UNIVERSIDAD DE MURCIA

FACULTAD DE QUÍMICA

Development of a Plataform for Metabolic Profiling and its Application to Biological Systems

Desarrollo de una Plataforma de Perfil Metabólico y su Aplicación al Estudio de Sistemas Biológicos

Dña. Cristina Bernal Martínez

2015

Trabajo presentado para optar al grado de

Doctor en Bioquímica con mención de

Doctorado Europeo.

Cristina Bernal Martínez

Murcia, Julio 2015.

RESUMEN GENERAL
(MENCIÓN EUROPEA)

Introducción

El metaboloma se refiere al conjunto de metabolitos (moléculas de bajo peso molecular) presente en una muestra biológica, tales como los intermedios metábolicos, las hormonas, las vitaminas o las moléculas de señalización (Wegner et al., 2012). Los cambios en el metaboloma son la última respuesta de un organismo a alteraciones genéticas, enfermedades o cambios ambientales (Clarke and Haselden, 2008). En este aspecto, el análisis del metaboloma puede ser una herramienta muy útil para estudiar el estado metabólico de los sistemas biológicos. Sin embargo, el metaboloma presenta una mayor complejidad frente a otras –omas como el transcriptoma o el proteoma. El transcriptoma se compone de cuatro tipos de unidades diferentes que son los ácidos nucleicos y el proteoma de veinte unidades que son los aminoácidos. En el caso del metaboloma, éste se compone de miles de pequeñas moléculas que son los metabolitos. La base de datos de metabolitos para la bacteria *Escherichia coli* (ECMDB) contiene más de 2.600 metabolitos (Guo et al., 2013), la base de datos de metabolitos para levaduras (YMDB) contiene más de 2.000 (Jewison et al., 2012) y la base de datos del metaboloma humano (HMDB) presenta más de 40.000 (Wishart et al., 2013).

El número de recambio de los metabolitos es del rango de segundos, por lo tanto, es necesaria una técnica apropiada para la paralización del metabolismo celular (quenching) que sea capaz de parar las reacciones bioquímicas que están teniendo lugar con la mínima pérdida del contenido intracelular (leakage). Se han descrito numerosos métodos de quenching en la literatura pero en esta Memoria se ha optado por usar la solución AMBIC, que consiste en metanol al 60% suplementado con bicarbonato amónico al 0.85% a -40 °C en base a los resultados obtenidos en trabajos anteriores (Sellick et al., 2009; Sellick et al., 2010; Sellick et al., 2011; Taymaz-Nikerel et al., 2009; Faijes et al., 2007). Por otro lado, existe una gran controversia sobre los métodos de quenching en el caso de los cultivos bacterianos debido al leakage o rotura. En el trabajo presente no se observó ninguna pérdida sustancial en el caso de los cultivos bacterianos (Capítulos 4 y 5) con el uso de AMBIC. Pero debido a la controversia actual acerca de este tema, se optó por no expresar los resultados de manera absoluta y hacerlo de manera relativa (fold-change) lo cual no

afectaba en absoluto al objetivo de estudio.

Con respecto a los protocolos de extracción de los metabolitos intracelulares, también se han aplicado numerosos en la literatura. El protocolo de extracción empleado en cada caso particular dependerá del tipo de muestra biológica así como de los metabolitos de interés (Faijes et al., 2007). Por ejemplo, en el trabajo de Sellick y colaboradores (2010) se describen numerosos procedimientos para estudiar los metabolitos intracelulares de las células de ovario de hámster chino (CHO). Los resultados mostraron distintas señales correspondientes a diferentes metabolitos de acuerdo con el protocolo empleado en cada caso. El protocolo de extracción de metabolitos intracelulares debe ser cuidadosamente validado ya que algunos procesos descritos tales como la liofilización pueden alterar la concentración de los metabolitos más lábiles (Oikawa et al., 2011).

El estudio de las concentraciones metabólicas se ha podido aplicar en diversos campos. Con respecto a la biomedicina, existen diversos trabajos centrados en distintas áreas como el cáncer (Beger 2013), enfermedades cardiovasculares (Mayr, 2011), o alimentación y nutrición (Wishart 2008), entre otros. Por ejemplo, en el trabajo de Aranibar y colaboradores (2011) los resultados obtenidos mostraron que los niveles de GSH y ATP eran más elevados cuando el medio, en el que se encontraban tejidos hepáticos, era suplementado con colina e histidina ya que estos componentes se agotaban antes en el medio. Con respecto a los bioprocesos, la cuantificación metabólica permite la formulación de medios químicamente definidos (Sonntag et al., 2011) y ayuda a la mejora de las técnicas de cultivo microbiano por medio de la ingeniería metabólica (Oldiges et al., 2014), entre otros. Por ejemplo, en el trabajo de Taymaz-Niquerel y colaboradores (2013) se estudió la red metabólica de *E.coli* en un cultivo continuo limitado por glucosa como fuente de carbono tras tres diferentes pulsos durante el cultivo (glucosa, piruvato y succinato). Las concentraciones metabólicas intracelulares así como el análisis de flujos metabólicos (MFA) mostraron un incremento en el flujo de la reacción catalizada por la enzima fosfoenolpiruvato carboxikinasa (PPCK) tras los pulsos de piruvato y succinato.

Objetivos

El objetivo de esta Tesis fue el desarrollo de una plataforma de perfil metabólico que permitiera identificar y cuantificar el mayor número posible de metabolitos pertenecientes a distintas rutas metabólicas en un amplio rango de muestras biológicas de distinta naturaleza.

Materiales y métodos

Se han empleado diversas muestras biológicas: (i) células murinas de leucemia sensibles y resistentes a la quimioterapia (Capítulo 2), (ii) muestras de tejido hepático de rata, de animales sanos y de animales con la enfermedad del hígado graso no alcohólico (EHGNA) (Capítulo 3) y (iii) muestras de cultivos bacterianos (*E.coli*), sometidos a estrés osmótico por altas concentraciones de NaCl (Capítulo 4) y en cultivos continuos de acetato como única fuente de carbono (Capítulo 5).

En nuestro estudio, se han empleado técnicas de cromatografía líquida-masas (LC-MS) para estudiar diferentes sistemas biológicos. Concretamente, se ha empleado cromatografía líquida de alta resolución acoplada a espectrometría de masas con ionización por electrospray (HPLC-ESI-MS) (Capítulos 3-5) que ha permitido identificar más de 70 metabolitos simultáneamente. Además de MS, en este trabajo también se han usado otros detectores acoplados a HPLC como el índice de refracción (RI) (Capítulos 4 y 5) y un detector ultravioleta que cubre un amplio rango de longitudes de onda (UV-diode array) que era capaz de identificar y cuantificar más de 20 metabolitos simultánemante (Capítulo 2). Para el tratamiento de datos se hizo uso de la web EASYLCMS (Fructuoso et al., 2012) que permite la cuantificación automática de cantidades masivas de datos obtenidos por LC-MS.

Con los datos obtenidos, se llevaron a cabo diversos procedimientos como el estudio de la varianza (ANOVA), el análisis de los componentes principales (PCA), el clustering bidimensional (agrupación bidimensional), el análisis de flujos metabólicos (MFA) o integración de vías metabólicas para agrupar datos de distinto origen (metaboloma y transcriptoma) (Integrative-pathway analysis).

Resultados y Discusión

En la presente memoria, se ha desarrollado una plataforma de perfil metabólico que incluye: la paralización del metabolismo celular (quenching), la extracción de los metabolitos intracelulares, el análisis cualitativo/cuantitativo de los metabolitos y el procesamiento de datos. La selección de un método apropiado, para llevar a cabo cada una de las etapas mencionadas anteriormente, es clave para obtener resultados concluyentes. En este aspecto, el protocolo de extracción de los metabolitos intracelulares ha sido cuidadosamente validado con la inclusión de algunos procedimientos comúnmente empleados tales como la liofilización. Los resultados obtenidos en este estudio mostraron que los metabolitos involucrados en el estado redox, NADP(H), NAD(H) y glutatión (formas reducida y oxidada), así como la relación de AcetilCoA/CoA, se modificaban cuando la liofilización se incluía en el proceso de extracción, o cuando se utilizaba metanol/agua como disolvente de extracción. En consecuencia, el protocolo de extracción basado en ACN/$CHCl_3$ resultó ser el más eficiente tras su validación con estándares de concentración conocida.

Una vez seleccionado el método de extracción, se procedió al estudio del análisis del metaboloma en diferentes sistemas. Algunas de las aplicaciones se centraron en el estudio de alteraciones metabólicas en el campo de la biomedicina, tales como la exposición de células leucémicas resistentes a múltiples fármacos (MDR) al fármaco quimioterapeútico daunomicina (DNM) (Capítulo 2) y en hígados de ratas con la enfermedad del hígado graso no alcohólico (EHGNA) (Capítulo 3). Además, el análisis del metaboloma también se aplicó en el campo de los bioprocesos bacterianos, para estudiar las alteraciones metabólicas durante una situación de choque osmótico por estrés salino (Capítulo 4), así como el efecto de la supresión del gen *cobB* en *Escherichia coli* en quimiostatos con acetato como una única fuente de carbono (Capítulo 5).

En el Capítulo 2, se ha detallado la elección del método de extracción más adecuado para las coenzimas, los cofactores redox y los nucleótidos, que resultó ser un protocolo basado en ACN/$CHCl_3$ que evita la liofilización. También en este capítulo, se mostró cómo el análisis metabólico contribuyó al

estudio de los mecanismos de resistencia a la quimioterapia. En este aspecto, se determinaron 21 metabolitos por LC-UV en diferentes cultivos de células leucémicas murinas antes y después de la exposición a DNM. Las líneas celulares estudiadas fueron: L1210 (sensible a DNM), L1210R (fenotipo MDR) y CBMC-6 (L1210 que expresan la glicoproteína P, P-gp). La actividad de P-gp es uno de los mecanismos más conocidos de resistencia a la quimioterapia, ya que es capaz de excretar el fármaco al exterior celular. Los resultados mostraron que L1210R y CBMC-6 presentaron 5 y 2 veces, respectivamente, la concentración de GSH con respecto a L1210. Este hecho sugiere que este metabolito juega un papel fundamental en la protección celular ya que se correlacionó con un porcentaje de supervivencia alta de estas células durante la exposición a DNM en contraposición a la línea sensible. Nuestros resultados sugirieron que uno de los mecanismos de resistencia a múltiples drogas podía ser la neutralización de las sustancias reactivas de oxígeno (ROS) (Fratelli et al., 2005) por medio del aumento de la concentración intracelular de GSH. Además, las relaciones $NADH/NAD^+$, AcCoA/CoA, la carga energética de adenilato (AEC), de uridilato (UEC) y de guanilato (GEC) fueron siempre mayores en L1210R que en L1210. Curiosamente, las células CBMC-6 presentaron un comportamiento intermedio entre las otras dos, posiblemente debido a la presencia de la P-gp.

En el capítulo 3, se analizó el metaboloma de hígados de ratas con la enfermedad del hígado graso no alcohólico (EHGNA), donde se identificaron y cuantificaron por LC-MS más de 70 metabolitos. Los resultados obtenidos mostraron diferentes perfiles metabólicos entre los hígados sanos y los hígados con EHGNA, lo cual estuvo en concordancia con los valores de los biomarcadores clásicos. Se debe mencionar que la alteración metabólica no sólo incluyó las moléculas redox (GSH, GSSG, NAD(P)(H)), sino también otros metabolitos como L-carnitina, CoA y diversos aminoácidos. Curiosamente, a diferencia de varios aminoácidos, la arginina (Arg) presentó una concentración de 8 veces en los hígados con EHGNA con respecto a los hígados sanos. Este hecho podría estar asociado al papel de la Arg en la regulación del metabolismo de lípidos, ya que modula la expresión y función de las enzimas involucradas en la lipólisis y lipogénesis (Jobgen et al., 2009).

En el Capítulo 4 de esta Memoria, también se estudiaron los eventos metabólicos que tuvieron lugar en *E. coli* durante la exposición a largo plazo de altas concentraciones de NaCl. Los resultados mostraron que las concentraciones intracelulares de determinados metabolitos tales como aminoácidos, nucleótidos, metabolitos redox, L-carnitina, fosfato y derivados de CoA se encontraban muy alterados en función de la concentración de NaCl. Además, tras el choque osmótico, tuvo lugar un descenso muy pronunciado en las concentraciones de los aminoácidos extracelulares presentes en el medio. Este hecho podría no deberse a su uso como osmoprotectores (Amezaga and Booth, 1999), sino a una manera de ahorrar energía redirigiendo los cofactores redox y las coenzimas hacia otras vías metabólicas ya que de esa manera se evitaría la síntesis *de novo* (Jozefczuk et al., 2010). Los datos metabólicos se integraron con los datos del análisis de transcriptómica por medio del análisis de rutas metabólicas (pathway-based analysis). La integración de ambos conjuntos de datos permitió resaltar las principales vías metabólicas alteradas que resultaron ser: el metabolismo del GSH, las vías glucólisis/gluconeogénesis, la biosíntesis/degradación de aminoácidos, el metabolismo de purinas, la fosforilación oxidativa y el ciclo de ácidos tricarboxilicos (CAT)/ciclo del glioxilato, entre otros. La concentración de GSH no se alteró apenas a la concentración de NaCl 0,5M pero estuvo bajo los límites de cuantificacíon a muy altas concentraciones de NaCl (0,8M). Este hecho sugirió que el GSH podría ser clave en la respuesta al choque osmótico ya que mutantes de *E. coli* incapaces de sintentizar o regenerar GSH, resultaron incapaces de crecer en un medio de alta osmolaridad (Smirnova et al., 2001). Además, se realizó el análisis de flujos metabólicos (MFA), que mostró una reorganización de los mismos orientada hacia la mayor síntesis de productos de fermentación, tales como etanol en el caso de NaCl 0.5M y lactato en el caso de NaCl 0.8M.

En el Capítulo 5, el análisis del metaboloma se aplicó al estudio del papel de la única deacetilasa conocida de *E. coli* (CobB) en quimiostatos con acetato como única fuente de carbono. Además, también se realizó el análisis del transcriptoma, y ambos conjuntos de datos se integraron por medio del análisis de rutas metabólicas (pathway-based analysis). Los resultados obtenidos no

mostraron diferencias estadísticas en el metabolismo central como ocurría en el caso de los cultivos continuos limitados por glucosa como fuente de carbono (Castaño-Cerezo et al., 2014). Sin embargo, los efectos más notables tuvieron lugar en el metabolismo del azufre y del nitrógeno, incluyendo alteraciones en las vías de CoA, taurina, pirimidinas y varios aminoácidos, sugiriendo que el metabolismo del nitrógeno podría estar directa o indirectamente regulado por la acetilación de proteínas. El análisis de las rutas metabólicas (pathway-based analysis) ha mostrado ser una herramienta muy efectiva para la integración de cantidades masivas de datos (metabolómica y transcriptómica) identificando las rutas metabolicas que se encuentran afectadas.

Conclusión

En conclusión, el análisis del metaboloma ha sido utilizado en conjunción con otras técnicas tales como la transcriptómica, la flujómica o biomarcadores clásicos. Asimismo, la cuantificación de los cofactores redox, los nucleótidos, las coenzimas y los aminoácidos es sumamente importante para la comprensión global del estado metabólico en los sistemas biológicos siendo clave GSH, ATP, CoA, AcCoA y diversos aminoácidos ya que al menos uno de los mencionados se ha encontrado alterado en las situaciones descritas en esta Tesis a lo largo de los Capítulos 2-5. Además, algunas de las moléculas clave mencionadas como GSH, AcCoA, CoA y también NAD(P)H han resultado ser lábiles durante el proceso de extracción, de modo que es esencial el uso de un protocolo que no altere *per se* estos metabolitos.

Referencias

Amezaga, M. R., Booth, I. R. (1999). Osmoprotection of *Escherichia coli* by peptone is mediated by the uptake and accumulation of free proline but not of proline-containing peptides. *Appl. Environ. Microbiol*., **65**, 5272-5278.

Aranibar, N., Borys, M., Mackin, N. A., Ly, V., Abu-Absi, N., Abu-Absi, S., Niemitz, M., Schilling, B., Li, Z. J., Brock, B., Russell, R. J., II, Tymiak, A., Reily, M. D. (2011). NMR-based metabolomics of mammalian cell and tissue cultures. J. Biomol. Nmr, 49, 195-206.

Beger, R. D. (2013). A review of applications of metabolomics in cancer. *Metabolites*, **3**, 552-574.

Castano-Cerezo, S., Bernal, V., Post, H., Fuhrer, T., Cappadona, S., Sanchez-Diaz, N. C., Sauer, U., Heck, A. J., Altelaar, A. F. and Canovas, M. (2014). Protein acetylation affects acetate metabolism, motility and acid stress response in *Escherichia coli*. Mol. Syst. Biol., **10**, 762. doi: 10.15252/msb.20145227**.**

Clarke, C. J., Haselden, J. N. (2008). Metabolic Profiling as a Tool for Understanding Mechanisms of *Toxicity. Toxicol. Pathol*., **36**, 140-147.

Faijes, M., Mars, A. E., Smid, E. J. (2007). Comparison of quenching and extraction methodologies for metabolome analysis of Lactobacillus plantarum. *Microb. Cell Fact*., **6**, 27. doi:10.1186/1475-2859-6-27.

Fratelli, M., Goodwin, L. O., Orom, U. A., Lombardi, S., Tonelli, R., Mengozzi, M. and Ghezzi, P. (2005). Gene expression profiling reveals a signaling role of glutathione in redox regulation. Proc. Natl. Acad. Sci. U. S. A., 102, 13998-14003.

Fructuoso, S., Sevilla, A., Bernal, C., Lozano, A. B., Iborra, J. L., Canovas, M. (2012). EasyLCMS: an asynchronous web application for the automated quantification of LC-MS data. BMC res. notes, 5, 428-428.

Guo, A. C., Jewison, T., Wilson, M., Liu, Y., Knox, C., Djoumbou, Y., Lo, P., Mandal, R., Krishnamurthy, R., Wishart, D. S. (2013). ECMDB: The E-coli Metabolome Database. *Nucleic Acids Res*., **41**, D625-D630.

Jewison, T., Knox, C., Neveu, V., Djoumbou, Y., Guo, A. C., Lee, J., Liu, P., Mandal, R., Krishnamurthy, R., Sinelnikov, I., Wilson, M., Wishart, D. S. (2012). YMDB: the Yeast Metabolome Database. *Nucleic Acids Res*., **40**, D815-D820.

Jobgen, W., Fu, W. J., Gao, H., Li, P., Meininger, C. J., Smith, S. B., Spencer, T. E., Wu, G. (2009). High fat feeding and dietary L-arginine supplementation differentially regulate gene expression in rat white adipose tissue. *Amino Acids*, **37**, 187-198.

Jozefczuk, S., Klie, S., Catchpole, G., Szymanski, J., Cuadros-Inostroza, A., Steinhauser, D., Selbig, J., Willmitzer, L. (2010). Metabolomic and transcriptomic stress response of *Escherichia coli*. *Mol. Syst. Biol*., **6**:364. doi: 10.1038/msb.2010.18.

Mayr, M. (2011). Recent highlights of metabolomics in cardiovascular research. Circulation. *Cardiovasc. genetics*, **4**, 463-464.

Oikawa, A., Otsuka, T., Jikumaru, Y., Yamaguchi, S., Matsuda, F., Nakabayashi, R., Takashina, T., Isuzugawa, K., Saito, K., Shiratake, K. (2011). Effects of freeze-drying of samples on metabolite levels in metabolome analyses. *J. Sep. Sci*., **34**, 3561-3567.

Oldiges, M., Eikmanns, B. J., Blombach, B. (2014). Application of metabolic engineering for the biotechnological production of L-valine. *Appl. Microbiol. Biotechnol.*, **98**, 5859-5870.

Sellick, C. A., Hansen, R., Maqsood, A. R., Dunn, W. B., Stephens, G. M., Goodacre, R., Dickson, A. J. (2009). Effective Quenching Processes for Physiologically Valid Metabolite Profiling of Suspension Cultured Mammalian Cells. Anal. Chem., 81, 174-183.

Sellick, C. A., Knight, D., Croxford, A. S., Maqsood, A. R., Stephens, G. M., Goodacre, R., Dickson, A. J. (2010). Evaluation of extraction processes for intracellular metabolite profiling of mammalian cells: matching extraction approaches to cell type and metabolite targets. *Metabolomics*, **6**, 427-438.

Sellick, C. A., Hansen, R., Stephens, G. M., Goodacre, R., Dickson, A. J. (2011). Metabolite extraction from suspension-cultured mammalian cells for global metabolite profiling. *Nat. Protoc*., **6**, 1241-1249.

Smirnova, G. V., Krasnykh, T. A., Oktyabrsky, O. N. (2001). Role of glutathione in the response of *Escherichia coli* to osmotic stress. *Biochem.-Moscow*, **66**, 973-978.

Sonntag, D., Scandurra, F. M., Friedrich, T., Urban, M., Weinberger, K. M. (2011). Targeted metabolomics for bioprocessing., in: 22nd European Society for Animal Cell Technology (ESACT) Meeting on Cell Based Technologies., p. 27. BMC Proceedings, Innsbruck, Austria.

Taymaz-Nikerel, H., de Mey, M., Ras, C., ten Pierick, A., Seifar, R. M., Van Dam, J. C., Heijnen, J. J., Van Glilik, W. M. (2009). Development and application of a differential method for reliable metabolome analysis in *Escherichia coli*. *Anal. Biochem.*, **386**, 9-19.

Wegner, A., Cordes, T., Michelucci, A., Hiller, K. (2012). The Application of Stable Isotope Assisted Metabolomics in Biomedicine. Curr. Biotechnol., 1, 88-97.

Wishart, D. S. (2008). Metabolomics: applications to food science and nutrition research. *Trends Food Sci. Technol.*, **19**, 482-493.

Wishart, D. S., Jewison, T., Guo, A. C., Wilson, M., Knox, C., Liu, Y., Djoumbou, Y., Mandal, R., Aziat, F., Dong, E., Bouatra, S., Sinelnikov, I., Arndt, D., Xia, J., Liu, P., Yallou, F., Bjorndahl, T., Perez-Pineiro, R., Eisner, R., Allen, F., Neveu, V., Greiner, R., Scalbert, A. (2013). HMDB 3.0-The Human Metabolome Database in 2013. *Nucleic Acids Res*., **41**, D801-D807.

UNIVERSIDAD DE
MURCIA

D. Manuel Cánovas Díaz, Catedrático de Universidad del Área de Bioquímica en el Departamento de Bioquímica y Biología Molecular B e Inmunología, AUTORIZA:

La presentación de la Tesis Doctoral titulada "Desarrollo de una plataforma de perfil metabólico y su aplicación al estudio de sistemas biológicos (Development of a Metabolic Profiling Platform and its Application to the Study of Biological Systems)", realizada por Dª. Cristina Bernal Martínez, bajo mi inmediata dirección y supervisión, y que presenta para la obtención del grado de Doctor por la Universidad de Murcia.

En Murcia, a 14 de Julio de 2015

UNIVERSIDAD DE
MURCIA

D. José Luis Iborra Pastor, Catedrático de Universidad del Área de Bioquímica en el Departamento de Bioquímica y Biología Molecular B e Inmunología, AUTORIZA:

La presentación de la Tesis Doctoral titulada "Desarrollo de una plataforma de perfil metabólico y su aplicación al estudio de sistemas biológicos (Development of a Metabolic Profiling Platform and its Application to the Study of Biological Systems)", realizada por Dª. Cristina Bernal Martínez, bajo mi inmediata dirección y supervisión, y que presenta para la obtención del grado de Doctor por la Universidad de Murcia.

En Murcia, a 16 de Julio de 2015

FDO. JOSE L. IBORRA

UNIVERSIDAD DE
MURCIA

D. Ángel Sevilla Camins, Doctor de Universidad del Área de Bioquímica en el Departamento de Bioquímica y Biología Molecular B e Inmunología, AUTORIZA:

La presentación de la Tesis Doctoral titulada "Desarrollo de una plataforma de perfil metabólico y su aplicación al estudio de sistemas biológicos (Development of a Metabolic Profiling Platform and its Application to the Study of Biological Systems)", realizada por Dª. Cristina Bernal Martínez, bajo mi inmediata dirección y supervisión, y que presenta para la obtención del grado de Doctor por la Universidad de Murcia.

En Murcia, a 14 de julio de 2015

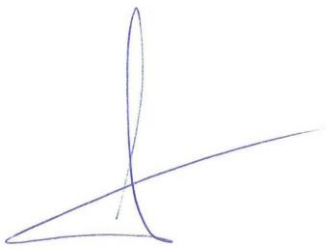

La firmante de esta Memoria ha disfrutado, durante el período de 2009-2013, de una beca del gobierno de España, para la Formación de Profesorado Universitario (FPU).

Este trabajo ha sido subvencionado por los siguientes proyectos:

- "Biotecnología de Sistemas para la mejora de bioprocesos relacionados con el metabolismo central de *E.coli:* Integración de la regulación transcripcional y posttransduccional", (BIO2011-29233-C02-01) concendido por MICIN (Ministerio de Ciencia e Innovacón).

- "Redirección de flujos metabólicos del metabolismo central de *E.coli* para la producción de succinato y L-carnitina", (BIO2008-04500-C02-01), concedido por MICIN.

- "Ingeniería metabólica y Biología de Sistemas aplicadas a la optimización de bioprocesos", (08660/PI/08) concedido por Séneca-CARM.

- "Biología de Sistemas y sintética de la acetilación/desacetilación del proteoma de *E.coli",* (BIO2014-54411-C2-1-R), concedido por MINECO (Ministerio de Economía).

- "Biotecnología de Sistemas para la mejora de bioprocesos relacionados con el metabolismo central de *E. coli*: Integración de la regulación del transcriptoma y post-traduccional en la producción de terpenos", (19236-PI/14), concedido por la Fundación Séneca.

Cristina Bernal Martínez

Murcia, Julio 2015

Some results obtained in this Thesis are contained in the following publications:

ARTICLES

- Cánovas, M., **Bernal, C**.,Sevilla, A., Iborra, J. L. (2007).In silico model of the mitochondrial role in cardiac cell undergoing angina pectoris. *J. Biotechnol*., **131**, S19.
- **Bernal, C**., Sevilla, A., Iborra, J. L., Canovas, M.(2009). Metabolic profiling of multi-drug resistant cells. *New Biotech*., **25**,S341-S341.
- Cerezo, D., Ruiz-Alcaraz, A.J., Lencina, M., **Bernal, C**., Cánovas, M., García-Peñarrubia, P. and Martín-Orozco, E. (2010). Molecular events during cold stress induced cell-death on multidrug resistant leukemic cells. *EJC Supplements* **8** no. 5, 145-146.
- Fructuoso, S., Sevilla, A., **Bernal, C**., Lozano, A. B.,Iborra, J. L., Canovas, M. (2012). EasyLCMS: An asynchronous web application for the automated quantification of LC-MS data. *BMC Res Notes*, **5**, 428.
- **Bernal, C**., Martin-Pozuelo, G., Sevilla, A., Lozano, A., Garcia-Alonso, J., Canovas, M., Periago, M. J. (2013). Lipid biomarkers and metabolic effects of lycopene from tomato juice on liver of rats with induced hepatic steatosis. *J. Nutr.Biochem*, **24**, 1870-1881.
- Monteiro, F., Bernal, V., Saelens, X., Lozano, A. B., **Bernal, C**., Sevilla, A., Carrondo, M. J. T. and Alves, P. M. (2014). Metabolic profiling of insect cell lines: Unveiling cell line determinants behind system's productivity. *Biotechnol. Bioeng*. **111**, 816-828.
- Montero, M., Rahimpour, M., Viale, A.M., Almagro, G., Eydallin, G., Sevilla, Á., Cánovas, M., **Bernal, C**., Lozano, A.B., Muñoz, F.J., Baroja-Fernández, E., Bahaji, A., Mori, H., Codoñer, F.M., Pozueta-Romero, J.(2014). Systematic production of inactivating and non-inactivating suppressor mutations at the relA locus that compensate the detrimental effects of complete spot loss and affect glycogen content in Escherichia coli. *PloS One* doi: 10.1371/journal.pone.0106938. eCollection 2014.

- **Bernal, C**., Sevilla, A., Ruiz-Alacaraz, A., Martin-Orozco, E., Iborra, J. L., Canovas, M., Metabolic Profiling of Multi Drug Resistance cells under cold-induced cell death. *Metabolomics*. (Submitted).
- Arense, P., **Bernal, C**., Sevilla, A., Iborra, J. L., Canovas, M. Integration of Fluxomics, Metabolomics and Trascriptomics to describe anaerobic long-term salt adaptation of E. coli using glycerol as C-source. *Metab. Eng*. (Submitted)

BOOK OF CHAPTER

- Sevilla, A., Bernal, V., Teruel, R., **Bernal, C**., Canovas, M., Iborra, J. L. (2006). Dynamic model for the optimization of L(-)-carnitine production by Escherichia coli, in: Understanding and Exploiting Systems Biology in *Bioprocess and Biomedicine* 249-259. ISBN: 284-611-1135-1134. Fundación Caja Murcia.

CONGRESS PRESENTATIONS

- Sevilla, A., Bernal, V., Teruel, R., **Bernal**, **C.,** Cánovas, M. and Iborra, J. L. Dynamic model for the optimization of L(-)-carnitine production by *Escherichia coli*. (2006). *1st International Symposium on Systems Biology: From genomes to In silico and back.* Murcia (Spain). Book of Abstracts.
- Teruel, R., Sevilla, A., **Bernal, C.**, Bernal, V., Arense, P., Masdemont, B., Cánovas, M. and Iborra, J. L. (2006). Análisis de flujos metabólicos del metabolismo central y el de carnitina en *Escherichia coli* para incrementar su biosíntesis. *Biospain-Biotec 2006.* Madrid (Spain). Book of Abstracts.
- Sevilla, A., **Bernal, C.**, Teruel, R., Bernal, V., Arense, P., Masdemont, B., Cánovas, M. and Iborra, J. L. (2006). La mejora de bioprocesos mediante el estudio de las redes de señalización: el caso de la

biotransformación de L(-)-carnitina. *Biospain-Biotec 2006*. Madrid (Spain). Book of Abstracts**. 3rd Prize Poster.**

- Sevilla, A., **Bernal, C.**, Teruel, R, Bernal, V., Arense, P., Masdemont, B., Cánovas, M. and Iborra, J. L. (2006). Uso de células durmientes, permeabilizadas y dañadas en la mejora de biotransformaciones con enterobacterias: la producción de L(-)-canitina. (2006). *Biospain-Biotec 2006.* Madrid (Spain). Book of Abstracts.
- Cánovas, M., **Bernal, C.**, Sevilla, A. and Iborra, J. L. In silico model of the mitochondrial role in the cardiac cell pathology (2007). *The Eight International Conference on Systems Biology ICSB.* Long Beach, California. USA. Book of Abstracts.
- **Bernal, C.**, Sevilla, A., Arense, P., Cánovas, M. and Iborra, J. L. In silico model of the mitochondrial metabolism in cardiac cell undergoing alterations in the ATP synthesis (2007). *4th Meeting of the Spanish Systems Biology Network (REBS)*. Valencia (Spain). Book of Abstracts.
- Cánovas, M., **Bernal, C.**, Sevilla, A. and Iborra, J. L. In silico model of the mitochondrial role in cardiac cell undergoing angina pectoris (2007). European Congress on Biotechnology, 2007. Barcelona (Spain). **Oral Presentation.**
- **Bernal, C.**, Sevilla, A., Cánovas, M. and Iborra, J. L. In silico model of the mitochondrial metabolism in cardiac cell undergoing hyperglycemia (2008). *Conference on Systems Biology of mammalian cells (SBMC2008).* Dresden (Germany). Book of Abstracts.
- **Bernal, C.**, Sevilla, A., Cánovas, M. and Iborra, J. L. In silico model of the mitochondrial metabolism in cardiac cell undergoing electron transport chain dysfunctions (2008). *7th European Symposium on Biochemical Engineering Science (ESBES-7).*Faro (Portugal). Book of Abstracts.
- Arense, P., Bernal, V., **Bernal, C.**, Sevilla, A., Cánovas, M. and Iborra, J. L. Salt stress effects on the central and carnitine production metabolisms of *Escherichia coli* (2008). *BioSpain Biotec 2008.*Granada (Spain). Book of Abstracts.
- Sevilla, A., **Bernal, C.**, Arense, P., Cánovas, M. and Iborra, J. L. Signalling model of E. coli L-carnitine metabolism for imparing the glucose catabolite

repression (2008). *4th Meeting of the Spanish Systems Biology Network (REBS 2008*). Valencia (Spain). Book of Abstracts.

- Sevilla, A., **Bernal, C.**, Arense, P., Cánovas, M. and Iborra, J. L. El uso de la Biología de Sistemas para evitar la Represión catabólica (2008). *BioSpain Biotec 2008.*Granada (Spain). Book of Abstracts. **Oral Presentation.**
- **Bernal, C.**, Sevilla, A., Iborra, J. L. and Cánovas, M. Metabolic Profiling of Multi-Drug resistant cells (2009). *14th European Congress on Biotechnology (Symbiosis 2009).* Barcelona (Spain). Book of Abstracts.
- **Bernal, C.**, Ruiz-Alacaraz, A., Martin-Orozco, E., Iborra, J. L. and Cánovas, M. Metabolomic Profiles of leukemic cell line: Understanding the multi-drug resistance and apoptosis (2009). *Cell line and Engineering 2009*. Berlin (Germany). Book of Abstracts. **Oral Presentation.**
- Cánovas, M., **Bernal, C.**, Sevilla, A. and Iborra, J. L. Systemics of leukemic cell lines: understanding multi-drug resistance and apoptosis (2009). *Fostering Systems & Synthetic Biology in Southern Europe*. Madrid (Spain). Book of Abstracts. **Oral Presentation.**
- Sevilla, A., **Bernal, C.**, Arense, P., Iborra, J. L. and Cánovas, M. Optimization of a bioprocess through Cofactor Engineering applying mathematical models (2009).
  European Systems & Synthetic Biology. Paris (France). Book of Abstracts. **Invited Oral Presentation (Plenary).**
- Sevilla, A., **Bernal, C.**, Arense, P., Iborra, J. L. and Cánovas, M. Metabolomics for Systems Biology (2009). *Industrial Biotechnology PhD Meeting*. Verbania (Italy). **Invited Oral Presentation (Plenary).**
- Sevilla, A., **Bernal, C.**, Iborra, J. L. and Cánovas, M. Integration of metabolic and biophysic models of mitochondria using linlog formalism (2010). *BioSpain Biotec 2010*. Pamplona (Spain). **Oral Presentation.**
- **Bernal, C.**, Sevilla, A., Iborra, J. L., Cerezo, D., Martin-Orozco, E. and Cánovas, M.
  Metabolic Differences between Sensitive And Multidrug-Resistance Leukaemic Cell Lines Under Daunomycin Treatment (2010). BioSpain Biotec 2010. Pamplona (Spain). **Oral Presentation. Second Award.**

- **Bernal, C.**, Lozano, A.B., Muñoz, P., Sevilla, A., Cerezo, D., Iborra, J. L. and Cánovas, M. The increment in agitation rate in spinner reactors causes different metabolic alterations in sensitive and multidrug-resistant human leukaemia cell lines (2010). *BioSpain Biotec 2010.* Pamplona (Spain). Book of Abstracts.
- **Bernal, C.**, Sevilla, A., Ruiz-Alacaraz, A., Martin-Orozco, E., Iborra, J. L. and Cánovas, M. Metabolomics of leukemic cell lines: understanding multi-drug resistance and apoptosis (2010). *SEBBM 2010.* Cordoba (Spain). **Invited Oral Presentation.**
- Sevilla, A., **Bernal, C.**, Iborra, J. L. and Cánovas, M. Inbionova. I Premio Proyecto Emprendedor Biotecnología (2010). *SEBBM 2010*. Cordoba (Spain). **Invited Oral Presentation.**
- Arense, P., Sevilla, A., **Bernal, C.**, Lozano, A.B., Vidal, R., Iborra, J. L. and Cánovas, M. Adaptation of E. coli to long-term high salt conditions: integrating metabolomics, transcriptomics and fluxomics data (2012). *BIOTEC 2012.* Bilbao (Spain). **Invited Oral Presentation.**
- Fructuoso, S., Sevilla, A., Lozano, A.B., **Bernal, C.**, Iborra, J. L. and Cánovas, M. EasyLCMS: From metabolomics raw data files to quantified data for bioprocess optimization (2012). *Applied Synthetic Biology in Europe 2012*. Barcelona (Spain). **Oral Presentation.**
- Vidal, R., **Bernal, C.**, Sevilla, A., Lozano, A.B., Cerezo, D., Martin-Orozco, E., Iborra, J. L. and Cánovas, M. Optimising sample preparation in proteomics: study of a human leukemia cell line CCL-159 (2012). *BIOTEC 2012*. Bilbao (Spain). **Oral Presentation.**

AGRADECIMIENTOS/ ACKNOWLEDGEMENTS

He tenido la gran suerte de poder contar con muchísimas personas a mi alrededor durante estos años. Todos y cada uno de ellos han contribuido de alguna manera a que esta memoria haya podido ver la luz.

A mis directores, *Manuel Cánovas, José Luis Iborra* y *Ángel Sevilla*, por darme la oportunidad y confiar en mí para la realización de este proyecto. Gracias por vuestros consejos y cariño.

A todos los compañeros del departamento de Bioquímica y Biología Molecular (B) e Inmunología, a los que están y a los que ya no están pero que dejaron su granito de arena. *Pedro, Vicente, Kimberly, Macarena, Natalie, Ann, Inés, Juana Mari, Berenice, José María, Corina, Sergio*…….. quiero darle una mención especial a *Teresa, Arturo y David* por su ayuda incondicional y con los que he compartido muchas horas de laboratorio y muchas risas. A *Arancha, Rebeca, Miguel*, por vuestra alegría y contribución a ese trabajo. También quiero resaltar la ayuda y colaboración de *Sara* en los últimos capítulos de esta memoria, gracias.

A mi *Ana*, una de mis mejores amigas, sin duda una de las personas más importantes para la realización de esta Tesis, el ejemplo más sublime de compañerismo y lealtad. Gracias por alegrarme cada día. A *Paula,* otra persona clave en estos años, gracias por tu ayuda y por los buenos ratos que hemos pasado (también a Jerusam). Gracias por el papel indispensable en uno de los capítulos de esta Tesis.

A *Elena, Antonio y David* de la parte de Inmunología, personas fundamentales en el comienzo del desarrollo de esta Tesis, con vosotros empecé mis primeros experimentos, gracias por todo lo que aprendí y por vuestra dedicación.

A *Maria Jesús y a Gala* del departamento de Bromatología de la Universidad de Murcia. Gracias por esa colaboración tan bonita que permitió trabajar en el análisis de tejidos.

An special mention for people from CSE in TUDELFT (Delft, Netherlands), where my stay there was key in the development of one chapter of this Thesis. To *Sef* and *Aljoscha* for the opportunity there, thanks for your supervision and kindness, to *Jinrui, Robin, Mihir, Anisha, Reza, Angie, Cor, Walter, Amit, Manuel, Peter, Katelijne,* thanks for your advices and the good moments, specially to Panchis and Hugo since you have become part of my family and very very specially, to *Camilo,* "my πφϚϞ", thanks for all the hours we spent in the lab specially with the srynges and tubes in the sink (☺), for your advices and patience, and for being key in the development of the present work.

A todos y cada uno de los miembros de la *Secretaria de la Facultad de Química*, indispensables en el edificio, ¡lo saben todo!, gracias por vuestra paciencia con "la fashion".

A *Javier, Medhi, Goizeder, Manuel* del CSIC de Navarra por su enriquecedora colaboración.

A los miembros del Oceanográfico, Marina, Antonio y a Diego de Toxicología, por lo mucho que hemos aprendido de las colaboraciones y los frutos que están dando.

A mi familia, *mis padres* y *mi hermano*, por preocuparse por mí y tratar de entenderlas cosas en las que trabajo, muchas gracias por vuestro apoyo y por quererme. A mi gran familia, *mis abuelos*, algunos de los cuales disfrutarán este trabajo desde un lugar privilegiado, *mis tíos*, *mis primos*, *mi madrina, mis sobrinas* y *mi suegra.* La familia no se elige, es la que te toca pero yo sin duda, os elegiría.

A mis amigos, *Mar, Mónica, Maribel,* por nuestras charlas interminables sobre cualquier tema*, a Silvia, Juanda, Manolo, Chemi,* por sobrevivir a las patiladas*, a Toñi, Óscar, María, Víctor, Lucas, Jacin, David, Paco, Yolanda, Óscar, Rafa, Reyes, Carla, Osqui, Alejandro, Juli y "la familia"* y sobre todo a mi *Belén* y mi *Anita*, para que la amistad que empezamos con 6 años nos dure hasta los 106 por lo menos.

Por último y más importante, a *Ángel*, la mejor parte de mi vida, a ti te lo debo todo, gracias por elegirme y compartir tu vida conmigo, contigo de la mano, cualquier obstáculo es un paseo y cualquier momento es un regalo. Ild.

A mis abuelos

TABLE OF CONTENTS

RESUMEN

El metaboloma se refiere al conjunto de metabolitos (moléculas de bajo peso molecular) presente en una muestra biológica, tales como los intermedios metábolicos, las hormonas, las vitaminas o las moléculas de señalización. Debido a la disponibilidad actual de técnicas analíticas novedosas, el análisis del metaboloma se utiliza ampliamente y presenta multitud de aplicaciones para el estudio de los sistemas biológicos.

En la presente memoria, se ha desarrollado una plataforma de perfil metabólico que incluye: la paralización del metabolismo celular (quenching), la extracción de los metabolitos intracelulares, el análisis cualitativo/cuantitativo de los metabolitos y el procesamiento de datos. La selección de un método apropiado, para llevar a cabo cada una de las etapas mencionadas anteriormente, es clave para obtener resultados concluyentes. En este aspecto, el protocolo de extracción de los metabolitos intracelulares ha sido cuidadosamente validado con la inclusión de algunos procedimientos comúnmente empleados tales como la liofilización. Los resultados obtenidos en este estudio mostraron que los metabolitos involucrados en el estado redox, NADP(H), NAD(H) y glutatión (formas reducida y oxidada), así como la relación de AcetilCoA/CoA, se modificaban cuando la liofilización se incluía en el proceso de extracción, o cuando se utilizaba metanol/agua como disolvente de extracción. En consecuencia, el protocolo de extracción basado en ACN/$CHCl_3$ resultó ser el más eficiente tras su validación con estándares de concentración conocida.

Una vez seleccionado el método de extracción, se procedió al estudio del análisis del metaboloma en diferentes sistemas. Algunas de las aplicaciones se centraron en el estudio de alteraciones metabólicas en el campo de la biomedicina, tales como la exposición de células leucémicas resistentes a múltiples fármacos (MDR) al fármaco quimioterapeútico daunomicina (DNM) (Capítulo 2) y en hígados de ratas con la enfermedad del hígado graso no alcohólico (EHGNA) (Capítulo 3). Además, el análisis del metaboloma también se aplicó en el campo de los bioprocesos bacterianos, para estudiar las alteraciones metabólicas durante una situación de choque osmótico por estrés salino (Capítulo 4), así como el efecto de la supresión del gen *cobB* en *Escherichia coli* en quimiostatos con acetato como una única fuente de carbono (Capítulo 5).

En el Capítulo 2, también se ha detallado la elección del método de extracción más adecuado para las coenzimas, los cofactores redox y los nucleótidos, que resultó ser un protocolo basado en ACN/$CHCl_3$ que evita la liofilización. También en este capítulo, se mostró cómo el análisis metabólico contribuyó al estudio de los mecanismos de resistencia a la quimioterapia. En este aspecto, se determinaron 21 metabolitos por LC-UV en diferentes cultivos de células leucémicas murinas antes y después de la exposición a DNM. Las líneas celulares estudiadas fueron: L1210 (sensible a DNM), L1210R (fenotipo MDR) y CBMC-6 (L1210 que expresan la glicoproteína P, P-gp). La actividad de P-gp es uno de los mecanismos más conocidos de resistencia a la quimioterapia, ya que es capaz de excretar el fármaco al exterior celular. Los resultados mostraron que L1210R y CBMC-6 presentaron 5 y 2 veces, respectivamente, la concentración de GSH con respecto a L1210. Este hecho sugiere que este metabolito juega un papel fundamental en la protección celular ya que se correlacionó con un porcentaje de supervivencia alta de estas células durante la exposición a DNM en contraposición a la línea sensible. Además, las relaciones NADH/NAD^+, AcCoA/CoA, la carga energética de adenilato (AEC), de uridilato (UEC) y de guanilato (GEC) fueron siempre mayores en L1210R que en L1210. Curiosamente, las células CBMC-6 presentaron un comportamiento intermedio entre las otras dos, posiblemente debido a la presencia de la P-gp.

En el capítulo 3, se analizó el metaboloma de hígados de ratas con la enfermedad del hígado graso no alcohólico (EHGNA), donde se identificaron y cuantificaron por LC-MS más de 70 metabolitos. Los resultados obtenidos mostraron diferentes perfiles metabólicos entre los hígados sanos y los hígados con EHGNA, lo cual estuvo en concordancia con los valores de los biomarcadores clásicos. Se debe mencionar que la alteración metabólica no sólo incluyó las moléculas redox (GSH, GSSG, NAD(P)(H)), sino también otros metabolitos como L-carnitina, CoA y diversos aminoácidos.

En el Capítulo 4 de esta Memoria, también se estudiaron los eventos metabólicos que tuvieron lugar en *E. coli* durante la exposición a largo plazo de altas concentraciones de NaCl. Los resultados mostraron que las concentraciones intracelulares de determinados metabolitos tales como

aminoácidos, nucleótidos, metabolitos redox, L-carnitina, fosfato y derivados de CoA se encontraban muy alterados en función de la concentración de NaCl. Además, tras el choque osmótico, tuvo lugar un descenso muy pronunciado en las concentraciones de los aminoácidos extracelulares presentes en el medio. Los datos metabólicos se integraron con los datos del análisis de transcriptómica por medio del análisis de rutas metabólicas (pathway-based analysis). La integración de ambos conjuntos de datos permitió resaltar las principales vías metabólicas alteradas que resultaron ser: el metabolismo del GSH, las vías glucólisis/gluconeogénesis, la biosíntesis/degradación de aminoácidos, el metabolismo de purinas, la fosforilación oxidativa y el ciclo de ácidos tricarboxilicos (CAT)/ciclo del glioxilato, entre otros. Además, se realizó el análisis de flujos metabólicos (MFA), que mostró una reorganización de los mismos orientada hacia la mayor síntesis de productos de fermentación, tales como etanol en el caso de NaCl 0.5M y lactato en el caso de NaCl 0.8M.

En el Capítulo 5, el análisis del metaboloma se aplicó al estudio del papel de la única deacetilasa conocida de *E. coli* (CobB) en quimiostatos con acetato como única fuente de carbono. Además, también se realizó el análisis del transcriptoma, y ambos conjuntos de datos se integraron por medio del análisis de rutas metabólicas (pathway-based analysis). Los resultados obtenidos no mostraron diferencias estadísticas en el metabolismo central. Sin embargo, los efectos más notables tuvieron lugar en el metabolismo del azufre y del nitrógeno, incluyendo alteraciones en las vías de CoA, taurina, pirimidinas y varios aminoácidos, sugiriendo que el metabolismo del nitrógeno podría estar directa o indirectamente regulado por la acetilación de proteínas. El análisis de las rutas metabólicas (pathway-based analysis) ha mostrado ser una herramienta muy efectiva para la integración de cantidades masivas de datos (metabolómica y transcriptómica) identificando las rutas metabolicas que se encuentran afectadas.

En conclusión, el análisis de metaboloma ha sido utilizado en conjunción con otras técnicas tales como la transcriptómica, la flujómica o biomarcadores clásicos. Asimismo, la cuantificación de los cofactores redox, los nucleótidos, las coenzimas y los aminoácidos es sumamente importante para la comprensión global del estado metabólico en los sistemas biológicos siendo

clave GSH, ATP, CoA, AcCoA y diversos aminoácidos ya que al menos uno de los mencionados se ha encontrado alterado en las situaciones descritas en esta Tesis a lo largo de los Capítulos 2-5. Además, algunas de las moléculas clave mencionadas como GSH, AcCoA, CoA y también NAD(P)H han resultado ser lábiles durante el proceso de extracción, de modo que es esencial el uso de un protocolo que no altere per se estos metabolitos.

THESIS ABSTRACT

Metabolome analysis is widely used in the study of biological systems due to the affordable analytical techniques currently available. Metabolome analysis refers to the analysis of the set metabolites present in a biological sample such as metabolic intermediates, hormones, vitamins or signaling molecules.

A metabolic profile platform has been carefully developed, including quenching of the cell metabolism, extraction of the intracellular metabolites, qualitative/quantitative analysis and data processing. The choice of an appropriate method to carry out any of the steps mentioned above is the key to obtaining reliable results. In fact, the metabolic quantification process has been thoroughly validated, including some commonly used steps such as lyophilization, since our results suggested that metabolites involved in the redox state ($NADPH/NADP^+$, $NADH/NAD^+$ and reduced/oxidized glutathione) and the AcetylCoA/CoA ratio were modified when lyophilization was included in the extraction process or when methanol/water is used as the extraction solvent. To avoid this, a highly efficient extraction protocol based on $ACN/CHCl_3$ was validated with standard mixtures.

Then, the metabolome analysis was applied to the study of metabolic alterations in biomedical fields such as in multidrug-resistant (MDR) leukaemia cells under daunomycin (DNM) exposure (Chapter 2) and in a non-alcoholic fatty liver disease (NAFLD) in rat-livers (Chapter 3). In addition, metabolome analysis was applied in the field of bacterial bioprocesses to study events such as the metabolic alterations that took place during an osmotic up-shock switch (Chapter 4) and the effect of the *cobB* gene deletion in acetate-feeding chemostats of *Escherichia coli* (Chapter 5).

Chapter 2 reports on the choice of the most suitable extraction method for coenzymes, redox metabolites and nucleotides, which was found to be a protocol based on acetonitrile/choloroform that avoids lyophilization. Also in this Chapter, it is shown how metabolic analysis contributed to the better understanding of the chemotherapy resistance mechanisms. For that purpose, 21 metabolites were determined by LC/UV before and after DNM exposure in different murine cell line cultures: L1210 (sensitive to DNM), L1210R (multidrug-resistance phenotype, MDR) and CBMC-6 (L1210 transfected with the

glycoprotein P, P-gp). P-gp is one of the known mechanisms of chemotherapy resistance since it is able to take out the drug outside the cell. The results showed that L1210R and CBMC-6 presented 5 and 2-fold, respectively, the concentrat on of GSH with respect to L1210, which suggest that this metabolite plays a protective role since it was correlated with the high survival percentage of these lines during DNM exposure. Additionally, the $NADH/NAD^+$, AcCoA/CoA, adenylate (AEC), uricilate (UEC) and guanylate (GEC) energy charge ratios were always higher in L1210R than in L1210. Interestingly, CBMC-6 cells presented an intermediate behaviour between the other two due to the presence of the P-gp.

In Chapter 3, the metabolome analysis of non-alcoholic fatty liver disease (NAFLD) in rat livers was carried out with more than 70 metabolites being identified and quantified by LC/MS. The metabolic pattern showed clear differences between healthy and NALFD-livers attending to the diet and as assessed by classical biomarkers. Interestingly, the metabolic alteration included not only redox molecules (GSH, GSSG, NAD(P)(H)), as expected, but also other metabolites such as L-carnitine, CoA and amino acids.

In Chapter 4, the long-term exposure of *E. coli* to osmotic stress has been studied from a metabolic point of view, where it was seen that intracellular metabolic levels were highly dependent on the NaCl concentration in the medium. The results obtained pointed to clear alterations in several metabolites, such as intracellular amino acids, nucleotides, redox coenzymes, acetyl phosphate and CoA derivatives. Moreover, the depletion of extracellular amino acids was measured when NaCl was added. These metabolic data were combined with the transcriptomic profile using integration pathway-based analysis, highlighting the main pathways affected, namely, GSH metabolism, glycolysis/gluconeogenesis, amino acid biosynthesis/degradation, purine metabolism, phosphorylative oxidation, and the TCA cycle/glyoxylate shunt. In addition, metabolic flux analysis pointed out a fermentation pattern that depended on the NaCl concentration.

In Chapter 5, metabolome analysis was carried out to shed light on the role of the only known deacetylase of *E.coli* (CobB) in acetate-feeding chemostats.

Moreover, transcriptomic analysis was performed and both data sets were integrated by using pathway-based analysis. The results showed no statistical differences in the central carbon metabolism. However, it was clear that the main effects were in both the sulfur and nitrogen pathways, including CoA, taurine, pyrimidines and several amino acid metabolisms, suggested that nitrogen metabolism is directly or indirectly regulated by protein acetylation. Pathway analysis using massive metabolomic and transcriptomic data was seen to be useful for integarating both data sets and for identifying pathways which are affected in a specific system.

To conclude, metabolome analysis can be used in conjuction with other techniques such as transcriptomics, fluxomics or classical experiments. The quantification of redox cofactors, nucleotides, coenzymes and amino acids is highly important for the understanding of the whole metabolic state in biological systems where key metabolites have been found such as GSH, ATP, AcCoA, CoA and some amino acids since at least one of them has resulted altered in any of the situations described along Chapters 2 to 5. Surprisingly, GSH, AcCoA, CoA and also NAD(P)H concentrations could be altered during the extraction process therefore the use of an appropriate extraction protocol has been proved to be essential.

CHAPTER 1

Introduction

METABOLOME

The term metabolome refers to the total set of low molecular weight molecules found in biological systems such as metabolic intermediates, hormones, vitamins or signaling molecules (Wegner et al., 2012). Changes in the metabolome are the ultimate answer of an organism to genetic alterations, disease, or environmental influences. Because of that metabolome analysis constitute a very useful tool for studying the metabolic state of biological systems (Clarke and Haselden, 2008). However, the metabolome presents more complexity than other 'omes' like transcriptome or proteome. Transcriptome consists of four different building blocks (nucleic acids) and proteome twenty (amino acids). By contrast, metabolome consists of thousands of small molecules (metabolites), for example: (i) the *Escherichia coli* metabolite database ECMDB contains more than 2,600 metabolites (Guo et al., 2013), (ii) the yeast metabolome database YMDB contains more than 2,000 entries for metabolites (Jewison et al., 2012) and (iii) the human metabolome database HMDB contains more than 40,000 metabolites in 2013 (Wishart et al., 2013). In Figure 1 an overview of the metabolome complexity is depicted.

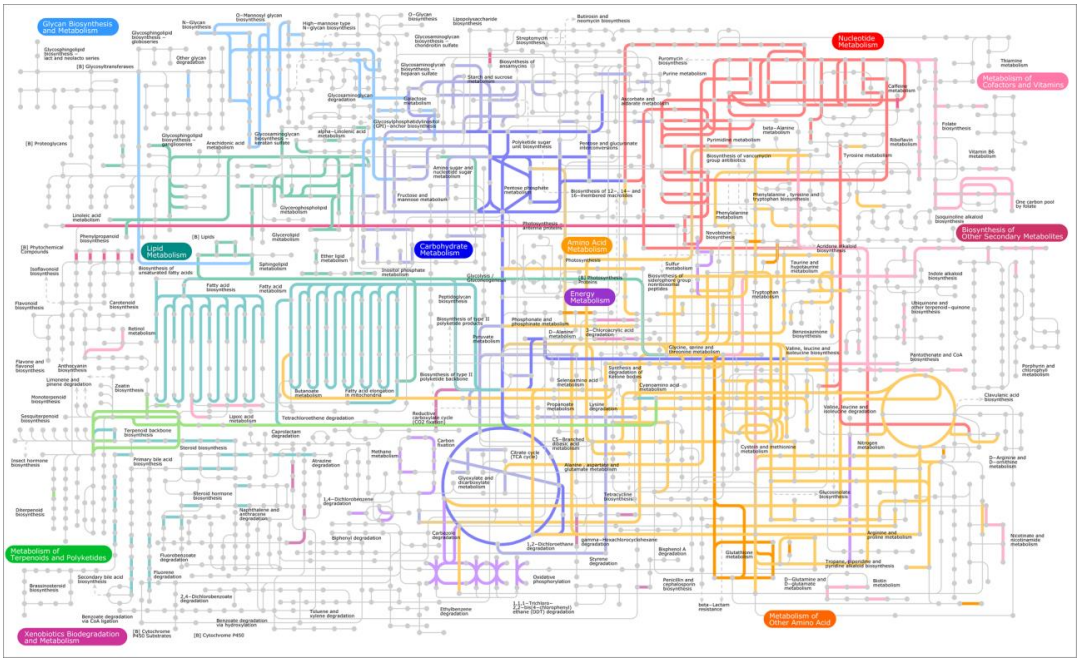

Figure 1. General overview of central metabolic pathways complexity. Picture taken from the KyotoEncyclopedia of Genes and Genomes (KEGG). http://www.kegg.jp.

METABOLOME ANALYSIS

Metabolome analysis refers to the analysis of metabolites in a biological organism and it could be classified into non-targeted and targeted analysis. The former gives extended information about all the metabolites detected (known and unknown) and the latter is able to provide absolute quantitative information (Hiller et al., 2011). Additionally, it is important to mention some concepts regarding these analyses, for example the term *Metabolomics* involves a comprehensive analysis of the whole metabolome present in a sample, but the term *Metabolic profiling* involves a specific group of metabolites that belong to the same class or are associated with a specific pathway. *Metabolic target analysis* refers to specific metabolites that would be directly affected by a perturbation, and *Metabolic fingerprinting* consists of the comparison of the metabolite patterns that change in response to a perturbation or disease (Ellis et al., 2007; Clarke and Haselden 2008).

Several key aspects are involved in metabolome analysis: sampling, metabolite detection and computational data analysis (Wegner et al., 2012). These aspects result in several steps: (i) quenching of the cell metabolism preventing the loss of its content (leakage), (ii) intracellular metabolites extraction, (iii) sensitive quantitative analysis and (iv) appropriate data processing (Schaub and Reuss 2008).

Quenching

The turnover of metabolites is in the range of seconds, therefore an effective quenching technique to immediately stop all the biochemical reactions that are taking place at the moment of sampling is required. This procedure has to be carefully validated to prevent the leakage of intracellular metabolites. The most common quenching methods use cold-methanol or cold-ethanol mixtures to abolish the tertiary structure of the enzymes (Wegner et al., 2012; Spura et al., 2009). In this work, 60% cold-methanol based methods are used for quenching (Sellick et al., 2009; Sellick et al., 2010; Sellick et al., 2011; Taymaz-Nikerel et al., 2009; Faijes et al., 2007). In the works of Sellick and collaborators the protocol described was validated for the recovery of most relevant metabolites from suspension-cultured mammalian cells. The cells were quenched in 60% methanol supplemented with 0.85% ammonium bicarbonate (AMBIC) at -40 °C. In the study

of Sellick et al. (2011) no substantial leakage in the case of small metabolites (TCA intermediates) was found when using this protocol. Based on these results, in the present work this solution was used to carry out the quenching of leukaemic murine cell lines studied (Chapter 2). Also, in the present work, metabolome analysis was applied to prokaryotic cells, specifically *Escherichia coli* strains. Previous studies such as those of Taymaz-Nikerel et al. (2009) and Faijes et al. (2007) have described quenching methods for bacteria based on 60% cold methanol. In the work of Faijes et al. (2007) the 60% (vol/vol) methanol/water supplemented with 0.85% ammonium bicarbonate solution at -40°C was selected as the most suitable quenching buffer for metabolomic studies in the bacteria *Lactobacillus plantarum,* since metabolite leakage was minimal compared to other solutions based on 60% (vol/vol) MeOH/water. Therefore, this quenching solution was also applied for bacterial strains (Chapter 4 and 5). During these experiments, no metabolite leakage was found in the quenching solution probably due to the fact that most of the measured metabolites have a high molecular weight since cell metabolite leakage has been shown to be size-dependent (Canelas et al., 2009) or due to the platform sensitivity. In any case, in the present work fold-change is used for bacterial metabolites determination due to the controversy regarding the above.

Intracellular metabolite extraction methods

Several extraction protocols have been widely applied in the literature. The exact sample preparation protocol used in any particular case will depend on the biological sample and also on the targeted metabolites (Faijes et al., 2007). In the work of Sellick et al. (2010) several metabolite extraction protocols were tested for chinese hamster ovary (CHO) cells: (i) methanol, (ii) methanol/water, (iii) hot ethanol, (iv) alkali (KOH), (v) acid (perchloric acid, PCA), (vi) two processes based on methanol/chloroform and (vii) methanol/chloroform adapted from Wu et al. (2008). The authors concluded that methanol/water extraction was the most suitable method to recover the greatest range of metabolites (210 signals), although, no single method provided the optimal conditions for extraction of all metabolites. Alkali (KOH) and acid (PCA) extractions resulted in fewer peaks, 152 and 59 respectively, although, in the latter the peak signal was increased. In that study, it was also found that hot ethanol was not suitable for the optimal recovery

of NAD^+ and NADH, the methanol extraction method being the most suitable. On the contrary, Dietmair et al. (2010) reported that the optimal extraction method for mammalian cells was cold extraction in 50% aqueous acetonitrile. Regarding bacterial strains, Faijes et al. (2007) reported that PCA extraction was the most suitable for their target metabolites. Besides these previous works, special attention was focused on the determination and quantification of some extremely labile compounds such as NADH, NADPH and CoA derivatives (Gao et al., 2007; Wu et al., 1986). Further, a recent work has highlighted that lyophilization could affect the levels of redox coenzymes such as glutathione and NAD^+ (Oikawa et al., 2011). Lazzarino et al. (2003) reported a reliable method for the study of parameters of redox and energy state, such as GSH, GSSG, NAD(P)(H) and CoASH among other metabolites extracted from rat livers, using ice-cold nitrogen-saturated CH_3CN + 10 mM KH_2PO_4 (3:1; v:v), pH 7.40 followed by several chloroform washing steps. With regards to the different extraction methods described above, Chapter 2 describes the careful validation of the most representative ones as well as the lyophilization step, applied to a known concentration defined standard mixture. In the present work the acetonitrile/chloroform extraction based on Lazzarino et al. (2003) was used in order to determine the intracellular metabolites since it was shown to be the most suitable extraction protocol for all the target metabolites (Chapter 2).

Analytical techniques

For specific metabolites quantification, analytical separation techniques are essential. Among these, chromatography is widely used to separate the specific metabolites. According to the IUPAC International Commission (1993), chromatography is a physical method of separation in which the components to be separated are distributed between two phases, one of which is stationary (stationary phase) while the other (the mobile phase) moves in a definite direction (Ettre 1993). This procedure is named after the mobile phase in each case: gas chromatography (GC), liquid chromatography (LC) or supercritical fluid chromatography (SFC) (Niessen 2006). In the case of GC the sample is normally introduced as a vapour onto the chromatographic column and the solubility of each component in the gas phase is dependent on its vapour pressure (Prichard et al.,

2003). Regarding LC, the mixture of compounds to be separated is introduced at the top of the column and washed through the column by the mobile phase. Depending on the magnitude of adsorption onto the surface of the solid stationary phase, one specific compound will travel down the column faster or slower compared to the other ones present in the mixture (Lindsay, 1992). With regard to SFC, principles are similar to those of LC, carbon dioxide being the most stable and excellent solvent compound normally used as mobile phase (Gopaliya et al., 2014). In the present work high performance liquid chromatography (HPLC) is used. In Figure 2 the main components involved in the process are depicted.

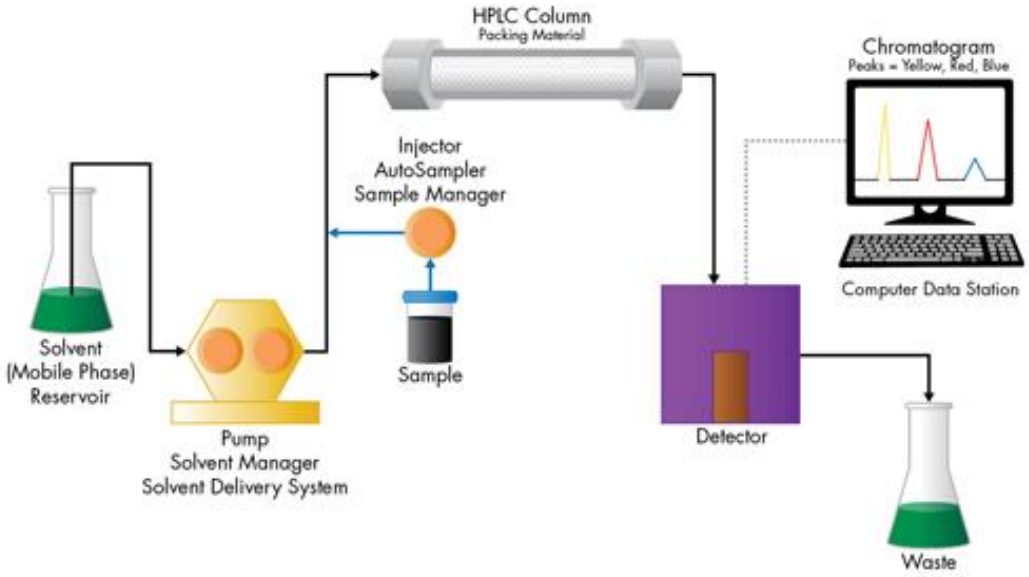

Figure 2. HPLC scheme showing how a chromatographic band is formed. The main components of the whole equipment are depicted (http://www.waters.com/waters/en_CA/Chromatographic-Bands,-Peaks-and-Band-Spreading/nav.htm?locale=en_CA&cid=134803614).

For most practical purposes, the two major analytical platforms for measuring metabolite levels are NMR (nuclear magnetic resonance) and MS (mass spectrometry). NMR relies on the magnetic properties of the atomic nucleus. Specific nuclei resonate at a characteristic frequency when a strong magnetic field is applied (Jacobsen, 2007). According to this resonance frequency, NMR yields specific positional information providing details about the molecular structure in which the atom is placed (Wegner et al., 2012). On the other hand, MS consists of ionizing the molecules generating charged molecule fragments. All these charged fragments are separated in the mass spectrometer according to their mass/charge (m/z) ratio. As a function of this ratio, the detected ions peaks are displayed as a

spectrum of their relative abundance. Most recent applications of MS have been oriented towards biochemical systems such as the study of the metabolome (Hoffmann and Stroobant, 2007). In our study LC-MS techniques are widely used to study different metabolic systems (Chapter 3-5), more specifically high performance liquid chromatography coupled to electrospray ionization mass spectrometry (HPLC-ESI-MS) since this has been widely used in previous works concerning biological applications. ESI is based on the use of electrical energy to transfer the ions from solution to gas phase before the mass spectrometric analysis takes place (Figure 3). Ionic and also neutral compounds can be studied by ESI-MS since these latter can be converted to an ionic form by protonation or cationisation (Ho et al., 2003). Besides MS, UV-diode array as well as refraction index (IR) methods coupled to HPLC are used in the present work (Chapter 2, 4 and 5).

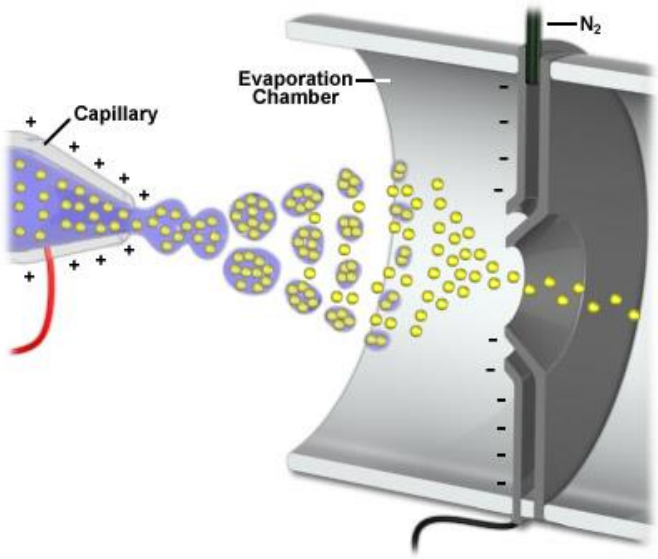

Figure 3. ESI-electrospray.The electrical energy transfer the ions from solution to gas phase before the mass spectrometric analysis takes place (https://nationalmaglab.org).

Data processing

By using LC-MS an important set of raw data is obtained since a wide range of different metabolites can be detected. Furthermore, the availability of a data processing method is essential. Sometimes LC-MS peak alignment is problematic since it is based on retention time which could present non-linear deviations during analysis (Pluskal et al., 2010). Moreover, the obtained results should be checked in order to verify the peak assignment. The asynchronous web application

EasyLCMS for the automated quantification of LC-MS data (Fructuoso et al., 2012) has been used for the data processing in the present work. This platform easily allows quantification of the targeted metabolites from raw LC-MS data. This web connects with popular databases to carry out the peak assignment with the result of clear chromatogram visualization.

SOME METABOLOME ANALYSIS EXAMPLES

The study of metabolite concentrations is a powerful tool that can be applied in different fields. As regards biomedicine, previous works have focused on several fields such as cancer (Beger 2013), cardiovascular diseases (Mayr, 2011), or food and nutrition (Wishart 2008) among others. Aranibar et al. (2011) reported that metabolomic analysis was applied to study the biochemical changes on the superfusion media in the model *in vitro* liver slices. It was reported that the addition of extra choline and histidine to the medium improves the long-term liver slice viability since these two components were depleted faster than the others. 94 h after incubation, the level of glutathione and ATP were higher in the tissues. Besides, in the same work, the quantification of several metabolites (amino acids, tricarboxylic acid cycle intermediates, activated sugars and cofactors among others) in CHO cell line cultures, indicated changes in energy utilization due to the bioreactor scale impact and the antiapoptotic agent addition. In the work of Liu et al. (2012), the measurement of specific metabolites (uric acid, hypoxanthine, xanthosine, guanosine, inosine and tryptophan) in human urine samples by high performance liquid chromatography-diode array detection (HPLC-DAD) and the use of statistical analysis permitted the discrimination to gout patients from the controls as well as the acute from the chronic gout .

With regard to bioprocesses, metabolite quantification allow the formulation of a chemically defined medium supplement (Sonntag et al., 2011) and improves knowledge of microbial cultivation technology by means of metabolic engineering (Oldiges et al., 2014), among other applications. A knowledge of intracellular metabolite concentrations could lead to the identification of potential metabolic bottlenecks and the quantitative understanding of intracellular reaction rates and the control of metabolic fluxes which enable design strategies in metabolic engineering (Schaub and Reuss 2008). These latter quantified intracellular

glycolytic intermediates in *E.coli* chemostats at different dilution rates in response to a glucose pulse. They concluded that the intracellular metabolite concentrations changed significantly at different dilution rates, providing information on the metabolic phenotype in specific conditions. Taymaz-Nikerel et al. (2013) reported on the flexibility of the metabolic network in *E. coli* after three different substrate pulses (glucose, pyruvate and succinate) in a glucose-limited steady state chemostat. Intracellular metabolic concentrations and metabolic flux analysis (MFA) identified the immediate onset of gluconeogenesis after pyruvate and succinate pulses, showing a higher flux in phosphoenolpyruvate carboxykinase PPCK which catalyzes the conversion of oxaloacetate to phosphoenolpyruvate, which in the end will generate pyruvate to feed the TCA cycle. However, the adenylate energy charge remained constant after these three pulses, showing the robustness and flexibility of the energy system in *E.coli.*

THESIS OUTLINE

The aim of this Thesis was to design a metabolic profile platform able to identify and quantify unequivocally as many metabolites as possible present in different kind of biological samples such as eukaryotic cells (Chapter 2), tissues (Chapter 3) and prokaryotic cells (Chapter 4 a 5).

In Chapter 2, the validation of the neutral extraction protocol based on ACN/$CHCl_3$ used in this Thesis is described. This method presents several advantages compared to others since specific labile standard metabolites such as AcCoA, GSH, NADH or NADPH are efficiently recovered after its application. After its validation, the method was applied to quantify different metabolites (nucleotides, coenzymes and redox state metabolites) in one murine leukaemia cell line L1210 (sensitive to daunomycin, DNM) and two derived sublines L1210R (multi-drug resistance, MDR phenotype) and CBMC-6 (glycoprotein P, P-gp expressed L1210). The results showed specific metabolic differences among these cell types before and after DNM exposure. In this chapter the analysis method used was based on HPLC-UV, which was able to identify and quantify 20 metabolites.

In Chapter 3, the main hepatic metabolic alterations in non-alcoholic fatty liver disease (NALFD) rat livers were studied. More than 70 metabolites were quantified and a statistical analysis was applied showing a completely different metabolic pattern able to discriminate between healthy and fatty rat liver. In this chapter the analysis method used was based on HPLC-MS, which was able to identify and quantify 80 metabolites.

Chapter 4 describes the main metabolic features, the integrative pathway analysis as well as the metabolic flux distribution for *E.coli* under 0.5M and 0.8M NaCl concentrations in the medium**.** A common NaCl concentration-dependent pattern was found, which was based on increasing the ATP generation processes, such as C-source consumption (glycerol) and decreasing the ATP consumption processes. In this chapter the same analytical method of Chapter 3 was used but applied to bacterial cultures instead of tissues.

In Chapter 5, the metabolic alterations due to the *cobB* gene deletion in *E.coli* were studied. Acetate-feeding chemostat cultures were used for *E.coli* WT and its derived Δ*cobB*. Statistically significant metabolic differences were found and their correspondence with transcriptomic analysis was reported since integrative pathway analysis was performed. In this chapter, the analytical method used was based on the HPLC-MS method described in Chapter 3 and 4.

REFERENCES

Aranibar, N., Borys, M., Mackin, N. A., Ly, V., Abu-Absi, N., Abu-Absi, S., Niemitz, M., Schilling, B., Li, Z. J., Brock, B., Russell, R. J., II, Tymiak, A., Reily, M. D. (2011). NMR-based metabolomics of mammalian cell and tissue cultures. *J. Biomol. Nmr*, **49**, 195-206.

Beger, R. D. (2013). A review of applications of metabolomics in cancer. *Metabolites*, **3**, 552-574.

Canelas, A. B., ten Pierick, A., Ras, C., Seifar, R. M., van Dam, J. C., van Gulik, W. M., Heijnen, J. J. (2009). Quantitative Evaluation of Intracellular Metabolite Extraction Techniques for Yeast Metabolomics. *Anal. Chem*., **81**, 7379-7389.

Clarke, C. J., Haselden, J. N. (2008). Metabolic Profiling as a Tool for Understanding Mechanisms of *Toxicity. Toxicol. Pathol*., **36**, 140-147.

Dietmair, S., Timmins, N. E., Gray, P. P., Nielsen, L. K., Kroemer, J. O. (2010). Towards quantitative metabolomics of mammalian cells: Development of a metabolite extraction protocol. *Anal. Biochem*., **404,** 155-164.

Ellis, D. I., Dunn, W. B., Griffin, J. L., Allwood, J. W., Goodacre, R. (2007). Metabolic fingerprinting as a diagnostic tool. *Pharmacogenomics*, **8**, 1243-1266.

Ettre, L. S. (1993). Nomenclature for chromatography. *Pure Appl. Chem.,* **65**, 819-872.

Faijes, M., Mars, A. E., Smid, E. J. (2007). Comparison of quenching and extraction methodologies for metabolome analysis of Lactobacillus plantarum. *Microb. Cell Fact*., **6**, 27. doi:10.1186/1475-2859-6-27.

Fructuoso, S., Sevilla, A., Bernal, C., Lozano, A. B., Iborra, J. L., Canovas, M. (2012). EasyLCMS: an asynchronous web application for the automated quantification of LC-MS data. *BMC res. notes*, **5**, 428-428.

Gao, L., Chiou, W., Tang, H., Cheng, X. H., Camp, H. S., Burns, D. J. (2007). Simultaneous quantification of malonyl-CoA and several other short-chain acyl-CoAs in animal tissues by ion-pairing reversed-phase HPLC/MS. *J. Chromatogr. B-Anal. Technol. Biomed. Life Sci*., **853**, 303-313.

Gopaliya, P., Kamble, P. R., Kamble, R., Chauhan, C. S. (2014). A review Article on Supercritical Fluid Chromatography. *Int. J. Pharma Res. Rev*., **3**, 7.

Guo, A. C., Jewison, T., Wilson, M., Liu, Y., Knox, C., Djoumbou, Y., Lo, P., Mandal, R., Krishnamurthy, R., Wishart, D. S. (2013). ECMDB: The E-coli Metabolome Database. *Nucleic Acids Res*., **41**, D625-D630.

Hiller, K., Metallo, C., Stephanopoulos, G. (2011). Elucidation of Cellular Metabolism Via Metabolomics and Stable-Isotope Assisted Metabolomics. *Curr. Pharm. Biotechnol*., **12**, 1075-1086.

Ho, C. S., Lam, C. W. K., Chan, M. H. M., Cheung, R. C. K., Law, L. K., Lit, L. C. W., Ng, K. F., Suen, M. W. M., Tai, H. L. (2003). Electrospray ionisation mass spectrometry: principles and clinical applications. The Clinical biochemist. Reviews /Australian Association of Clinical Biochemists, 24, 3-12.

Hoffmann, E. d., Stroobant, V. (2007). Mass Spectrometry. Principles and Applications. 3rd edition. John Wiley & Sons, England.

Jacobsen, N. E. (2007). NMR Spectroscopy Explained. Simplified Theory, Applications and Examples for Organic Chemistry and Structural Biology. John Wiley & Sons, Inc., New Yersey, U.S and Canada.

Jewison, T., Knox, C., Neveu, V., Djoumbou, Y., Guo, A. C., Lee, J., Liu, P., Mandal, R., Krishnamurthy, R., Sinelnikov, I., Wilson, M., Wishart, D. S. (2012). YMDB: the Yeast Metabolome Database. *Nucleic Acids Res*., **40**, D815-D820.

Lazzarino, G., Amorini, A. M., Fazzina, G., Vagnozzi, R., Signoretti, S., Donzelli, S., Di Stasio, E., Giardina, B., Tavazzi, B. (2003). Single-sample preparation for simultaneous cellular redox and energy state determination. *Anal. Biochem*., **322**, 51-59.

Lindsay, S. (1992). High Performance Liquid Chromatography 2nd edition. John Wiley & Sons Ltd., London, UK.

Liu, Y., Yu, P., Sun, X., Di, D. (2012). Metabolite target analysis of human urine combined with pattern recognition techniques for the study of symptomatic gout. *Mol. Biosyst*., **8**, 2956-2963.

Mayr, M. (2011). Recent highlights of metabolomics in cardiovascular research. Circulation. *Cardiovasc. genetics*, **4**, 463-464.

Niessen, W. M. A. (2006). Liquid Chromatography-Mass Spectrometry. United States.

Oikawa, A., Otsuka, T., Jikumaru, Y., Yamaguchi, S., Matsuda, F., Nakabayashi, R., Takashina, T., Isuzugawa, K., Saito, K., Shiratake, K. (2011). Effects of freeze-drying of samples on metabolite levels in metabolome analyses. *J. Sep. Sci*., **34**, 3561-3567.

Oldiges, M., Eikmanns, B. J., Blombach, B. (2014). Application of metabolic engineering for the biotechnological production of L-valine. *Appl. Microbiol. Biotechnol.*, **98**, 5859-5870.

Pluskal, T., Castillo, S., Villar-Briones, A., Oresic, M. (2010). MZmine 2: Modular framework for processing, visualizing, and analyzing mass spectrometry-based molecular profile data. *Bmc Bioinformatics*, **11**.

Prichard, E., Ho, W. F., Stuart, B. (2003). High Performance Liquid Chromatography. LGC, Teddington, UK.

Schaub, J., Reuss, M. (2008). In Vivo Dynamics of Glycolysis in Escherichia coli Shows Need for Growth-Rate Dependent Metabolome Analysis. *Biotechnol. Progr*., **24**, 1402-1407.

Sellick, C. A., Hansen, R., Maqsood, A. R., Dunn, W. B., Stephens, G. M., Goodacre, R., Dickson, A. J. (2009). Effective Quenching Processes for Physiologically Valid Metabolite Profiling of Suspension Cultured Mammalian *Cells. Anal. Chem*., **81**, 174-183.

Sellick, C. A., Knight, D., Croxford, A. S., Maqsood, A. R., Stephens, G. M., Goodacre, R., Dickson, A. J. (2010). Evaluation of extraction processes for intracellular metabolite profiling of mammalian cells: matching extraction approaches to cell type and metabolite targets. *Metabolomics*, **6**, 427-438.

Sellick, C. A., Hansen, R., Stephens, G. M., Goodacre, R., Dickson, A. J. (2011). Metabolite extraction from suspension-cultured mammalian cells for global metabolite profiling. *Nat. Protoc*., **6**, 1241-1249.

Sonntag, D., Scandurra, F. M., Friedrich, T., Urban, M., Weinberger, K. M. (2011). Targeted metabolomics for bioprocessing., in: 22nd European Society for Animal Cell Technology (ESACT) Meeting on Cell Based Technologies., p. 27. BMC Proceedings, Innsbruck, Austria.

Spura, J., Reimer, L. C., Wieloch, P., Schreiber, K., Buchinger, S., Schomburg, D. (2009). A method for enzyme quenching in microbial metabolome analysis successfully applied to gram-positive and gram-negative bacteria and yeast. Anal.l *Biochem.*, **394,** 192-201.

Taymaz-Nikerel, H., de Mey, M., Ras, C., ten Pierick, A., Seifar, R. M., Van Dam, J. C., Heijnen, J. J., Van Glilik, W. M. (2009). Development and application of a differential method for reliable metabolome analysis in *Escherichia coli*. *Anal. Biochem.*, **386**, 9-19.

Taymaz-Nikerel, H., De Mey, M., Baart, G., Maertens, J., Heijnen, J. J., van Gulik, W. (2013). Changes in substrate availability in *Escherichia coli* lead to rapid metabolite, flux and growth rate responses. *Metab. Eng*., **16**, 115-129.

Wegner, A., Cordes, T., Michelucci, A., Hiller, K. (2012). The Application of Stable Isotope Assisted Metabolomics in Biomedicine. *Curr. Biotechnol*., **1**, 88-97.

Wishart, D. S. (2008). Metabolomics: applications to food science and nutrition research. *Trends Food Sci. Technol.*, **19**, 482-493.

Wishart, D. S., Jewison, T., Guo, A. C., Wilson, M., Knox, C., Liu, Y., Djoumbou, Y., Mandal, R., Aziat, F., Dong, E., Bouatra, S., Sinelnikov, I., Arndt, D., Xia, J., Liu, P., Yallou, F., Bjorndahl, T., Perez-Pineiro, R., Eisner, R., Allen, F., Neveu, V., Greiner, R., Scalbert, A. (2013). HMDB 3.0-The Human Metabolome Database in 2013. *Nucleic Acids Res*., **41,** D801-D807.

Wu, J. T., Wu, L. H., Knight, J. A. (1986). Stability of NADPH - effect of various factors on the kinetics of degradation. *Clin. Chem*., **32,** 314-319.

Wu, H., Southam, A.D., Hines, A., Viant, M.R. (2008). High-throughput tissue extraction protocol for NMR- and MS-based metabolomics. *Anal. Biochem*., **372** (2), 204-212.

CHAPTER 2

Metabolic analysis in Biomedicine:

Unbiased extraction method to study the metabolic characterization of leukemia cells exposed to daunomycin

The extraction protocol used in this chapter has been applied in the publication:

Monteiro, F., Bernal, V., Saelens, X., Lozano, A. B., Bernal, C., Sevilla, A., Carrondo, M. J. T. and Alves, P. M. (2014). Metabolic profiling of insect cell lines: Unveiling cell line determinants behind system's productivity. *Biotechnol. Bioeng*. **111**, 816-828.

The content of this chapter has generated the following manuscript:

Bernal, C., Sevilla, A., Cerezo, D., Martín-Orozco, E., Iborra, J.L and Cánovas, M. Unbiased extraction method to study the metabolic characterization of leukemia cells exposed to daunomycin *(Metabolites*, submitted).

ABSTRACT

Metabolic analysis has been used to describe the metabolic behaviour of chemotherapy sensitive cell lines in contrast to those that present a multidrug-resistance phenotype (MDR). However, the metabolic quantification protocol needed be thoroughly optimized and validated, including some commonly used steps such as lyophilisation, since our results suggested that the redox state (measured by NADPH/$NADP^+$, NADH/NAD^+ and reduced/oxidized glutathione ratios) and the AcetylCoA/CoA ratio were modified when lyophilization was included in the extraction protocol or when methanol/water was used as the extraction solvent. To avoid this, a highly efficient extraction protocol based on ACN/$CHCl_3$ was validated with defined standard mixtures. Afterwards, it was applied for the determination of 21 metabolites before and after daunomycin (DNM) exposure in different murine cell line cultures: L1210 (sensitive to DNM), L1210R (MDR) and CBMC-6 (L1210 that express glycoprotein-P, pg-P). L1210R cells presented 5-fold and CBMC-6 2-fold of GSH with respect to L1210, which suggested that GSH content strongly influenced cell survival to DNM since a high percent of these derived sublines survived during DNM exposure in contrast to the sensitive one that only survived in 12%. Besides, NADH/NAD^+ ratio, AcCoA/CoA ratio, and the adenylate (AEC), uridilate (UEC) and guanylate (GEC) energy charge levels resulted always higher in L1210R than in L1210, while CBMC-6 cells presented an intermediate behaviour between these two in almost all the cases. In base of these results, metabolic analysis could help to understand chemotherapy resistance mechanisms.

INTRODUCTION

The use of antineoplastic drugs for cancer treatment is frequently associated with the acquisition of multidrug-resistant (MDR) phenotype that renders tumoural cells insensitive to antineoplastics (Gottesman and Pastan, 1993). One of the best-characterized resistance mechanisms is the expression of P-glycoprotein (P-gp, MDR-1, Abcb1a), a plasma membrane ATPase which is a member of the ABC transporter family. This glycoprotein, which is encoded by the MDR-1 gene, is responsible for drug efflux (Fazlina et al., 2008) and represents a real obstacle in the effective chemotherapeutic treatment of leukaemia (Gibalova et al., 2009). In Figure 1, this mechanism is depicted.

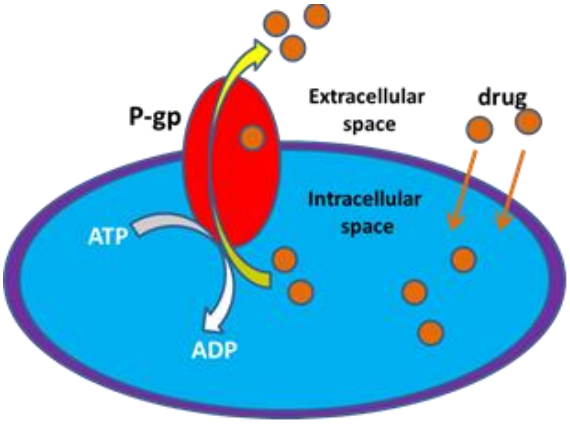

Figure 1. Schematic representation of P-glycoprotein (P-gp), a transmembrane protein able to eject the drugs from the cells.

Anticancer anthracycline antibiotic daunomycin (DNM) has been used for nearly 40 years, primarily for the treatment of leukaemia (cancer of blood forming cells). DNM consists of a tetracyclic aglycon chromophore, whose B, C, and D rings constitute an aromatic moiety, and an amino-sugar group, which is positively charged under physiological conditions. In Figure 2 the structure of DNM is depicted.

The proposed action mechanism of this antibiotic seems to involve DNA as the primary target, with the result of inhibiting DNA replication and RNA transcription. For this reason, extensive research has been reported about the intercalation of DNM in DNA (Figure 3), its involvement in free-radical generation (ROS) and its interaction with topoisomerases and other proteins (Barone et al., 2008).

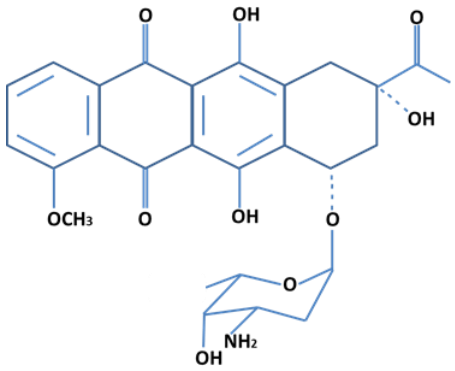

Figure 2. Chemical structure of daunomycin.

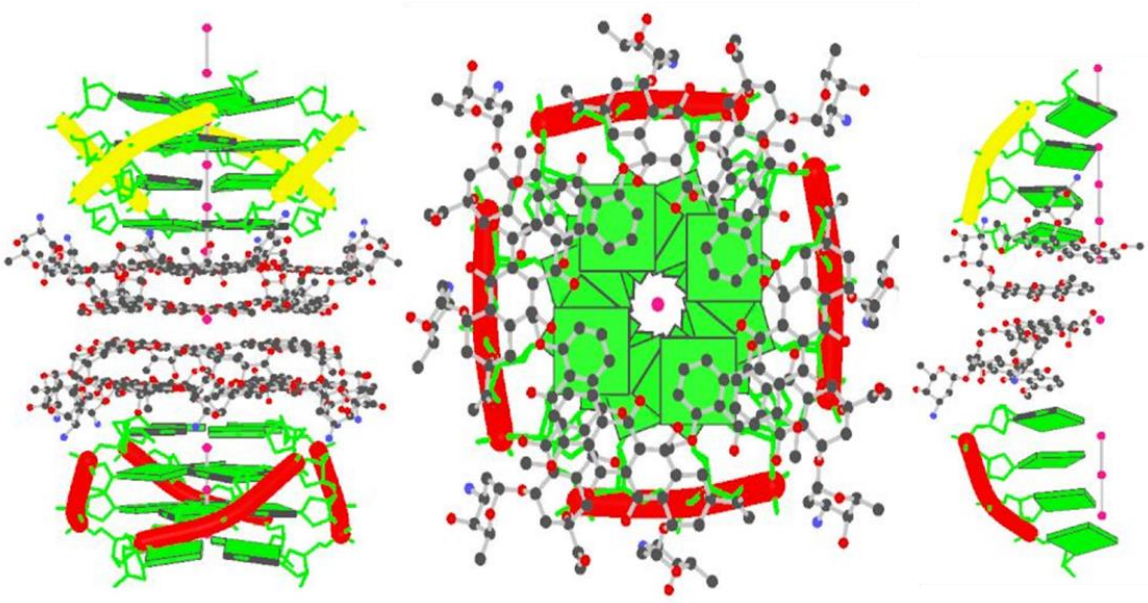

Figure 3. Different points of view of the highly symmetric DNA quadruplex/daunomycin complex. In this picture is depicted the intercalation of daunomycin in the DNA grooves. (http://www.rcsb.org/pdb/explore/images.do?structureId=3TVB).

In previous works (Martín-Orozco et al., 2005, Cerezo et al., 2012) the parental leukaemic murine cell line L1210 and the derived subline L1210R (MDR phenotype) have been studied in order to withdraw more information about the protein expression patterns under specific stimuli. In the latter, also another derived subline CBMC-6 (parental line with P-gp expression) was used. The present work uses metabolic analysis to unveil whether metabolic alterations take place in these cell lines during culture and daunomycin exposure. It was reported that P-gp expression and the metabolic switch of tumour cells from oxidative phosphorylation towards glycolysis are closely related (Wartenberg et al., 2010). Further, it has been hypothesized that the relationship between therapeutic

resistance and glycolysis may, at least partially, be due to the radical scavenging potential of glycolytic intermediates, mainly pyruvate, and to the link between these metabolites and the cellular redox state (Sattler et al., 2007). Kuznetsov et al. (2011) described that drug treatment may cause adaptive responses through the mitochondria and various cellular antioxidant defence systems, potentially contributing to the development of multidrug resistance. In fact, cancer researchers have amassed substantial information about the metabolic alterations that take place in cancer cells and the differences between sensitive and drug-resistant cells. For example, in the work of Harper et al. (2002), four cell lines were studied: L1210, HL60 (sensitive), L1210/DDP (resistant to methotrexate and cisplatin) and HL60.MDR (multidrug-resistant). In that work, it was demonstrated the higher glycolysis in drug-resistant cells to obtain ATP. Additionally, it was reported that total ATP content was higher whereas oxygen consumption and ATP production per mitochondrium were lower in drug-resistant than in drug-sensitive cells.

However, there is little information available about certain metabolites such as NADH, NADPH and CoA derivatives due to the complexity involved in their quantification since they are extremely labile (Gao et al., 2007; Wu et al., 1986). Moreover, a recent work has highlighted that lyophilization could alter the levels of some metabolites, including redox coenzymes such as glutathione and NAD^+ (Oikawa et al., 2011), hence, extraction effects should be tested in these metabolites to avoid biased results. Furthermore, the development of a combined quenching/extraction method which does not alter the redox state *per se,* was thought to be essential.

The aim of this work was to design a specific extraction protocol to determine the intracellular level of metabolites in murine leukaemia cells testing different procedures described previously in the literature. The election of these protocols was based on previous studies that reported the higher number of metabolites were determined (Dietmair et al., 2010; Sellick et al., 2010 and Lazzarino et al., 2003). The specific protocol based on ACN/CHCl3 was applied to the study of the metabolic effects in both sensitive and resistant cells during culture and under daunomycin exposure. In Figure 4, a scheme of the different metabolic pathways

concerned is depicted, with red circles indicating the metabolites that have been studied.

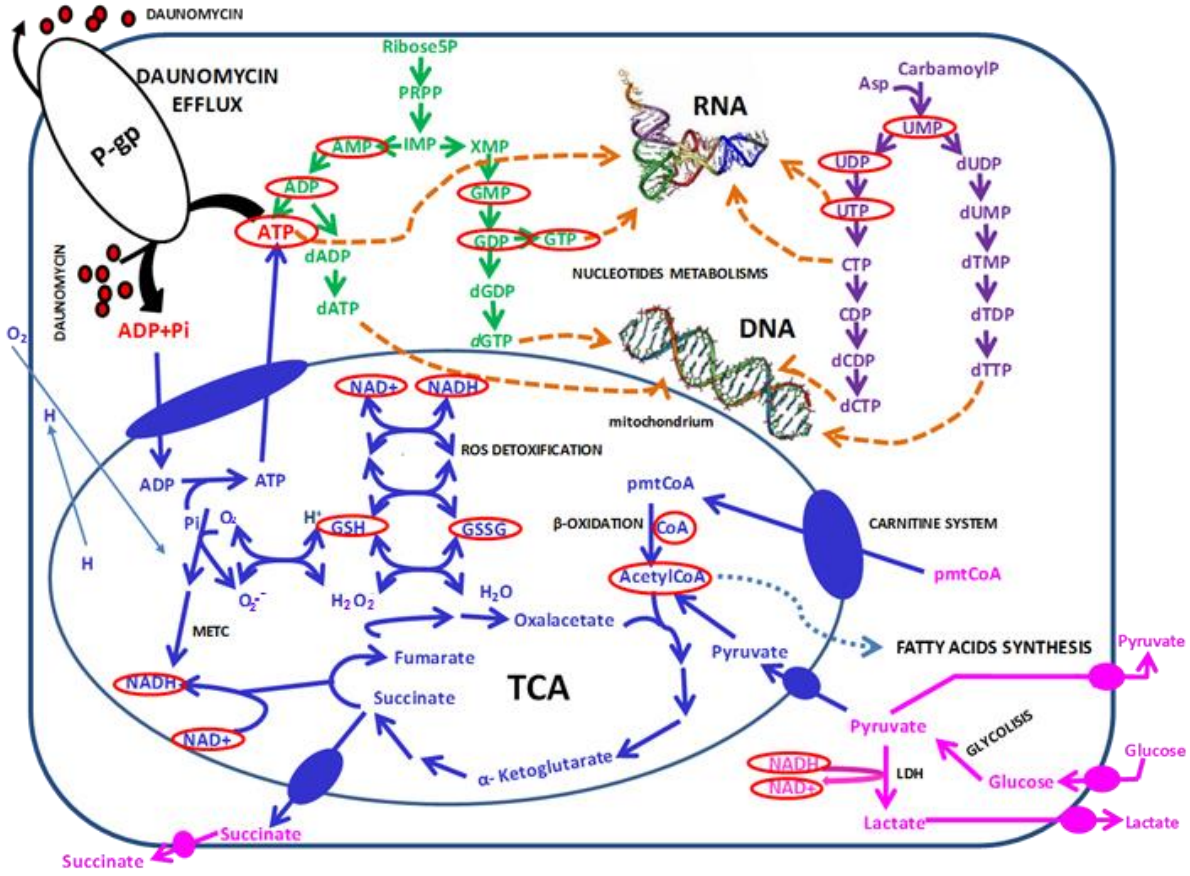

Figure 4. Most relevant metabolic pathways in drug-resistance including ATPase P-glycoprotein (P-gp). metabolites quantified in this work are shown In red circles

MATERIALS AND METHODS

Reagents

Standard metabolites were supplied by Sigma Aldrich (St Louis MO, USA). The chemicals used as eluents (acetonitrile, acetic acid, ammonium acetate, ammonium hydroxide and water) were obtained from Panreac (Barcelona, Spain). All chemicals were of at least HPLC grade quality.

Test of extraction protocols using a mixture of standards

To check concentration recoveries after different extraction protocols, a mixture of standards containing reduced glutathione (GSH), oxidized glutathione (GSSG), ATP, ADP, AMP, cAMP, GTP, GDP, GMP, cGMP, UTP UDP, UMP, CTP, CDP, AcetylCoA, CoA, NADPH, $NADP^+$, NADH and NAD^+ was prepared. The concentration of each standard in the mixture was 50 µM. This fresh mixture, that was not frozen nor lyophilized, was subjected to four protocols, three of them were extraction protocols based on the literature, whereas the fourth one consisted of lyophilizating the mixture described above to check the effect of this process. To quantify the recovery, a calibration curve was built with the same standard defined mixture from 5 µM to 100 µM.

Protocols:

(1) Methanol/water extraction (meoh) based on Sellick et al. (2010)

Briefly, 500 µL of the standard mixture were resuspended in pure methanol and flushed with liquid nitrogen. After centrifugation, the supernatant was collected and the previous step was repeated. The pellet was extracted with cold un-buffered water, and then flushed with liquid nitrogen. Finally, the supernatants were pooled, centrifuged and lyophilized.

(2) Acetonitrile/water (acn) extraction based on Dietmair et al. (2010)

Briefly, 500 µL of the standard mixture were extracted with 50% acetonitrile/water, and then the extracts were lyophilized.

(3) Acetonitrile/chloroform extraction (acn + chloro) based on Lazzarino et al. (2003)

500 µL of the standard mixture was resuspended in 2 mL of extraction solution (acetonitrile + 10mM KH_2PO_4 (3:1 v/v) at pH 7.4) before incubating in a wheel for 30 minutes at 4°C. The homogenate was centrifuged at 15,000 xg for 20 min at 4°C and then was added to 4 mL of ice-cold chloroform before centrifuging again at 15,000 xg for 5 min. This gave a biphasic system, from which the aqueous phase was harvested. This process was repeated twice more. It must be remarked that this method does not involve lyophilizing or freezing during or after extraction

and the samples are prepared when the analysis platform is ready to avoid potential metabolic degradation.

(4) Lyophilization (lyo)

Additionally, standard mixtures were lyophilized and resuspended in water to check lyophilization effect on the above mentioned metabolites.

All the procedures finished with a filtering step through a sterile 0.2 µm filter before the analyses were carried out.

Cell lines cultures

One cancer cell line (L1210) and two derived sublines (L1210R and CBMC-6) were kindly donated by Dr. Ferragut and Dr. Saceda of the Miguel Hernández University, Elche, Alicante (Spain). The parental murine L1210 cell line, a leukaemic cell line of DBA/2 origin, was used as tumour model. L1210R cells are 160-fold resistant to daunomycin (DNM-resistant). CBMC-6 (stands for Centro de Biología Molecular y Celular, University Miguel Hernández) cells were obtained by transfecting L1210 cells with the plasmid pcDNA 3-mpgp that contains the mouse *mdr1a* P-gp cDNA under control of the CMV promoter. All cell lines were maintained in RPMI 1640 Glutamax™ I medium, which contained the dipeptide, L-alanyl-L-glutamine substituted on a molar equivalent basis for L-glutamine, supplemented with 10% FBS and 1% penicillin-streptomycin mix (10,000 U/mL penicillin, 10,000 µg/mL streptomycin). All these products were supplied by GIBCO®, Invitrogen, USA. All cells were grown at 37°C in a 5% CO_2 atmosphere in flask reactors.

Sampling protocol

Samples before DNM incubation (controls) were during exponential growth phase ((3-7)·10^5cells/mL). Before sampling, cells were passed into fresh medium. Harvested samples were subjected to quenching, which was performed as described by Sellick et al. (2010). In short, 2·10^7 cells were harvested and added into the quenching solution, 60% (vol/vol) methanol/water supplemented with

0.85% ammonium bicarbonate (AMBIC), kept at -40°C. Afterwards, cells were pelleted by centrifugation at 1,000 x g for 1 min at -12°C. The supernatant was removed by aspiration and kept for subsequent analysis to check for potential leakage (Dietmair et al., 2010). The extraction protocol chosen for samples was acn+chloro, as previously explained.

Daunomycin incubation experiment

For daunomycin-induced apoptosis, cells were incubated in the presence of 0.15 µM daunomycin for 60 minutes and samples were withdrawn at different sampling times in order to determine cell viability by evaluating whether necrosis or apoptosis was occurring. This experiment was carried out by the Immunology group of the University of Murcia as reported in the Appendix. Harvested samples were subjected to quenching and extraction as described above.

Antibodies and Western-blot experiments

The antibodies used and western-blot experiments are described in Appendix.

Quantification of intracellular metabolites

The analytical method (acn+chloro) carried out was based on Lazzarino et al. (2003) as follows: The HPLC apparatus consisted of a SHIMADZU 20A HPLC station equipped with a high sensitive SPD-M20A diode array and multiple wavelength detectors. The cell length was 10 mm, and measurements were made between 190 and 950 nm. Data were acquired and analysed by a PC using the SHIMADZU LC Solution software package provided by the HPLC manufacturer. Separation was carried out with 120 µl of sample or 50 µl of standard solutions using a Supelco LC-18-T 158x4.6 mm, 3 µm particle-size column, provided with its own guard column. The step gradient from buffer A (10 mM tetrabutylammonium hydroxide, 10 mM KH_2PO_4, 0.125% methanol, pH 7.00) to buffer B (2.8 mM tetrabutylammonium hydroxide, 100 mM KH_2PO_4, 30% methanol, pH 5.50) was as follows: 10 min 100% buffer A, 3 min to reach 80% buffer A, 10 min to reach 70% buffer A, 12 min to reach 55% buffer A, 11 min to reach 40% buffer A, 9 min

to reach 35% buffer A, 10 min to reach 25% buffer A, 15 min 0% buffer A, and 80 min 0% buffer A; The flow rate was 1.0 ml/min. For each cell sample, the adenylate energy charge value (AEC), uracilate energy charge value (UEC) as well as guanylate energy charge value (GEC) were calculated as in Atkinson and Walton (1967):

$$AEC = \frac{ATP + 0.5 \cdot ADP}{ATP + ADP + AMP}$$

$$UEC = \frac{UTP + 0.5 \cdot UDP}{UTP + UDP + UMP}$$

$$GEC = \frac{GTP + 0.5 \cdot GDP}{GTP + GDP + GMP}$$

Statistical analyses

To validate the extraction protocol, the experimental values were calculated as mean ± standard error of the mean (s.e.m.) of 5 samples. The statistical analysis was performed by one-way ANOVA and p-values were adjusted using FDR (Benjamini and Hochberg, 1995). For the daunomycin incubation experiments, the experimental values were represented as mean ± s.e.m. of 3 independent experiments. The statistical analysis was performed by one-way ANOVA followed by Tukey's HSD post hoc tests and p-values were adjusted using FDR (Benjamini and Hochberg, 1995) for all pairwise combinations. All these statistical analyses were carried out using the web-application metaboanalyst (Xia et al., 2009) and statistical significance was accepted as $p<0.05$.

RESULTS AND DISCUSSION

Validation of the extraction protocol

Since some metabolites have been difficult to quantify due to their instability under several conditions (Gao et al., 2007; Wu et al., 1986; Oikawa et al., 2011) the lyophilization step as well as different extraction protocols were tested in order to optimize the protocol.

A mixture of 21 metabolite 50 µM each were subjected to 3 extraction protocols, namely acn+chloro, meoh and acn, as described in materials and methods section. Additionally, standard mixtures were lyophilized and resuspended in water to check the potential consequences of lyophilization (lyo).

The results showed some important facts related with these extraction protocols (Figure 5). Firstly, out of 21 metabolites, 4 showed significant differences with an ANOVA p-value <0.001 (NADH, NADPH, AcCoA and GSSG), whereas the remaining recoveries were close to 100%. This fact indicates that extraction methods used did not generally alter metabolite levels as they were previously optimised (Dietmair et al., 2010; Sellick et al., 2010).

The results suggest that lyophilization does indeed alter the composition of metabolic mixtures, mainly in the case of GSSG, CoA and AcCoA where the recoveries were significantly lower (60%, 65% and 50%, respectively). Also with the use of the protocols that implied lyophilization (meoh and acn), the recoveries of these metabolites were close to the ones mentioned. Alterations in the glutathione ox/red ratio due to freeze-drying has been previously described using plant extracts (Oikawa et al., 2011) and also when solvent evaporation is involved (Villas-Boas et al., 2005). The present study demonstrates, in addition, the inefficient recovery of AcetyCoA and CoA as a result of lyophilization. These results are of enormous importance since lyophilization and also solvent evaporation, which have been widely used in literature, may not be suitable for measuring the redox and AcCoA/CoA ratios.

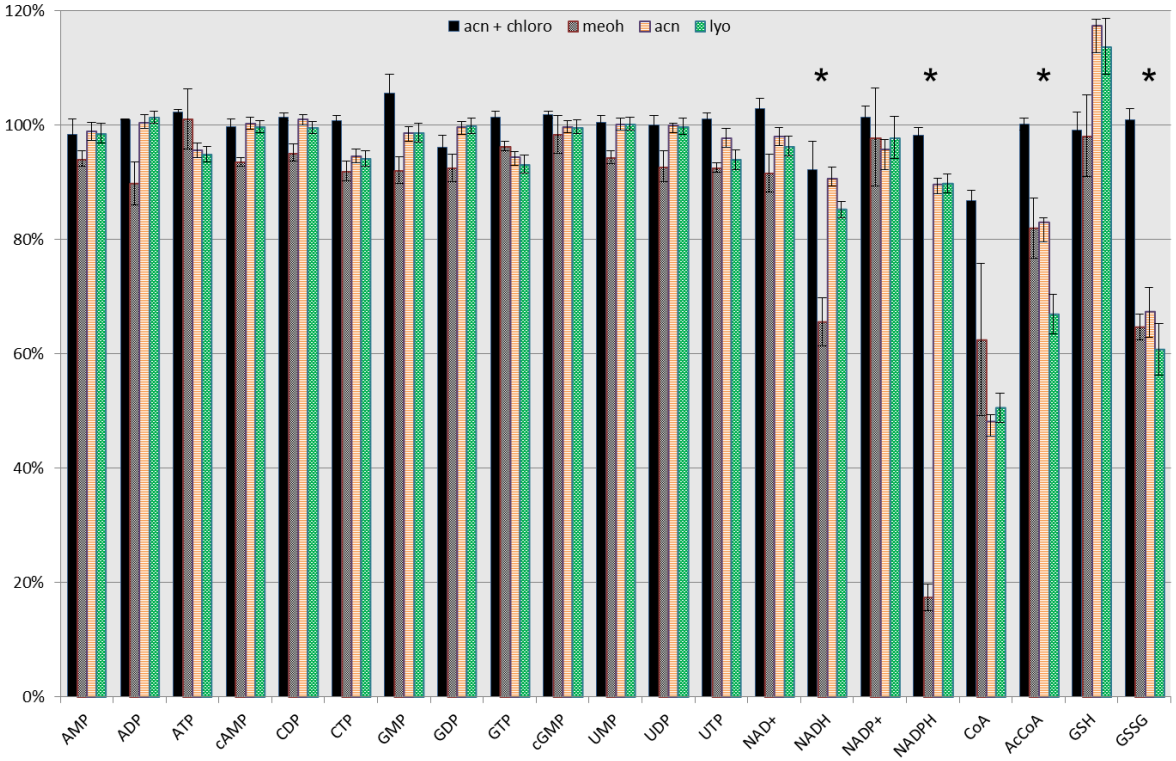

Figure 5. The recovery (%) of each metabolite after the different protocols used. In black it is shown the results obtained with the acetonitrile/chloroform extraction method (acn+chloro), in grey with the methanol extraction method (meoh), in orange the extraction protocol based in acetonitrile (acn) and the green bars represented the recoveries obtained after the lyophilization process (lyo). One-way ANOVA p-values FDR adjusted <0.05 are highlighted with an asterisk.

Regarding meoh extraction, the recoveries of NADH and NADPH decreased to 66% and 17%, respectively. This fact was apparently independent of the lyophilization step, since other extraction methods did not alter so strongly the recoveries of these metabolites. Besides, meoh extraction slightly lowered the recoveries of the remaining metabolites.

On the other hand, the recoveries obtained with the acn+chloro extraction method were higher than 85% for all the analysed metabolites and, therefore, this method was used in the subsequent experiments. It should also be mentioned that CoA seemed to be inefficiently recovered, with values below 40%, except when using the acn+chloro method (86% of recovery), which could be the result of the chemical instability of this metabolite (Haynes, 2011). These results agree with those of Dietmair et al., (2010) and Rabinowitz and Kimball (2007), who demonstrated that acetonitrile could be better extractant than methanol regarding the metabolite conservation. This effect was especially evident for the reduced species (NADH and NADPH).

In light of these results, it was seen that the extraction with acetonitrile and without lyophilization is recommended, especially when the quantification of redox metabolites is to be carried out. One known problem with acetonitrile is that lipids are also extracted (Lin et al., 2007), which can be avoided by using multiple chloroform extractions (Sellick et al., 2011). Surprisingly, this step was also recommended for the determination of CoA derivatives (Haynes, 2011). Furthermore, degradation of some metabolites is pH dependent, as it occurs with NADH and NADPH, which are more stable in basic solutions (Wu et al., 1986), whereas NAD^+ and $NADP^+$ are more stable at low pH (Johnson and Tuazon, 1977). Therefore, extraction in aqueous solution (with addition of acetonitrile) should be buffered to neutral pH in order to avoid both degradation rates. Taking all this into account, the extraction method used to determine the redox state, CoA derivatives and nucleotides should use acetonitrile with a buffered solution and complemented with several chloroform extractions afterwards (Lazzarino et al., 2003). The validation performed herein also points to high extraction efficiency (higher than 85%) for all the tested metabolites.

Quenching

As regards quenching of mammalian cells, Sellick et al. (2010) concluded that an optimal quenching solution could be 60 % methanol supplemented with 0.85% AMBIC at -40ºC, although, Dietmair et al. (2010) stated different conclusions, demonstrating that the above solution could lead to metabolite leakage from the quenched cells and proposed 0.9 NaCl (w/v) at 0ºC as the optimal quenching solution. Recently, Sellick et al. (2011) did not find any substantial leakage in the case of small metabolites (TCA intermediates), even though leakage has been shown to be size dependent (Canelas et al., 2009). However, a low quenching temperature is critical for stopping enzymatic activity although metabolite interconversions might not be completely prevented even at -50ºC (Wellerdiek et al., 2009). Whatever the case, Sellick's method has been used in this work and checks were carried out for leakage of the metabolites analysed. The results showed no relevant leakage, probably due to the fact that the measured metabolites have a high molecular weight (Canelas et al., 2009).

Daunomycin-induced cell death

The results of daunomycin-induced cell death in the three cancer cell lines are shown in Figure 6C. Thus, during incubation with daunomycin, 88% of the L1210, 37% of the CBMC-6 and less than 10% of the L1210R cells died. a finding that points to the activity of P-gp as a drug extrusion pump, able to export the drug outside the cells. As a result, we observed a survival level for CBMC-6 (63%), relatively close to that of the L1210R. P-gp expression was also analysed in the corresponding L1210, L1210R and CBMC-6 cell lines by western blot (Figure 6A and 6B). These experiments were carried out by Dr. Cerezo and Dr. Martín-Orozco (Immunology Group, University of Murcia). These results were of the same order as previously described in the work of Cerezo et al. (2012), in which basal P-gp expression was higher in L1210R than in CBMC-6 cells, while no expression was detected in the parental cell line L1210.

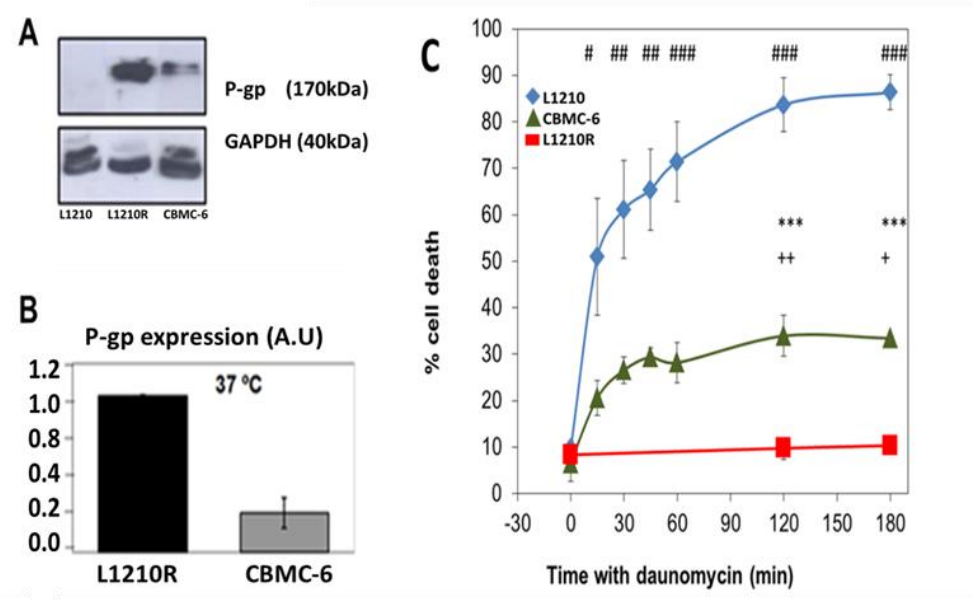

Figure 6. In section A, P-gp and GAPDH western blot for sensitive (L1210), resistant (L1210R) and P-gp overexpressed (CBMC-6) cells are depicted. In section B, the expression of P-gp (A.U) in the resistant cells is shown, the expression has been normalized with respect to L1210R cells since no expression of P-gp in parental cells was detected. Data are represented as the mean ± s.e.m. To measure protein bands intensity the Scion software was used. In section C, the average death percent is depicted for each cell type (L1210 in blue, L1210R in red and CBMC-6 in green) during daunomycin time exposure. Differences are considered statistically significant between L1210R and CBMC-6 when Tukey's HSD post hoc tests FDR adjusted were **+**, $p<0.05$; **++**, $p<0.01$; **+++**, $p<0.001$ as well as between L1210R and L1210 were *, $p<0.05$; **, $p<0.01$; ***, $p<0.001$ and between L1210 and CBMC-6 were #, $p<0.05$; ##, $p<0.01$; ###, $p<0.001$. These experiments were carried out by Dr. Cerezo and Dr. Martín-Orozco (Immunology Group, University of Murcia) and described in the work of Cerezo et al. (2012).

Metabolic state of L1210, L1210R and CBMC-6

The selected extraction protocol was used to study the metabolic state among L1210, L1210R and CBMC-6 cell lines.

Regarding redox state (GSH), before daunomycin treatment, GSH concentration was five-fold higher in L1210R ($p<0.001$) and two-fold higher in CBMC-6 than in the parental cell line, L1210 (Figure 7). GSH is the most abundant non-protein thiol in mammalian cells, where it acts as a major antioxidant by maintaining tight control of the cell redox status (Marí et al., 2009). The difference in GSH levels between chemotherapy-resistant and sensitive cell lines agreed with results of Suzukake et al., (1982) who demonstrated that melphalan-resistant cell lines derived from the same cell line (L1210) presented a higher GSH content. Moreover, this effect was also observed when P388 murine cell line was in the presence of doxorubicin (Ramu et al., 1984), another anthracycline. Therefore, it was thought that higher GSH content could be related to the difference in cell sensitivity. However, several works (Bohacova et al., 2000; Ramu et al., 1984) have shown contradictory results by the use of GSH depletion agents such as L-buthionine sulfoximne (LBSO). Surprisingly, in CBMC-6 cells, where P-gp expression is approximately 20% of that of L1210R, GSH concentration was two-fold higher than in L1210 cells. This fact could suggest a positive correlation between P-gp expression and GSH level as was shown in the work of Wu et al., 2009, where GSH depletion in cells of the rat blood-brain barrier promoted the up-regulation of P-gp (Wu et al., 2009). In addition, $NADH/NAD^+$ ratio was higher in MDR cells than in both L1210 and CBMC-6 cell lines ($p<0.05$ for both), as shown in Figure 7, which may protect cells from ROS-induced cell death (Kuznetsov et al., 2011).

With regard to AcetylCoA/CoA ratio, it was higher in L1210R and CBMC-6 cell lines ($p<0.05$) than in L1210 parental cell line (Figure 7). This is a very surprising finding since the main function of P-gp is to actively pump xenobiotics out of the cells. However, P-gp is also involved in the movement of lipids (Aye et al., 2009). In fact, recently, Foucaud-Vignault et al. (2011) demonstrated that obesity and liver steatosis are originated as a consequence of P-gp deficiency, thus confirming the involvement of P-gp in lipid trafficking and homeostasis. Moreover, the

AcetylCoA/CoA ratio has been linearly correlated with the acetylcarnitine/carnitine ratio (Pearson and Tubbs, 1967). As shown in our results, the AcetylCoA/CoA ratio increased in both L1210R and CBMC-6 cell lines, which could also be related with an alteration in the carnitine system. Again, a small increment in P-gp concentration could be sufficient to provoke large differences in this ratio (see Figure 7). AcetylCoA determination is especially important since it is a key factor connecting glycolysis and fatty acid oxidation, both pathways being relevant in cancer metabolism (Chajes et al., 2006).

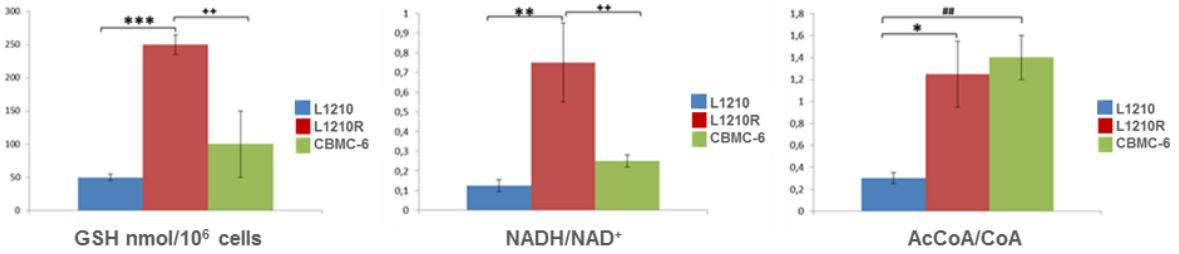

Figure 7. Metabolic levels (average ± s.e.m. of 3 values) of GSH nmol/10^6 cells, NADH/NAD^+ ratio and AcCoA/CoA ratio before daunomicin exposure. Differences are considered statistically significant between L1210R and CBMC-6 when Tukey's HSD post hoc tests FDR adjusted were **+**, p<0.05; **++**, p<0.01; **+++**, p<0.001 as well as between L1210R and L1210 were *****, p<0.05; ******, p<0.01; *******, p<0.001 and between L1210 and CBMC-6 were #, p<0.05; ##, p<0.01; ###, p<0.001.

The nucleotide content could be key in cancer chemotherapy since ATP depletion is involved in cell death by apoptosis (Eguchi et al., 1997) and GTP is involved in several signalling pathways (Traut, 1994). However, it might be more appropriate rather than paying attention to triphosphates (XTP) to look at their balance with the corresponding diphosphates (XDP) and monophosphates (XMP), since several enzymatic reactions are devoted to their interconversion. In 1967, Atkinson and Walton proposed the concept of “Energy Charge” for the adenylate phosphates (AMP, ADP and ATP), which is indeed a commonly used relation for the energy status of cells (Atkinson and Walton, 1967). Moreover, the AEC has been higher in several leukaemic cell lines compared with lymphocytes from healthy human subjects (Baranowska-Bosiacka et al., 2005). Recently, this concept has been extended to the rest of the nitrogenous bases, for example, the guanylate energy charge (GEC) is related to the energy available for protein synthesis (Ataullakhanov and Vitvitsky, 2002) and the uracilate energy charge (UEC) is involved in polysaccharide synthesis (Hisanaga et al., 1986). Our results showed

(Figure 8) that AEC was higher in MDR than in parental ($p<0.01$) and CBMC-6 cells ($p<0.05$). This fact may point to the high energy requirement of MDR cells due to over-expression of P-gp ATPase, which could exhaust the ATP pools, among other mecachisms involved. It could contribute to the slight higher AEC in CBMC-6 cells since this subline presents 20% P-gp expression of MDR cells. In this sense, ATP depletion along with inhibition of the P-gp ATPase activity showed a strong inhibition of the P-gp efflux pump and the overall drastic sensitization of MDR tumors (Oberlies et al., 1997). Furthermore, our results showed that UEC and GEC depicted the same behaviour as AEC, both being higher in L1210R than in L1210 ($p<0.01$, UEC and $p<0.05$, GEC) and CBMC-6 ($p<0.05$, UEC and $p<0.001$, GEC) cell lines. Surprisingly, the overexpression of P-gp did not reduce the energy charges, even though P-gp is an ATPase. On the contrary, the energy charges seemed to increase (Figure 8). It is tempting to speculate that this could be due to the greater activity ATP source pathways in the CMBC-6 and L1210R cell lines.

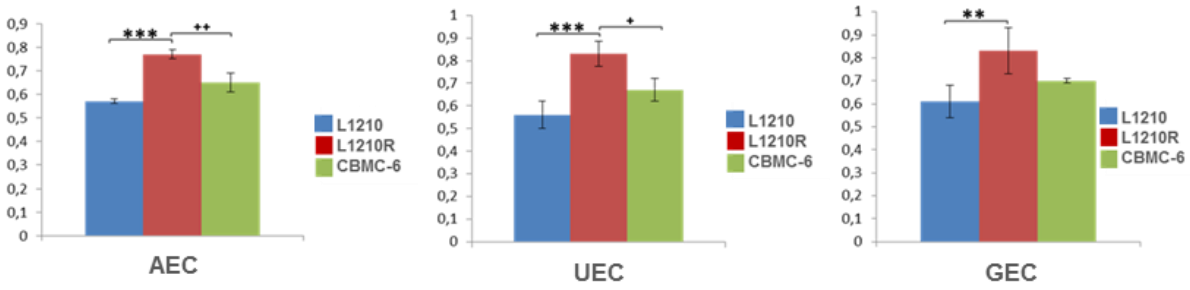

Figure 8. Adenylate Energy Charge (AEC), Uracilate Energy Charge (UEC) and Guanylate Energy Charge (GEC) before daunomicin exposure (average ± s.e.m. of 3 values). Differences are considered statistically significant between L1210R and CBMC-6 when Tukey's HSD post hoc tests FDR adjusted were **+**, $p<0.05$; **++**, $p<0.01$; **+++**, $p<0.001$ as well as between L1210R and L1210 were *****, $p<0.05$; ******, $p<0.01$; *******, $p<0.001$ and between L1210 and CBMC-6 were #, $p<0.05$; ##, $p<0.01$; ###, $p<0.001$.

Metabolic response of L1210, L1210R and CBMC-6 cell lines to daunomycin exposure

After 60 minutes of daunomycin addition, only 12% of the L1210 cells survived. In contrast, CBMC-6 (63%) survival was closer to that of the L1210R cell line (90%) (Figure 6). In Figure 9, different metabolic concentrations are depicted. GSH showed a higher content in the L1210R cell line than CBMC-6 cells and parental line. It has been demonstrated that anthracyclin exposure leads to rapid reactive

oxygen species (ROS) production through various mechanisms (Kuznetsov et al., 2011). Thus, our results suggest that one of the multidrug resistance mechanisms of leukaemic cells could be based on ROS neutralization (Fratelli et al., 2005) by higher intracellular GSH, thus avoiding ROS-induced cell death after daunomycin treatment. In contrast, parental cell line presented lower GSH decreasing until depletion during DNM exposure. In the work of Lasso de la Vega et al., (1994) it was also reported that GSH depletion caused higher cellular sensitivity to cytotoxic chemotherapy. In fact, nuclear and cytosolic GSH depletion by BCNU (an inhibitor of glutathione reductase), resulted in enhanced sensitivity to the topoisomerase II inhibitor adriamycin (doxorubicin), which is closely related with the natural compound from *Streptomyces*, daunomycin (Leitner et al., 2007). Furthermore, a high antioxidative capacity is associated with poor prognosis or resistance against therapy (Andreadis et al., 2007).

Interestingly, regarding NADH/NAD^+ ratio only L1210R cells presented an initial sharp increase after daunomycin addition and, therefore, this effect might not only be due to the presence of P-gp. In this regard, MDR cells could have developed mechanisms to increase NADH levels in order to be protected from ROS-induced cell death, as also shown by Kuznetsov et al., (2011). At this point, it should be remembered that both cellular redox state and overall cellular NAD(H) pool depend on the complex interrelations of many cellular systems. In fact, the regenerative function of many antioxidative and ROS-scavenging enzymes in the cell requires NADH or NADPH, both of which are produced by various dehydrogenases and by the mitochondrial Krebs cycle.

On the other hand, AcetylCoA/CoA ratio strongly decreased in the MDR and CBMC-6 cells after daunomycin treatment. In this sense, global gene expression arrays in cardiac tissue indicate that the inhibition of mitochondrial oxidative phosphorylation by doxorubicin, a broad-spectrum antineoplasic agent closely related to daunomycin, was accompanied by lower expression of genes related to aerobic fatty acid oxidation and higher expression of genes involved in anaerobic glycolysis, possibly as an alternative source of ATP production (Carvalho et al., 2010). Besides, the major role of mitochondrial oxidative phosphorylation in maintaining the energy status in human carcinoma cells despite the expected

bioenergetic shift towards a more glycolytic pathway, which is a widely accepted characteristic of all cancers (Warburg effect) (Kuznetsov et al., 2011).

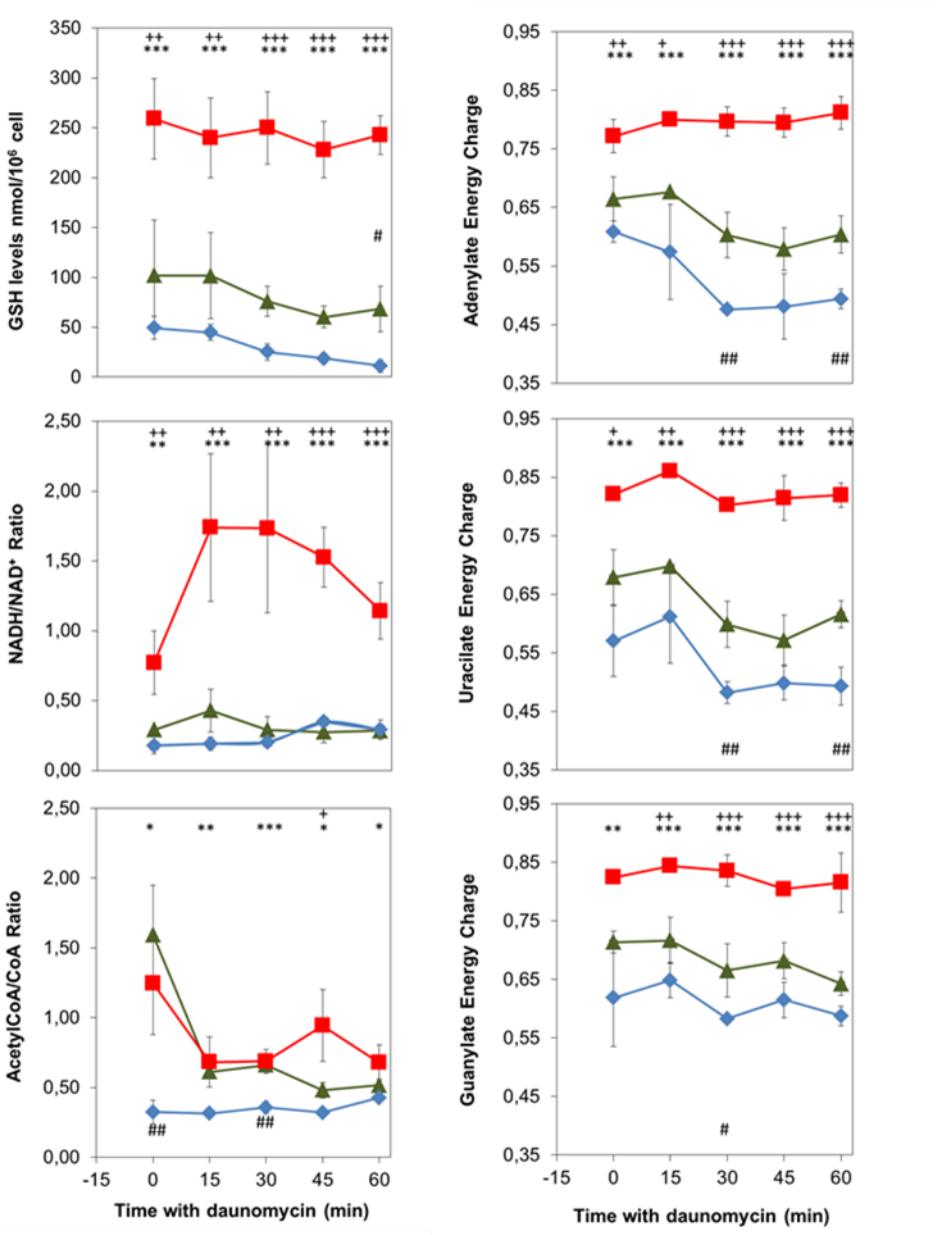

Figure 9. GSH levels (A), NADH/NAD$^+$ ratio (B) AcetylCoA/CoA ratio (C) Adenylate (D), Uracilate (E) and Guanylate (F) Energy Charges measured during daunomycin incubation for L1210 (blue, ◆), L1210R (red, ■) and CBMC-6 (green, ▲) cultured cell lines (for a detailed description, see Methods section). At time t=0, daunomycin was added. Results are averages ± s.e.m. of 3 values. Differences are considered statistically significant between L1210R and CBMC-6 when **+**, p<0.05; **++**, p<0.01; **+++**, p<0.001 as well as between L1210R and L1210 when *****, p<0.05; ******, p<0.01; *******, p<0.001 and between L1210 and CBMC-6 when #, p<0.05; ##, p<0.01; ###, p<0.001.

Moreover, after daunomycin treatment, AEC was kept higher in L1210R than CBMC-6 and the parental line perhaps because L1210R cells were adapted to the presence of daunomycin, developing the capacity to reach the high energy levels

necessary for maintaining P-gp activity. Therefore, the L1210R cells were forced to increase their metabolic rate in order to increase the amount of ATP to satisfy their demand during incubation with daunomycin. This observation is consistent with the NADH/NAD^+ ratio profile (Figure 9). Interestingly, AEC level in CBMC-6 cells, was in between L1210R and the parental cell line, probably as these cells did not develop a mechanism to increase the ATP supply or P-gp activity was not enough in CBMC-6. Whatsoever the case, among the different alterations observed in MDR cells, the developed mechanism to produce high AEC levels to maintain the P-gp activity should be taken into account. However, such mechanisms do not seem to exist in P-gp expressing cell line as demonstrated in Figure 9, as well as in previous reports (Alakhova et al., 2010).

Similarly, GEC, which has been identified in previous works as a mediator specifically linked to the apoptotic phenotype, was higher in L1210R cells, demostrating that enhanced GEC recovery had a profound beneficial effect on cell survival (Kelly et al., 2003). In addition, the level of UEC was higher in the L1210R cell line. This could be related to the protective role of UTP, as previously reported by Yitzhaki and co-workers (Yitzhaki et al., 2007) since UTP protects the mitochondrial function after chemical stress and keeps ATP levels high. Moreover, the CBMC-6 cells seemed to present an intermediate value between L1210 and L1210R cells.

CONCLUDING REMARKS

A metabolic extraction protocol able to efficiently recover more than 20 metabolites, including labile redox molecules (NADH, NADPH, GSH), CoA, AcCoA and nucleotides has been validated. Lyophilization has been avoided since this procedure altered the concentration of some labile metabolites, and acetonitrile/chloroform was used as the extraction solvent. The metabolomic platform used in this work was able to provide a specific metabolic profile for each cell line. Moreover, the main metabolic differences after the daunomycin addition were demonstrated concerning GSH concentration and AEC. Based on these results we can hypothesized that cell survival during DNM exposure is highly influenced by cellular GSH content behaviour since this metabolite is depleted in

sensitive-cells after one hour of DNM-exposure (12% cell survival) and GSH highly constant in MDR cells during DNM exposure (90% cell survival). Regarding AEC, it could be concluded that MDR cells have developed different metabolic strategies in order to keep high values of AEC. This metabolic approach led to a better understanding of the defence mechanisms developed by leukaemia-MDR cells under DNM treatment. Regarding the metabolic alterations due to the contribution of P-gp to this process further experiments are necessary to corroborate this hypothesis. Thus, loss-of-functions experiments could be implemented in order to highlight the actual dependence of the observed metabolic profiles upon P-gp expression, i.e., down-regulating P-gp expression in L1210R and CBMC-6 cells.

REFERENCES

Alakhova, D. Y., Rapoport, N. Y., Batrakova, E. V., Timoshin, A. A., Li, S., Nicholls, D., Alakhov, V. Y. and Kabanov, A. V. (2010). Differential metabolic responses to pluronic in MDR and non-MDR cells: A novel pathway for chemosensitization of drug resistant cancers. *J. Control. Release*, **142**, 89-100.

Andreadis, C., Gimotty, P. A., Wahl, P., Hammond, R., Houldsworth, J., Schuster, S. J. and Rebbeck, T. R. (2007). Members of the glutathione and ABC-transporter families are associated with clinical outcome in patients with diffuse large B-cell lymphoma. *Blood*, **109**, 3409-3416.

Ataullakhanov, F. I. and Vitvitsky, V. M. (2002). What determines the intracellular ATP concentration. *Biosci. Rep*., **22**, 501-511.

Atkinson, D. E. and Walton, G. M. (1967). Adenosine triphosphate conservation in metabolic regulation - rat liver citrate cleavage enzyme. *J. Biol. Chem*., **242**, 3239-3241.

Aye, I., Singh, A. T. and Keelan, J. A. (2009). Transport of lipids by ABC proteins: Interactions and implications for cellular toxicity, viability and function. *Chem. Biol. Interact*., **180**, 327-339.

Baranowska-Bosiacka, I., Machalinski, B. and Tarasiuk, J. (2005). The purine nucleotide content in human leukemia cell lines. *Cell. Mol. Biol. Lett*., **10**, 217-226.

Barone, G., Guerra, C. F., Gambino, N., Silvestri, A., Lauria, A., Almerico, A. M. and Bickelhaupt, F. M. (2008). Intercalation of daunomycin into stacked DNA base pairs. DFT study of an anticancer drug. *J. Biomol. Struct. Dyn*., **26**, 115-129.

Benjamini, Y. and Hochberg, Y. (1995). Controlling the false discovery rate - A practical and powerful approach to multiple testing. *J. R. Stat. Soc. Ser. B-Methodol*., **57**, 289-300.

Bohacova, V., Kvackajova, J., Barancik, M., Drobna, Z. and Breier, A. (2000). Glutathione S-transferase does not play a role in multidrug resistance of L1210/VCR cell line. *Physiol. Res.,* **49**, 447-453.

Canelas, A. B., ten Pierick, A., Ras, C., Seifar, R. M., van Dam, J. C., van Gulik, W. M. and Heijnen, J. J. (2009). Quantitative Evaluation of Intracellular Metabolite Extraction Techniques for Yeast Metabolomics. *Anal. Chem*., **81**, 7379-7389.

Carvalho, R. A., Sousa, R. P. B., Cadete, V. J. J., Lopaschuk, G. D., Palmeira, C. M. M., Bjork, J. A. and Wallace, K. B. (2010). Metabolic remodeling associated with subchronic doxorubicin cardiomyopathy. *Toxicol.,* **270**, 92-98.

Cerezo, D., Lencina, M., Ruiz-Alcaraz, A. J., Ferragut, J. A., Saceda, M., Sanchez, M., Canovas, M., Garcia-Penarrubia, P. and Martin-Orozco, E. (2012). Acquisition of MDR phenotype by leukemic cells is associated with increased caspase-3 activity and a collateral sensitivity to cold stress. *J. Cell. Biochem*., **113**, 1416-1425.

Chajes, V., Cambot, M., Moreau, K., Lenoir, G. M. and Joulin, V. (2006). Acetyl-CoA carboxylase alpha is essential to breast cancer cell survival. *Cancer Res*., **66**, 5287-94.

Dietmair, S., Timmins, N. E., Gray, P. P., Nielsen, L. K. and Kroemer, J. O. (2010). Towards quantitative metabolomics of mammalian cells: Development of a metabolite extraction protocol. *Anal. Biochem*., **404**, 155-164.

Eguchi, Y., Shimizu, S. and Tsujimoto, Y. (1997). Intracellular ATP levels determine cell death fate by apoptosis or necrosis. *Cancer Res*., **57**, 1835-1840.

Fazlina, N., Maha, A., Zarina, A. L., Hamidah, A., Zulkifli, S. Z., Cheong, S. K., Ainoon, O., Jamal, R. and Hamidah, N. H. (2008). Assessment of P-gp and MRP1 activities using MultiDrugQuant Assay Kit: a preliminary study of correlation between protein expressions and its functional activities in newly diagnosed acute leukaemia patients. *Malays. J. Pathol*., **30**, 87-93.

Foucaud-Vignault, M., Soayfane, Z., Menez, C., Bertrand-Michel, J., Guy, P., Martin, P., Guillou, H., Collet, X. and Lespine, A. (2011). P-glycoprotein Dysfunction Contributes to Hepatic Steatosis and Obesity in Mice. *PLoS One,* **6**: e23614. doi: 10.1371/journal.pone.0023614.

Fratelli, M., Goodwin, L. O., Orom, U. A., Lombardi, S., Tonelli, R., Mengozzi, M. and Ghezzi, P. (2005). Gene expression profiling reveals a signaling role of glutathione in redox regulation. *Proc. Natl. Acad. Sci. U. S. A*., **102**, 13998-14003.

Gao, L., Chiou, W., Tang, H., Cheng, X., Camp, H. S. and Burns, D. J. (2007). Simultaneous quantification of malonyl-CoA and several other short-chain acyl-CoAs in animal tissues by ion-pairing reversed-phase HPLC/MS. *J. Chromatogr. B Analyt. Technol. Biomed. Life. Sci.,* **853**, 303-313.

Gibalova, L., Sedlak, J., Labudova, M., Barancik, M., Rehakova, A., Breier, A. and Sulova, Z. (2009). Multidrug resistant P-glycoprotein positive L1210/VCR cells are also cross-resistant to cisplatin via a mechanism distinct from P-glycoprotein-mediated drug efflux activity. *Gen. Physiol. Biophys*., **28**, 391-403.

Gottesman, M. M. and Pastan, I. (1993). Biochemistry of multidrug-resistance mediated by the multidrug transporter. *Annu. Rev. Biochem*., **62**, 385-427.

Harper, M. E., Antoniou, A., Villalobos-Menuey, E., Russo, A., Trauger, R., Vendemelio, M., George, A., Bartholomew, R., Carlo, D., Shaikh, A., Kupperman, J., Newell, E. W., Bespalov, I. A., Wallace, S. S., Liu, Y., Rogers, J. R., Gibbs, G. L., Leahy, J. L., Camley, R. E., Melamede, R. and Newell, M. K. (2002). Characterization of a novel metabolic strategy used by drug-resistant tumor cells. *FASEB J*., **16**, 1550-1557.

Haynes, C. A. (2011). Analysis of mammalian fatty acyl-coenzyme A species by mass spectrometry and tandem mass spectrometry. *Biochim. Biophys. Acta*, **1811**, 663-668.

Hisanaga, K., Onodera, H. and Kogure, K. (1986). Changes in levels of purine and pyrimidine nucleotides during acute-hypoxia and recovery in neonatal rat-brain. *J. Neurochem*., **47**, 1344-1350.

Hobbs, R. P., Amargo, E. V., Somasundaram, A., Simpson, C. L., Prakriya, M., Denning, M. F. and Green, K. J. (2011). The calcium ATPase SERCA2 regulates desmoplakin dynamics and intercellular adhesive strength through modulation of PKCα signaling. *FASEB J*., **25**, 990-1001.

Johnson, S. L. and Tuazon, P. T. (1977). Acid-catalyzed hydration of reduced nicotinamide adenine-dinucleotide and its analogs. Biochemistry*,* **16**, 1175-1183.

Kelly, K. J., Plotkin, Z., Vulgamott, S. L. and Dagher, P. C. (2003). P53 mediates the apoptotic response to GTP depletion after renal ischemia-reperfusion: Protective role of a p53 inhibitor. *J. Am. Soc. Nephrol*., **14**, 128-138.

Kuznetsov, A. V., Margreiter, R., Amberger, A., Saks, V. and Grimm, M. (2011). Changes in mitochondrial redox state, membrane potential and calcium precede mitochondrial dysfunction in doxorubicin-induced cell death. *Biochim. Biophys. Acta*, **1813**, 1144-52.

Lasso de la Vega, M. C., Terradez, P., Obrador, E., Navarro, J., Pellicer, J. A. and Estrela, J. M. (1994). Inhibition of cancer growth and selective glutathione depletion in Ehrlich tumour cells in vivo by extracellular ATP. *Biochem. J*., **298** (1), 99-105.

Lazzarino, G., Amorini, A. M., Fazzina, G., Vagnozzi, R., Signoretti, S., Donzelli, S., Di Stasio, E., Giardina, B. and Tavazzi, B. (2003). Single-sample preparation for simultaneous cellular redox and energy state determination. *Anal. Biochem*., **322**, 51-59.

Leitner, H. M., Kachadourian, R. and Day, B. J. (2007). Harnessing drug resistance: Using ABC transporter proteins to target cancer cells. *Biochem. Pharmacol*., **74**, 1677-1685.

Lin, C. Y., Wu, H. F., Tjeerdema, R. S. and Viant, M. R. (2007). Evaluation of metabolite extraction strategies from tissue samples using NMR metabolomics. *Metabolomics,* **3**, 55-67.

Marí, M., Morales, A., Colell, A., García-Ruiz, C., & Fernández-Checa, J. C. (2009). Mitochondrial Glutathione, a Key Survival Antioxidant. *Antioxid. Redox Signaling*, **11**(11), 2685–2700.

Martin-Orozco, E., Ferragut, J. A., Garcia-Penarrubia, P. and Ferrer-Montiel, A. (2005). Acquisition of multidrug resistance by L1210 leukemia cells decreases their tumorigenicity and enhances their susceptibility to the host immune response. *Cancer Immunol. Immunother*., **54**, 328-36.

Mumenthaler, S. M., Ng, P. Y., Hodge, A., Bearss, D., Berk, G., Kanekal, S., Redkar, S., Taverna, P., Agus, D. B. and Jain, A. (2009). Pharmacologic inhibition of Pim kinases alters prostate cancer cell growth and resensitizes chemoresistant cells to taxanes. *Mol. Cancer Ther*., **8**, 2882-93.

Oberlies, N. H., Croy, V. L., Harrison, M. L. and McLaughlin, J. L. (1997). The Annonaceous acetogenin bullatacin is cytotoxic against multidrug-resistant human mammary adenocarcinoma cells. *Cancer Lett*., **115**, 73-79.

Oikawa, A., Otsuka, T., Jikumaru, Y., Yamaguchi, S., Matsuda, F., Nakabayashi, R., Takashina, T., Isuzugawa, K., Saito, K. and Shiratake, K. (2011). Effects of freeze-drying of samples on metabolite levels in metabolome analyses. *J. Sep. Sci*., **34**, 3561-3567.

Pearson, D. J. and Tubbs, P. K. (1967). Carnitine and derivatives in rat tissues. *Biochem. J.,* **105**, 953-&.

Rabinowitz, J. D. and Kimball, E. (2007). Acidic acetonitrile for cellular metabolome extraction from *Escherichia coli*. *Anal. Chem*., **79**, 6167-6173.

Ramu, A., Cohen, L. and Glaubiger, D. (1984). Oxygen radical detoxification enzymes in doxorubicin-sensitive and doxorubicin-resistant P388 murine leukemia-cells. *Cancer Res.,* **44**, 1976-1980.

Sattler, U. G. A., Walenta, S. and Mueller-Klieser, W. (2007). Lactate and redox status in malignant tumors. *Anaesthesist*, **56**, 466-469.

Sellick, C. A., Hansen, R., Stephens, G. M., Goodacre, R. and Dickson, A. J. (2011). Metabolite extraction from suspension-cultured mammalian cells for global metabolite profiling. *Nat. Protoc*., **6,** 1241-1249.

Sellick, C. A., Knight, D., Croxford, A. S., Maqsood, A. R., Stephens, G. M., Goodacre, R. and Dickson, A. J. (2010). Evaluation of extraction processes for intracellular metabolite profiling of mammalian cells: matching extraction approaches to cell type and metabolite targets. *Metabolomics*, **6**, 427-438.

Suzukake, K., Petro, B. J. and Vistica, D. T. (1982). Reduction in glutathione content of L-pam resistant L1210 cells confers drug sensitivity. *Biochem. Pharmacol*., **31**, 121-124.

Traut, T. W. (1994). Physiological concentrations of purines and pyrimidines. *Mol. Cell. Biochem.,* **140**, 1-22.
Traut, T. W. (1994). Physiological concentrations of purines and pyrimidines. *Mol. Cell. Biochem.*, **140**, 1-22.

Villas-Boas, S. G., Hojer-Pedersen, J., Akesson, M., Smedsgaard, J. and Nielsen, J. (2005). Global metabolite analysis of yeast: evaluation of sample preparation methods. *Yeast,* **22**, 1155-1169.

Wartenberg, M., Richter, M., Datchev, A., Gunther, S., Milosevic, N., Bekhite, M. M., Figulla, H. R., Aran, J. M., Petriz, J. and Sauer, H. (2010). Glycolytic Pyruvate Regulates P-Glycoprotein Expression in Multicellular Tumor Spheroids via Modulation of the Intracellular Redox State. *J. Cell. Biochem*., **109**, 434-446.

Wellerdiek, M., Winterhoff, D., Reule, W., Brandner, J. and Oldiges, M. (2009). Metabolic quenching of *Corynebacterium glutamicum*: efficiency of methods and impact of cold shock. *Bioprocess Biosyst. Eng.,* **32**, 581-592.

Wu, J., Hong, H., Ji, H., Wang, Y. Y., Wang, Y., Li, Y. Q., Li, W. G., Long, Y. and Xia, Y. Z. (2009). Glutathione depletion upregulates P-glycoprotein expression at the blood-brain barrier in rats. *J. Pharm. Pharmacol*., **61**, 819-824.

Wu, J. T., Wu, L. H. and Knight, J. A. (1986). Stability of NADPH - effect of various factors on the kinetics of degradation. *Clin. Chem*., **32**, 314-319.

Xia, J. G., Psychogios, N., Young, N. and Wishart, D. S. (2009). MetaboAnalyst: a web server for metabolomic data analysis and interpretation. *Nucleic Acids Res*., **37**, W652-W660.

Yitzhaki, S., Hochhauser, E., Porat, E. and Shainberg, A. (2007). Uridine-5'-triphosphate (UTP) maintains cardiac mitochondrial function following chemical and hypoxic stress. *J. Mol. Cell. Cardiol*., **43**, 653-62.

APPENDIX

Daunomycin-induced apoptosis

For daunomycin-induced apoptosis, cells were incubated in the presence of 0.15 µM daunomycin for 60 minutes and samples were withdrawn at different sampling times in order to determine cell viability by evaluating whether necrosis or apoptosis was occurring. Samples were withdrawn at different sampling time during the 60 minutes of daunomycin incubation. Cell death was evaluated by using propidium iodide (PI) assay (BD Pharmingen, Franklin Lakes, NJ, USA) according to the manufacturer´s instructions. Apoptotic cells were detected using flow cytometry. The analysis was performed in a Flow cytometer (Becton Dickinson) argon laser of 15 mW at 488 nm. Ten thousand events were collected and analysed using CellQuest software (Beckton Dickinson).

Antibodies and Western-blot experiments

To prepare cellular extracts, cells were plated at $3x10^5$ cells/mL in six-well culture plates and incubated at 37 ºC for 24 hours. Cell protein extracts were obtained by collecting total cells, washing them with phosphate buffer saline (PBS) and resuspending them in Cell Signaling lysis buffer (Cell Signaling Technologies, Beverly, MA) following the manufacturer´s instructions.

Equal amounts of cell extract proteins (15 g/lane) were subjected to polyacrylamide gel electrophoresis and transferred to polyvinylidine difluoride membranes (Bio-Rad, Hercules, CA, USA). After blocking (2 % BSA-TBS-T or 5 % Non-fat Milk-PBS-T), membranes were incubated with the corresponding primary antibody, followed by incubation with a horseradish peroxidase-conjugated secondary antibody. Protein bands were visualized using the ECL detection system (Amersham Biosciences, Buckinghamshire, UK). The antibodies used in our study were the following: anti-MDR-1 (clone D-11) (Mumenthaler et al., 2009), anti-GAPDH pAb (Sigma-Aldrich) (Hobbs et al., 2011). Quantification was carried out by Scion Image Software, normalized to the respective loading control and finally the expression results represented relative to P-gp expression levels in L1210R cells since no expression of this protein was detected in parental cells.

CHAPTER 3

Metabolic Analysis in Biomedicine:

Metabolic alterations in rat livers in early-state Induced non-alcoholic fatty liver disease (NAFLD)

The contents of this chapter has generated the following publication:

Bernal, C., Martín-Pozuelo, G., Sevilla, A., Lozano, A., García-Alonso, J., Cánovas, M., Periago, M. J. (2013) Lipid biomarkers and metabolic effects of lycopene from tomato juice on liver of rats with induced hepatic steatosis. *J. Nutr. Biochem.,* **24**, 1870-1881.

ABSTRACT

Non-alcoholic fatty liver disease (NAFLD) is one of the most common hepatic diseases and consists on liver fatty accumulation without any other liver disease or excessive alcohol consumption. This desease presents a wide range of states, from simple steatosis to non-alcoholic steatohepatitis (NASH). In the present work, a LC-MS metabolomic analysis platform able to measure more than 70 metabolites has been used to study the metabolic profile of healthy and early state induced NAFLD in rat livers. This pathology was induced using a hypercholesterolemic and high-fat diet. Out of the analysed metabolites, fifty-one were able to be quantified and twenty-six presented differences with statistical significance (Welch's t-test P values<0.05) between healthy NAFLD livers. To study the metabolic pattern, PCA and two-way hierarchical clustering were applied showing marked differences attending to the diet, which agreed with the biochemical parameters. Interestingly, the metabolic alteration between the high-fat diet (NAFLD livers) and the normal diet (healthy livers) was detected in several metabolites such as CoA, GSH, L-carnitine, UDP, L-Lysine and L-Tyrosine, among others, which were found impaired in NAFLD samples. CoA and L-carnitine are essential in the fatty acid transport into mitochondria, and therefore, it was not surprising to find them at low concentration when a high fatty acid was supplied. Similarly, GSH is a redox cofactor that plays an important role as a cellular protector. In contrast, ATP, NADH, GDP and Arg were found higher in the high-fat diet samples. Probably because of the higher caloric content of the high-fat diet, the ATP content was 5-fold in NAFLD livers compared to healthy samples. Interestingly, Arg, which seems to be involved in the regulation lipid metabolism, was also found higher in NAFLD livers. These results could lead to new targets for therapeutic agents against NAFLD and to achieve a better understanding of this disease.

INTRODUCTION

Non-alcoholic fatty liver disease (NAFLD) has been progressively diagnosed worldwide and is considered to be the most common liver disorder in western countries. NAFLD is characterized by fatty infiltration in the absence of an excess of alcohol consumption or any other liver disease. NAFLD covers a wide range of hepatic pathologies from simple steatosis to non-alcoholic steatohepatitis (NASH). Simple steatosis, largely benign, is an accumulation of abnormal amounts of fat in the liver generally due to a metabolic abnormality, insulin resistance or excess of dietary fat. Once steatosis has been established, the progression to NASH is mainly due to oxidative stress, lipid peroxidation, mitochondrial dysfunction, high cytokine production and inflammation (Tessari et al., 2009; Tilg and Moschen 2010; Liu et al., 2011). NASH is defined by the presence of more events as hepatocyte injury, inflammation and/or fibrosis which can lead to cirrhosis, liver failure, and finally to hepatocellular carcinoma (Vanni et al., 2010). In Figure 1, the light microscopic pictures from healthy and NALFD rat livers used in this work are shown. The picture on the left corresponds to healthy liver whereas the one on the right depicts the fat accumulation in a liver with steatosis, an early stage of NAFLD. In addition to the changes in lipid metabolism caused by fat accumulation, the aminotransferase activity of the liver is also altered in NALFD since the presence of an elevated value of alanine aminotransferase (ALT) and aspartate aminotransferase (AST), which is one of the first signs for its diagnosis (Stacklies et al., 2007). Moreover, epidemiological studies, such as the Hoorn and Firenze Bagno a Ripoli (FIBAR)

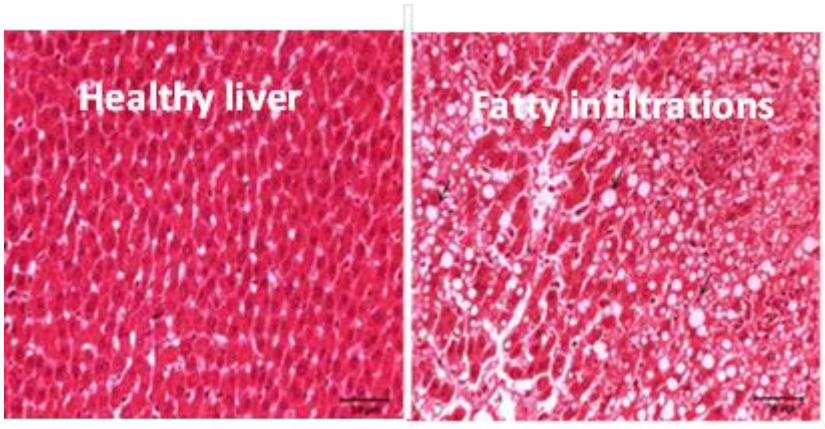

Figure.1. Light microscopic study of a healthy rat liver (left picture) and early stage induced NALFD liver (right picture) (Bernal et al., 2013).

(Monami et al., 2008) have shown that an increase in ALT and AST can be used to evaluate cardiovascular events independently of traditional risk factors and the features of metabolic syndrome (Schindhelm et al., 2007; Monami et al., 2008). Besides these values, other biochemical parameters as isoprostanes or inflammation biomarkers (TNF-α) are measured to evaluate the state of NAFLD. Despite these well recognized facts in NAFLD, this disease has been found related to important metabolic perturbations, including (i) energy metabolism, (ii) lipid metabolism, (iii) amino acids concentration and (iv) antioxidant capacity (García-Valverde et al., 2013). In this regard, metabolomics is a valuable tool that may provide better knowledge through the evaluation of changes in the metabolic profile present in the liver during shifts from health to disease. In particular, Metabolic profiling, which is focused on the simultaneous quantification of numerous targeted metabolites, could help to understand the exact mechanisms underlying the progression of NAFLD, and to predict as well as prevent further complications. The use of metabolomics has contributed to understand other diseases or alterations since some metabolic biomarkers have been previously used to study different hepatic disorders. For example, in the work of Vinaixa et al. (2010) is reported a significant variation in the hepatic concentration of some amino acids and derivatives (taurine, glutathione, methionine, and L-carnitine) about the cholesterol diet effects. Another example is the work of Casals et al. (2013) where gas chromatography/mass spectrometry (GC-MS) has been used to study urinary steroid metabolome of acute intermittent porphyria (AIP) patients, showing that a significant proportion of AIP patients presented abnormally increased the etiocholanolone/androsterone and THF/5α-THF ratios. The aim of the present study has been to evaluate the main metabolic alterations in liver from rats with induced NAFLD by a hypercholesterolemic and high-fat diet in contrast to rats that have been fed with a normal diet to achieve a better understanding of the metabolic alterations in this disease.

MATERIALS AND METHODS

Biological samples

Samples were kindly donated from the Department of Nutrition and Bromatology, University of Murcia (Murcia, Spain). Rats were maintained under controlled

parameters as 12h light-dark cycles, 55% of humidity and 22^{o}C for seven weeks. During this period they had free access to the diet and tap water. Animals were divided into two groups (5 in each one). One was fed a standard laboratory diet (Teklad Global 14% Protein Rodent Maintenance diet, Harland Laboratories) and was shown as N diet. The second group was fed with a hypercholesterolemic and high-fat diet (Atherogenic rodent diet TD-02028, Harland Laboratories) and was shown as H diet. The animal study was carried out under appropriate guidelines and was approved by the Bioethics Committee of Murcia University. At the end of the experiment, all rats were deprived of food overnight, anaesthetised with isofluorane, and sacrificed using an intraperitoneal injection of sodium pentobarbital. Livers were collected from the 10 animals as biological samples. Livers were immediately cut into small pieces and then frozen with liquid nitrogen. Liver samples were stored at -80ºC until the analytical procedures were carried out.

Weigh, histopathological examination and biochemical parameters

Initial and final body weights, food and drink intakes, histopathological description, excreted faeces and urine, ALT, AST, TNF-α in plasma and urine isoprostane levels of experimental groups (N, normal diet) and (H, hypercholesterolemic and high fat diet) were determined as reported in Appendix.

Chemicals

Standard metabolites were generally supplied by Sigma Aldrich (St Louis MO, USA), but glycine and L-histidine were from by Merck (Madrid, Spain). L-phenylalanine, L-tryptophan, and the chemicals used as eluents (acetonitrile, acetic acid, ammonium acetate, ammonium hydroxide, and water) were obtained from Panreac (Barcelona, Spain). All chemicals were of HPLC grade quality.

Extraction method validation

The extraction method used based on Lazzarino et al., (2003) was previously validated (see chapter 2) by the use of several standard mixtures. Additionally, more metabolites (amino acids and other derivatives) were tested since a more complete metabolic analysis platform was available. Indeed, more than 70 metabolites could be quantified. The recovery was again more than 85% in all cases (results not shown). Besides, lyophilizing or freezing during and after the extraction procedure were avoided. For this reason, samples were prepared when the analysis platform was ready to avoid potential metabolic degradation, since lyophilization has been proven to alter the composition of metabolic mixtures (Oikawa et al., 2011) due to the presence of specific labile metabolites.

Intracellular metabolite extraction protocol

Metabolite extraction was based on Lazzarino et al. (2003). 2mL of extraction solution (ice-cold nitrogen-saturated acetonitrile + 10 mM KH_2PO_4 (3:1 v/v) at pH 7.4) were added to liver tissues to homogenate with a basic ultra turrax (IKA T10, Cole Palmer). During the whole process, samples tubes were kept in ice in order to prevent tissue degradation. Homogenated samples were incubated afterwards in a wheel for 30 minutes at 4^{o}C. This homogenate was then centrifuged at 15,000 x g for 20 min at 4^{o}C. The supernatant was split and added to 4 mL of chloroform and centrifuged again at 15,000 x g for 5 min. This yielded a biphasic system, from which the aqueous phase was harvested. This process was carried out three times more. The extraction procedure was finished by filtering through a sterile 0.2 µm filter before the sample being analyzed.

Analysis method

The separation was carried out as previously described (Preinerstorfer et al., 2010) using an injection volume of 10 µl and a ZIC-HILIC as stationary phase: 150 mm x 4.6 mm internal diameter, and 5 µm particle size, provided with a guard column, 20 x 2.1 mm, 5 µm (Merck SeQuant, Marl, Germany) at a temperature of 25^{o}C. For metabolite elution, a gradient method was used with a flow rate of 0.5 ml/min. Mobile

phases were 20 mM ammonium acetate (adjusted to pH 7.5 with NH_4OH) in H_2O (solvent A) and 20 mM ammonium acetate in AcN (solvent B). Gradient elution was performed, starting with 0% A and increasing to 80% A over 30 minutes, then return to starting conditions (80-0% A) for 1 minute followed by a re-equilibration period (0% A) of 14 minutes (total run time, 45 minutes). Data were acquired by a PC using the Agilent Chemstation software package provided by the HPLC manufacturer. Measurements for quantification were conducted using single ion monitoring (Bravo et al., 2011). The measured metabolites and the SIM ions used for quantification are summarized in Table 1. LC-MS experiments were performed on a 1200 series HPLC instrument (Agilent Technologies; California, USA) coupled to an Agilent 6120 single quadrupole mass spectrometer with orthogonal ESI source. The apparatus can be used in positive or negative ionization mode in either SCAN or SIM mode (Agilent Technologies). The mass spectrometer was operated in the positive ESI mode, using the SIM mode for the m/z of each compound. The ion spray voltage was set at 4000 V. Nitrogen with a flux of 12 L/min was used as the sheath gas (35 psi) and the auxiliary gas. The ion transfer capillary was heated to 300ºC. The fragmentation voltage was set at 100 V.

Metabolites identification

Prior to the quantification process, the metabolites were identified using the retention time and relative intensities of the diagnostic ions of a pool of samples. For that, the mass spectra of single and pure standards were recorded and compared with the mass spectra of a pool of samples at the corresponding retention time. At least three diagnostic ions (preferably including the molecular ion) must be found, and their relative intensities should correspond to those of the sample (see recent EU regulation for details) (Document No. SANCO/12495/2011). If the concentration of the metabolites in the sample was not sufficient to generate a clear spectrum, and a metabolite could not be unequivocally identified, pure calibration standards were spiked and the mass spectrum was recorded again. The diagnostic ions used as well as their relative intensities are summarized in Table 1. Due to the limitations of a single quadrupole for identifying isobaric compounds, their separation was confirmed by chromatography.

Table 1. LC-ESI-MS analytical parameters and method performance for compound standards of the quantified metabolites.

Metabolite	Abbreviation	Parent ion formula	Diagnostic ions (relative abundance)	RT (min)	SIM ion	LOD[a] (nmol/mL)	LOQ[b] (nmol/nM)	R^2	Intraday[c] RSD (%)	Interday[c] RSD (%)
Glycine	**Gly**	$C_2H_6NO_2^+$	76 (82), 98 (8), 150 (52)	15.0	76	4.71	15.71	0.9782	8.75	12.2
L-Alanine	**Ala**	$C_3H_8NO_2^+$	90 (100),112 (13), 134 (5)	14.3	90	4.81	16.03	0.9944	1.94	8.4
L-Serine	**Ser**	$C_3H_8NO_3^+$	88 (20), 106 (100),128 (10)	13.2	106	0.02	0.05	0.9826	1.50	9.3
L-Proline	**Pro**	$C_5H_{10}NO_2^+$	70 (2), 116 (100),138 (10)	25.8	116	0.90	3.0	0.9905	1.38	18.2
L-Valine	**Val**	$C_5H_{12}NO_2^+$	72 (5), 118 (80), 140 (15)	12.6	118	0.83	2.77	0.9935	1.14	11.5
L-Threonine	**Thr**	$C_4H_8NO_3^+$	74 (5), 120 (100),142 (10)	10.0	120[d]	0.91	3.03	0.9824	28.85	6.5
L-Homoserine	**HomoSer**	$C_4H_{10}NO^+$	74 (5), 120 (100),142 (8)	14.2	120[d]	0.28	0.94	0.9981	0.79	15.2
L-Cysteine	**Cys**	$C_3H_8NO_2S^+$	102 (10), 122 (42), 144 (44)	11.7	122	0.91	3.02	0.9992	1.36	7.9
Taurine	**Taurine**	$C_2H_6NO_3S^+$	126 (100), 146 (10), 148 (12), 251 (15)	12.1	126	3.11	10.36	0.9950	2.40	5.8
Thymine	**Thymine**	$C_5H_7N_2O_2^+$	127 (100),149 (10), 171 (10)	4.0	127	0.07	0.22	0.9991	0.45	13.7
L-Hydroxyproline	**HydroxyPro**	$C_5H_9NO_3^+$	86 (50), 132 (100),154 (10)	10.7	132[d]	1.73	5.77	0.9947	13.41	18.6
L-Isoleucine	**Ileu**	$C_6H_{14}NO_2^+$	86 (50), 132 (100),154 (10)	11.3	132[d]	0.45	1.5	0.9899	0.33	5.2
L-Leucine	**Leu**	$C_6H_{14}NO_2^+$	86 (10), 132 (100),154 (20)	14.1	132[d]	0.07	0.25	0.9926	1.22	16.7
L-Asparagine	**Asn**	$C_4H_9N_2O_3^+$	87 (10), 133 (100),155 (10)	14.5	133[d]	1.10	3.66	0.9834	1.31	0.9
L-Ornithine	**Orn**	$C_5H_{13}N_2O_2^+$	115 (25), 133 (100),155 (10)	26.5	133[d]	0.43	1.43	0.9902	0.44	2.5
L-Aspartic acid	**Asp**	$C_4H_6NO_4^+$	121 (20), 134 (100), 200 (75)	15.2	134	6.28	20.93	0.9837	2.78	4.9
L-Homocysteine	**HomoCys**	$C_4H_{10}NO_2S^+$	90 (10), 136 (100),158 (10)	12.4	136	1.14	3.82	0.9859	0.37	6.7
Hypoxanthine	**Hypoxan**	$C_5H_5N_4O^+$	137 (70),159 (100), 175 (10)	11.0	137	0.23	0.77	0.9986	2.52	10.2
Acetylphosphate	**Acetyl-P**	$C_2H_4O_5P^+$	116 (100), 141 (23),163 (13)	15.3	141	0.76	2.53	0.9910	7.76	11.9
O-Phosphorylethanolamine	**OPE**	$C_2H_8NO_4P^+$	111 (5), 142 (100), 164 (10)	18.0	142	26.34	87.80	0.9705	4.0	8.4
L-Lysine	**Lys**	$C_6H_{15}N_2O_2^+$	84 (8), 130 (30), 147 (100),169 (8)	25.9	147[d]	0.10	0.35	0.9892	1.10	12.6
L-Glutamine	**Gln**	$C_5H_{11}N_2O_3^+$	130 (50), 147 (100),169 (67)	14.7	147[d]	0.73	2.45	0.9901	3.91	9.9
L-Glutamic acid	**Glu**	$C_5H_{10}NO_4^+$	102 (60), 148 (100), 170 (30),	14.9	148	0.37	1.23	0.9882	0.64	5.4
L-Methionine	**Met**	$C_5H_{12}NO_2S^+$	104 (8), 150 (100),172 (15)	11.6	150	0.01	0.04	0.99	1.50	3.4
L-Histidine	**His**	$C_6H_{10}N_3O_2^+$	137 (25), 156 (100), 178 (5)	15.0	156	0.24	0.79	0.9801	7.08	21.5
L-Carnitine	**Carnitine**	$C_7H_{16}NO_3^+$	149 (1), 162 (100),184 (5)	15.7	162	0.02	0.08	0.9899	4.04	7.9
L-Phenylalanine	**Phe**	$C_9H_{12}NO_2^+$	137 (35), 166 (100), 188 (20)	9.9	166	0.74	2.47	0.9987	2.08	12.5
L-Arginine	**Arg**	$C_6H_{13}N_4O_2^+$	140 (5), 175 (100),197 (2)	24.5	175	0.02	0.08	0.9950	1.47	16.4
L-Citrulline	**CIR**	$C_6H_{12}N_3O_3^+$	159 (19), 176 (100),198 (18)	15.3	176	0.38	1.26	0.9846	26.65	14.2
Glucosamine	**Glucosamine**	$C6H14NO_{5+}$	162 (35), 180 (100), 202 (10)	14.4	180	3.45	10.95	0.9940	14.3	7.9
L-Tyrosine	**Tyr**	$C_9H_{12}NO_3^+$	163 (15), 182 (100),204 (5)	12.1	182	0.76	2.55	0.9892	0.97	6.4

O-Phospho-L-Serine	**P-serine**	$C_3H_9NO_6P^+$	88 (18), 186 (100), 208 (5)	16.3	186	3.24	10.8	0.9923	1.19	0.5
2-Phosphogliceric acid	**2PG**	$C_3H_7O_7P^+$	187 (92),209 (33), 231 (19)	16.1	187 [d]	1.87	6.23	0.9924	0.70	3.1
3-Phosphogliceric acid	**3PG**	$C_3H_7O_7P^+$	187 (92),209 (33), 231 (19)	17.1	187 [d]	0.37	1.24	0.9932	0.82	4.0
N-Acetyl-L-Glutamine	**Ac-Gln**	$C_7H_{12}N_2O_4^+$	172 (15), 189 (80), 211 (60)	13.3	189	5.8	17.9	0.9812	2.6	0.6
L-Tryptophan	**Trp**	$C_{11}H_{13}N_2O_2^+$	177 (10), 205 (100),227 (30)	10.1	205	2.99	9.97	0.9897	5.13	2.4
L-Cystine	**Cystin**	$C_6H_{12}N_2O_4S_2^+$	156 (100), 241 (30), 263 (18)	17.0	241	12.07	40.24	0.9577	3.97	0.8
Thymidine	**Thymidine**	$C_{10}H_{13}N_2O_5^+$	243 (38), 265 (100), 281 (38)	4.2	243	0.17	0.57	0.9949	0.19	1.4
Biotin	**Biotin**	$C_{10}H_{17}N_2O_3S^+$	245 (43),267 (30), 527 (55)	10.8	245	1.52	5.07	0.9974	4.87	16.1
2'-Deoxyadenosine	**DA**	$C_{10}H_{14}N_5O_3^+$	139 (10), 252 (100), 274 (15)	5.2	252	0.04	0.13	0.9946	0.55	13.0
Glucosamine 6-phosphate	**GlucN6P**	$C_6H_{15}NO_8P^+$	242 (32), 260 (100),282 (8)	17.4	260	7.83	26.12	0.9993	2.06	5.1
L-Glutathione	**GSH**	$C_{10}H_{18}N_3O_6S^+$	308 (100),330 (10),618 (10)	14.6	308	5.64	18.82	0.9864	0.30	6.4
Thymidine monophosphate	**TMP**	$C_{10}H_{16}N_2O_8P^+$	207 (25), 323 (100),345 (50)	14.4	323	15.8	52.4	0.9799	4.1	0.8
Cytidine monophosphate	**CMP**	$C_9H_{15}N_3O_8P^+$	112 (20), 266 (10), 324 (100)	16.0	324	1.25	4.18	0.9881	5.07	0.9
Uridine monophosphate	**UMP**	$C_9H_{14}N_2O_9P^+$	172 (90), 325 (100), 342 (25)	15.0	325	26.55	88.51	0.9820	3.53	10.6
Thiamine monophosphate	**ThiaMP**	$C_{12}H_{18}N_4O_4PS^+$	122 (25), 345 (100), 367 (15)	20.5	345	2.3	7.6	0.9812	12.4	14.6
Adenosine monophosphate	**AMP**	$C_{10}H_{11}N_5O_6P^+$	268 (15), 348 (100), 370 (10)	14.7	348	0.64	2.15	0.9910	2.04	18.4
Inosine monophosphate	**IMP**	$C_{10}H_{14}N_4O_8P^+$	138 (50), 349 (100),371 (41)	15.4	349	93.71	312.39	0.9810	11.13	23.1
Guanosine monophosphate	**GMP**	$C_{10}H_{15}N_5O_8P^+$	344 (18), 364 (100), 386 (42)	16.3	364	4.48	14.92	0.9885	10.29	9.1
Xanthosine monophosphate	**XMP**	$C_{10}H_{14}N_4O_9P^+$	157 (50), 365 (100),387 (27)	15.7	365	17.85	59.49	0.9945	2.57	5.4
Cytidine diphosphate	**CDP**	$C_9H_{14}N_3O_{11}P_2^+$	381 (40),404 (100),426 (48)	16.0	404	2.32	7.74	0.9822	5.48	8.8
Uridine diphosphate	**UDP**	$C_9H_{13}N_2O_{12}P_2^+$	301 (95), 405 (100), 427 (60)	15.4	405	73.50	350.02	0.9949	2.42	0.9
Adenosine diphosphate	**ADP**	$C_{10}H_{14}N_5O_{10}P_2^+$	348 (40),428 (100), 450 (20)	15.7	428	1.95	5.50	0.9941	2.07	9.4
Guanosine diphosphate	**GDP**	$C_{10}H_{14}N_5O_{11}P_2^+$	150 (85), 444 (100),466 (38)	16.0	444	4.70	15.67	0.9940	5.33	5.4
Tetrahydrofolic acid	**THF**	$C_{19}H_{23}N_7O_6^+$	399 (100), 446 (20), 468 (17)	16.0	446	1.06	3.54	0.9930	1.55	16.4
Riboflavin-5'-monophosphate	**FMN**	$C_{17}H_{20}N_4O_9P^+$	399 (30), 457 (100),479 (30)	13.6	457	2.33	7.76	0.9942	2.17	11.5
Deoxycytidine triphosphate	**dCTP**	$C_9H_{15}N_3O_{13}P_3^+$	397 (50), 468 (100), 490 (75)	16.5	468	10.8	30.7	0.9991	18.6	22.1
Deoxythymidine triphosphate	**TTP**	$C_{10}H_{16}N_2O_{14}P_3^+$	419 (40), 483 (100), 505 (50)	15.2	483	34.72	115.75	0.9811	0.96	10.0
Cytidine triphosphate	**CTP**	$C_9H_{15}N_3O_{14}P_3^+$	177 (43) , 484 (100),506 (60)	16.7	484	0.62	2.08	0.9501	12.17	8.4
Uridine triphosphate	**UTP**	$C_9H_{14}N_2O_{15}P_3^+$	485 (100), 507 (50), 589 (20)	15.9	485	2.25	7.49	0.9961	5.56	13.7
CDP-choline	**CDP-choline**	$C_{14}H_{27}N_4O_{11}P_2^+$	112 (20), 489 (100), 511 (80)	17.0	489	9.41	31.38	0.9949	5.70	4.6
Deoxyadenosine triphosphate	**dATP**	$C_{10}H_{15}N_5O_{12}P_3^+$	252 (100), 492 (20),512 (5)	15.3	492	5.9	18.1	0.9926	9.7	5.7
adenosine triphosphate	**ATP**	$C_{10}H_{15}N_5O_{13}P_3^+$	410 (15),508 (100),530 (20)	15.6	508	7.68	25.62	0.9877	1.74	12.5
Inosine triphosphate	**ITP**	$C_{10}H_{14}N_4O_{14}P_3^+$	475 (50), 509 (100),531 (49), 553 (35)	16.4	509	11.71	30.06	0.9722	2.12	8.4
Guanosine triphosphate	**GTP**	$C_{10}H_{15}N_5O_{14}P_3^+$	213 (15), 524 (100),546 (30)	16.5	524	22.16	73.86	0.9883	9.11	20.4
L-Glutathione oxidised form	**GSSG**	$C_{20}H_{33}N_6O_{12}S_2^+$	307 (100),613 (100),635 (50)	16.5	613	4.09	13.63	0.9913	4.84	5.4

Nicotinamide adenine dinucleotide oxidised form	**NAD$^+$**	$C_{21}H_{26}N_7O_{14}P_2^+$	123 (20), 333 (30), 664 (100),686 (50)	15.2	664	3.44	11.46	0.9943	3.08	6.7
Nicotinamide adenine dinucleotide reduced form	**NADH**	$C_{21}H_{28}N_7O_{14}P_2^+$	334 (70), 666 (80),688 (50)	16.0	666	49.24	164.15	0.9834	4.51	7.8
Nicotinamide adenine dinucleotide phosphate oxidised form	**NADP$^+$**	$C_{21}H_{29}N_7O_{17}P_3^+$	123 (50), 744 (100),766 (37)	16.6	744	3.91	13.03	0.9947	2.12	0.8
Nicotinamide adenine dinucleotide phosphate reduced form	**NADPH**	$C_{21}H_{27}N_7O_{17}P_3^+$	315 (25), 746 (25), 768 (10)	16.0	746	0.33	1.12	0.9875	2.52	0.4
Coenzyme A	**CoA**	$C_{21}H_{37}N_7O_{16}P_3S^+$	385 (60),768 (100),790 (25)	14.8	768	18.65	62.18	0.9913	6.79	9.7
Acetyl-CoA	**AcCoA**	$C_{23}H_{39}N_7O_{17}P_3S^+$	406 (100),810 (95),832 (25)	14.1	810	16.38	54.60	0.9881	2.89	1.4

[a] LOD calculated from standard deviation of memory peak areas of blank runs: 3 x standard deviation of memory peak area (n=6)/slope of calibration function with neat standard solutions.

[b] LOD calculated from standard deviation of memory peak areas of blank runs: 10 x standard deviation of memory peak area (n=6)/slope of calibration function with neat standard solutions.

[c] The intra- and inter-day precision were determined by analyzing six replicates of the standards at the same concentration level and calculated as the relative standard deviation (RSD) defined as the ratio of the standard deviation to the mean response factor of each metabolite.

[d] Chromatographically separated.

Quantitative analysis

The platform EasyLCMS (Fructuoso et al., 2012) was used for automated quantification. Standard and sample areas were normalized using the following formula, as previous established (Bunk et al., 2006):

$$A_N = \frac{A \cdot N}{A_{IS}}$$

In the above formula A is the standard or sample area without normalization, A_N is the normalized area, N is the normalization value (10^6 by default), and A_{IS} is the internal standard area. Although the use of at least one internal standard representative is recommended for each chemical class, it has been reported that normalization with N-acetyl-glutamine gave similar results to isotope-labelled standards for several metabolic groups including nucleoside bases, nucleosides, nucleotides, amino acids, redox carriers (NAD^+, $NADP^+$, …), and vitamins, among others (Bajad et al., 2006), and therefore this has been selected as an internal standard for all of the analyzed metabolites.

Quality control

The quality of the results was assessed by: (i) checking the extraction method with standard mixtures, (ii) internal standard (IS), and (iii) quality control samples (QC). The extraction method was validated by comparing the concentration of standard mixtures with and without the extraction process. Recoveries were higher than 85% in all of the analysed metabolites (results not shown). N-acetyl-L-glutamine (m/z 189) was added as IS (Bajad et al., 2006), reaching a final concentration of 50 µM in each analysed sample, and the analysis was monitored by confirming that the internal standard area and retention time were always within an acceptable range. An acceptable coefficient of variation was set at 20% for the peak area and 2% for retention time. With respect to quality control samples, two types of QC were incorporated in the analysis: (i) a pool of samples and (ii) a pool of standards. QC analysis was performed in all of the analysed metabolites in the standard

pool of samples and in all those in which concentrations were over the quantification limits of the sample pools. This was carried out by comparing the corrected areas. For the standard pool, the theoretical corrected area was calculated for the measured concentration. Regarding the pool of samples, the corrected areas were compared among all of the samples. An acceptable coefficient of variation was set at 20% for the peak area and 2% for retention time. QC samples were included in the analysis of the whole set of 20 biological samples. Additionally, samples were analysed randomly.

Statistical Analysis

With regard to the statistical analysis of hepatic metabolites, concentrations for the selected metabolites were normalized by the weight of the tissue, scaled by mean subtraction, and divided by the standard deviation of each metabolite (autoscaling), due to metabolite concentrations were separated by several orders of magnitude and PCA is scale dependent. Moreover, this scaling method has been demonstrated to perform optimally in attending to biological expectations (van den Berg et al., 2006). Afterwards, Welch's t-tests were applied and family wise error rate was corrected using FDR with a 5% proportion of false discovery. Those metabolites with statistical significance ($p<0.05$) were selected for ulterior analysis. Metaboanalyst 2.0 web application (Xia et al., 2009) was used to perform the PCA. Additionally, a two-way hierarchical clustering was performed, in which one clustering regroups the samples, while the other one regroups the 26 significant metabolites previously filtered. In both clusterings, Pearson distance method and Ward clustering algorithm were used to measure the distance between the samples. Both dendrograms are related through a colour-gradient matrix, which allows a simpler view of which metabolites are in higher concentration and which ones are in lower concentrations in the high-fat diet samples with respect to the normal diet ones.

RESULTS

Weigh and biochemical parameters

The results of the initial and final body weights, food and drink intakes, excreted faeces and urine, TNF-α in plasma and urine isoprostane levels of experimental groups (N, normal diet) and (H, hypercholesterolemic and high fat diet) are shown in Appendix.

Pairwise comparison

Welch's t-test was applied to the 51 concentrations for the quantified metabolites and family wise error rate was corrected using FDR with a 5% proportion of false discovery. Those metabolites with statistical significance are depicted in Table 2.

PCA of Liver Metabolites.

Figure 2 depicts the PCA for the relevant metabolites (Welch's t-test p-value <0.05). PC1 and PC2 conglomerated more than 89% of the total variance. The PCA score plot showed that there was a clear separation accounted for the diet (N vs H). This fact could mean that the hypercholesterolemic diet resulted in a different metabolic pattern, which is in concordance with previous studies (Vinaixa et al., 2010; Xie et al., 2010). According to the loadings plots in Figure 3, almost all statistical relevant metabolites were involved in the PC1 variations, which suggested that the change of the feed altered enormously the global metabolic pattern.

Table 2. Metabolites with a statistical significance (Welch's t-test FDR adjusted) in livers with high-fat diet compared to the normal diet.

Name	p-value	FDR
ATP	3.75E-06	1.73E-04
NADH	8.16E-06	1.73E-04
CoA	1.02E-05	1.73E-04
Arg	2.23E-05	2.84E-04
GDP	6.87E-05	7.01E-04
UDP	1.65E-04	0.0010914
Pro	1.71E-04	0.0010914
GSH	1.71E-04	0.0010914
Tyr	4.52E-04	0.0025586
HydroxyPro	5.65E-04	0.0028811
Biotin	9.06E-04	0.0041996
HomoCys	0.0012848	0.0054603
Ala	0.0019359	0.0071888
ITP	0.0019734	0.0071888
Gly	0.0033839	0.011505
GMP	0.0042304	0.013263
GSSG	0.0044351	0.013263
Carnitine	0.0046811	0.013263
Val	0.00782	0.020436
P-serine	0.0080142	0.020436
Glu	0.011469	0.027852
Lys	0.013143	0.030467
Asp	0.014132	0.031337
ThiaMP	0.018688	0.039712
Hypoxan	0.01969	0.040168
Acetyl-P	0.024039	0.047154

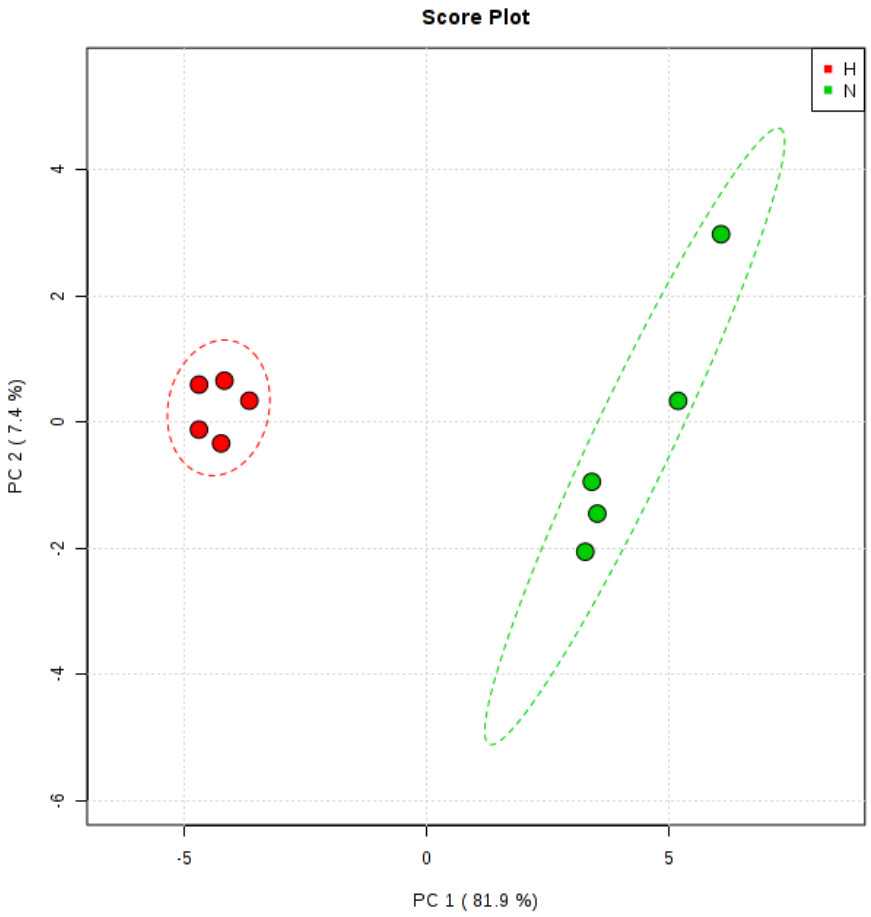

Figure 2. PCA scores plot for the statistically relevant metabolites (Welch's t-test FDR adjusted P-value<0.05) in normal diet (N) and high fatty acids diet (H).

Intracellular concentration of liver metabolites (clustering)

Main results of metabolite analysis are summarized in Figure 4. In a general view, hypercholesterolemic and high-fat diet changed metabolic pattern, showing several metabolic alterations compared to the animals that intake the normal diet. This figure shows how in the case of the high-fat diet the majority of metabolite levels were lower (blue tones) and only a few ones were higher (red tones) (NADH, ATP, Arg, GDP, HomoCys, GMP and ITP) than those of the normal diet. As can be seen, the two groups of different samples (NAi and HAi, normal and high-fat diet respectively) are assembled in two differentiated clusters.

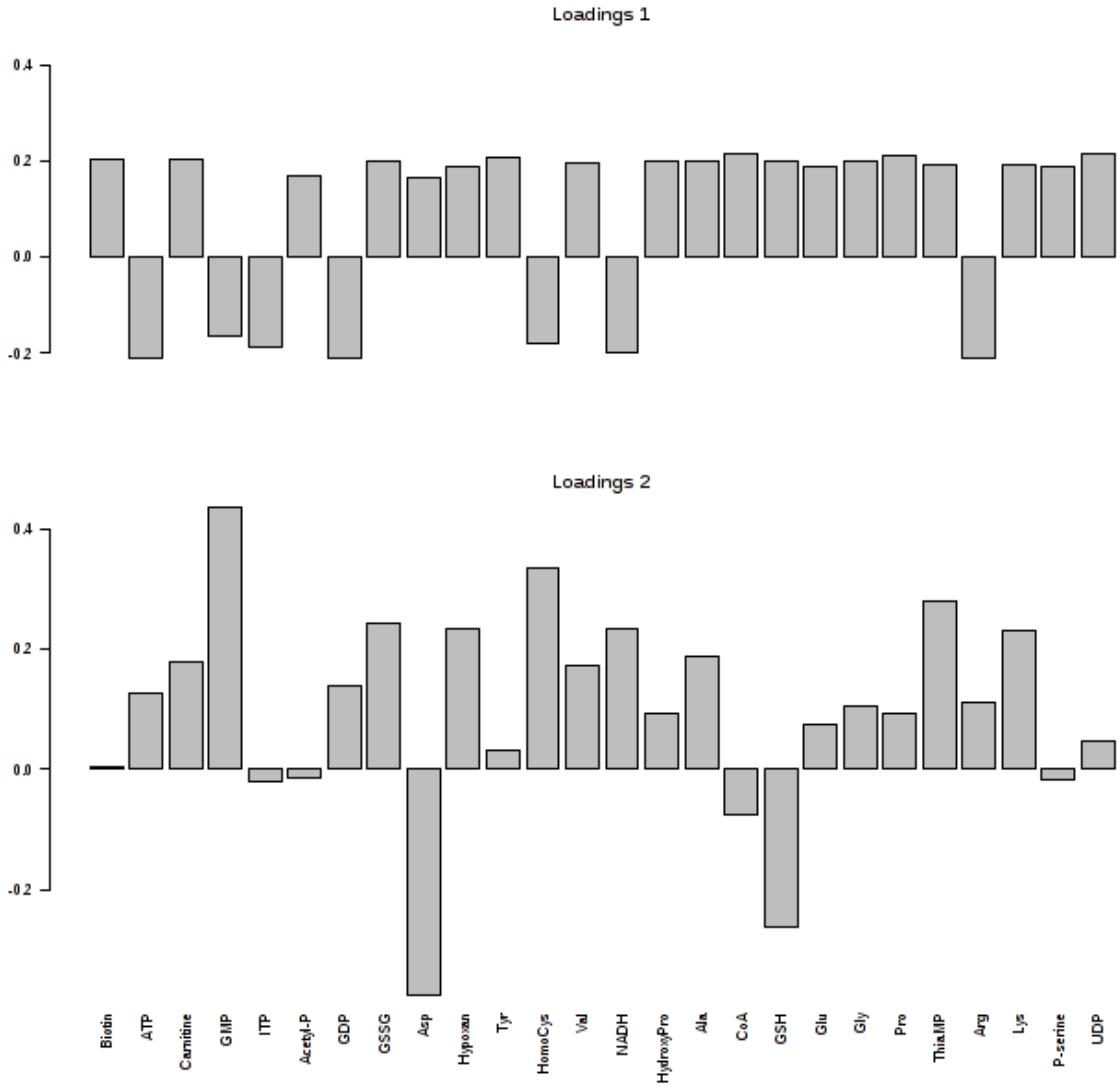

Figure 3. PCA loadings plot for the statistically relevant metabolites (Welch's t-test FDR adjusted P-value<0.05) in normal diet (N) and high fatty acids diet (H). Loading 1 and 2 correspond to PC1 and PC2, respectively.

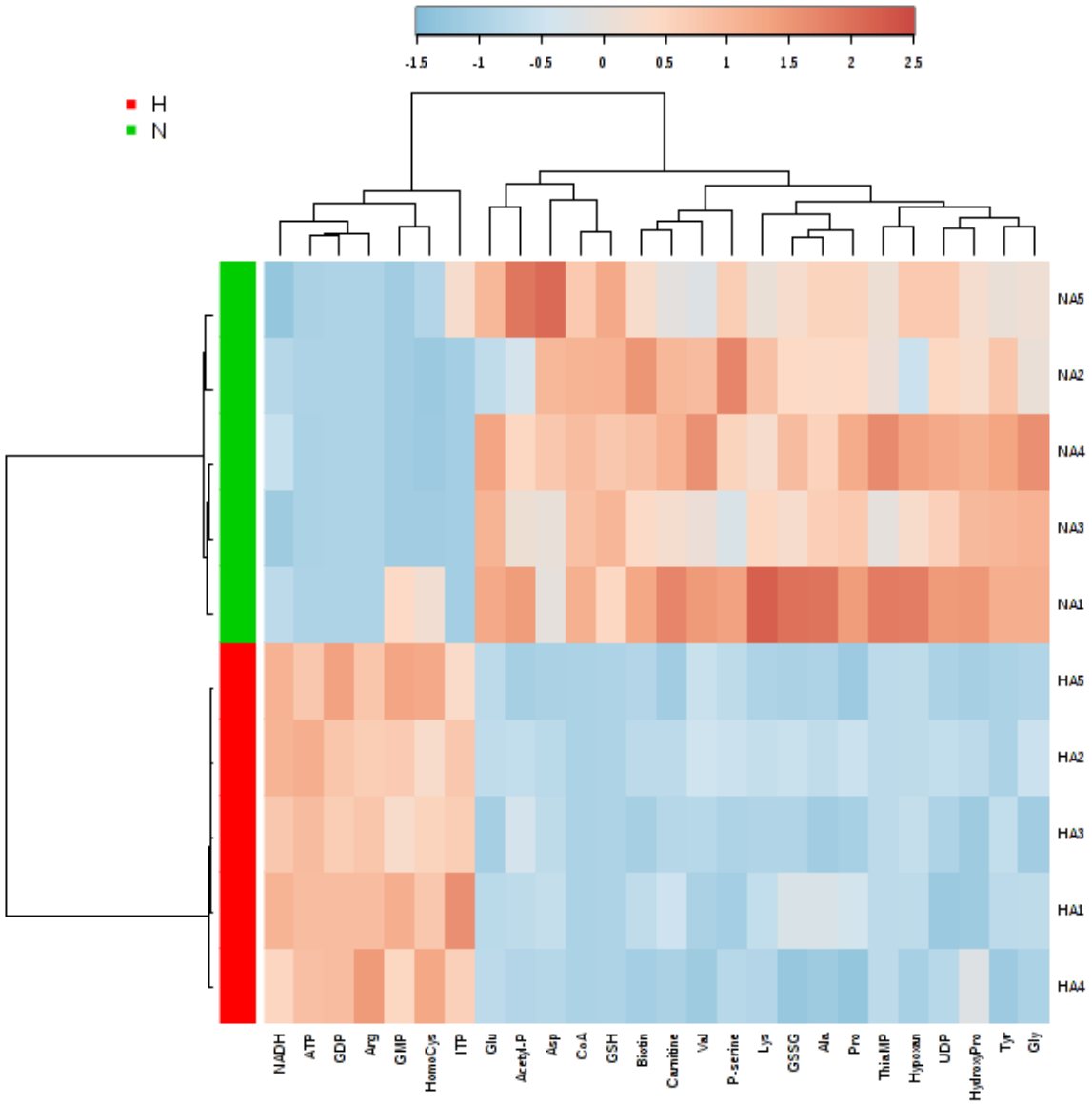

Figure 4. Two-way hierarchical clustering of the metabolic pattern in hypercholesterolemic and high-fat diet samples (H, red cluster) and normal diet samples (N, green cluster).

The absolute concentrations of the most relevant metabolites are shown in Figures 5 and 6. The majority of the levels of the measured metabolites were lower when the animals were fed a hypercholesterolemic diet (Figure 5). However, only a few ones such as Arg or ATP were higher in these samples (Figure 6).

Regarding the redox state, there were significant differences between these two experimental groups. The ratios of NAD/NADH and GSH/GSSG decreased with the hypercholesterolemic and high-fat diet as shown in Table 3.

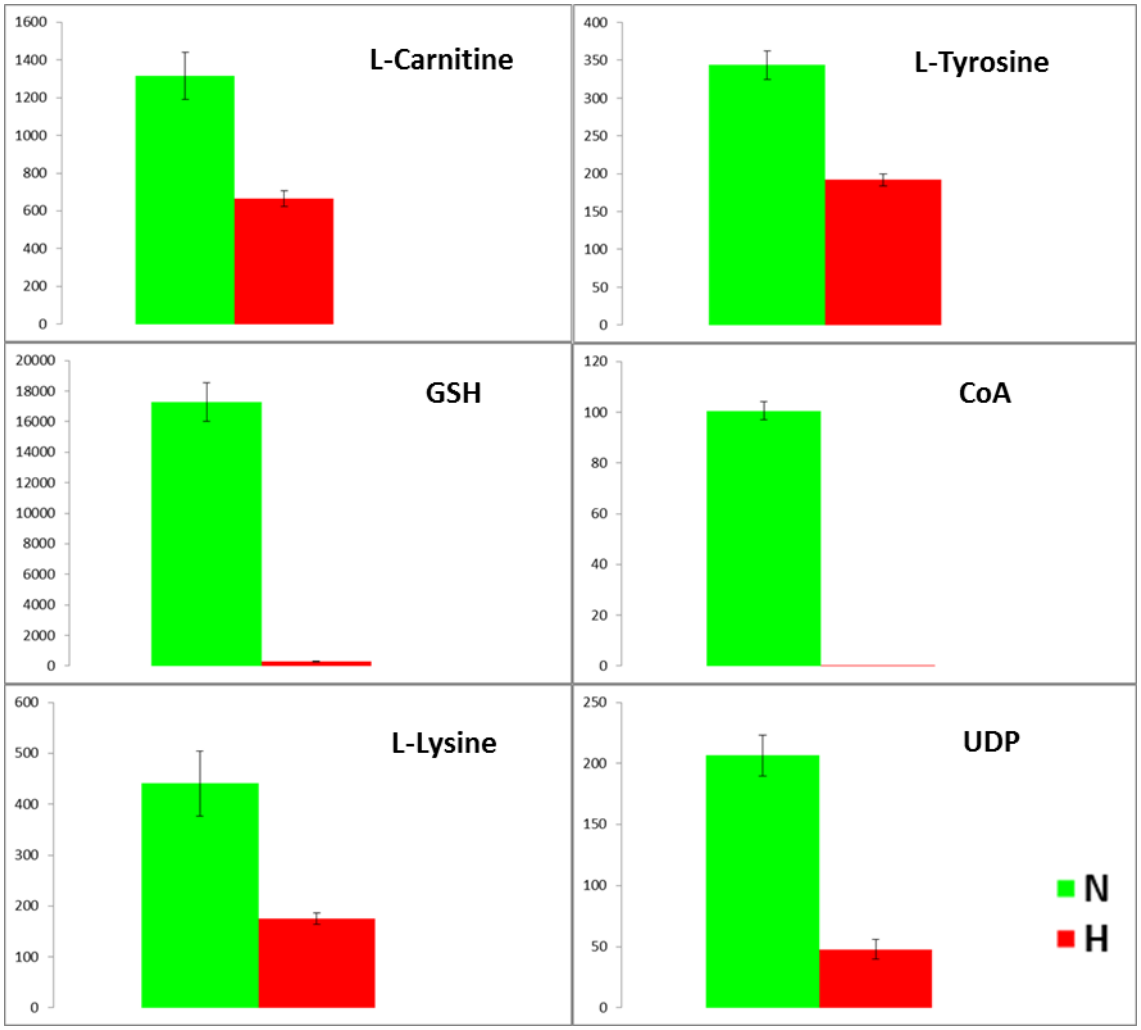

Figure 5. Absolute concentrations of the most relevant metabolites found lower in the case of high fatty acids diet (H, red) compared to those of normal diet (N, green). Bar height indicates mean value (nmol/g) of each diet condition, and error bars indicate the s.e.m.

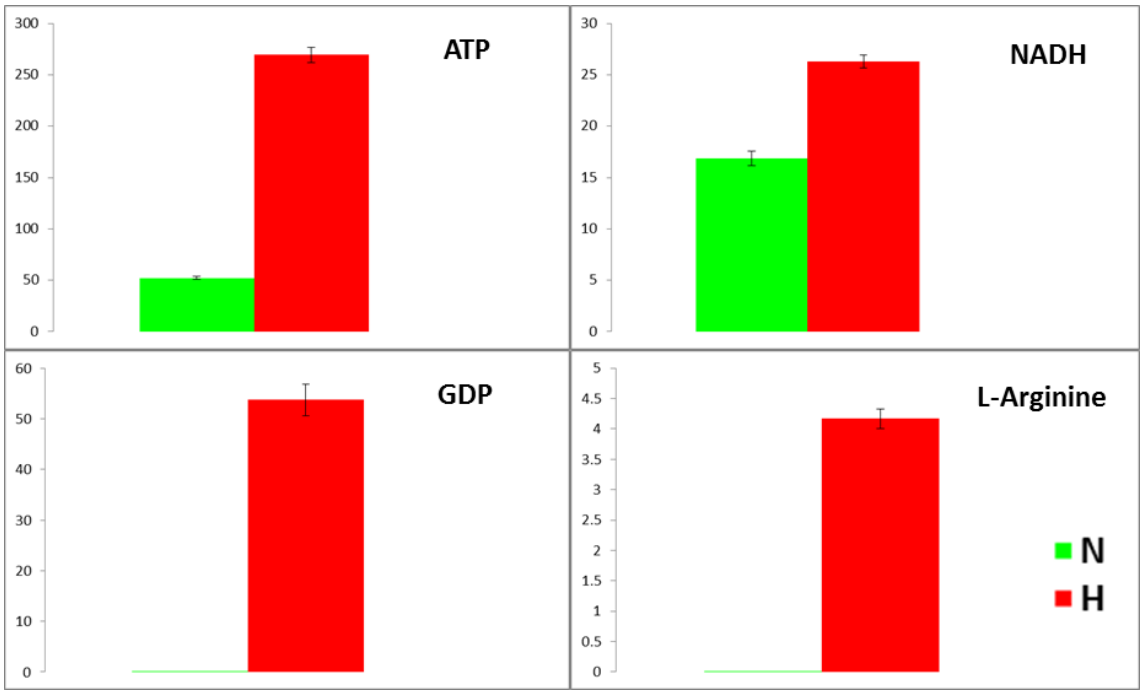

Figure 6. Absolute concentrations of the most relevant metabolites found higher in the case of high fatty acids diet (H, red) compared to those of normal diet (N, green). Bar height indicates mean value (nmol/g) of each diet condition, and error bars indicate the s.e.m.

Table 3. Redox ratios in the liver of the rats of two experimental groups group N (normal diet) and group H (hypercholesterolemic and high-fat diet).

Samples	N (average± s.e.m)	H (average± s.e.m)
NAD^+/NADH	15.1±3.0	3.9±0.7
GSH/GSSG	3.7±0.6	0.1±0.0

DISCUSSION

Obesity increases the prevalence of NAFLD, and present changes observed in biochemical parameters confirm the liver dysfunction. Rats fed with a hypercholesterolemic diet used in this study could be considered obese since their body weight increased a 30% more than rats fed the maintenance diet (Appendix, Table 1). The liver dysfunction of the rats used in this study was

classified as steatosis, an early stage of NAFLD with accumulation of fat in the hepatocyte. After seven weeks with high fat diet *ad lib*, higher values of AST and ALT (Appendix, Table 1) were found in the animals of study, which is one of the first signs of diagnosis of NAFLD. Also these animals presented significant changes in the lipid profiles since the level of LDL cholesterol, triglycerides and total cholesterol resulted increased and the level of HDL cholesterol decreased compared to the ones fed with N diet (Appendix, Table 1). These results agree with the ones described previously by other authors (Amin and Nagy 2009). Whatsmore, these rats fed with hypercholesterolemic and high-fat diet showed an increased in isoprostanes but no differences were observed in plasmatic TNF-α and pro-inflammatory cytokines (Appendix, Table 1) that have been considered a biomarker for the progression of NAFLD to NASH. Based on these findings and since inflammation and fibrosis did not take place, it was considered an early stage of NAFLD specifically a steatosis.

Once these classical biomarkers were established, the intracellular metabolite concentrations were measured in order to check whether the correlation between classical biomarkers and metabolism alterations took place in induced NAFLD rats.

After seven weeks of hypercholrestorlemic diet strong alterations were found in the energy metabolism such as the increase of ATP and NADH compared to rats fed with normal diet (Table 2, 3 and Figure 6). Indeed, ATP concentration was 5-fold higher in the former rats, which is in concordance to the high-fat intake.

The lipid metabolism was also altered in high-fat diet rats since CoA was completely depleted and carnitine was two-fold lower compared to rats fed with normal diet. Both CoA and carnitine are essential in the fatty acid metabolism (Table 2, Figure 5).

Moreover, these metabolites have been lower in NAFLD in rat and human models in previous studies (Vinaixa et al., 2010; Kim et al., 2011). The decreased L-carnitine levels in the liver might be accompanied by marked perturbations in mitochondrial activity, including low rates of complete fatty acid oxidation (Noland et al., 2009; Vinaixa et al., 2010).

Regarding amino acid concentrations, Lys and Tyr were two-fold lower, whereas arginine was 8 times higher in NALFD rats (Figure 5 and 6). Previous studies have confirmed amino acid depletion in liver with a high-fat diet (Xie et al., 2010; Garcia-Canaveras et al., 2011; Kim et al., 2011). On the contrary, the increase of Arg in the livers of animals fed with a high-fat diet could be associated with decreasing lipogenesis, since this amino acid regulates lipid metabolism, modulating the expression and function of the enzymes involved in lipolysis and lipogenesis (Jobgen et al., 2009).

It is generally accepted that oxidative stress is related to the development of NAFLD affecting the trans-sulphuration pathway (Bravo et al., 2011). Therefore, it is not surprising that some downstream products from methionine metabolism, like Homocys, GSH, and GSSG resulted altered when a hypercholesterolemic and high-fat diet was supplied (Table 2, 3 and Figure 5). The results could indicate impairment in glutathione synthesis (Abdelmalek et al., 2009) in animals in the H group, which can be confirmed by the abrupt GSH decrease (almost 60 fold). Moreover, glutathione is formed from three amino acids, L-cysteine, L-glutamate and glycine (Figure 4 , 5, Table 3), which are also diminished in rats fed a hypercholesterolemic and high-fat diet. The redox state is also affected regarding the NAD^+/NADH since the level of NADH was very high in the case of high-fat diet fed rats. This alteration could be due to the fact that NAD^+ acts as electron acceptor in the β-oxidation.

The targeted metabolite levels mentioned above agree with the metabolic alterations previously resported (García-Valverde et al., 2013) such as the changes in energy metabolism, lipid metabolism, amino acids concentration, and the impairment of antioxidant capacity. Most of the previous metabolomic studies related to NASH and NAFLD have been performed in non-targeted platforms (Barr et al., 2010; Xie et al., 2010; Garcia-Canaveras et al., 2011; Kim et al., 2011) and are related to fold-change *vs.* a 'normal state'. Only a few determined absolute concentrations in terms of µmol/mg tissue (Vinaixa et al., 2010; Kim et al., 2011). Moreover, not many metabolites were unambiguously quantified in these works. In contrast, more than 70 metabolites were measured in this work in the liver extracts of rats in the initial phase of the NAFLD. 51 metabolites were quantified and 26 metabolites presented a statistically

significant ($p<0.05$ in Welch's t-test) alteration when animals were fed with a hypercholesterolemic diet. In general, our results confirm and validate those previously obtained, however, the values for GSH are in disagreement with those of Bahcecioglu et al. (2010) who found no significant difference in reduced glutathione concentration between rats fed with high-fat and normal diets. A plausible explanation for these differences could be the quantification method for GSH used by these authors, which was based on the reaction of GSH with DTNB. This reaction is obviously not specific for GSH since, for instance, L-cysteine yields the same reaction (Sedlak and Lindsay 1968). Moreover, no separation method was indicated in the quantification procedure and, therefore, the authors' results might be related to total non-protein sulfhydryl groups rather than the specific GSH concentration.

CONCLUDING REMARKS

In summary, the metabolic profile platform used in this work is able to easily differentiate between healthy and NALFD liver samples providing a specific metabolic profile pattern for each type of sample. An unknown sample of these groups could be easily classified into the group fed with normal diet or the high-fat diet if it is analyzed with the method described in this work. The metabolic results agreed with the classical biomarkers and this targeted metabolic study presents some advantages compared to previous works since it is able to provide absolute concentrations and not only fold changes.

REFERENCES

Abdelmalek, M. F., Sanderson, S. O., Angulo, P., Soldevila-Pico, C., Liu, C., Peter, J., Keach, J., Cave, M., Chen, T., McClain, C. J., Lindor, K. D. (2009). Betaine for Nonalcoholic Fatty Liver Disease: Results of a Randomized Placebo-Controlled Trial. *Hepatology*, **50**, 1818-1826.

Amin, K. A., Nagy, M. A. (2009). Effect of Carnitine and herbal mixture extract on obesity induced by high fat diet in rats. *Diabetol. Metab. Syndr.*, **1;** doi:10.1186/1758-5996-1-17.

Bahcecioglu, I. H., Kuzu, N., Metin, K., Ozercan, I. H., Ustundag, B., Sahin, K., Kucuk, O. (2010). Lycopene prevents development of steatohepatitis in experimental nonalcoholic steatohepatitis model induced by high-fat diet. *Vet. Med. Int.*, doi:10.4061/2010/262179.

Bajad, S. U., Lu, W., Kimball, E. H., Yuan, J., Peterson, C., Rabinowitz, J. D. (2006). Separation and quantitation of water soluble cellular metabolites by hydrophilic interaction chromatography-tandem mass spectrometry. *J. Chromatogr. A*, **1125**, 76-88.

Barr, J., Vazquez-Chantada, M., Alonso, C., Perez-Cormenzana, M., Mayo, R., Galan, A., Caballeria, J., Martin-Duce, A., Tran, A., Wagner, C., Luka, Z., Lu, S. C., Castro, A., Le Marchand-Brustel, Y., Martinez-Chantar, M. L., Veyrie, N., Clement, K., Tordjman, J., Gual, P., Mato, J. M. (2010). Liquid Chromatography-Mass Spectrometry-Based Parallel Metabolic Profiling of Human and Mouse Model Serum Reveals Putative Biomarkers Associated with the Progression of Nonalcoholic Fatty Liver Disease. *J. Proteome Res.*, **9**, 4501-4512.

Bernal, C., Martin-Pozuelo, G., Sevilla, A., Lozano, A., Garcia-Alonso, J., Canovas, M., Periago, M. J. (2013) Lipid biomarkers and metabolic effects of lycopene from tomato juice on liver of rats with induced hepatic steatosis. *J. Nutr. Biochem*., **24**, 1870-1881.

Bravo, E., Palleschi, S., Aspichueta, P., Buque, X., Rossi, B., Cano, A., Napolitano, M., Ochoa, B., Botham, K. M. (2011). High fat diet-induced non alcoholic fatty liver disease in rats is associated with hyperhomocysteinemia caused by down regulation of the transsulphuration pathway. *Lipids Health Dis.*, **10;** doi:10.1186/1476-511x-10-60.

Brunt, E.M., Janney, C.G., Di Bisceglie, A.M., Neuschwander-Tetri, B.A., Bacon, B.R. (1999). Nonalcoholic steatohepatitis: A proposal for grading and staging the histological lesions. *Am. J. Gastroenterol*., **94**:2467-74.

Bunk, B., Kucklick, M., Jonas, R., Munch, R., Schobert, M., Jahn, D., Hiller, K. (2006). MetaQuant: a tool for the automatic quantification of GC/MS-based metabolome data. *Bioinformatics*, **22**, 2962-2965.

Casals, G., Marcos, J., Pozo, O. J., Aguilera, P., Herrero, C., To-Figueras, J. (2013). Gas chromatography-mass spectrometry profiling of steroids in urine of patients with acute intermittent porphyria. *Clin. Biochem.*, **46**, 819-824.

Document No. SANCO/12495/2011, Method Validation and Quality Control procedures for pesticide residues analysis in food and feed. http://ec.europa.eu/food/plant/protection/pesticides/docs/qualcontrol_en.pdf.

Fructuoso, S., Sevilla, A., Bernal, C., Lozano, A. B., Iborra, J. L., Canovas, M. (2012). EasyLCMS: An asynchronous web application for the automated quantification of LC-MS data. *BMC Res. Notes*, **5**, 428.

Garcia-Canaveras, J. C., Donato, M. T., Castell, J. V., Lahoz, A. (2011). A Comprehensive Untargeted Metabonomic Analysis of Human Steatotic Liver

Tissue by RP and HILIC Chromatography Coupled to Mass Spectrometry Reveals Important Metabolic Alterations. *J. Proteome Res.*, **10**, 4825-4834.

García-Valverde, V., Navarro-González, I., García-Alonso, J., Periago, M. (2013). Antioxidant Bioactive Compounds in Selected Industrial Processing and Fresh Consumption Tomato Cultivars. *Food Bioprocess Technol.*, **6,** 391-402.

Helger, R., Rindfrey, H., Hilgenfe, .J. (1974) Method for direct estimation of creatinine in serum and urine. *Z. Klin. Chem. Klin. Biochem*., **12**, 344-9.

Jobgen, W., Fu, W. J., Gao, H., Li, P., Meininger, C. J., Smith, S. B., Spencer, T. E., Wu, G. (2009). High fat feeding and dietary L-arginine supplementation differentially regulate gene expression in rat white adipose tissue. *Amino Acids*, **37**, 187-198.

Kim, H. J., Kim, J. H., Noh, S., Hur, H. J., Sung, M. J., Hwang, J. T., Park, J. H., Yang, H. J., Kim, M. S., Kwon, D. Y., Yoon, S. H. (2011). Metabolomic Analysis of Livers and Serum from High-Fat Diet Induced Obese Mice. *J. Proteome Res.*, **10**, 722-731.

Lazzarino, G., Amorini, A. M., Fazzina, G., Vagnozzi, R., Signoretti, S., Donzelli, S., Di Stasio, E., Giardina, B., Tavazzi, B. (2003). Single-sample preparation for simultaneous cellular redox and energy state determination. *Anal. Biochem.*, **322**, 51-59.

Liu, Y., Wang, D., Zhang, D., Lv, Y., Wei, Y., Wu, W., Zhou, F., Tang, M., Mao, T., Li, M., Ji, B. (2011). Inhibitory Effect of Blueberry Polyphenolic Compounds on Oleic Acid-Induced Hepatic Steatosis in Vitro. *J. Agric. Food Chem.*, **59**, 12254-12263.

Monami, M., Bardini, G., Lamanna, C., Pala, L., Cresci, B., Francesconi, P., Buiatti, E., Rotella, C. M., Mannucci, E. (2008). Liver enzymes and risk of diabetes and cardiovascular disease: Results of the Firenze Bagno a Ripoli (FIBAR) study. *Metab. Clin. Exp.*, **57**, 387-392.

Noland, R. C., Koves, T. R., Seiler, S. E., Lum, H., Lust, R. M., Ilkayeva, O., Stevens, R. D., Hegardt, F. G., Muoio, D. M. (2009). Carnitine Insufficiency Caused by Aging and Overnutrition Compromises Mitochondrial Performance and Metabolic Control. *J. Biol. Chem.*, **284**, 22840-22852.

Oikawa, A., Otsuka, T., Jikumaru, Y., Yamaguchi, S., Matsuda, F., Nakabayashi, R., Takashina, T., Isuzugawa, K., Saito, K., Shiratake, K. (2011). Effects of freeze-drying of samples on metabolite levels in metabolome analyses. *J. Sep. Sci.*, **34**, 3561-3567.

Preinerstorfer, B., Schiesel, S., Lammerhofer, M. L., Lindner, W. (2010). Metabolic profiling of intracellular metabolites in fermentation broths from beta-lactam antibiotics production by liquid chromatography-tandem mass spectrometry methods. *J. Chromatogr. A*, **1217**, 312-328.

Roberts, L.J., Morrow, J.D. (2000). Measurement of F-2-isoprostanes as an index of oxidative stress in vivo. *Free Radic. Biol. Med*., **28**:505-13.

Schindhelm, R. K., Dekker, J. M., Nijpels, G., Bouter, L. M., Stehouwer, C. D. A., Heine, R. J., Diamant, M. (2007). Alanine aminotransferase predicts coronary heart disease events: A 10-year follow-up of the Hoorn Study. *Atherosclerosis*, **191**, 391-396.

Sedlak, J., Lindsay, R. H. (1968). Estimation of total protein-bound and nonprotein sulfhydryl groups in tissue with Ellmans reagent. *Anal. Biochem.*, **25**, 192-205.

Stacklies, W., Redestig, H., Scholz, M., Walther, D., Selbig, J. (2007). pcaMethods—a bioconductor package providing PCA methods for incomplete data. *Bioinformatics*, **23**, 1164-1167.

Tessari, P., Coracina, A., Cosma, A., Tiengo, A. (2009). Hepatic lipid metabolism and non-alcoholic fatty liver disease. *Nutr. Metab. Cardiovasc. Dis.*, **19**, 291-302.

Tilg, H., Moschen, A. R. (2010). Evolution of Inflammation in Nonalcoholic Fatty Liver Disease: The Multiple Parallel Hits Hypothesis. *Hepatology*, **52**, 1836-1846.

van den Berg, R. A., Hoefsloot, H. C. J., Westerhuis, J. A., Smilde, A. K., van der Werf, M. J. (2006). Centering, scaling, and transformations: improving the biological information content of metabolomics data. *BMC Genomics*, **7**; doi:10.1186/1471-2164-7-142.

Vanni, E., Bugianesi, E., Kotronen, A., De Minicis, S., Yki-Jarvinen, H., Svegliati-Baroni, G. (2010). From the metabolic syndrome to NAFLD or vice versa? *Dig. Liver Dis.*, **42**, 320-330.

Vinaixa, M., Rodriguez, M. A., Rull, A., Beltran, R., Blade, C., Brezmes, J., Canellas, N., Joven, J., Correig, X. (2010). Metabolomic Assessment of the Effect of Dietary Cholesterol in the Progressive Development of Fatty Liver Disease. *J. Proteome Res.*, **9**, 2527-2538.

Xia, J. G., Psychogios, N., Young, N., Wishart, D. S. (2009). MetaboAnalyst: a web server for metabolomic data analysis and interpretation. *Nucleic Acids Res.*, **37**, W652-W660.

Xie, Z. Q., Li, H. K., Wang, K., Lin, J. C., Wang, Q., Zhao, G. P., Jia, W., Zhang, Q. H. (2010). Analysis of transcriptome and metabolome profiles alterations in fatty liver induced by high-fat diet in rat. *Metab.-Clin. Exp.*, **59**, 554-560.

APPENDIX

Analyses of plasma

Blood samples were transferred into heparin-containing tubes. Plasma was obtained by centrifugation (3000 g, 10 min, 4ºC). Total cholesterol, its fractions HDL-cholesterol and LDL-cholesterol, total triglycerides, and AST (aspartate aminotransferase) and ALT (alanine aminotransferase) enzymes were analysed in plasma samples using an automatic analyser (AU 600 Olympus Life, Germany). In addition, tumour necrosis factor (TNF-α) was measured as a biomarker of inflammation related to NAFLD using an ELISA kit (Rat TNFα Single Analyte Elisarray kit SER06411A, Sabiosciences). All analyses were performed in triplicate.

Determination of isoprostanes

Isoprostanes are a very specific marker for free radical-induced peroxidation of arachidonic acid. Measurement of the urinary excretion of the F_2-isoprostane metabolite 15-F_{2t}-isoprostane (8-*epi*-$PGF_{2\alpha}$) is considered to be an accurate tool to determine endogenous isoprostane production (Roberts et al., 2000). An enzyme immunoassay kit (OxiSelectTm 8-iso-Prostaglandin F2α Elisa Kit, STA-337, Cell Biolabs) was used to quantify the content of this biomarker in urine samples. Urine creatinine was determined by the Jaffe picric acid spectrophotometrical method (Helger et al., 1974) to normalize isoprostane content. For each urine sample, the isoprostane and creatinine contents were analysed in triplicate.

Weight gain and volume of feed consume

The initial and final body weight of rats in the experimental period were determined (Appendix, Table 1). A significant increase in the body weights was registered after the intervention period. The diet has a significant effect in the final body weights, showing H group higher values than N group. The food and drink intakes, the

excreted faeces and urine are shown in Appendix, Table 1. Despite the fact that the animals in the two groups were fed *ad lib*, significant differences were found in this parameter between animals fed the standard diet and animals fed the hypercholesterolemic and high-fat diet. The N group showed a significantly higher feed intake than the H group, as was also observed in the excreted faeces. Related to liquid intake, all animals drank a similar amount of water (around 30 ml/day), and no significant differences were found in the amounts of daily excreted urine.

Histopathological examination

Paraffin blocks were prepared, and cross-sections (4 μm thick) were stained with haematoxylin eosin (H&E) for light microscope examination. Steatosis was graded according to the Brunt and collaborators classification (Brunt et al., 1999), which assigns grade 0 when <5% of fat is found in the liver, grade 1 when fat vacuoles are seen in less than 33% of hepatocytes, grade 2 when 33%–66% of hepatocytes are affected by fat vacuoles, and grade 3 when fat vacuoles are found in more than 66% of hepatocytes.

Biochemical parameters

Biochemical parameters were measured in urine and plasma to determine the status of NAFLD during the intervention study (Appendix, Table 1). Parameters were measured after two weeks of experiment and at the end (seven weeks). Final urine isoprostanes were measured as a better biomarker of oxidative stress, showing a significant effect associated with the feed. Isoprostanes increased in rats fed diet H compared with diet N. Related to inflammation biomarkers, no significant differences were found in the plasma level of TNF-α among the two groups (Appendix, Table 1), which is in concordance with the histopathological description.The feed influenced significantly the lipid profiles. Animals fed with the H diet showed a significant decrease in total and LDL cholesterol and an increase in HDL cholesterol. The pathological status in the liver is also confirmed by the abnormal aminotransferase levels (AST and ALT enzymes), which increased significantly at the end of the study in H group.

Table 1. Food and drink intakes, excreted faeces and urine, TNF-α in plasma and urine isoprostanes levels, total cholesterol, LDL cholesterol, HDL cholesterol, triglycerides, AST and ALT (mean ± s.e.m. (n=5 per group)) of experimental groups (N: normal diet and H: hypercholesterolemic and high fat diet). Some values were determined after 2 weeks of experiments were other were determined after 7 weeks (Final).

Parameters	N	H
Body weight (g) (2 weeks of experiment)	300.0±8.9	295.8±7.2
Final body weight (g)	423.8±6.9	479.5±9.5
Food intake (g/day)	21.12±0.82	17.92±0.26
Water intake (ml/day)	28.83±2.42	31.09±3.54
Excreted feaces (g/day)	8.60±0.40	2.77±0.16
Excreted urine (ml/day)	10.11±1.46	8.61±2.13
Final urine isoprostanes (ng/mg creatinine)	2.22±0.12	9.87±0.81
Final plasma TNFα (pg/ml)	32.75±1.20	29.96±1.36
Total cholesterol (mg/dL) (2 weeksof experiment)	105±3.3	305.5±40.9
Final total cholesterol (mg/dL)	99.2 ±4.1	167±14.4
LDL cholesterol (mg/dL) (2 weeks of experiment)	21.9±1.4	215.6±39.2
LDL cholesterol (mg/dL)	25.5±1.4	93.7±11.1
HDL cholesterol (mg/dL) (2 weeks of experiment)	53.4±1.5	31.1±5.4
Final HDL cholesterol (mg/dL)	54.4±2.3	39.7±2.1
Triglycerides (mg/dL) (2 weeks of experiment)	96±4.4	89.4±9.1
Final Triglycerides (mg/dL)	80.1±4.6	121.2±7.1
ALT (U/L) (2 weeks of experiment)	43.3±3.6	42.3±3.7
Final AST (U/L)	32.4±1.9	78.7±10.5
ALT (U/L) (2 weeks of experiment)	88±9.4	106.4±5.1
Final AST (U/L)	63.8±7.1	150.4±7.6

Chapter 4

Metabolic analysis in Bioprocess:

Integration of metabolomics and trascriptomics datasets by pathway-based analysis to describe anaerobic long-term NaCl adaptation of *E. coli* using glycerol as C-source

The contents of this chapter has been submitted as:

Arense, P*., Bernal, C*., Sevilla, A., Iborra, J. L., Cánovas, M. Integration of Fluxomics, Metabolomics and Trascriptomics to describe anaerobic long-term NaCl adaptation of *E. coli* using glycerol as C-source. (*Metab. Eng.*, submitted).(*equal contribution).

The analytical methods used in this chapter has been published as:

Montero, M., Rahimpour, M., Viale, A.M., Almagro, G., Eydallin, G., Sevilla, Á., Cánovas, M., Bernal, C., Lozano, A.B., Muñoz, F.J., Baroja-Fernández, E., Bahaji, A., Mori, H., Codoñer, F.M., Pozueta-Romero, J. (2014) Systematic production of inactivating and non-inactivating suppressor mutations at the relA locus that compensate the detrimental effects of complete spot loss and affect glycogen content in *Escherichia coli*. *PloS one,* **9**(9):e106938.

ABSTRACT

Glycerol is used as C-source due to its cheap price since it is a by-product of the biodiesel and bioethanol industries. However, this glycerol is contaminated with NaCl, even processed. According to that, it seems important to study the impact of the NaCl concentration in *E. coli* metabolism when glycerol is used as C-source. After short-term exposure of osmotic stress the initial state is rapidly returned. However, in the case of long-term exposure a different cellular physiological state is involved in order to achieve the cellular osmoadaption. Additionally, complex medium, such as peptone, is able to enhance growth more than compatible solutes after an osmotic stress. In industrial environments, anaerobic processes are preferred as they are cheaper to maintain in industrial size biofermenters. However, there is a lack of information integrating these conditions.

The aim of the present work was to throw light about the intracellular metabolic and transcriptomic profile and the metabolic flux distribution of *E.coli* in three NaCl concentrations (0.085, 0.5 and 0.8M) in anaerobic chemostats using glycerol as C-source in a complex medium.

The results obtained highlighted a common pattern regarding the NaCl concentration including total depletion of extracellular amino acids accompanied with an intracellular amino acid accumulation (except Cys and His) and the increase of intracellular carnitine, glycerol assimilation intermediates and CoA derivatives. Additionally, redox coenzyme ratio alterations were observed, stronger at 0.8M of NaCl. Regarding metabolic fluxes, fermentation pattern was altered, increasing the relative ethanol synthesis in the case of 0.5M of NaCl, whereas relative lactate synthesis was increased in the case of 0.8M of NaCl. Metabolic data of the present work were combined with the transcriptomic data to carry out the integration by pathway-based analysis. This highlighted the main pathways affected, namely, GSH metabolism, glycolysis/glyconeogenesis, amino acid biosynthesis/degradation, purine metabolism, phosphorilative oxidation, pyruvate metabolism and the TCA cycle/glyoxylate shunt among others. This work shows how metabolomics is a powerful tool to complete the information given by other –omics in the long-term osmoadaptation of *E. coli*. However, further studies should be carried out to establish the relevance of the switch of redox cofactors observed and the effect of the oxidation state under these conditions.

INTRODUCTION

The use of glycerol as C-source is increasingly for several bioprocesses (Murarka et al., 2008) because its price has fallen drastically. This fact is due to its generation as a by-product of the biodiesel and bioethanol production (Yazdani and Gonzalez, 2007). However, crude glycerol is highly contaminated with ash, whose principal component is NaCl (Yong et al., 2011). Ashby et al. (2004) reported that NaCl may affect productivity as was studied in the case of polyhydroxyalcanoate synthesis. On the other hand, the use of osmoprotectants, such as L-carnitine or crotonobetaine (a by-product of L-carnitine chemical synthesis) could alleviate the harmful effects of high NaCl concentrations (Canovas et al., 2007). Curiously enough, these conditions are closer to the natural environment of *Escherichia coli* (high osmolarity, complex medium and anaerobic conditions).

E.coli is a natural inhabitant of the mammalian intestine so that it withstands diverse conditions of growth depending on the diet of its host. In fact, both rich medium and anaerobically grown cells are of special importance in the osmoadaptation process because they allow cells to acquire favorable genetic and metabolic features to overcome osmotic upshift (Rozen et al., 2002; Weber et al., 2006). As regards high osmolarity, the intestine may present NaCl concentrations of 0.3 M or even higher (Gupta and Chowdhury, 1997) and, although osmoprotectans molecules such as L-carnitine are also present, hardly any reports have described high osmolarity with osmoprotectans (Santos et al., 2012). Moreover, it has been recently demonstrated that fumarate is the most important electron acceptor for *E. coli* to colonize the mouse intestine (Jones et al., 2011). However, very few studies can be found regarding bioprocesses using anaerobic conditions and using fumarate as electron acceptor, even though these conditions are closer to the natural environment of *E. coli* and fumarate improves both cell growth and productivity in anaerobic conditions, for example, during L-carnitine biotransformation (Sevilla et al., 2005b; Torres Darias et al., 2009) and 1,3 propanediol biosynthesis (Zhu et al., 2002).

To our knowledge, few works have dealt with the anaerobic cultivations of *E. coli* compensated with an electron acceptor such as fumarate, and where the high concentratios of NaCl is alleviated with an osmoprotectant such as crotonobetaine.

Moreover, glycerol and both fumarate and crotonobetaine are inexpensive to obtain (Moon et al., 2004; Sevilla et al., 2005a; Yang et al., 2012) and can be transformed into high value compounds (lactate, ethanol, formate, succinate and L-carnitine). Furthermore, glycerol fermentation is facilitated with the tryptone or corn steep liquor (Dharmadi et al., 2006) and some biotechnological processes such as recombinant dengue protein (Tripathi et al., 2009) or bioethanol (Thapa et al., 2013) have demonstrated the positive effect of tryptone in the production. Peptone or tryptone may not be ideal for high-scale biotechnological processes as they are costly. However, corn steep liquor, a low-priced by-product of the corn processing industry, is amenable for industrial applications (Dharmadi et al., 2006).

E. coli adaptation to stress conditions by different molecular mechanisms in conditions of osmolarity up-shifts has been described (Wood 1999). In that work different progressive strategies to achieve the cell osmoadaption were reported: First, dehydration, respiration and transport cease and a transiently increment of ATP level takes place. Second, rehydration, glutamate and other solutes accumulation, respiration at lower rate and ATP level restoration are the key events. Finally, the cell wall is remodeled, protein and DNA synthesis take up again and the cycle is established with the consequent osmoresponsive genes expression. Generally, the initial state is rapidly returned after short-term exposure (Cánovas et al., 2007).

On the other hand, the response to long-term high NaCl exposure involves different cellular physiological states due to the osmoadaptation to the new stress conditions as was reported in Arense et al., (2010). In that work it is shown the relevance of central carbon metabolism in NaCl stress adaptation. In that study the strain O44K74 (DSM 8828) that overexpresses the genes of carnitine metabolism (Kleber 1997) was grown in several chemostats under standard salt conditions (0.085M NaCl). After reaching the steady state, different salt concentrations (0.3, 0.5 and 0.8M NaCl) were assayed for the osmotic up-shifts. At the highest salt concentration, longer time was needed to achieve the new steady state. That fact can be related with the high energy requirement to maintain cellular homeostasis (Arense et al., 2010). In that work the different effects of high salt concentration were also reported, such as a lower biomass as a function of NaCl concentration and the impact in extracellular concentration of L-carnitine, which can be due to its accumulation within the cells as

osmoprotectant. Glycerol was used as C-source and the specific consumption rate resulted higher when the osmotic up-shifts took place. Besides, intracellular ATP level was also studied resulting in a sharp increase in the case of both 0.5 and 0.8M NaCl experiments, therefore coinciding with the NaCl up-shifts. This transient effect could be due to the energy demand to protect the cell against the osmotic shock. That work concluded that the metabolic flux distribution plays an important role in cell survival as well as adaptation during long-term high NaCl exposure, pointing out to the participation of the TCA cycle, glyoxylate cycle, anaplerotic pathways, glycolysis and AcCoA/acetate metabolism. However, the results indicated that further research was needed to determine the level of internal and external metabolites and monitoring their evolution through flux analysis.

The aim of this work was to provide extensive metabolic information as well as to carry out the metabolic flux analysis at the three different NaCl concentration conditions (0.08, 0.5 and 0.8M) described above, thus completing the results obtained in the work of Arense et al., (2010). The results obtained at metabolic level identify metabolic targets which can be modified in order to enforce desirable cellular properties and improve biotechnological processes. Moreover, in this work we complete the information obtained with the use of other -omic technologies such transcriptomics, which have identified groups of genes involved in the osmoadaptation process (Franzel et al., 2010). In order to estimate the critical modifications undergone to overcome stress and to develop tolerance to salt, the metabolism was examined by pathway-based integrative analysis of the metabolomic and transcriptomic levels, whose results were corroborated by fluxomics data. The internal and external metabolites and energetic cofactors showed an altered pattern with respect to that observed in control conditions (0.085 M NaCl). Interestingly, all amino acids of the culture medium were taken up as soon as the osmotic up-shift took place and important changes in redox cofactors were observed.

MATERIALS AND METHODS

Chemicals

Standard metabolites were generally supplied by Sigma Aldrich (St Louis MO, USA), but glycine and histidine were from by Merck (Madrid, Spain). Phenylalanine, tryptophan, and the chemicals used as eluents (acetonitrile, acetic acid, ammonium acetate, ammonium hydroxide, and water) were obtained from Panreac (Barcelona, Spain). All chemicals were of HPLC grade quality.

Culture conditions

The strain *E. coli* O44K74 (DSM 8828), which contains the complete *cai* and *fix* operons, was used. The standard complex medium (CM) used contained (g/L): bacteriological peptone, 20; NaCl, 5; glycerol (carbon source), 12.6; crotonobetaine, 4; and fumarate, 2. The NaCl concentration was 0.085M as stated in the text. The pH of the media was adjusted to 7.5 with 1 M KOH prior to autoclaving (Cánovas et al., 2003; Cánovas et al., 2002). Experiments were performed in Biostat B (Braun Biotech International GMBH, Melsungen, Germany) reactors equipped with temperature, pH and oxygen probes, using pump controls for continuous operation. A 2 L culture vessel with 1.8 L working volume was used. Strict anaerobiosis was maintained by bubbling nitrogen. After inoculation continuous operation was started by feeding with the complex medium at a dilution rate of 0.1 h^{-1}. At the steady state, 0.5 g/L biomass dry weight was reached. After the steady state was reached, the feeding was switched to another medium containing the new NaCl concentration (0.5 and 0.8 M, respectively).

Extracellular samples

Samples for the analysis of extracellular metabolites were withdrawn from the reactor and immediately centrifuged at 16,000 xg at 4ºC. Supernatants were used to determine fermentation products as described in Appendix (section 1). Supernatants were also used for amino acid determination with the analysis method based on HPLC-MS described below for the endometabolome analysis.

Endometabolome analysis

Quenching

Quenching was performed by harvesting cells and introducing them into the quenching solution, 60% (vol/vol) methanol/water supplemented with 0.85% ammonium bicarbonate (AMBIC), kept at -40°C. AMBIC is compatible with LC-MS analysis AMBIC, moreover it seemed to reduce osmotic shock and leakage in bacteria (Faijes et al., 2007) as well as in eukaryotic cells (Sellick et al., 2011) despite controversial results (Kronthaler et al., 2012). Afterwards, the cells were pelleted by centrifugation at 3,000 x g for 5 min at -12ºC. The contact time with the methanol solution was kept as short as possible and the temperature was always kept below -12°C, since both factors have been demonstrated to be critical (Schadel et al., 2011). The supernatant was removed by aspiration and kept for subsequent analysis to check and quantify leakage (Dietmair et al., 2010). Samples were kept at -86°C until extraction. Although, no leaking was detected, the results are expressed as fold-change and not as absolute concentrations since it is possible that no leakage was detected due to the sensitivity of the platform.

Extraction Method Validation

The extraction method used based on Lazzarino et al., (2003) was previously validated (see chapter 2) by the use of several standard mixtures. Additionally, more metabolites (amino acids and other derivatives) were tested since a more complete metabolic analysis platform was available. Indeed, more than 70 metabolites were detected. The recovery was again more than 85% in all cases (results not shown). Besides, lyophilizing or freezing during and after the extraction procedure were avoided. For this reason, samples were prepared when the analysis platform was ready to avoid potential metabolic degradation, since lyophilization has been proven to alter the composition of metabolic mixtures (Oikawa et al., 2011) due to the presence of specific labile metabolites. Additionally, this method has been successfully tested in *E. coli* samples (Montero et al., 2014).

Extraction Method Description

Metabolite extraction was based on Lazzarino et al. (2003). Samples from quenching step were re-suspended in 2 mL of extraction solution (acetonitrile + 10 mM KH2PO4 (3:1 v/v) at pH 7.4) and then incubated in a wheel for 30 minutes at 4ºC. This homogenate was centrifuged at 15,000 x g for 20 min at 4ºC. The supernatant was separated and added to 4 mL of cold chloroform and centrifuged again at 15,000 x g for 5 min. This yielded a biphasic system, from which the aqueous phase was harvested. This process was carried out twice more. The extraction procedure was finished by filtering through a sterile 0.2 µm filter before being analyzed.

Analysis Method

The separation was carried out as previously described (Preinerstorfer et al., 2010) using an injection volume of 10 µl and a ZIC-HILIC as stationary phase: 150 mm x 4.6 mm internal diameter, and 5 µm particle size, provided with a guard column, 20 x 2.1 mm, 5 µm (Merck SeQuant, Marl, Germany) at a temperature of 25oC. For metabolite elution, a gradient method was used with a flow rate of 0.5 ml/min. Mobile phases were 20 mM ammonium acetate (adjusted to pH 7.5 with NH4OH) in H2O (solvent A) and 20 mM ammonium acetate in AcN (solvent B). Gradient elution was performed, starting with 0% A and increasing to 80% A over 30 minutes, then return to starting conditions (80-0% A) for 1 minute followed by a re-equilibration period (0% A) of 14 minutes (total run time, 45 minutes). Data were acquired by a PC using the Agilent Chemstation software package provided by the HPLC manufacturer. Measurements for quantification were conducted using single ion monitoring (Bravo et al., 2011). The measured metabolites and the SIM ions used for quantification are summarized in Table 1. LC-MS experiments were performed on a 1200 series HPLC instrument (Agilent Technologies; California, USA) coupled to an Agilent 6120 single quadrupole mass spectrometer with orthogonal ESI source. The apparatus can be used in positive or negative ionization mode in either SCAN or SIM mode (Agilent Technologies). The mass spectrometer was operated in the positive ESI mode, using the SIM mode for the m/z of each compound. The ion spray voltage was set at 4000 V. Nitrogen with a flux of 12 L/min was used as the sheath gas (35 psi) and the

auxiliary gas. The ion transfer capillary was heated to 300ºC. The fragmentation voltage was set at 100 V.

Metabolite Identification

Prior to the quantification process, the metabolites were identified using the retention time and relative intensities of the diagnostic ions of a pool of samples. For that, the mass spectra of single and pure standards were recorded and compared with the mass spectra of a pool of samples at the corresponding retention time. At least three diagnostic ions (preferably including the molecular ion) must be found, and their relative intensities should correspond to those of the sample (see recent EU regulation for details) (Document No. SANCO/12495/2011). If the concentration of the metabolites in the sample was not sufficient to generate a clear spectrum, and a metabolite could not be unequivocally identified, pure calibration standards were spiked and the mass spectrum was recorded again. The diagnostic ions used as well as their relative intensities are summarized in Table 1. Due to the limitations of a single quadrupole for identifying isobaric compounds, their separation was confirmed by chromatography.

Quality Control

The quality of the results was assessed by: (i) checking the extraction method with standard mixtures, (ii) internal standard (IS), and (iii) quality control samples (QC). The extraction method was validated by comparing the concentration of standard mixtures with and without the extraction process. Recoveries were higher than 85% in all of the analysed metabolites (results not shown). N-acetyl-L-glutamine (m/z 189) was added as IS (Bajad et al., 2006), reaching a final concentration of 50 µM in each analyzed sample, and the analysis was monitored by controlling that the internal standard area and retention time were always within an acceptable range. Acceptable coefficient of variation was set at 20% for the peak area and 2% for retention time.

With respect to quality control samples, two types of QC were incorporated in the analysis: (i) a pool of samples and (ii) a pool of standards. QC analysis was performed in all of the analysed metabolites in the standard pool and in all those in

which concentrations were over the quantification limits of the sample pools. This was carried out by comparing the corrected areas. For the standard pool, the theoretical corrected area was calculated for the measured concentration. Regarding the pool of samples, the corrected areas were compared among all of the samples. An acceptable coefficient of variation was set at 20% for the peak area and 2% for retention time. QC samples were included in the analysis of the whole set of 20 biological samples. Additionally, random samples were analysed.

Quantitative Analysis

The platform EasyLCMS (Fructuoso et al., 2012) was used for automated quantification. Standard and sample areas were normalized using the following formula, as previous established (Bunk et al., 2006):

$$A_N = \frac{A \cdot N}{A_{IS}}$$

In the formula above A is the standard or sample area without normalization, A_N is the normalized area, N is the normalization value (10^6 by default), and A_{IS} is the internal standard area. Although the use of at least one internal standard representative is recommended for each chemical class, it has been reported that normalization with N-acetyl-glutamine gave similar results to isotope-labelled standards for several metabolic groups including nucleoside bases, nucleosides, nucleotides, amino acids, redox carriers, and vitamins, among others (Bajad et al., 2006), and therefore this has been selected as an internal standard for all of the analyzed metabolites.

Statistical analysis

The statistical analysis was performed using the Bioconductor suite (Gentleman et al., 2005) in R (R Development Core Team, 2014). Missing values were replaced by the half of the minimum positive value in the original uploaded file. The resultant data were normalized by the dry weight of the samples, scaled by mean subtraction, and divided by the standard deviation of each metabolite (autoscaling), since this scaling

method has been demonstrated to perform optimally in attending to biological expectations (van den Berg et al., 2006). Afterwards, differentially metabolite concentrations were identified by one-way ANOVA, followed, by Tukey's HSD post-hoc test were used to analyse between-group differences when variance was assumed to be homogeneous, or Welch ANOVA followed, by Games–Howell post-hoc test was used when the data violated the assumption of homogeneity of variance with a p-value cut-off of 0.05, adjusted with Benjamini and Hochberg's method (Benjamini and Hochberg, 1995). Shapiro-Wilk and Bartlett tests were used to check for normality and homoscedascity respectively. Furthermore, the fold-change had to exceed a factor of 2 at 0.8 M NaCl and 1.3 at 0.5 M NaCl compared with the initial steady state values for metabolites to be considered.

Transcriptomic analysis

Time-course microarray experiment design; RNA extraction and microarray sample preparation; microarray data analysis and GO enrichment analysis were performed as described in Appendix (section 2).

Pathway-based integrative analysis

Transcriptomic data (Appendix, section 3) and intra-metabolomic results were integrated using pathway analysis based on KEGG pathways. Genes were annotated using the KEGG Escherichia coli K-12 MG1655 database. Similarly, traditional metabolite names were translated into KEGG compound database identifiers. KEGG XML data files were downloaded from the *Escherichia coli* K-12 MG1655 database, which are freely available for academic users from the KEGG website (Kanehisa et al., 2014). SubpathwayMiner (Li et al., 2009) was used for mapping previously identified genes and metabolites to pathways for overrepresentation analysis using the hypergeometric test. P-values were adjusted with Benjamini and Hochberg's method (Benjamini and Hochberg, 1995) and a cut-off value of 0.05 was set. This analysis led to a list of overrepresented pathways, which were visualized using the Pathview R package (Luo and Brouwer, 2013).

Metabolic Flux Analysis

A previously developed *E. coli* large-scale stationary model (Sevilla et al., 2005a), including a model of carnitine metabolism (Sevilla et al., 2005b) and anaerobic conditions was used. The software used was Insilico Discovery (Insilico Biotechnology AG, Stuttgart, Germany), version 2.00, which allowed us to perform the Metabolic Flux Analysis for the different conditions. The model had 13 degrees of freedom, which could be solved with experimental fluxes: (i) glycerol, fumarate and crotonobetaine in the feeding medium, (ii) fermentation products (ethanol, pyruvate, acetate and lactate) and (iii) crotonobetaine derivates (L-carnitine and γ-butyrobetaine) in the effluent medium (Appendix, section 4). Pro U and biomass fluxes were determined as previously described (Sevilla et al., 2005a).

Table 1. LC-ESI-MS analytical parameters and method performance for compound standards of the quantified metabolites.

Metabolite	Abbreviation	Parent ion formula	Diagnostic ions (relative abundance)	RT (min)	SIM ion	LOD[a] (nmol/mL)	LOQ[b] (nmol/nM)	R^2	Intraday[c] RSD (%)	Interday[c] RSD (%)
Glycine	**Gly**	$C_2H_6NO_2^+$	76 (82), 98 (8), 150 (52)	15.0	76	4.71	15.71	0.9782	8.75	12.2
L-Alanine	**Ala**	$C_3H_8NO_2^+$	90 (100),112 (13), 134 (5)	14.3	90	4.81	16.03	0.9944	1.94	8.4
L-Serine	**Ser**	$C_3H_8NO_3^+$	88 (20), 106 (100),128 (10)	13.2	106	0.02	0.05	0.9826	1.50	9.3
L-Proline	**Pro**	$C_5H_{10}NO_2^+$	70 (2), 116 (100),138 (10)	25.8	116	0.90	3.0	0.9905	1.38	18.2
L-Valine	**Val**	$C_5H_{12}NO_2^+$	72 (5), 118 (80), 140 (15)	12.6	118	0.83	2.77	0.9935	1.14	11.5
L-Threonine	**Thr**	$C_4H_8NO_3^+$	74 (5), 120 (100),142 (10)	10.0	120[d]	0.91	3.03	0.9824	28.85	6.5
L-Homoserine	**HomoSer**	$C_4H_{10}NO^+$	74 (5), 120 (100),142 (8)	14.2	120[d]	0.28	0.94	0.9981	0.79	15.2
L-Cysteine	**Cys**	$C_3H_8NO_2S^+$	102 (10), 122 (42), 144 (44)	11.7	122	0.91	3.02	0.9992	1.36	7.9
Taurine	**Taurine**	$C_2H_6NO_3S^+$	126 (100), 146 (10), 148 (12), 251 (15)	12.1	126	3.11	10.36	0.9950	2.40	5.8
Thymine	**Thymine**	$C_5H_7N_2O_2^+$	127 (100),149 (10), 171 (10)	4.0	127	0.07	0.22	0.9991	0.45	13.7
L-Hydroxyproline	**HydroxyPro**	$C_5H_9NO_3^+$	86 (50), 132 (100),154 (10)	10.7	132[d]	1.73	5.77	0.9947	13.41	18.6
L-Isoleucine	**Ile**	$C_6H_{14}NO_2^+$	86 (50), 132 (100),154 (10)	11.3	132[d]	0.45	1.5	0.9899	0.33	5.2
L-Leucine	**Leu**	$C_6H_{14}NO_2^+$	86 (10), 132 (100),154 (20)	14.1	132[d]	0.07	0.25	0.9926	1.22	16.7
L-Asparagine	**Asn**	$C_4H_9N_2O_3^+$	87 (10), 133 (100),155 (10)	14.5	133[d]	1.10	3.66	0.9834	1.31	0.9
L-Ornithine	**Orn**	$C_5H_{13}N_2O_2^+$	115 (25), 133 (100),155 (10)	26.5	133[d]	0.43	1.43	0.9902	0.44	2.5
L-Aspartic acid	**Asp**	$C_4H_6NO_4^+$	121 (20), 134 (100), 200 (75)	15.2	134	6.28	20.93	0.9837	2.78	4.9
L-Homocysteine	**HomoCys**	$C_4H_{10}NO_2S^+$	90 (10), 136 (100),158 (10)	12.4	136	1.14	3.82	0.9859	0.37	6.7
Hypoxanthine	**Hypoxan**	$C_5H_5N_4O^+$	137 (70),159 (100), 175 (10)	11.0	137	0.23	0.77	0.9986	2.52	10.2
Acetylphosphate	**Acetyl-P**	$C_2H_4O_5P^+$	116 (100), 141 (23),163 (13)	15.3	141	0.76	2.53	0.9910	7.76	11.9
O-Phosphorylethanolamine	**OPE**	$C_2H_8NO_4P^+$	111 (5), 142 (100), 164 (10)	18.0	142	26.34	87.80	0.9705	4.0	8.4
L-Lysine	**Lys**	$C_6H_{15}N_2O_2^+$	84 (8), 130 (30), 147 (100),169 (8)	25.9	147[d]	0.10	0.35	0.9892	1.10	12.6
L-Glutamine	**Gln**	$C_5H_{11}N_2O_3^+$	130 (50), 147 (100),169 (67)	14.7	147[d]	0.73	2.45	0.9901	3.91	9.9
L-Glutamic acid	**Glu**	$C_5H_{10}NO_4^+$	102 (60), 148 (100), 170 (30),	14.9	148	0.37	1.23	0.9882	0.64	5.4
L-Methionine	**Met**	$C_5H_{12}NO_2S^+$	104 (8), 150 (100),172 (15)	11.6	150	0.01	0.04	0.99	1.50	3.4
L-Histidine	**His**	$C_6H_{10}N_3O_2^+$	137 (25), 156 (100), 178 (5)	15.0	156	0.24	0.79	0.9801	7.08	21.5
L-Carnitine	**Carnitine**	$C_7H_{16}NO_3^+$	149 (1), 162 (100),184 (5)	15.7	162	0.02	0.08	0.9899	4.04	7.9

L-Phenylalanine	**Phe**	$C_9H_{12}NO_2^+$	137 (35), 166 (100), 188 (20)	9.9	166	0.74	2.47	0.9987	2.08	12.5
L-Arginine	**Arg**	$C_6H_{13}N_4O_2^+$	140 (5), 175 (100),197 (2)	24.5	175	0.02	0.08	0.9950	1.47	16.4
L-Citrulline	**CIR**	$C_6H_{12}N_3O_3^+$	159 (19), 176 (100),198 (18)	15.3	176	0.38	1.26	0.9846	26.65	14.2
Glucosamine	**Glucosamine**	$C6H14NO_{5+}$	162 (35), 180 (100), 202 (10)	14.4	180	3.45	10.95	0.9940	14.3	7.9
L-Tyrosine	**Tyr**	$C_9H_{12}NO_3^+$	163 (15), 182 (100),204 (5)	12.1	182	0.76	2.55	0.9892	0.97	6.4
O-Phospho-L-Serine	**P-serine**	$C_3H_9NO_6P^+$	88 (18), 186 (100), 208 (5)	16.3	186	3.24	10.8	0.9923	1.19	0.5
2-Phosphogliceric acid	**2PG**	$C_3H_7O_7P^+$	187 (92),209 (33), 231 (19)	16.1	187 [d]	1.87	6.23	0.9924	0.70	3.1
3-Phosphogliceric acid	**3PG**	$C_3H_7O_7P^+$	187 (92),209 (33), 231 (19)	17.1	187 [d]	0.37	1.24	0.9932	0.82	4.0
N-Acetyl-L-Glutamine	**Ac-Gln**	$C_7H_{12}N_2O_4^+$	172 (15), 189 (80), 211 (60)	13.3	189	5.8	17.9	0.9812	2.6	0.6
L-Tryptophan	**Trp**	$C_{11}H_{13}N_2O_2^+$	177 (10), 205 (100),227 (30)	10.1	205	2.99	9.97	0.9897	5.13	2.4
L-Cystine	**Cystin**	$C_6H_{12}N_2O_4S_2^+$	156 (100), 241 (30), 263 (18)	17.0	241	12.07	40.24	0.9577	3.97	0.8
Thymidine	**Thymidine**	$C_{10}H_{13}N_2O_5^+$	243 (38), 265 (100), 281 (38)	4.2	243	0.17	0.57	0.9949	0.19	1.4
Biotin	**Biotin**	$C_{10}H_{17}N_2O_3S^+$	245 (43),267 (30), 527 (55)	10.8	245	1.52	5.07	0.9974	4.87	16.1
2'-Deoxyadenosine	**DA**	$C_{10}H_{14}N_5O_3^+$	139 (10), 252 (100), 274 (15)	5.2	252	0.04	0.13	0.9946	0.55	13.0
Glucosamine 6-phosphate	**GlucN6P**	$C_6H_{15}NO_8P^+$	242 (32), 260 (100),282 (8)	17.4	260	7.83	26.12	0.9993	2.06	5.1
L-Glutathione	**GSH**	$C_{10}H_{18}N_3O_6S^+$	308 (100),330 (10),618 (10)	14.6	308	5.64	18.82	0.9864	0.30	6.4
Thymidine monophosphate	**TMP**	$C_{10}H_{16}N_2O_8P^+$	207 (25), 323 (100),345 (50)	14.4	323	15.8	52.4	0.9799	4.1	0.8
Cytidine monophosphate	**CMP**	$C_9H_{15}N_3O_8P^+$	112 (20), 266 (10), 324 (100)	16.0	324	1.25	4.18	0.9881	5.07	0.9
Uridine monophosphate	**UMP**	$C_9H_{14}N_2O_9P^+$	172 (90), 325 (100), 342 (25)	15.0	325	26.55	88.51	0.9820	3.53	10.6
Thiamine monophosphate	**ThiaMP**	$C_{12}H_{18}N_4O_4PS^+$	122 (25), 345 (100), 367 (15)	20.5	345	2.3	7.6	0.9812	12.4	14.6
Adenosine monophosphate	**AMP**	$C_{10}H_{11}N_5O_6P^+$	268 (15), 348 (100), 370 (10)	14.7	348	0.64	2.15	0.9910	2.04	18.4
Inosine monophosphate	**IMP**	$C_{10}H_{14}N_4O_8P^+$	138 (50), 349 (100),371 (41)	15.4	349	93.71	312.39	0.9810	11.13	23.1
Guanosine monophosphate	**GMP**	$C_{10}H_{15}N_5O_8P^+$	344 (18), 364 (100), 386 (42)	16.3	364	4.48	14.92	0.9885	10.29	9.1
Xanthosine monophosphate	**XMP**	$C_{10}H_{14}N_4O_9P^+$	157 (50), 365 (100),387 (27)	15.7	365	17.85	59.49	0.9945	2.57	5.4
Cytidine diphosphate	**CDP**	$C_9H_{14}N_3O_{11}P_2^+$	381 (40),404 (100),426 (48)	16.0	404	2.32	7.74	0.9822	5.48	8.8
Uridine diphosphate	**UDP**	$C_9H_{13}N_2O_{12}P_2^+$	301 (95), 405 (100), 427 (60)	15.4	405	73.50	350.02	0.9949	2.42	0.9
Adenosine diphosphate	**ADP**	$C_{10}H_{14}N_5O_{10}P_2^+$	348 (40),428 (100), 450 (20)	15.7	428	1.95	5.50	0.9941	2.07	9.4
Guanosine diphosphate	**GDP**	$C_{10}H_{14}N_5O_{11}P_2^+$	150 (85), 444 (100),466 (38)	16.0	444	4.70	15.67	0.9940	5.33	5.4

Tetrahydrofolic acid	**THF**	$C_{19}H_{23}N_7O_6^+$	399 (100), 446 (20), 468 (17)	16.0	446	1.06	3.54	0.9930	1.55	16.4
Riboflavin-5'-monophosphate	**FMN**	$C_{17}H_{20}N_4O_9P^+$	399 (30), 457 (100),479 (30)	13.6	457	2.33	7.76	0.9942	2.17	11.5
Deoxycytidine triphosphate	**dCTP**	$C_9H_{15}N_3O_{13}P_3^+$	397 (50), 468 (100), 490 (75)	16.5	468	10.8	30.7	0.9991	18.6	22.1
Deoxythymidine triphosphate	**TTP**	$C_{10}H_{16}N_2O_{14}P_3^+$	419 (40), 483 (100), 505 (50)	15.2	483	34.72	115.75	0.9811	0.96	10.0
Cytidine triphosphate	**CTP**	$C_9H_{15}N_3O_{14}P_3^+$	177 (43) , 484 (100),506 (60)	16.7	484	0.62	2.08	0.9501	12.17	8.4
Uridine triphosphate	**UTP**	$C_9H_{14}N_2O_{15}P_3^+$	485 (100), 507 (50), 589 (20)	15.9	485	2.25	7.49	0.9961	5.56	13.7
CDP-choline	**CDP-choline**	$C_{14}H_{27}N_4O_{11}P_2^+$	112 (20), 489 (100), 511 (80)	17.0	489	9.41	31.38	0.9949	5.70	4.6
Deoxyadenosine triphosphate	**dATP**	$C_{10}H_{15}N_5O_{12}P_3^+$	252 (100), 492 (20),512 (5)	15.3	492	5.9	18.1	0.9926	9.7	5.7
adenosine triphosphate	**ATP**	$C_{10}H_{15}N_5O_{13}P_3^+$	410 (15),508 (100),530 (20)	15.6	508	7.68	25.62	0.9877	1.74	12.5
Inosine triphosphate	**ITP**	$C_{10}H_{14}N_4O_{14}P_3^+$	475 (50), 509 (100),531 (49), 553 (35)	16.4	509	11.71	30.06	0.9722	2.12	8.4
Guanosine triphosphate	**GTP**	$C_{10}H_{15}N_5O_{14}P_3^+$	213 (15), 524 (100),546 (30)	16.5	524	22.16	73.86	0.9883	9.11	20.4
L-Glutathione oxidised form	**GSSG**	$C_{20}H_{33}N_6O_{12}S_2^+$	307 (100),613 (100),635 (50)	16.5	613	4.09	13.63	0.9913	4.84	5.4
Nicotinamide adenine dinucleotide oxidised form	**NAD^+**	$C_{21}H_{26}N_7O_{14}P_2^+$	123 (20), 333 (30), 664 (100),686 (50)	15.2	664	3.44	11.46	0.9943	3.08	6.7
Nicotinamide adenine dinucleotide reduced form	**NADH**	$C_{21}H_{28}N_7O_{14}P_2^+$	334 (70), 666 (80),688 (50)	16.0	666	49.24	164.15	0.9834	4.51	7.8
Nicotinamide adenine dinucleotide phosphate oxidised form	**$NADP^+$**	$C_{21}H_{29}N_7O_{17}P_3^+$	123 (50), 744 (100),766 (37)	16.6	744	3.91	13.03	0.9947	2.12	0.8
Nicotinamide adenine dinucleotide phosphate reduced form	**NADPH**	$C_{21}H_{27}N_7O_{17}P_3^+$	315 (25), 746 (25), 768 (10)	16.0	746	0.33	1.12	0.9875	2.52	0.4
Coenzyme A	**CoA**	$C_{21}H_{37}N_7O_{16}P_3S^+$	385 (60),768 (100),790 (25)	14.8	768	18.65	62.18	0.9913	6.79	9.7
Acetyl-CoA	**AcCoA**	$C_{23}H_{39}N_7O_{17}P_3S^+$	406 (100),810 (95),832 (25)	14.1	810	16.38	54.60	0.9881	2.89	1.4

[a] LOD calculated from standard deviation of memory peak areas of blank runs: 3 x standard deviation of memory peak area (n=6)/slope of calibration function with neat standard solutions.

[b] LOD calculated from standard deviation of memory peak areas of blank runs: 10 x standard deviation of memory peak area (n=6)/slope of calibration function with neat standard solutions.

[c] The intra- and inter-day precision were determined by analyzing six replicates of the standards at the same concentration level and calculated as the relative standard deviation (RSD) defined as the ratio of the standard deviation to the mean response factor of each metabolite.

[d] Chromatographically separated.

RESULTS

Extracellular amino acids depletion after osmotic up-shifts

Evolution of amino acid intake was correlated (Figure 1) with the NaCl concentration (0.5 and 0.8 M NaCl). In general, all the amino acids in the medium reached a steady state during the system evolution at control NaCl concentration (0.085M, before t = 0), indicating a constant uptake rate. Surprisingly, after medium was switched over to high or very high NaCl concentrations, all measured amino acids (Asp, Glu, Asn, Thr, Tyr, Pro, Ala, Met, Val, Leu, Iso, His, Lys and Arg) depleted. Moreover, this effect was more dramatic at 0.8 M than at 0.5 M NaCl (Figure 1), since amino acid total depletion took place after 20h of adding 0.5M NaCl supplemented medium and 7h after the addition of 0.8M NaCl supplemented medium.

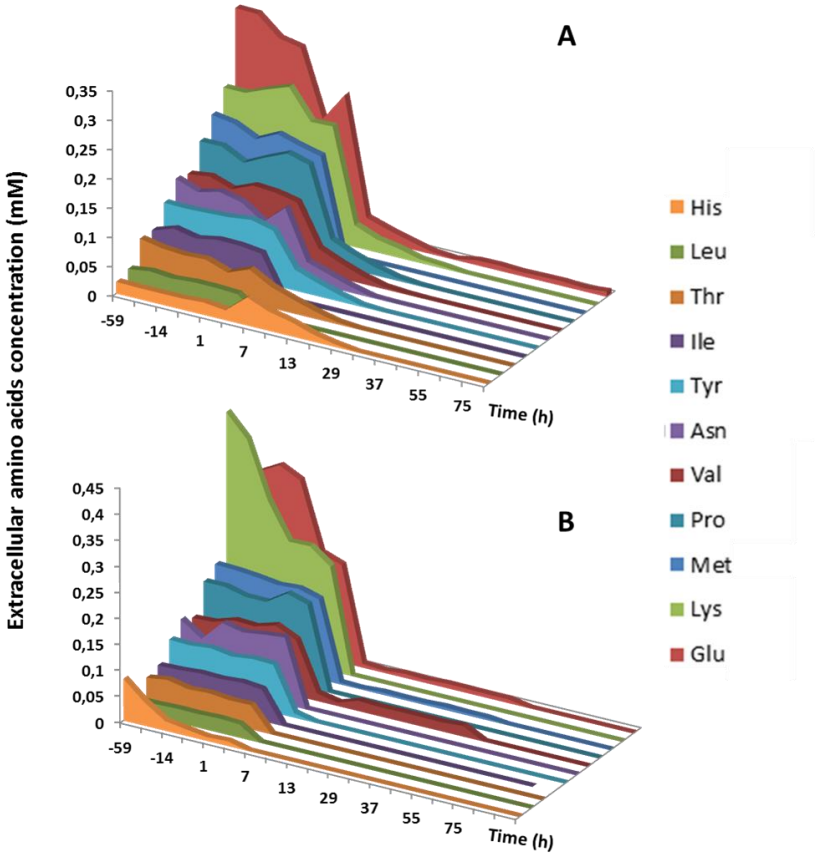

Figure 1. Extracellular amino acid concentration profiles during the chemostat culture. Before t=0 the chemostat corresponds to control NaCl concentration (0.085M). After t=0 the osmotic up-shift took place with: A) high NaCl concetration (0.5 M) and B) very high NaCl concetration (0.8M).

Principal component analysis (PCA) of the intra-metabolome

In Figure 2, PCA of the intra-metabolome long-term adaptation to osmotic up-shift at high (0.5 M) and very high (0.8 M) NaCl concentrations is depicted. PC1 encompass more than 90% of total variance showing clear differences among sample bundles.

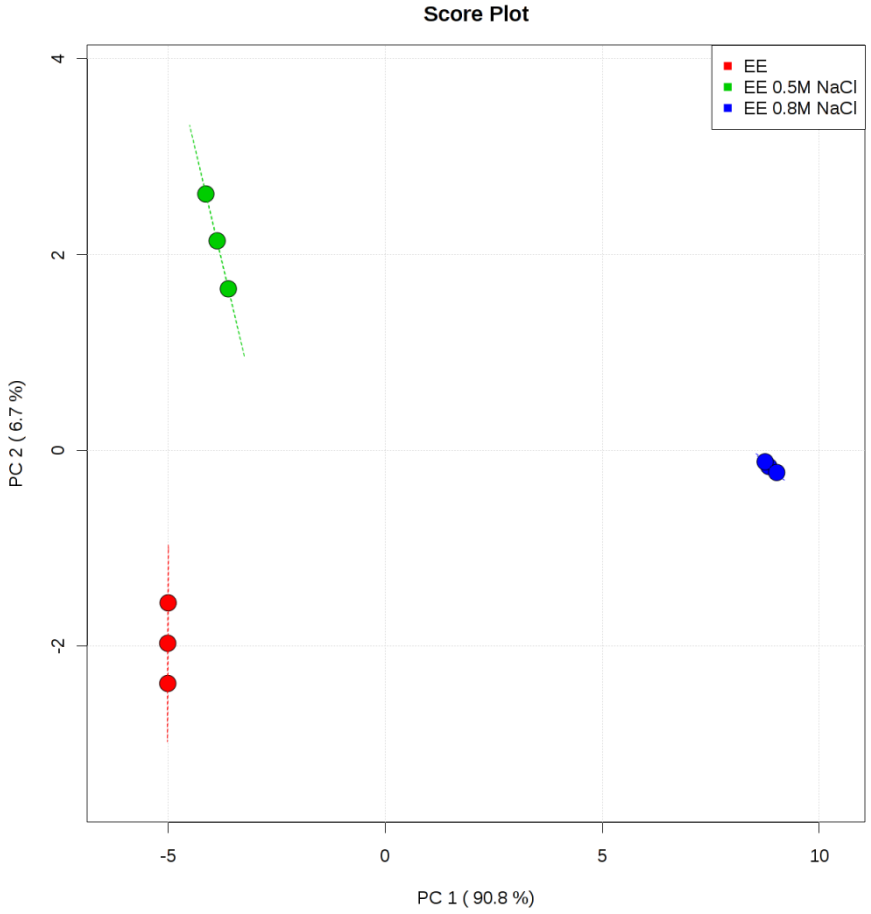

Figure 2. Scores plot of the PCA of the intracellular metabolome at the three stationary states reached (red, control NaCl concentration; green, 0.5M NaCl and blue, 0.8M NaCl).

Regarding samples that correspond to 0.8M NaCl steady-state (blue), it is important to highlight that this group presents the most pronounced separation which shows the drastic effect in the metabolic profile. In Table 2, 3 and 4 the fold-changes and p-values of the metabolites after reaching a new steady state in the presence of 0.5 or 0.8 M NaCl are shown.

Major differences between intracellular metabolic concentrations

Redox metabolites

NADH and GSH were almost depleted at 0.8 M NaCl and, as a consequence, NADH/NAD^+ and GSH/GSSG ratios were reduced. However, the concentration of NADPH and $NADP^+$ increased according to NaCl concentration, particularly at 0.8 M when their concentrations were almost 150 and 290 times respectively higher than the control condition. Table 2 depicts the intracellular concentrations of redox metabolites.

Table 2. Fold changes and p-values of redox metabolites after reaching a new steady state in the presence of 0.5 or 0.8 M NaCl. One-way ANOVA, followed, by Tukey's HSD post-hoc test were used to analyse between-group differences when variance was assumed to be homogeneous, or Welch ANOVA followed, by Games–Howell post-hoc test with the Benjamini-Hochberg FDR correction was used when the data violated the assumption of homogeneity of variance. Shapiro-Wilk and Bartlett tests were used to check for normality and homoscedascity respectively. Abbreviations are described in Table 1.

Redox metabolite	KEGG Id	Fold change 0.5M NaCl	Fold change 0.8 M NaCl	ANOVA	Post hoc p-value 0.5M NaCl-Control	Post hoc p-value 0.8M NaCl-Control	Post hoc p-value 0.5M NaCl-0.8M NaCl
NADH	C00004	-3.3	**<-200**[#]	<0.001***	<0.001***	<0.001***	0.025*
GSH	C00051	1	**<-150**[#]	<0.001***		0.007**	<0.001***
NAD	C00003	-1	**2.8**	<0.001***		<0.001***	<0.001***
NADPH	C00005	2.9	**143.4**	<0.001***		0.006**	0.006**
FMN	C00061	8.6	**159.7**	<0.001***	0.025*	0.006**	0.006**
NADP	C00006	3.1	**285.1**	<0.001***		0.006**	0.006**
GSSG	C00127	>300[#]	**>20000**[#]	<0.001***		<0.001***	<0.001***

#Estimated taking into account detection limits since these metabolites were below quantification limits

Amino acids

Some intracellular amino acids such as His and Cys were almost depleted in situations of high and very high concentration of NaCl (Table 3). The remaining amino acid concentrations were higher at 0.5 M than control conditions, some of them (Arg, Gly and Asp) being 2-fold and even more 0.8 M NaCl where Val even showed a 100-fold and Gln more than 2000.

Table 3. Fold changes and p-values of amino acids after reaching a new steady state in the presence of 0.5 or 0.8 M NaCl. One-way ANOVA, followed, by Tukey's HSD post-hoc test were used to analyse between-group differences when variance was assumed to be homogeneous, or Welch ANOVA followed, by Games–Howell post-hoc test with the Benjamini-Hochberg FDR correction was used when the data violated the assumption of homogeneity of variance. Shapiro-Wilk and Bartlett tests were used to check for normality and homoscedascity respectively. Abbreviations are described in Table 1.

Amino acid	KEGG Id	Fold change 0.5M NaCl	Fold change 0.8 M NaCl	ANOVA	Post hoc p-value 0.5M NaCl-Control	Post hoc p-value 0.8M NaCl-Control	Post hoc p-value 0.5M NaCl-0.8M NaCl
Cys	C00097	<-50[#]	**<-50[#]**	<0.001***	<0.001***	<0.001***	
His	C00135	-12.3	**<-40[#]**	<0.001***	<0.001***	<0.001***	
Cystin	C00491	2.7	**-2.7**	<0.001***		0.003**	0.023*
P-serine	C01005	1.2	**7.9**	<0.001***	<0.001***	0.006**	0.006**
HomoCys	C00155	1.5	**8.5**	<0.001***	0.015*	0.006**	0.006**
Trp	C00078	1	**12.1**	<0.001***	0.019*	0.006**	0.006**
Taurine	C00245	1.5	**12.2**	<0.001***		<0.001***	<0.001***
Thr	C00188	1.7	**12.3**	0.002**		0.006**	0.006**
Tyr	C00082	1.5	**12.4**	<0.001***	<0.001***	0.006**	0.006**
Glu	C00025	1.4	**12.8**	<0.001***	0.018*	0.006**	0.006**
Gly	C00037	1.4	**13.2**	<0.001***	<0.001***	0.006**	0.006**
Ala	C00041	1.4	**13.3**	<0.001***	0.019*	0.006**	0.006**
Arg	C00062	1.6	**14.6**	<0.001***	<0.001***	0.006**	0.006**
Ileu	C00407	1.6	**15.9**	<0.001***	0.049*	0.006**	0.006**
Phe	C00079	1.5	**16.1**	<0.001***	0.013*	0.006**	0.006**
HydroxyPro	C01157	1.6	**16.3**	<0.001***	0.01***	0.006**	0.006**
Leu	C00123	1.5	**18.2**	<0.001***	0.018*	0.006**	0.006**
Lys	C00047	1.3	**20.3**	<0.001***	<0.001***	0.006**	0.006**
Asp	C00049	2.3	**22.5**	<0.001***	0.033*	0.006**	0.006**
HomoSer	C00263	3.3	**50.7**	<0.001***		<0.001***	<0.001***
3PG	C00197	6.2	**79.6**	<0.001***	0.004**	0.006**	0.006**
Val	C00183	4.9	**105.3**	<0.001***	<0.001***	0.006**	0.006**
Gln	C00064	1	**>2000[#]**	<0.001***		<0.001***	<0.001***

#Estimated taking into account detection limits since these metabolites were below quantification limits.

Nucleotides, CoA derivatives and other metabolites

The levels of ATP and GMP were almost depleted at 0.8 M salt (Table 4). However, the remaining nucleotide concentrations increased when the concentration of NaCl was higher, this being much higher in the case of 0.8M of NaCl. Despite the stress exerted on the environment of cells, their metabolism

tended to withstand the robustness of the system. In fact, the AcCoA/CoA ratio did not have important alterations during the three assayed conditions: control, 0.5 and 0.8 M salt concentration (Figure 3).

Table 4. Fold changes and p-values of the metabolites after reaching a new steady state in the presence of 0.5 or 0.8 M NaCl. One-way ANOVA, followed, by Tukey's HSD post-hoc test were used to analyse between-group differences when variance was assumed to be homogeneous, or Welch ANOVA followed, by Games–Howell post-hoc test with the Benjamini-Hochberg FDR correction was used when the data violated the assumption of homogeneity of variance. Shapiro-Wilk and Bartlett tests were used to check for normality and homoscedascity respectively. Abbreviations are described in Table 1.

Metabolite	KEGG Id	Fold change 0.5M NaCl	Fold change 0.8 M NaCl	ANOVA	Post hoc p-value 0.5M NaCl-Control	Post hoc p-value 0.8M NaCl-Control	Post hoc p-value 0.5M NaCl-0.8M NaCl
ATP	C00002	-4	**<-20**[#]	<0.001***	0.002**	<0.001***	
GMP	C00144	<-20	**<-2**	0.03*	0.045*	0.045*	
CoA	C00010	-1.3	**7.1**	0.002**		0.006**	0.006**
AcCoA	C00024	-1.1	**7.3**	<0.001***		<0.001***	<0.001***
ITP	C0081	>20[#]	**>8**[#]	<0.001***		<0.001***	<0.001***
ADP	C00008	1.9	**9.5**	<0.001***		<0.001***	<0.001***
Biotin	C00120	2.3	**9.9**	<0.001***		<0.001***	<0.001***
ThiaMP	C01081	1.4	**14.5**	<0.001***	0.013*	0.006**	0.006**
Carnitine	C00318	1.9	**15.9**	<0.001***	<0.001***	0.006**	0.006**
IMP	C00130	1.2	**17.4**	<0.001***		0.006**	0.006**
UMP	C00105	3	**27.2**	<0.001***	0.003**	0.006**	0.006**
TMP	C00364	3	**29.3**	<0.001***	0.013*	0.006**	0.006**
CTP	C00063	1.4	**32**	<0.001***		<0.001***	<0.001***
CMP	C00055	3.3	**32.3**	<0.001***	0.005**	0.006**	0.006**
3PG	C00197	6.2	**79.6**	<0.001***	0.004**	0.006**	0.006**
Acetyl-P	C00227	4.5	**85.7**	<0.001***	<0.001***	0.006**	0.006**
OPE	C00346	5.9	**120.3**	<0.001***	<0.001***	0.006**	0.006**
2PG	C00631	97.8	**2886**	<0.001***	0.004**	0.006**	0.006**
Hypoxan	C00262	1	**>1400**[#]	<0.001***		<0.001***	<0.001***
UTP	C00075	>80[#]	**>5000**[#]	<0.001***		<0.001***	<0.001***

#Estimated taking into account detection limits since these metabolites were below quantification limits

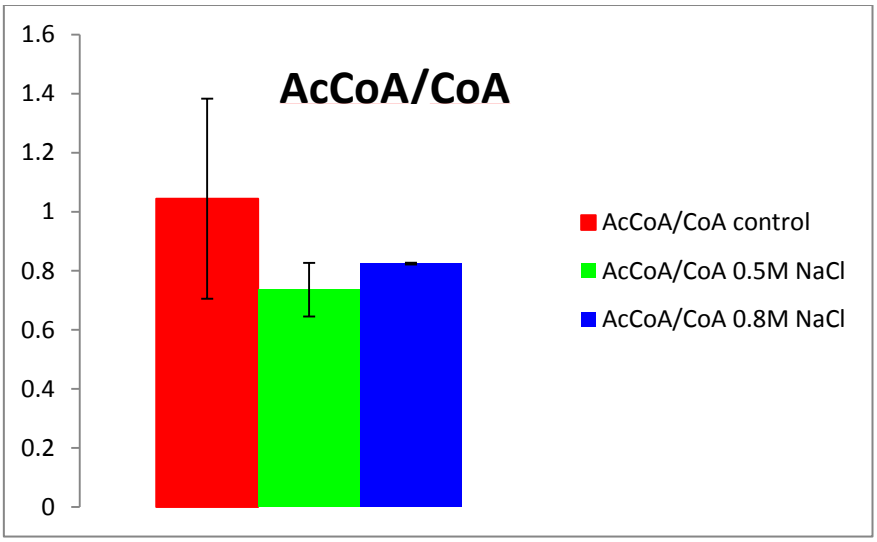

Figure 3. AccoA/CoA ratio (average ± s.e.m.) in the steady-state of the chemostats carried out (see Materials and Methods for details).

Metabolic flux analysis at two different NaCl concentrations with a large-scale stationary *E. coli* model

In order to compare the metabolic flux distribution in the different NaCl conditions, a large-scale stationary *E. coli* model (Sevilla et al., 2005a) was used to perform a metabolic flux analysis at three stationary states (control, 0.5 and 0.8 M NaCl). To deal with 13 degrees of freedom of this model, 14 fluxes were used. The experimental fluxes perfectly matched those obtained with the model, confirming the correlation between the model results and the experimental data. Figure 4 depicts a general overview of the fluxes in the large-scale stationary in which metabolic fluxes were normalized using the glycerol income flux to compare them during the different steady states. The principal outcome of this analysis was the evident different fermentation pattern in each case: (i) the acetate production was decreased for both NaCl concentrations (0.5 and 0.8M); (ii) at 0.5M NaCl the ethanol production was higher than at control conditions; (iii) at 0.8M NaCl, the lactate generation was more than double but ethanol production was lower. At 0.5M NaCl, pyruvate conversion to AcCoA through PDH was reduced which means lower NADH formation. On the other hand, at 0.8M, PDH flux was completely abolished, whereas PYRFL flux increased. The glyoxylate pathway flux increased at 0.5 and 0.8 M NaCl, being higher at very high NaCl concentration (0.8 M).

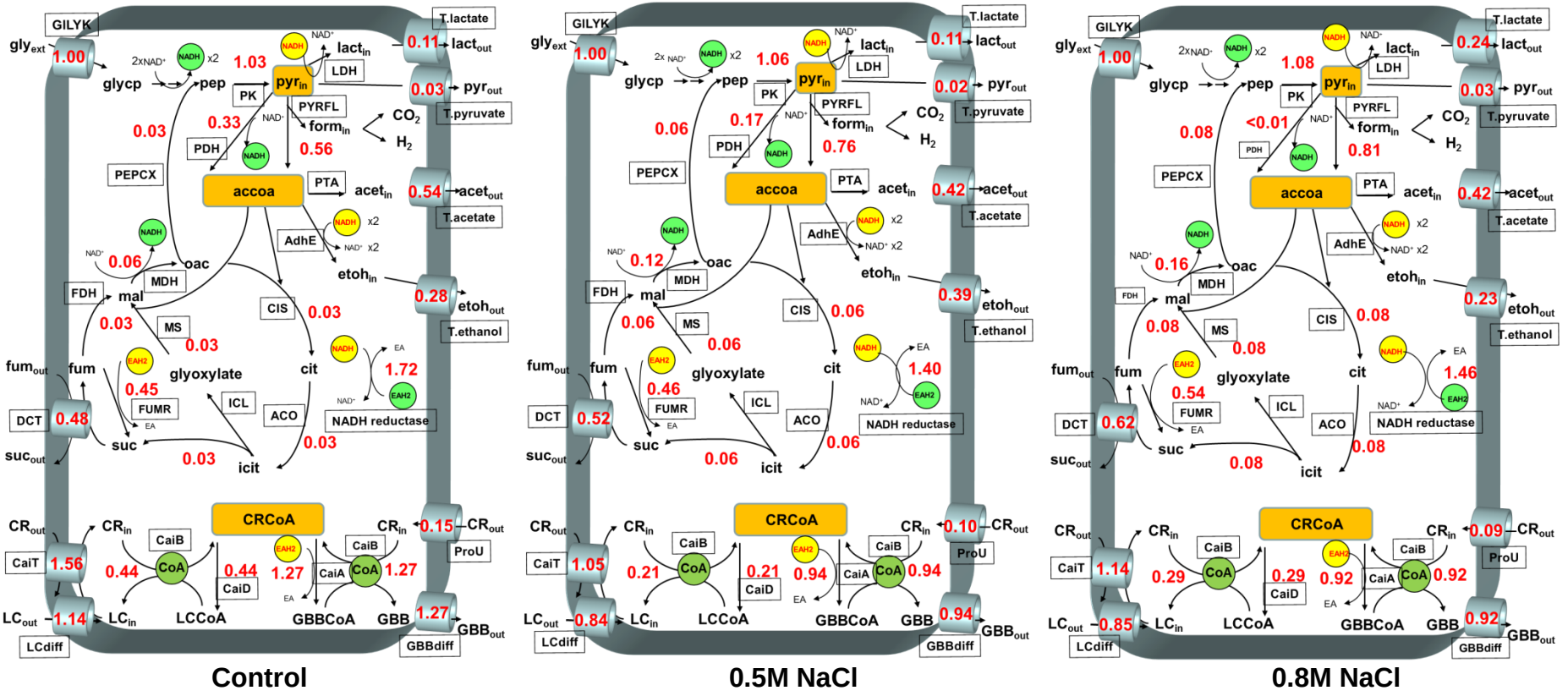

Figure 4. Overview of the fluxes in the large-scale stationary *E. coli* model in the steady state of control NaCl concentration, 0.5M NaCl, and 0.8M NaCl. Metabolic fluxes were normalized using the glycerol income flux (Appendix, Table 3).

Pathway Analysis

The results of the pathway analysis are shown in Table 5 (0.5M NaCl) and 6 (0.8M NaCl). A selection of the obtained pathways is depicted in Figure 4 and the whole set can be found in the Appendix. In general, both genetic and metabolic results were similar in both conditions, although the response was more intense at 0.8 M NaCl (Table 5 and 6). As expected, several genes of enzymes from *de novo* nucleotide metabolism were upregulated (Appendix, Table 2 and Figure 1A), whereas ATP concentration was lower in both conditions (Table 4), which could be the cause of the former genetic response. Regarding peptidoglycan biosynthesis, it was not only genetically upregulated (Appendix, Figure 1D) but also UTP (a necessary precursor) and UMP (a product) were higher in both conditions, as shown in Table 4. Similarly, the sulfur metabolism was genetically upregulated (Appendix, Figure 1C), which could be driven by L-cysteine deficiency at both NaCl concentrations (Table 4). In contrast, CoA biosynthesis seemed to present a different regulation control (Appendix, Figure 1E), which led to different CoA levels depending on the NaCl concentration (Table 4). Besides, oxidative phosphorylation was also highlighted in both conditions (Table 5 and 6). At 0.8 M NaCl, several genes were upregulated from the fumarate reductase and cytochrome c oxidase complexes (Figure 5C). Moreover, FMN, NAD^+ and ADP were higher, whereas ATP and NADH went down (Table 2 and 4). In general, these results suggest that ATP depletion and/or a higher ADP could increase the genetic expression of critical oxidative phosphorylation proteins, which might lead to the NADH depletion and increasing, as a consequence, the NAD^+ level. Similar results were obtained at 0.5 M NaCl, although the metabolic and genetic expression effects were less pronounced (Table 2 and 4). With regard to the nicotinate and nicotinamide metabolism, it was also found statistically relevant at 0.8 M NaCl (Table 6 and Appendix, Figure 1B), pointing to the overexpression of the pyridine nucleotide transhydrogenase (*sthA*, EC: 1.6.1.1). This enzyme catalyzes the reaction $NADPH+NAP^+ = NADH + NADP^+$. This gene was overexpressed almost 4 fold and could have been responsible of the extreme levels of NADP(H) as was shown in Table 2. With regard to central metabolism, several pathways have been found statistically relevant only at 0.8M NaCl,

namely, glycolysis/gluconeogenesis, TCA and glyoxylate and dicarboxylate metabolism (Table 6 and Figure 5A, D y E). The genetic and metabolic alterations suggested an increment in the glycerol assimilation since several intermediates, such as 3PG, 2PG and AcCoA were accumulated (Table 4). Additionally, several pathways related to transport (ABC Transporters) and amino acid metabolism were also found to be statistically relevant in the pathway analysis (Table 5 and 6), highlighting the importance of these metabolites in the adaptation process at both NaCl concentrations.

Table 5. KEGG pathway-based integrative analysis of metabolomic and transcriptomic data tested for overrepresentation using the hypergeometric distribution at 0.5 NaCl. annMoleculeRatio is the number of molecules present in the pathway divided by the total number of provided molecules, annBgRatio is the number of molecules present in the pathway divided by the total number of molecules considering the whole set of pathways, p value for the hypergeometric test and FDR are the previous p values adjusted by the Benjamini–Hochberg false discovery rate.

Pathway KEGG Id	Pathway Name	annMoleculeRatio	annBgRatio	p-value	FDR
eco02010	ABC transporters	22/211	280/19425	4.67E-13	4.67E-11
eco00920	Sulfur metabolism	8/211	60/19425	2.67E-07	1.34E-05
eco00290	Valine, leucine and isoleucine biosynthesis	6/211	39/19425	3.70E-06	1.23E-04
eco00460	Cyanoamino acid metabolism	6/211	41/19425	5.01E-06	1.25E-04
eco00260	Glycine, serine and threonine metabolism	7/211	84/19425	3.60E-05	7.00E-04
eco00270	Cysteine and methionine metabolism	7/211	86/19425	4.20E-05	7.00E-04
eco00430	Taurine and hypotaurine metabolism	4/211	28/19425	2.26E-04	3.23E-03
eco03070	Bacterial secretion system	4/211	31/19425	3.38E-04	4.23E-03
eco00450	Selenocompound metabolism	4/211	37/19425	6.75E-04	7.50E-03
eco00730	Thiamine metabolism	4/211	39/19425	8.26E-04	8.26E-03
eco02020	Two-component system	8/211	184/19425	9.27E-04	8.43E-03
eco00770	Pantothenate and CoA biosynthesis	4/211	49/19425	1.96E-03	1.62E-02
eco00550	Peptidoglycan biosynthesis	4/211	50/19425	2.11E-03	1.62E-02
eco00250	Alanine, aspartate and glutamate metabolism	4/211	55/19425	2.99E-03	2.14E-02
eco00190	Oxidative phosphorylation	4/211	57/19425	3.41E-03	2.24E-02
eco00230	Purine metabolism	7/211	180/19425	3.59E-03	2.24E-02
eco00680	Methane metabolism	5/211	101/19425	4.92E-03	2.89E-02

Table 6. KEGG pathway-based integrative analysis of metabolomics and transcriptomic data tested for overrepresentation using the hypergeometric distribution at 0.8 NaCl. annMoleculeRatio is the number of molecules present in the pathway divided by the total number of provided molecules, annBgRatio is the number of molecules present in the pathway divided by the total number of molecules considering the whole set of pathways, p value for the hypergeometric test and FDR are the previous p values adjusted by the Benjamini–Hochberg false discovery rate.

Pathway KEGG Id	Pathway Name	annMoleculeRatio	annBgRatio	p value	FDR
eco02010	ABC transporters	30/226	280/19425	0.00E+00	0.00E+00
eco00230	Purine metabolism	18/226	180/19425	3.74E-12	1.87E-10
eco00920	Sulfur metabolism	11/226	60/19425	8.61E-11	2.87E-09
eco00190	Oxidative phosphorylation	10/226	57/19425	9.97E-10	2.49E-08
eco00480	Glutathione metabolism	8/226	56/19425	2.61E-07	5.21E-06
eco00260	Glycine, serine and threonine metabolism	9/226	84/19425	5.75E-07	8.82E-06
eco00270	Cysteine and methionine metabolism	9/226	86/19425	7.04E-07	8.82E-06
eco00430	Taurine and hypotaurine metabolism	6/226	28/19425	7.06E-07	8.82E-06
eco00550	Peptidoglycan biosynthesis	7/226	50/19425	1.72E-06	1.91E-05
eco00290	Valine, leucine and isoleucine biosynthesis	6/226	39/19425	5.49E-06	5.49E-05
eco00460	Cyanoamino acid metabolism	6/226	41/19425	7.43E-06	6.75E-05
eco00240	Pyrimidine metabolism	9/226	127/19425	1.80E-05	1.50E-04
eco00680	Methane metabolism	8/226	101/19425	2.37E-05	1.82E-04
eco00250	Alanine, aspartate and glutamate metabolism	6/226	55/19425	4.18E-05	2.99E-04
eco00300	Lysine biosynthesis	5/226	42/19425	1.22E-04	8.14E-04
eco00630	Glyoxylate and dicarboxylate metabolism	7/226	98/19425	1.48E-04	9.27E-04
eco00770	Pantothenate and CoA biosynthesis	5/226	49/19425	2.56E-04	1.51E-03
eco00400	Phenylalanine, tyrosine and tryptophan biosynthesis	5/226	51/19425	3.10E-04	1.72E-03
eco03018	RNA degradation	3/226	16/19425	7.78E-04	4.10E-03
eco00471	D-Glutamine and D-glutamate metabolism	3/226	17/19425	9.37E-04	4.68E-03
eco00730	Thiamine metabolism	4/226	39/19425	1.07E-03	5.08E-03
eco00010	Glycolysis / Gluconeogenesis	5/226	70/19425	1.34E-03	6.07E-03
eco00620	Pyruvate metabolism	5/226	75/19425	1.82E-03	7.90E-03
eco00410	beta-Alanine metabolism	4/226	46/19425	1.99E-03	8.13E-03
eco00670	One carbon pool by folate	3/226	22/19425	2.03E-03	8.13E-03
eco00020	Citrate cycle (TCA cycle)	4/226	48/19425	2.32E-03	8.94E-03
eco00280	Valine, leucine and isoleucine degradation	4/226	52/19425	3.12E-03	1.16E-02
eco00780	Biotin metabolism	3/226	27/19425	3.70E-03	1.28E-02
eco03440	Homologous recombination	3/226	27/19425	3.70E-03	1.28E-02
eco00760	Nicotinate and nicotinamide metabolism	4/226	63/19425	6.22E-03	2.07E-02
eco00650	Butanoate metabolism	4/226	74/19425	1.09E-02	3.51E-02

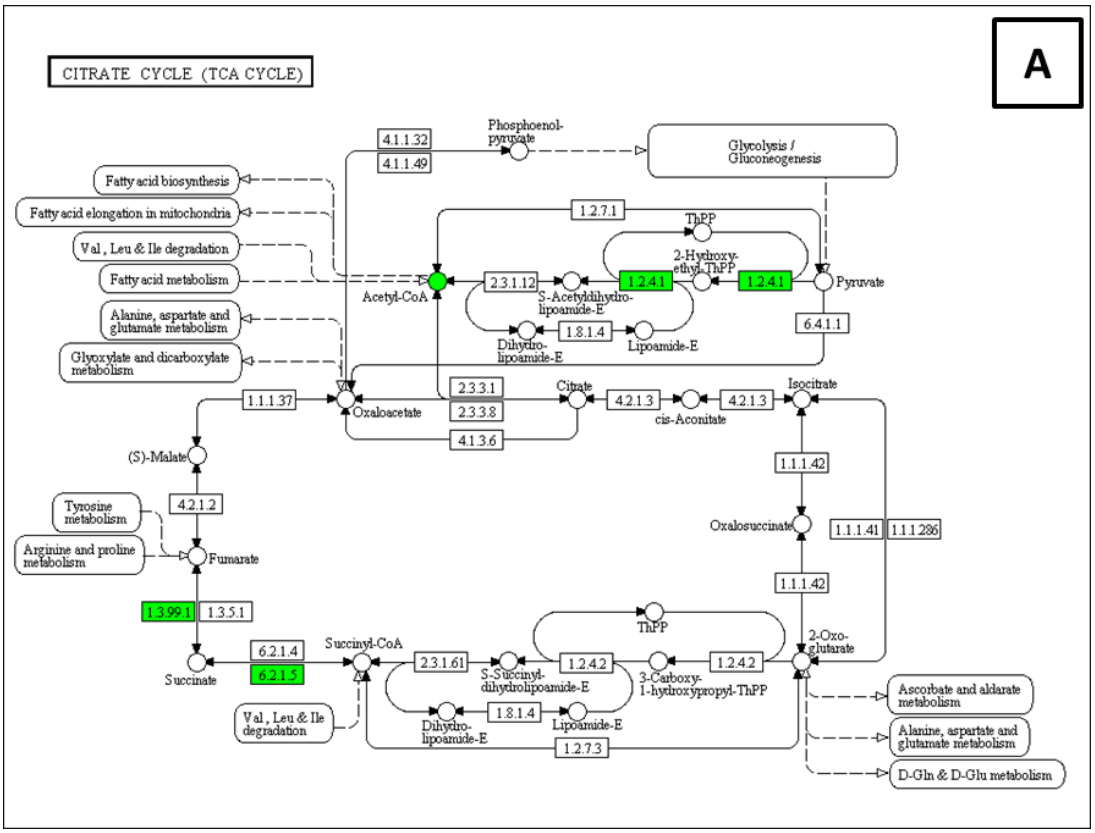
A
CITRATE CYCLE (TCA CYCLE)
Phosphoenol-pyruvate
Glycolysis / Gluconeogenesis
Fatty acid biosynthesis
Fatty acid elongation in mitochondria
Val, Leu & Ile degradation
Fatty acid metabolism
Alanine, aspartate and glutamate metabolism
Glyoxylate and dicarboxylate metabolism
ThPP
2-Hydroxy-ethyl-ThPP
Acetyl-CoA
S-Acetyldihydro-lipoamide-E
Dihydro-lipoamide-E
Lipoamide-E
Pyruvate
Oxaloacetate
Citrate
cis-Aconitate
Isocitrate
(S)-Malate
Tyrosine metabolism
Arginine and proline metabolism
Fumarate
Oxalosuccinate
Succinate
Succinyl-CoA
S-Succinyl-dihydrolipoamide-E
3-Carboxy-1-hydroxypropyl-ThPP
2-Oxo-glutarate
Val, Leu & Ile degradation
Ascorbate and aldarate metabolism
Alanine, aspartate and glutamate metabolism
D-Gln & D-Glu metabolism

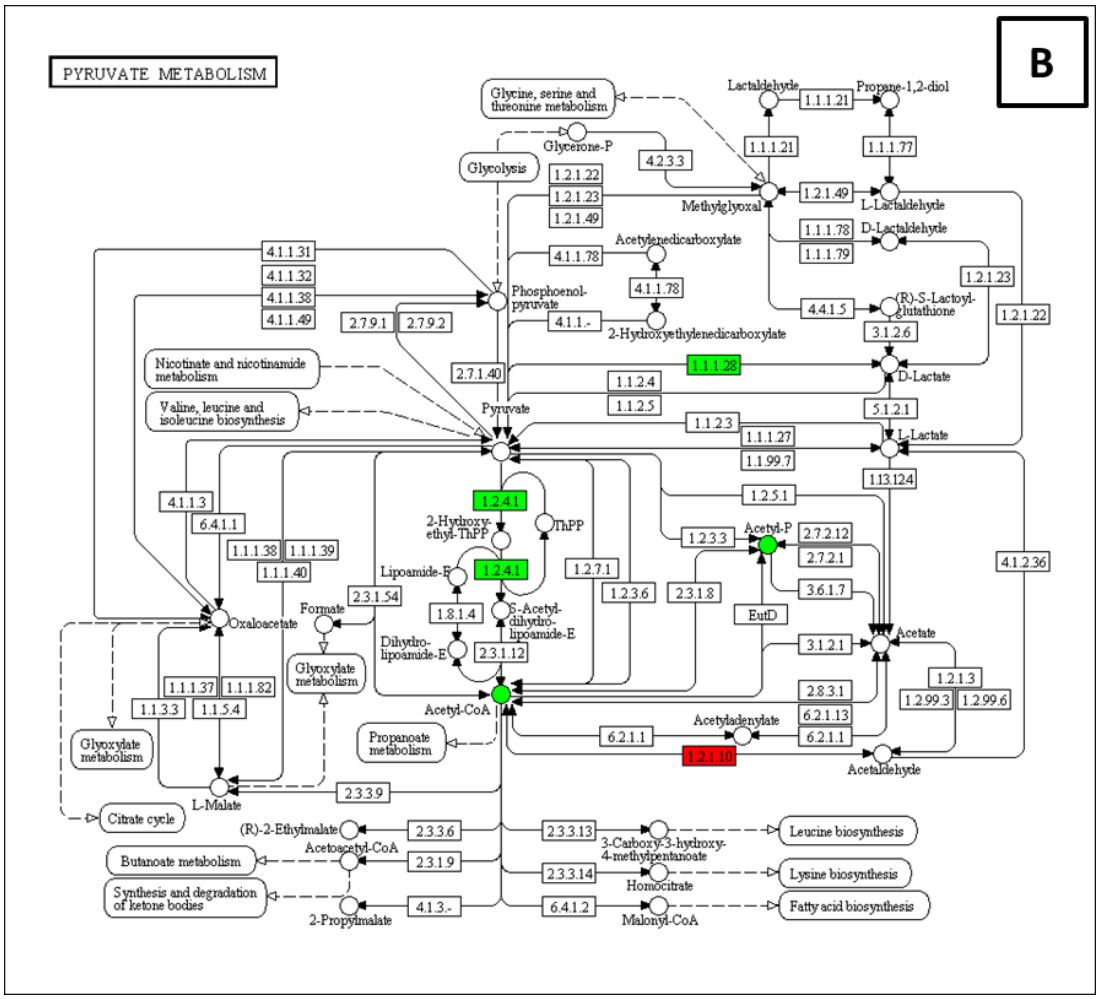
B
PYRUVATE METABOLISM
Glycine, serine and threonine metabolism
Glycerone-P
Glycolysis
Lactaldehyde
Propane-1,2-diol
Methylglyoxal
L-Lactaldehyde
D-Lactaldehyde
Acetylenedicarboxylate
Phosphoenol-pyruvate
2-Hydroxyethylenedicarboxylate
(R)-S-Lactoyl-glutathione
D-Lactate
L-Lactate
Nicotinate and nicotinamide metabolism
Valine, leucine and isoleucine biosynthesis
Pyruvate
2-Hydroxy-ethyl-ThPP
ThPP
Lipoamide-E
S-Acetyl-dihydro-lipoamide-E
Dihydro-lipoamide-E
Acetyl-P
Acetate
EutD
Oxaloacetate
Formate
Glyoxylate metabolism
Acetyl-CoA
Propanoate metabolism
Acetyladenylate
Acetaldehyde
L-Malate
Citrate cycle
(R)-2-Ethylmalate
Acetoacetyl-CoA
Butanoate metabolism
Synthesis and degradation of ketone bodies
2-Propylmalate
3-Carboxy-3-hydroxy-4-methylpentanoate
Homocitrate
Malonyl-CoA
Leucine biosynthesis
Lysine biosynthesis
Fatty acid biosynthesis

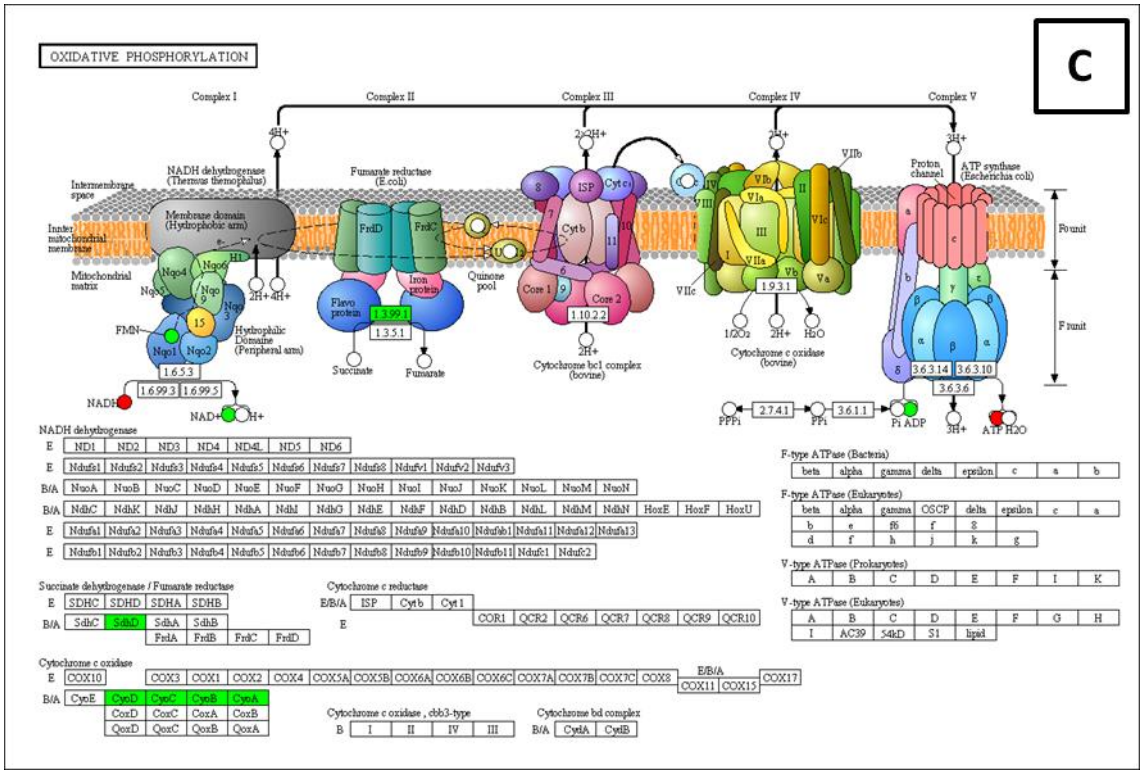
C
OXIDATIVE PHOSPHORYLATION
Complex I
Complex II
Complex III
Complex IV
Complex V
NADH dehydrogenase
Succinate dehydrogenase / Fumarate reductase
Cytochrome c reductase
Cytochrome c oxidase
F-type ATPase (Bacteria)
F-type ATPase (Eukaryotes)
V-type ATPase (Prokaryotes)
V-type ATPase (Eukaryotes)

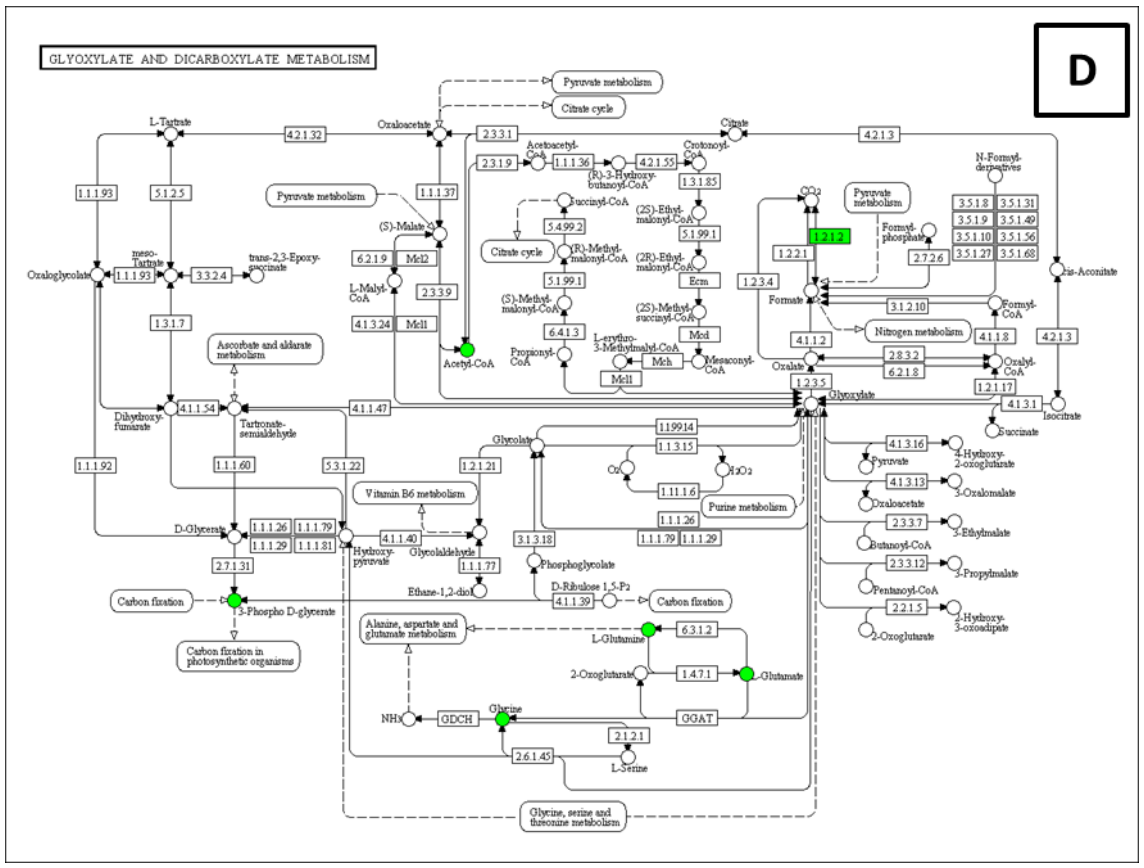
D
GLYOXYLATE AND DICARBOXYLATE METABOLISM

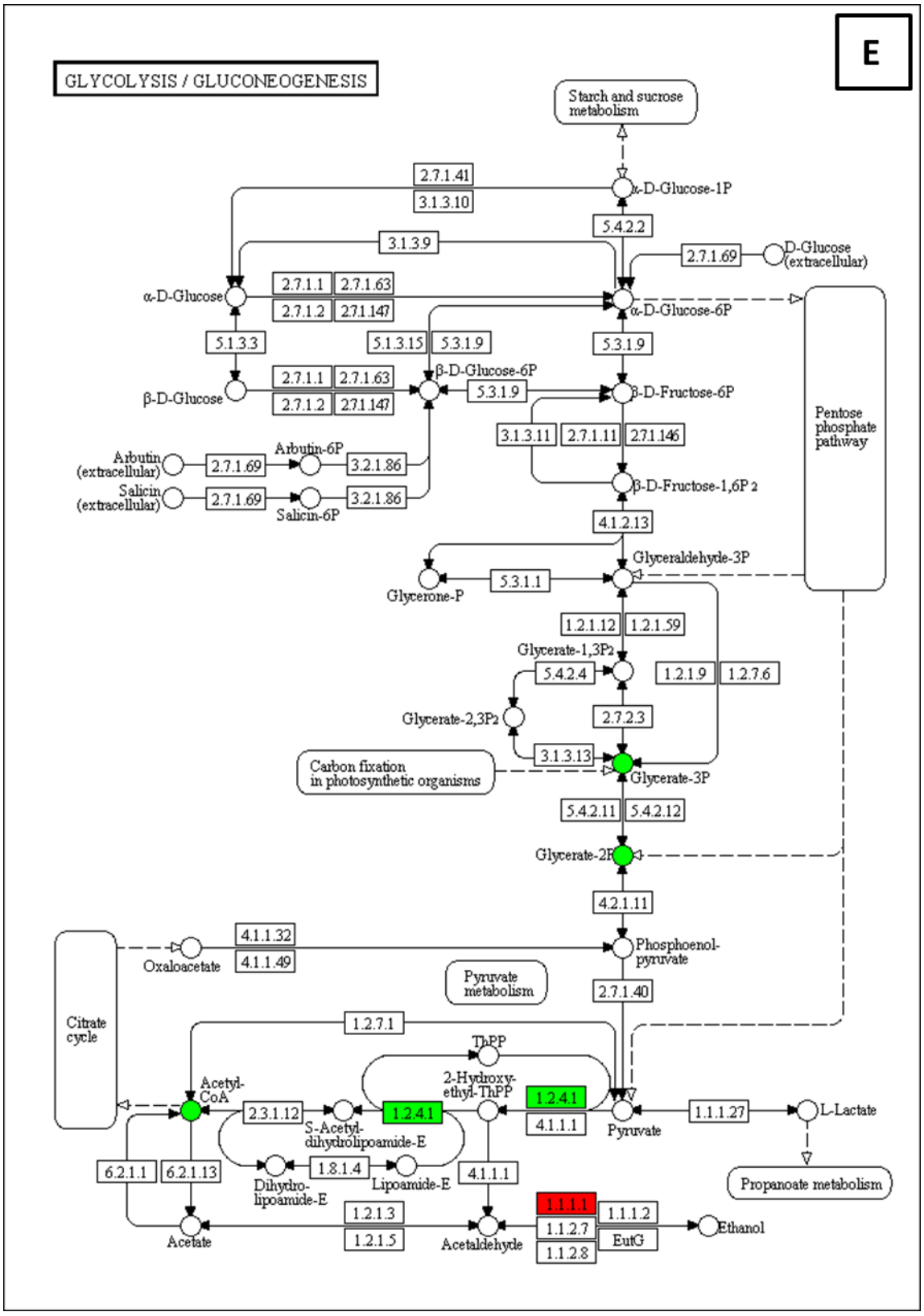

Figure 4. KEEG pathways highlighted by pathway-based integrative analysis: A. Citrate cycle. B. Pyruvate metabolism. C. Oxidative phosphorylation. D. Glyoxylate and dicarbolxylate metabolism. E. Glycolysis/gluconeogenesis. Upregulated genes and metabolites with higher levels after reaching a new steady state in the presence 0.8 M NaCl are highlighted in green, whereas downregulated genes or metabolites lower levels are in red. As established in the Materials and Methods section, the minimum fold change was set to 2.

DISCUSSION

To study the metabolic response of the *E. coli* anaerobic osmoadaptation, two NaCl concentrations (0.5 and 0.8 M) were selected according to the previous work carried out in our group (Arense et al., 2010). In general, our results showed that the strain developed a strategy to keep the cellular homeostasis since osmotic stress could result in a high demand of energy. Below, it is explained the most relevant metabolic features of this long-term osmoadaptation.

Extracellular concentration of amino acids depleted after NaCl up-shift (Figure 1). Although most studies have focused on the role of proline and betaines in stress conditions (Csonka and Epstein, 1996; LeRudulier et al., 1984; Lucht and Bremer, 1994; Verheul et al., 1998), the presence of amino acids in the medium seems to exert a positive effect on the adaptation process. In this regard, several works have reported the capacity of cells to use resources of the environment in order to economize energetic costs (Burkovski and Kramer, 2002; Chalova et al., 2009; Cosquer et al., 1999). However, extracellular amino acids depletion might not be due to their use as osmoprotectors (Amezaga and Booth, 1999), but a way of saving energy and redirecting cofactor redox and coenzymes to other pathways since this would avoid their *de novo* synthesis and they would be available for the turnover of proteins and enzyme machinery if necessary (Jozefczuk et al., 2010). Moreover, a recent publication of our group pointed out the necessary consumption of peptone (Santos et al., 2012) and, furthermore, peptone enhanced the growth of *E. coli* even more than glycine-betaine, which is the most powerful compatible solute in bacteria (Amezaga and Booth, 1999). Additionally, our results could be of relevance taking into account that tryptone has been demonstrated not to be a source of electron acceptors and can be substituted by a mixture of proteogenic acids with similar results in cell growth even with different *E. coli* strains (Murarka et al., 2008). In our work, amino acid depletion was faster in the case of very high salt (0.8M) compared to the 0.5M NaCl situation (Figure 1) which agrees with transcriptomic analysis since four genes (*pheP, proW, proV* and *proX*) with the GO term “amino acid transport” resulted significantly upregulated in the NaCl

exposure conditions (Appendix, Table 2A) with a concentration-dependent pattern.

In order to study the intracellular amino acid accumulation and other interesting molecules, more than 70 intracellular metabolites were measured by LC-MS in different samples corresponding to steady state chemostats at control (0.085M), 0.5M and 0.8M NaCl. The PCA analysis showed clear different intracellular metabolic patterns for these three situations (Figure 2). However, control concentration and 0.5M NaCl presented similar metabolic profiles, whereas the main metabolic differences were found in the case of 0.8M NaCl. Intracellular amino acids presented two tendencies, strong accumulation or depletion in the case of high concentration of salt. For example, intracellular L-histidine and L-cysteine concentrations went down until depletion when osmotic up-shift took place (Table 3). Sulfur metabolism was affected in both situations (0.5 and 0.8M NaCl) (Table 5 and 6). Besides, genes related to sulfur transport as well as sulfate assimilation were strongly overexpressed at both concentrations (even more at 0.8M NaCl) (Appendix, Figure 1C). On the contrary, other amino acids such as L-lysine, L-arginine, L-leucine, L-tryptophan, L-alanine, L-aspartic acid, L-glutamic acid, L-asparagine and L-glutamine resulted highly accumulated in the case of 0.8 M NaCl (Table 3). It has been reported that proline accumulation ceases if carnitine or betaine are supplemented since they act as osmoprotectants (Verheul 1998) although its accumulation was not significantly relevant. Our results in complex medium showed a different behavior, highlighting that the depletion of amino acids in the medium might not be due to their use as osmoprotectors, as previously mentioned. In the work of Glaasker et al. (1996), in *Lactobacillus plantarum* an intracellular accumulation of several amino acids was reported, namely, L-alanine, L-glutamine, glycine, L-valine and L-glutamic acid when the osmolarity of the growth media increased, fact that agrees with our results. However, both L-lysine and L-arginine were lower in that work. The case of L-glutamine and L-valine are very drastic since they showed a >2000 and 100-fold increase respectively in the case of 0.8M NaCl. It has been reported that valine is also one of the organic osmolytes that plants accumulate in the case of salt stress (Parida and Das 2005). Glutamine was also one of the amino acids with the highest accumulation achieved in the study

of osmotic stress in wheat (Kovács et al., 2012). With regard to L-carnitine, it can play an osmoprotector role since its concentration was twice the control condition value at 0.5M NaCl and 10 times higher at very high salt concentration (0.8 M) (Table 4). This fact is in agreement with the strong overexpression of genes involved in its transport (Appendix, Table 2A).

Even though AcCoA and CoA levels were strongly higher at 0.8M NaCl (Table 4), the AcCoA/CoA ratio did not significantly change in all the assayed conditions showing the flexibility of the metabolic network in *E. coli* (Figure 3). Therefore, the system could therefore be considered robust and stable. This flexibility has been previously reported in other work (Taymaz-Nikerel et al., 2013) in which AcCoA/CoA ratio was constant also in a glucose-limited chemostat after three different pulses (glucose, pyruvate and succinate).

Metabolic flux analysis was carried out using a large-scale stationary *E. coli* model (Sevilla et al., 2005a) and extracellular metabolic data (Appendix, section 4). The reorganization of the metabolic fluxes seemed to be focused on the adaptive response whose tendency would help to maintain cellular survival, although the response at 0.8 M NaCl was stronger (Figure 4). The metabolic flux analysis showed the different fermentation patterns in each case: ethanol production was relative higher at 0.5 M NaCl, whereas lactate was 2-fold at 0.8 M. Surprisingly, the acetate flux proportion was reduced compared with the control condition in both NaCl concentrations, suggesting potential saturation of this reaction which is supported by the high intracellular concentration of Acetyl-P and AcCoA in the case of 0.8M (Table 4). In order to increase ATP production, glycerol consumption rate was higher (Arense et al., 2010) as well as the conversion of succinate to fumarate. In both NaCl conditions, decreased the relative flux through PDH and increased flux through PYRFL/Formate dHase, this being higher in 0.8M NaCl (Figure 4). This result is supported by transcriptomic analysis since the gene *fdoI*, which codifies for formate dehydrogenase activity, was also upregulated (Appendix, Table 2B). It is shown that the metabolic fluxes reorganized to minimize the NADH production (decreased flux of PDH) increasing the flux in NADH regeneration steps such as fermentation product formation, for instance ethanol in the case of 0.5M of

salt and lactate in the case of 0.8M of salt. Also the results obtained from the flux analysis corroborate the previous results reported by our group (Arense et al., 2010) about the fact that the glyoxylate pathway flux increased at 0.8 M NaCl.

By integrating metabolic and transcriptomic results using pathway analysis, some salt-tolerance strategies were found to be similar at both NaCl concentrations, although they were more pronounced at 0.8 M. Among them were: (i) higher glycerol consumption, which was confirmed by the MFA and the increased glycerol specific consumption rate (Arense et al., 2010), (ii) increased flux through oxidative phosphorylation pathway supported by the increase in the relative flux through fumarate in the MFA (Figure 4), (iii) alteration of the transport and metabolism of amino acids, confirmed by the increase in extracellular amino acid uptake (Figure 1), and (iv) increased *de novo* synthesis of purine nucleotides, probably driven by the reduction in the ATP concentration (Table 4 and Appendix, Figure 1A).

In addition to the above mentioned results, different salt-dependent concentration strategies were found in the pathway analysis regarding 0.8M NaCl situation. First, the fermentation pattern was drastically altered at 0.8 M NaCl, probably because *adhE* expression (alcohol dehydrogenase activity) was downregulated, whereas *ldhA* (lactate dehydrogenase activity) was upregulated at 0.8 M (Appendix, Table 2B). This was supported by the fluxomics results, which showed that relative ethanol synthesis increased at 0.5 M NaCl, but decreased at 0.8 M, in contrast to lactate, that was approximately double at 0.8 M (Figure 4). Therefore, these alterations could be considered as an adaptation mechanism results from long-term adaptation. Secondly, pathway analysis (Table 5, 6, Figure 4 and Appendix, Figure 1) highlighted the NaCl-dependent alteration of redox cofactors, which was confirmed in the intra-metabolome results by the higher values of the NADPH and NADP forms, whereas NADH was almost depleted (Table 2). Besides, an increase in oxidative phosporylation (Figure 5C), which led to an increment in the NAD^+ concentration, and pyridine nucleotide transhydrogenase (*sthA*, EC: 1.6.1.1) was also probably involved. Thirdly, pathway analysis pointed to an increase in sulfur pathway expression at both NaCl concentrations, probably provoked by the depletion of L-cysteine

(Table 5, 6 and Appendix, Figure 1C), which is a precursor for both CoA and GSH. The regulation profiles of the CoA biosynthesis pathway depended on the NaCl concentration and CoA levels were higher at 0.8 M NaCl than at both control and 0.5 M NaCl (Table 4). Similarly, differences in the level of GSH and GSSG were found, confirming alternative processes to long-term osmoadaptation that depend on the salt concentration. However, the level of GSH was similar in control and 0.5 M conditions, while it was not detected at 0.8 M (Table 2). Meanwhile, the level of GSSG showed the opposite behaviour since it was not observed in control conditions, whereas it presented a very low concentration at 0.5 M, and increased at 0.8 M (Table 2). These findings suggest that a complex process regarding L-cysteine, CoA and redox adaptation was being carried out in order to ensure cell survival at very high salt concentrations. GSH was probably involved, since *E. coli* mutants deficient in their synthesis or regeneration were unable to grow in a medium of high osmolarity (Smirnova et al., 2001).

Taking all toghether, metabolic flux analysis and integration pathway analysis constitute a useful tool for a better understanding of the survival strategies in long-term exposure to high osmotic environment in *E. coli.*

CONCLUDING REMARKS

The present work describes relevant metabolic events that take place during the response to the long-term anaerobic NaCl exposure in *E.coli* improving the knowledge of the system previously described (Arense et al., 2010). Besides, fluxomic data confirmed most of the outcomes of the pathway analysis, showing how the integration of these –omics technologies can throw light on the reorganization of these metabolic networks.

The redistribution of metabolic fluxes pointed to a behavior that depended on NaCl concentration. The main conclusions about the metabolic events described in this work regarding the high osmotic medium adaption are: i) total depletion of extracellular aminoacids being faster at higher NaCl concentration, ii) intracellular amino acids accumulation (except Cys and His), being more

accused at higher NaCl concentration, iii) accumulation of carnitine, glycerol assimilation intermediates and CoA derivatives in the case of 0.8M of NaCl, iv) alterations in the redox coenzymes ratios and v) metabolic fluxes reorganization changing the formation of fermentation products, ethanol relative rate was increased in the case of 0.5M of NaCl and lactate relative rate in the case of 0.8M of NaCl. In addition, the information as a whole could be used to enhance biotechnological processes in which glycerol is used as C-source. The integration pathway analysis was in concordance with the metabolic flux analysis showing also the main affected pathways such as GSH metabolism, glycolysis/glyconeogenesis, amino acid biosynthesis/degradation, purine metabolism, phosphorylative oxidation, pyruvate metabolism or TCA cycle and glyoxylate shunt among others. Finally, further studies should be carried out to establish the relevance of the switch of redox cofactors observed and the effect of the oxidation state in the stressing conditions.

REFERENCES

Arense, P., Bernal, V., Iborra, J. L., Cánovas, M. (2010). Metabolic adaptation of *Escherichia coli* to long-term exposure to salt stress. *Process Biochem.*, **45**, 1459-1467.

Amezaga, M. R., Booth, I. R. (1999). Osmoprotection of *Escherichia coli* by peptone is mediated by the uptake and accumulation of free proline but not of proline-containing peptides. *Appl. Environ. Microbiol*., **65**, 5272-5278.

Ashby, R. D., Solaiman, D. K. Y., Foglia, T. A. (2004). Bacterial poly(hydroxyalkanoate) polymer production from the biodiesel co-product stream. *J. Polym. Environ*., **12**, 105-112.

Bajad, S. U., Lu, W., Kimball, E. H., Yuan, J., Peterson, C., Rabinowitz, J. D. (2006). Separation and quantitation of water soluble cellular metabolites by hydrophilic interaction chromatography-tandem mass spectrometry. *J. Chromatogr. A*, **1125**, 76-88.

Benjamini, Y., Hochberg, Y., (1995). Controlling the false discovery rate - A practical and powerful approach to multiple testing. *J. R. Stat. Soc. Ser. B-Methodol.*, **57**, 289-300.

Bravo, E., Palleschi, S., Aspichueta, P., Buque, X., Rossi, B., Cano, A., Napolitano, M., Ochoa, B., Botham, K. M. (2011). High fat diet-induced non

alcoholic fatty liver disease in rats is associated with hyperhomoCysteinemia caused by down regulation of the transsulphuration pathway. *Lipids Health Dis*., **10**:60. doi:10.1186/1476-511x-10-60.

Bunk, B., Kucklick, M., Jonas, R., Munch, R., Schobert, M., Jahn, D., Hiller, K. (2006). MetaQuant: a tool for the automatic quantification of GC/MS-based metabolome data. *Bioinformatics*, **22**(23), 2962-2965.

Burkovski, A., Kramer, R. (2002). Bacterial amino acid transport proteins: occurrence, functions, and significance for biotechnological applications. *Appl. Microbiol. Biotechnol*. **58**, 265-274.

Cánovas, M., Bernal, V., Sevilla, A., Iborra, J. L. (2007). Salt stress effects on the central and carnitine metabolisms of *Escherichia coli*. *Biotechnol. Bioeng.*, **96**, 722-737.

Canovas, M., Bernal, V., Torroglosa, T., Ramirez, J. L., Iborra, J. L. (2003). Link between primary and secondary metabolism in the biotransformation of trimethylammonium compounds by *Escherichia coli*. *Biotechnol. Bioeng*., **84**, 686-699.

Canovas, M., Maiquez, J. R., Obon, J. M., Iborra, J. L. (2002). Modeling of the biotransformation of crotonobetaine into L-(-)-carnitine by *Escherichia coli* strains. *Biotechnol. Bioeng*., **77**, 764-775.

Chalova, V. I., Sirsat, S. A., O'Bryan, C. A., Crandall, P. G., Ricke, S. C. (2009). *Escherichia coli*, an intestinal microorganism, as a biosensor for quantification of amino acid bioavailability. *Sensors,* **9**, 7038-7057.

Conesa, A., Nueda, M. J., Ferrer, A., Talon, M. (2006). maSigPro: a method to identify significantly differential expression profiles in time-course microarray experiments. *Bioinformatics*, **22**, 1096-1102.

Cosquer, A., Pichereau, V., Pocard, J. A., Minet, J., Cormier, M., Bernard, T. (1999). Nanomolar levels of dimethylsulfoniopropionate, dimethylsulfonioacetate, and glycine betaine are sufficient to confer osmoprotection to *Escherichia coli*. *Appl. Environ. Microbiol*., **65**, 3304-3311

Csonka, L. N., Epstein, W. (1996). Osmoregulation. *Escherichia* and *Salmonella*: cellular and molecular biology. ASM Press, Washington D.C. (U.S.A.), pp. 1210–1223.

Dharmadi, Y., Murarka, A., Gonzalez, R. (2006). Anaerobic fermentation of glycerol by *Escherichia coli*: A new platform for metabolic engineering. *Biotechnol. Bioeng*., **94**, 821-829.

Dietmair, S., Timmins, N. E., Gray, P. P., Nielsen, L. K., Kroemer, J. O. (2010). Towards quantitative metabolomics of mammalian cells: Development of a metabolite extraction protocol. *Anal. Biochem.*, **404**, 155-164.

Document No. SANCO/12495/2011 (2011). Method Validation and Quality Control procedures for pesticide residues analysis in food and feed. http://ec.europa.eu/food/plant/protection/pesticides/docs/qualcontrol_en.pdf.

Faijes, M., Mars, A. E., Smid, E. J. (2007). Comparison of quenching and extraction methodologies for metabolome analysis of *Lactobacillus plantarum*. *Microb. Cell. Fact.*, **6**, 27. doi:10.1186/1475-2859-6-27.

Falcon, S., Gentleman, R. (2007). Using GOstats to test gene lists for GO term association. *Bioinformatics*, **23**, 257-258.

Franzel, B., Trotschel, C., Ruckert, C., Kalinowski, J., Poetsch, A., Wolters, D. A. (2010). Adaptation of *Corynebacterium glutamicum* to salt-stress conditions. *Proteomics*, **10**, 445-457.

Fructuoso, S., Sevilla Camins, A., Bernal, C., Lozano, A. B., Iborra, J. L., Cánovas, M. (2012). EasyLCMS: An asynchronous web application for the automated quantification of LC-MS data. *BMC Res. Notes*, **5**, 428.

Gautier, L., Cope, L, Bolstad, B.M., Irizarry, R.A. (2004). affy—analysis of Affymetrix GeneChip data at the probe level. *Bioinformatics*, **20**, 307–315.

Gentleman, R. C., Carey, V. J., Bates, D. M., Bolstad, B., Dettling, M., Dudoit, S., Ellis, B., Gautier, L., Ge, Y., Gentry, J., Hornik, K., Hothorn, T., Huber, W., Iacus, S., Irizarry, R., Leisch, F., Li, C., Maechler, M., Rossini, A. J., Sawitzki, G., Smith, C., Smyth, G., Tierney, L., Yang, J. Y. and Zhang, J. (2004). Bioconductor: open software development for computational biology and bioinformatics. *Genome Biol*., **5**, R80.

Glaasker, E., Konings, W. N., Poolman, B. (1996). Osmotic regulation of intracellular solute pools in Lactobacillus plantarum. *J. Bacteriol.*, **178**, 575-582.

Gupta, S., Chowdhury, R. (1997). Bile affects production of virulence factors and motility of *Vibrio cholerae. Infect. Immun*., **65**, 1131-1134.

Irizarry, R. A., Hobbs, B., Collin, F., Beazer-Barclay, Y. D., Antonellis, K. J., Scherf, U., Speed, T. P. (2003). Exploration, normalization, and summaries of high density oligonucleotide array probe level data. *Biostatistics,* **4**, 249-264.

Jones, S. A., Gibson, T., Maltby, R. C., Chowdhury, F. Z., Stewart, V., Cohen, P. S., Conway, T. (2011). Anaerobic respiration of *Escherichia coli* in the mouse intestine. *Infect. Immun*., **79**, 4218-4226.

Jozefczuk, S., Klie, S., Catchpole, G., Szymanski, J., Cuadros-Inostroza, A., Steinhauser, D., Selbig, J., Willmitzer, L. (2010). Metabolomic and transcriptomic stress response of *Escherichia coli*. *Mol. Syst. Biol*., **6**:364. doi: 10.1038/msb.2010.18.

Kanehisa, M., Goto, S., Sato, Y., Kawashima, M., Furumichi, M., Tanabe, M. (2014). Data, information, knowledge and principle: back to metabolism in KEGG. Nucleic Acids Res., **42**, D199-205.

Kleber, H.P. (1997). Bacterial carnitine metabolism. *FEMS Microbiol. Lett*., **147**, 1-9.

Kovács, Z., Simon-Sarkadi, L., Vashegyi, I. and Kocsy, G. (2012). Different accumulation of free amino acids during short- and long-term osmotic stress in wheat. ScientificWorldJournal, **2012**, 216521.

Kronthaler, J., Gstraunthaler, G., Heel, C. (2012). Optimizing High-Throughput Metabolomic Biomarker Screening: A Study of Quenching Solutions to Freeze Intracellular Metabolism in CHO Cells. *OMICS*, **16**, 90-97.

Lazzarino, G., Amorini, A. M., Fazzina, G., Vagnozzi, R., Signoretti, S., Donzelli, S., Di Stasio, E., Giardina, B., Tavazzi, B. (2003). Single-sample preparation for simultaneous cellular redox and energy state determination. *Anal. Biochem.*, **322**, 51-59.

LeRudulier, D., Strom, A. R., Dandekar, A. M., Smith, L. T., Valentine, R. C. (1984). Molecular-Biology of osmoregulation. Science, **224**, 1064-1068.

Li, C. Q., Li, X., Miao, Y. B., Wang, Q. H., Jiang, W., Xu, C., Li, J., Han, J. W., Zhang, F., Gong, B. S., Xu, L. D. (2009). SubpathwayMiner: a software package for flexible identification of pathways. *Nucleic Acids Res*., **37**(19): e131. doi: 10.1093/nar/gkp667.

Luo, W. J., Brouwer, C. (2013). Pathview: an R/Bioconductor package for pathway-based data integration and visualization. *Bioinformatics*. **29**, 1830-1831.

Lucht, J. M., Bremer, E. (1994). Adaptation of *Escherichia coli* to high osmolarity environments - osmoregulation of the high-affinity glycine betaine transport-system *proU*. *FEMS Microbiol. Rev*., **14**, 3-20.

Montero, M., Rahimpour, M., Viale, A. M., Almagro, G., Eydallin, G., Sevilla, A., Canovas, M., Bernal, C., Lozano, A. B., Munoz, F. J., Baroja-Fernandez, E., Bahaji, A., Mori, H., Codoner, F. M. and Pozueta-Romero, J. (2014). Systematic production of inactivating and non-inactivating suppressor mutations at the *relA* locus that compensate the detrimental effects of complete *spoT* loss and affect

glycogen content in E*scherichia coli*. *PLoS One,* **9**(9): e106938. doi:10.1371/journal.pone.0106938.

Moon, S. K., Wee, Y. J., Yun, J. S., Ryu, H. W. (2004). Production of fumaric acid using rice bran and subsequent conversion to succinic acid through a two-step process. *Appl. Biochem. Biotechnol*., **113**, 843-855.

Murarka, A., Dharmadi, Y., Yazdani, S. S., Gonzalez, R. (2008). Fermentative utilization of glycerol by *Escherichia coli* and its implications for the production of fuels and chemicals. *Appl. Environ. Microbiol.,* **74**, 1124-1135

Oikawa, A., Otsuka, T., Jikumaru, Y., Yamaguchi, S., Matsuda, F., Nakabayashi, R., Takashina, T., Isuzugawa, K., Saito, K., Shiratake, K. (2011). Effects of freeze-drying of samples on metabolite levels in metabolome analyses. *J. Sep. Sci.*, **34**, 3561-3567.

Parida, A.K., Das, A.B. (2005). Salt tolerance and salinity effects on plants: a review. *Ecotoxicol. Environ. Saf.*, **60,** 324-49**.**

Preinerstorfer, B., Schiesel, S., Lammerhofer, M. L., Lindner, W. (2010). Metabolic profiling of intracellular metabolites in fermentation broths from beta-lactam antibiotics production by liquid chromatography-tandem mass spectrometry methods. *J. Chromatogr. A*, **1217**, 312-328.

R Development Core Team. R: A Language and Environment for Statistical Computing (R Foundation for Statistical Computing, 2014).

Rozen, Y., LaRossa, R. A., Templeton, L. J., Smulski, D. R., Belkin, S. (2002). Gene expression analysis of the response by *Escherichia coli* to seawater. Antonie Van Leeuwenhoek, **81**, 15-25.

Santos, G., Hormiga, J. A., Arense, P., Canovas, M., Torres, N. V. (2012). Modelling and analysis of central metabolism operating regulatory interactions in salt stress conditions in a L-carnitine overproducing *E. coli* strain. *PLoS One,* **7**(4): e34533. doi:10.1371/journal.pone.0034533.

Schadel, F., David, F., Franco-Lara, E. (2011). Evaluation of cell damage caused by cold sampling and quenching for metabolome analysis. *Appl. Microbiol. Biotechnol.*, **92**, 1261-1274.

Sellick, C. A., Hansen, R., Stephens, G. M., Goodacre, R., Dickson, A. J. (2011). Metabolite extraction from suspension-cultured mammalian cells for global metabolite profiling. *Nat. Protoc.*, **6**, 1241-1249.

Sevilla, A., Schmid, J. W., Mauch, K., Iborra, J. L., Reuss, M., Cánovas, M. (2005a). Model of central and trimethylammonium metabolism for optimizing L-carnitine production by *E. coli*. *Metab. Eng.*, **7**, 401-425.

Sevilla, A., Vera, J., Diaz, Z., Cánovas, M., Torres, N. V., Iborra, J. L. (2005b). Design of metabolic engineering strategies for maximizing L-(-)-carnitine production by *Escherichia coli*. Integration of the metabolic and bioreactor levels. *Biotechnol. Prog.*, **21**, 329-337.

Smirnova, G. V., Krasnykh, T. A., Oktyabrsky, O. N. (2001). Role of glutathione in the response of *Escherichia coli* to osmotic stress. *Biochem.-Moscow*, **66**, 973-978.

Taymaz-Nikerel, H., de Mey, M., Ras, C., ten Pierick, A., Seifar, R. M., Van Dam, J. C., Heijnen, J. J., Van Glilik, W. M. (2009). Development and application of a differential method for reliable metabolome analysis in *Escherichia coli*. *Anal. Biochem*., **386**, 9-19.

Thapa, L. P., Lee, S. J., Yoo, H. Y., Choi, H. S., Park, C., Kim, S. W. (2013). Development of glycerol-utilizing *Escherichia coli* strain for the production of bioethanol. *Enzyme Microb. Technol*., **53**, 206-215.

Torres Darias, N., Hormiga Cerdena, J., Sevilla, A., Canovas, M., Gonzalez Alcon, C. (2009). A system biology approach to the L-carnitine biosynthesis optimization in *E. coli* through the analysis of the regulatory signalling pathway. *New Biotech*., **25**, S355-S356.

Tripathi, N. K., Shrivastva, A., Biswal, K. C., Rao, P. V. L. (2009). Optimization of culture medium for production of recombinant dengue protein in *Escherichia coli*. *Ind. Biotechnol*., **5**, 179-183.

van den Berg, R.A., Hoefsloot, H.C.J., Westerhuis, J.A., Smilde, A.K., van der Werf, M.J. (2006). Centering, scaling, and transformations: improving the biological information content of metabolomics data. *BMC Genomics*, **7**:142.

Verheul, A., Wouters, J. A., Rombouts, F. M., Abee, T. (1998). A possible role of ProP, ProU and CaiT in osmoprotection of *Escherichia coli* by carnitine. *J. Appl. Microbiol.,* **85**, 1036-1046.

Weber, A., Kogl, S. A., Jung, K. (2006). Time-dependent proteome alterations under osmotic stress during aerobic and anaerobic growth in *Escherichia coli*. *J. Bacteriol*., **188**, 7165-7175.

Wood, J. M. (1999). Osmosensing by bacteria: Signals and membrane-based sensors. *Microbiol. Mol. Biol. Rev.*, **63**, 230-262.

Yang, F., Hanna, M. A., Sun, R. (2012). Value-added uses for crude glycerol-a byproduct of biodiesel production. *Biotechnol. Biofuels*, **5**:13. doi 10.1186/1754-6834-5-13.

Yazdani, S. S., Gonzalez, R. (2007). Anaerobic fermentation of glycerol: a path to economic viability for the biofuels industry. *Curr. Opin. Biotechnol*., **18**, 213-219.

Yong, K. C., Ooi, T. L., Dzulkefly, K., Wan Yunus, W. M. Z., Hazimah, A. H. (2011). Characterization of glycerol residue from a palm kernel oil methyl ester plant. *J. Oil. Palm. Res*., **13**, 1-6.

Zelder, O., Hauer, B. (2000). Environmentally directed mutations and their impact on industrial biotransformation and fermentation processes. *Curr. Opin. Microbiol.*, **3**, 248-251.

Zhu, M. M., Lawman, P. D., Cameron, D. C. (2002). Improving 1,3-propanediol production from glycerol in a metabolically engineered *Escherichia coli* by reducing accumulation of sn-glycerol-3-phosphate. *Biotechnol. Prog.*, **18**, 694-699.

APPENDIX

1. Fermentation products analysis method

Extracellular metabolites (acetate, ethanol, fumarate, pyruvate, lactate, succinate) were determined by an HPLC system from Shimadzu (Kyoto, Japan) with a cation exchange Aminex HPX-87H column supplied by BioRad Labs (Hercules, CA). The isocratic mobile phase was 5 mM H2SO4 at a flow rate of 0.5 mL min-1. The effluent was monitored using a refractive index detector (Shimadzu, Kioto, Japan).

2. Transcriptomic analysis

Time-course microarray experiment design

Cells were grown as described in the main text in the Material and Methods section using continuous reactors. The stationary state was confirmed after 5 residential times (50 h) when no modification in biomass concentration was observed, after which the samples were harvested (t= 0 h). From this moment, the medium was switched to another with a higher NaCl concentration (0.5 M or 0.8 M). Samples were harvested at different time points to cover not only the new stationary state (confirmed previously at t=75 h), but also the transition phase (t = 29 h).

RNA extraction and microarray sample preparation.

At every time point described above, the cultures were pelleted by centrifugation at 15000 x g and 4°C for 30 s. Total RNA was isolated by Qiagen Rneasy® Mini Kit (QIAGEN Ibérica, Madrid, Spain). Additionally, Dnase I digestion of the isolated RNA was performed using the Rnase-Free Dnase Set (QIAGEN Ibérica, Madrid, Spain) to avoid DNA interferences during PCR steps. RNA quality and quantity were evaluated by microfluidic capillary electrophoresis on an Agilent 2100 Bioanalyzer (Agilent Technologies, Palo Alto, CA) using Agilent RNA 6000 Pico kit. The GeneChip *E. coli* Genome 2.0 array of the Affymetrix system was used to compare gene expression of *E. coli*

O44K74 during the osmoadaptation process. The processing of extracted RNA, cDNA labeling, hybridization, and slide-scanning procedures were performed according to the manufacturer's instructions (Affymetrix).

Microarray data analysis

The statistical analysis was performed using the Bioconductor suite (Gentleman 2005) in R (R Development Core Team, 2011). Affymentrix data files were processed with affy package (Gautier et al., 2004). All of the microarrays were pre-processed simultaneously using Robust Multichip Average (RMA), as described by Irizarry et al. (2003). Afterwards, differentially expressed genes were identified from the time-course experiment using the maSigPro package (Conesa et al., 2006). A quadratic regression model was used for gene selection with a p-value cut-off of 0.05, adjusted with Benjamini and Hochberg's method (Benjamini and Hochberg, 1995). Furthermore, the fold-change in expression had to exceed a factor of 2 at 0.8 M NaCl and 1.3 at 0.5M NaCl compared with the initial steady state values for genes to be considered differentially expressed.

GO enrichment analysis.

Genes were analysed for gene term enriched analysis with the conditional hypergeometric test algorithm included in the GOstats Bioconductor package (Falcon and Gentleman, 2007). P-value cut-off was set at 0.05. GO terms in the three categories, namely, BiologicalProcess (BP), Molecular Function (MF) and Cellular Component (CC), were included.

3. Transcriptomic results

Selected common genes of *E. coli* in long-term adaptation to high and very high NaCl concentration (0.5 and 0.8 M) are shown below in Table 1. Fold-change is always more remarkable in the case of 0.8M NaCl. In Table 2, selected Enriched Gene Ontology groups for common genes of *E. coli* in long-term

adaptation to high and very high NaCl concentrations (0.5 and 0.8 M) are summarized.

Table 1: Selected common genes of *E. coli* in long-term adaptation to high and very high NaCl concentration (0.5 and 0.8 M).

Ecocyc Ids	Gene Title	p-value		Fold-Change	
		0.5 M	0.8 M	0.5 M	0.8 M
	Long-term downregulated Genes				
cheW	purine-binding chemotaxis protein	1.75E-02	1.81E-02	-6.03	-7.57
flgK	flagellar hook-associated protein FlgK	2.57E-02	2.66E-03	-2.19	-3.25
	Long-term upregulated Genes				
pheP	phenylalanine transporter	1.91E-03	1.56E-03	2.84	3.35
proV	glycine betaine transporter ATP-binding subunit	3.45E-02	1.69E-02	9.59	26.62
proW	glycine betaine transporter membrane protein	9.43E-03	2.03E-03	14.77	83.95
proX	glycine betaine transporter periplasmic subunit	2.38E-02	3.80E-03	11.26	68.25
cysJ	sulfite reductase subunit alpha	2.18E-02	2.23E-03	2.04	11.64
purE	phosphoribosylaminoimidazole carboxylase	1.52E-02	3.90E-03	4.28	18.70
purK	phosphoribosylaminoimidazole carboxylase	9.02E-03	3.40E-03	3.24	10.18
cysP	thiosulfate transporter subunit	8.28E-03	5.00E-03	5.73	8.94

Table 2A: Selected Enriched Gene Ontology groups for common genes of *E. coli* in long-term adaptation to high and very high NaCl concentrations (0.5 and 0.8 M).

GO number	GO name	Count[1]	%[2]	p-value	Gene Ecocyc Ids
	Long-term downregulated Genes				
	Biological Process				
GO:0040011	locomotion	2	3.08	4.48E-02	*cheW*, *flgK*
	Long-term upregulated Genes				
	Biological Process				
GO:0006865	amino acid transport	4	4.08	9.47E-03	*pheP*, *proW*, *proV*, *proX*
GO:0000097	sulfur amino acid biosynthetic process	2	5.13	4.37E-02	*cysK*, *cysJ*
GO:0009168	purine ribonucleoside monophosphate biosynthetic process	2	8.50	9.03E-03	*purK*, *purE*
	Molecular Function				
GO:0008271	secondary active sulfate transmembrane transporter activity	1	16.67	4.93E-02	*cysP*

[1]Number of genes found for each GO term.
[2]Coverage of the total number of genes for this GO term.

Table 2B: Selected Enriched Gene Ontology clusters of E. coli in long-term adaptation to very high NaCl concentration (0.8 M).

GO number	GO name	Count[1]	%[2]	P-value	Gene Ecocyc Ids[3]
Cluster I. Long-term downregulated Genes					
Biological Process					
GO:0009296	flagellum assembly	2	11.74	5.91E-03	*flgK, flhD*
GO:0009173	pyrimidine ribonucleoside monophosphate metabolic process	1	25.00	2.74E-02	*yeiA*
Molecular Function					
GO:0004022	alcohol dehydrogenase (NAD) activity	1	16.67	3.15E-02	*adhE*
Cluster II. Long-term upregulated Genes					
Biological Process					
GO:0009127	purine nucleoside monophosphate biosynthetic process	9	52.94	1.27E-10	*guaB, guaA, purH, purK, purM, purL, purB, purN, purE*
GO:0009408	response to heat	4	14.81	5.67E-03	*hslJ, ldhA, pspA, yhbO*
GO:0015741	fumarate transport	1	100.00	2.72E-02	*dctA*
Molecular Function					
GO:0015419	sulfatetransmembrane-transporting ATPase activity	2	28.57	1.29E-02	*cysA, cysP*
GO:0008863	formate dehydrogenase activity	2	18.18	3.16E-02	*fdhF, fdoI*

[1]Number of genes found for each GO term.
[2]Coverage of the total number of genes for this GO term.

4. Metabolic Flux Analysis Data

Experimental and theoretical fluxes for control, 0.5M NaCl and 0.8M NaCl are shown in Table 3.

Table 3. Experimental and theoretical fluxes obtained in the steady states of anaerobic continuous reactors of *E. coli* with different concentrations of NaCl using complex medium and glycerol as C-source. Metabolic fluxes were normalized using the glycerol income flux and expressed as mean ± standard deviation.

Transformation	Control		0.5 M NaCl		0.8 M NaCl	
	Experimental Flux	Theoretical Flux	Experimental Flux	Theoretical Flux	Experimental Flux	Theoretical Flux
Feed glycerol	5.36 ± 0.12	5.36	5.82 ± 0.13	5.82	7.91 ± 0.17	7.91
Feed fumarate	0.49 ± 0.04	0.49	0.53 ± 0.04	0.53	0.72 ± 0.06	0.72
Feed CR	1.96 ± 0.04	1.96	2.13 ± 0.04	2.13	2.90 ± 0.06	2.90
Efflluent glycerol	4.36 ± 0.13	4.36	4.82 ± 0.31	4.82	6.91 ± 0.43	6.91
Effluent LC	0.42 ± 0.08	0.42	0.21 ± 0.04	0.21	0.29 ± 0.06	0.29
Effluent CR	0.25 ± 0.05	0.25	0.98 ± 0.05	0.98	1.67 ± 0.07	1.67
Effluent GBB	1.27 ± 0.05	1.27	0.94 ± 0.05	0.94	0.92 ± 0.07	0.92
Ex.ethanol	0.28 ± 0.04	0.28	0.39 ± 0.03	0.39	0.23 ± 0.02	0.23
Ex.pyruvate	0.03 ± 0.00	0.03	0.02 ± 0.00	0.02	0.03 ± 0.00	0.03
Ex.fumarate	0.01 ± 0.00	0.01	0.01 ± 0.00	0.01	0.10 ± 0.04	0.10
Ex.acetate	0.54 ± 0.09	0.54	0.42 ± 0.04	0.42	0.42 ± 0.05	0.42
Ex.lactate	0.11 ± 0.00	0.11	0.11 ± 0.01	0.11	0.24 ± 0.01	0.24
Pro U	0.15 ± 0.00	0.15	0.10 ± 0.00	0.10	0.09 ± 0.00	0.09
T.bio	6.27E-04 ± 0.78E-05	6.27E-04	4.26E-04 ± 0.00E-04	4.26E-04	0.58E-04 ± 0.00E-04	0.58E-04

5. Integration pathway analysis

Additional figures of Integration pathway analysis are depicted in Figure 1.

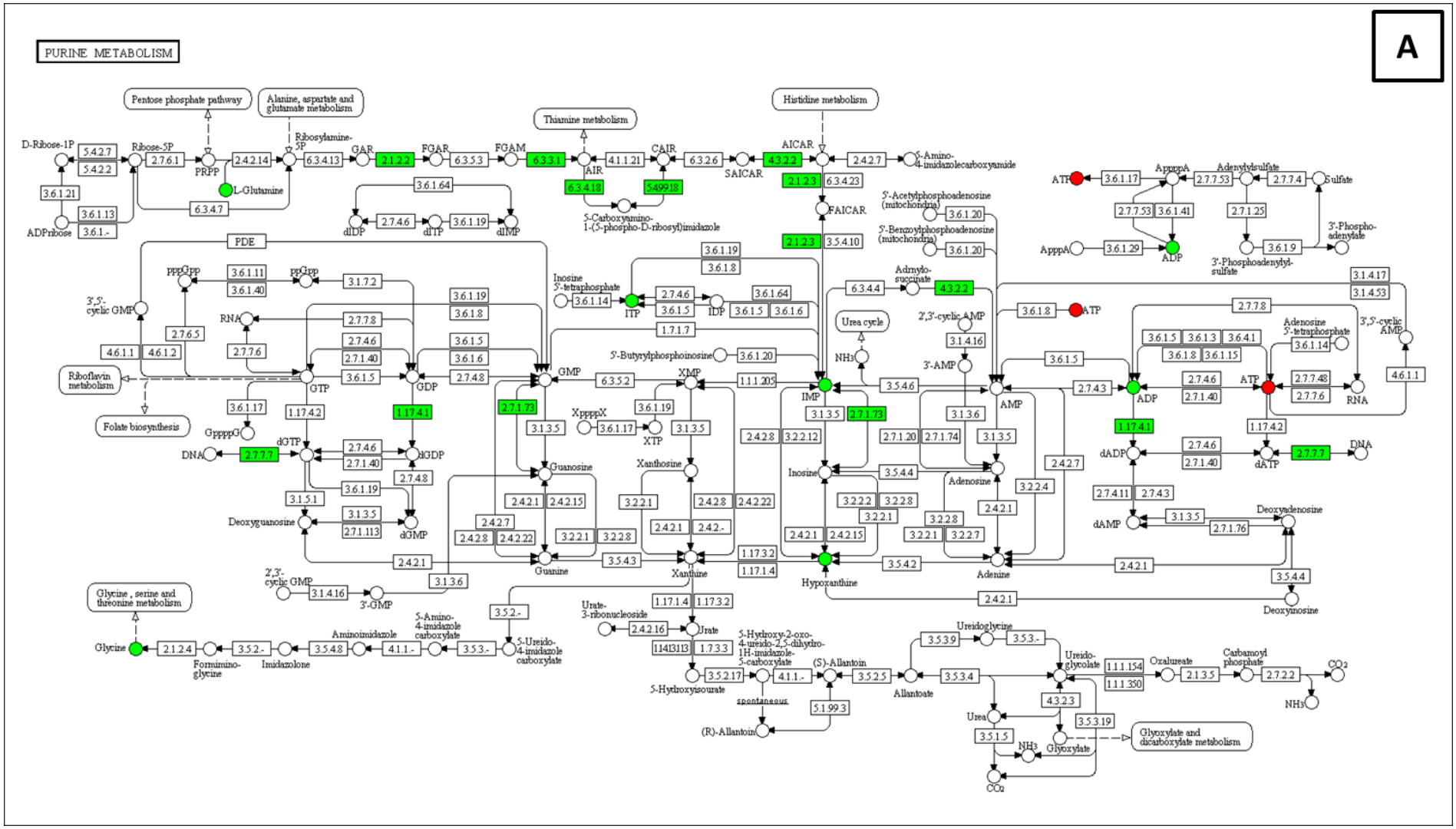
A
PURINE METABOLISM
Pentose phosphate pathway
Alanine, aspartate and glutamate metabolism
Thiamine metabolism
Histidine metabolism
Riboflavin metabolism
Folate biosynthesis
Glycine , serine and threonine metabolism
Urea cycle
Glyoxylate and dicarboxylate metabolism
D-Ribose-1P
Ribose-5P
PRPP
L-Glutamine
ADPribose
Ribosylamine-5P
GAR
FGAR
FGAM
AIR
CAIR
AICAR
SAICAR
FAICAR
5-Amino-4-imidazolecarboxyamide
5-Carboxyamino-1-(5-phospho-D-ribosyl)imidazole
dIDP
dITP
dIMP
PDE
3',5'-cyclic GMP
RNA
GTP
GDP
GMP
IMP
XMP
ITP
IDP
Inosine 5'-tetraphosphate
5'-Butyrylphosphoinosine
Admylo-succinate
2',3'-cyclic AMP
3'-AMP
AMP
ADP
ATP
Adenosine 5'-tetraphosphate
3',5'-cyclic AMP
dGTP
dGDP
dGMP
DNA
Guanosine
Xanthosine
Inosine
Adenosine
dADP
dATP
dAMP
Deoxyguanosine
Deoxyadenosine
Guanine
Xanthine
Hypoxanthine
Adenine
Deoxyinosine
2',3'-cyclic GMP
3'-GMP
Urate-3-ribonucleoside
Urate
5-Hydroxy-2-oxo-4-ureido-2,5-dihydro-1H-imidazole-5-carboxylate
(S)-Allantoin
5-Hydroxyisourate
spontaneous
(R)-Allantoin
Allantoate
Ureidoglycine
Ureido-glycolate
Oxalureate
Carbamoyl phosphate
Urea
Glyoxylate
Glycine
Formimino-glycine
Imidazolone
Aminoimidazole carboxylate
5-Amino-4-imidazole carboxylate
5-Ureido-4-imidazole carboxylate
ApppA
Adenylylsulfate
Sulfate
3'-Phospho-adenylate
3'-Phosphoadenylyl-sulfate
5'-Acetylphosphoadenosine (mitochondria)
5'-Benzoylphosphoadenosine (mitochondria)
PPGpp
ppGpp
GppppG
XppppX
XTP
Riboflavin metabolism
Folate biosynthesis
Glycine , serine and threonine metabolism
Urea cycle
Glyoxylate and dicarboxylate metabolism

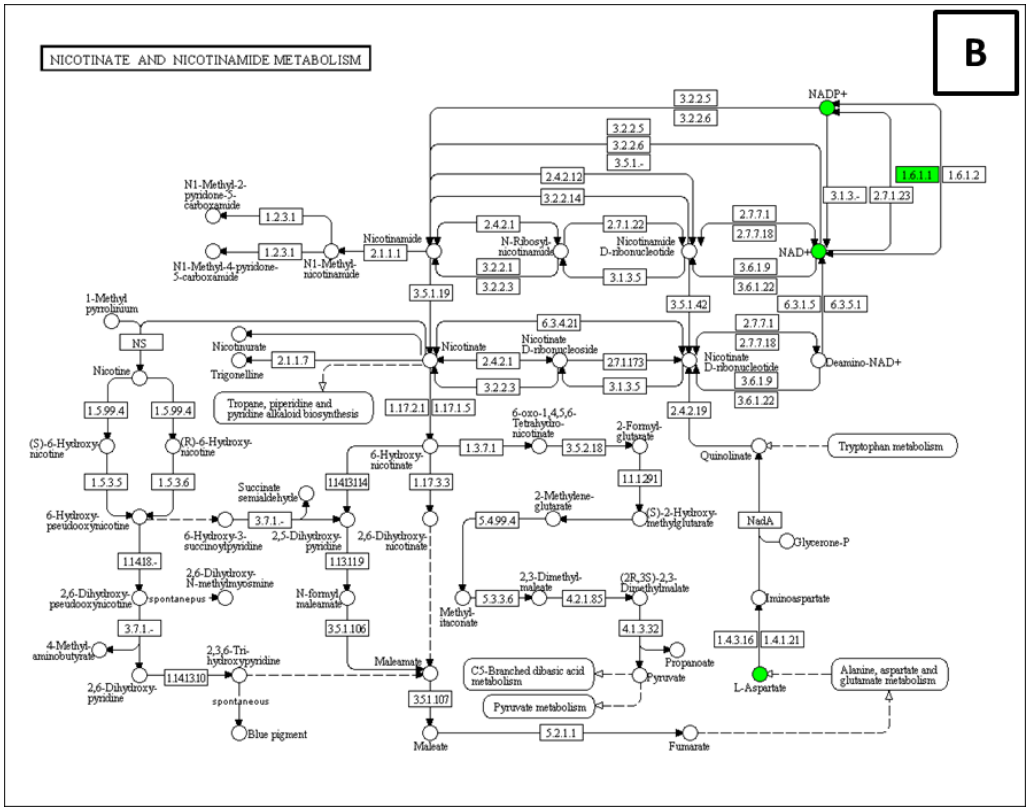
B
NICOTINATE AND NICOTINAMIDE METABOLISM
NADP+
NAD+
Nicotinamide
N-Ribosyl-nicotinamide
Nicotinamide D-ribonucleotide
N1-Methyl-2-pyridone-5-carboxamide
N1-Methyl-4-pyridone-5-carboxamide
N1-Methyl-nicotinamide
1-Methyl pyrrolinium
NS
Nicotine
Nicotinurate
Trigonelline
Tropane, piperidine and pyridine alkaloid biosynthesis
Nicotinate
Nicotinate D-ribonucleoside
Nicotinate D-ribonucleotide
Deamino-NAD+
(S)-6-Hydroxy-nicotine
(R)-6-Hydroxy-nicotine
6-Hydroxy-nicotinate
6-oxo-1,4,5,6-Tetrahydro-nicotinate
2-Formyl-glutarate
Quinolinate
Tryptophan metabolism
6-Hydroxy-pseudooxynicotine
6-Hydroxy-3-succinoylpyridine
2,5-Dihydroxy-pyridine
2,6-Dihydroxy-nicotinate
Succinate semialdehyde
2-Methylene-glutarate
(S)-2-Hydroxy-methylglutarate
NadA
Glycerone-P
2,6-Dihydroxy-pseudooxynicotine
2,6-Dihydroxy-N-methylmyosmine
N-formyl-maleamate
2,3-Dimethyl-malate
(2R,3S)-2,3-Dimethylmalate
Methyl-itaconate
Iminoaspartate
4-Methyl-aminobutyrate
2,3,6-Tri-hydroxypyridine
2,6-Dihydroxy-pyridine
Maleamate
C5-Branched dibasic acid metabolism
Propanoate
Pyruvate
L-Aspartate
Alanine, aspartate and glutamate metabolism
Pyruvate metabolism
Blue pigment
Malate
Fumarate
spontaneous
spontaneous

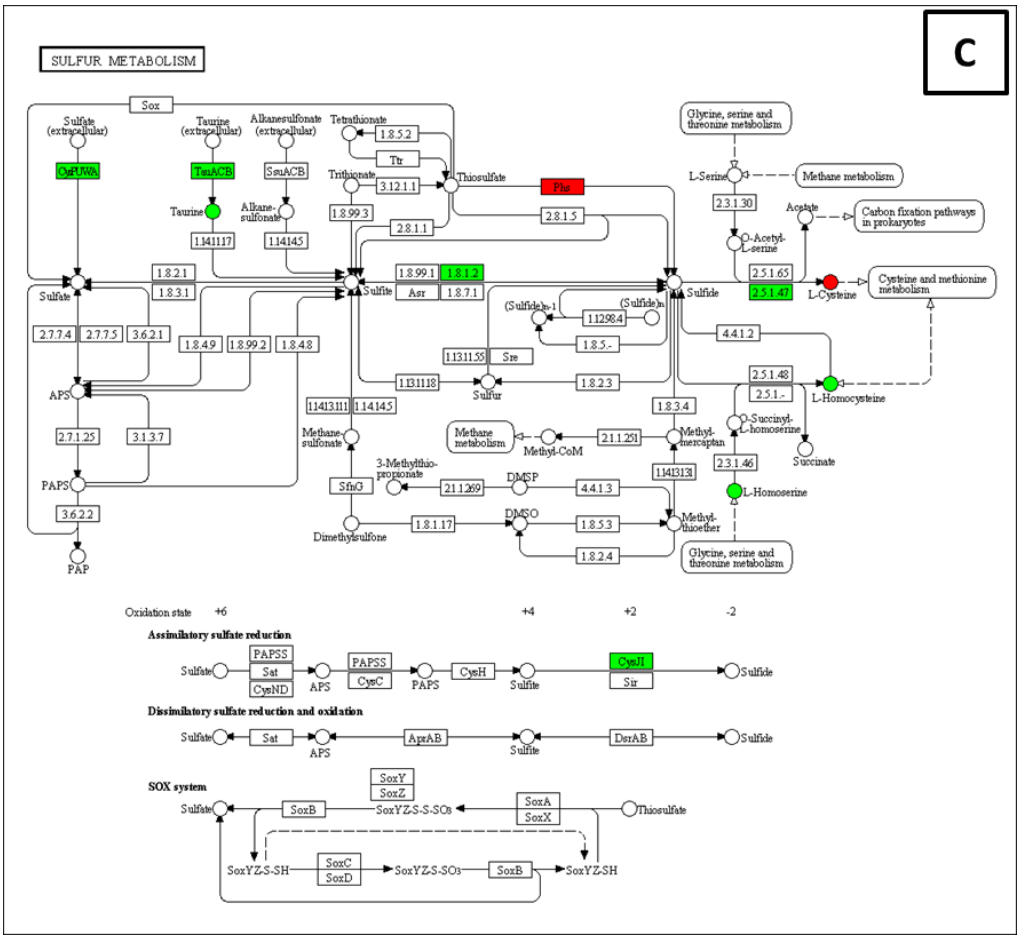
C
SULFUR METABOLISM
Sox
Sulfate (extracellular)
Taurine (extracellular)
Alkanesulfonate (extracellular)
Tetrathionate
CysPUWA
TauACB
SsuACB
Trithionate
Thiosulfate
Phs
Taurine
Alkane-sulfonate
Sulfate
Sulfite
Asr
Sulfide
L-Cysteine
Sre
Sulfur
APS
PAPS
PAP
Methane-sulfonate
Methane metabolism
Methyl-CoM
Methyl-mercaptan
3-Methylthio-propionate
SfnG
DMSP
DMSO
Dimethylsulfone
Methyl-thioether
L-Homocysteine
O-Succinyl-L-homoserine
Succinate
L-Homoserine
L-Serine
Glycine, serine and threonine metabolism
Methane metabolism
Acetate
Carbon fixation pathways in prokaryotes
O-Acetyl-L-serine
Cysteine and methionine metabolism
Oxidation state
+6
+4
+2
-2
Assimilatory sulfate reduction
PAPSS
Sat
CysND
APS
CysC
PAPS
CysH
Sulfite
CysJI
Sir
Sulfide
Dissimilatory sulfate reduction and oxidation
AprAB
DsrAB
SOX system
SoxY
SoxZ
SoxB
SoxYZ-S-SO3
SoxA
SoxX
Thiosulfate
SoxYZ-S-SH
SoxC
SoxD
SoxYZ-SO3

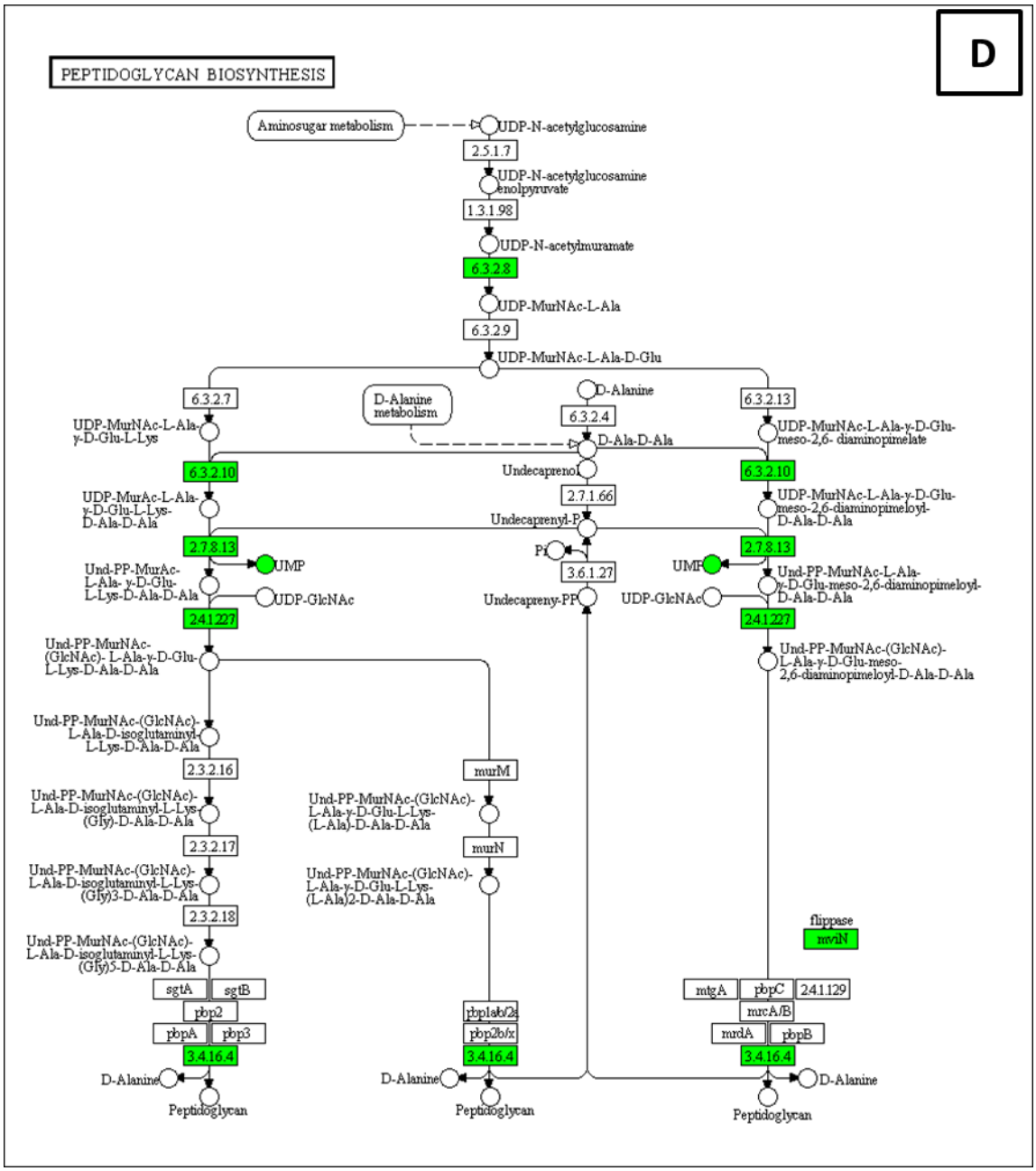
D
PEPTIDOGLYCAN BIOSYNTHESIS
Aminosugar metabolism
UDP-N-acetylglucosamine
2.5.1.7
UDP-N-acetylglucosamine enolpyruvate
1.3.1.98
UDP-N-acetylmuramate
6.3.2.8
UDP-MurNAc-L-Ala
6.3.2.9
UDP-MurNAc-L-Ala-D-Glu
6.3.2.7
UDP-MurNAc-L-Ala-γ-D-Glu-L-Lys
D-Alanine metabolism
D-Alanine
6.3.2.4
D-Ala-D-Ala
6.3.2.13
UDP-MurNAc-L-Ala-γ-D-Glu-meso-2,6- diaminopimelate
6.3.2.10
UDP-MurAc-L-Ala-γ-D-Glu-L-Lys-D-Ala-D-Ala
Undecaprenol
2.7.1.66
Undecaprenyl-P
6.3.2.10
UDP-MurNAc-L-Ala-γ-D-Glu-meso-2,6-diaminopimeloyl-D-Ala-D-Ala
2.7.8.13
UMP
Und-PP-MurAc-L-Ala-γ-D-Glu-L-Lys-D-Ala-D-Ala
UDP-GlcNAc
Pi
3.6.1.27
Undecapreny-PP
UMP
UDP-GlcNAc
2.7.8.13
Und-PP-MurNAc-L-Ala-γ-D-Glu-meso-2,6-diaminopimeloyl-D-Ala-D-Ala
2.4.1.227
Und-PP-MurNAc-(GlcNAc)-L-Ala-γ-D-Glu-L-Lys-D-Ala-D-Ala
2.4.1.227
Und-PP-MurNAc-(GlcNAc)-L-Ala-γ-D-Glu-meso-2,6-diaminopimeloyl-D-Ala-D-Ala
Und-PP-MurNAc-(GlcNAc)-L-Ala-D-isoglutaminyl-L-Lys-D-Ala-D-Ala
2.3.2.16
murM
Und-PP-MurNAc-(GlcNAc)-L-Ala-γ-D-Glu-L-Lys-(L-Ala)-D-Ala-D-Ala
2.3.2.17
murN
Und-PP-MurNAc-(GlcNAc)-L-Ala-γ-D-Glu-L-Lys-(L-Ala)2-D-Ala-D-Ala
Und-PP-MurNAc-(GlcNAc)-L-Ala-D-isoglutaminyl-L-Lys-(Gly)-D-Ala-D-Ala
2.3.2.17
Und-PP-MurNAc-(GlcNAc)-L-Ala-D-isoglutaminyl-L-Lys-(Gly)3-D-Ala-D-Ala
2.3.2.18
Und-PP-MurNAc-(GlcNAc)-L-Ala-D-isoglutaminyl-L-Lys-(Gly)5-D-Ala-D-Ala
flippase
mviN
sgtA
sgtB
pbp2
pbpA
pbp3
3.4.16.4
pbp1a/b/2a
pbp2b/x
3.4.16.4
mtgA
pbpC
2.4.1.129
mrcA/B
mrdA
pbpB
3.4.16.4
D-Alanine
Peptidoglycan
D-Alanine
Peptidoglycan
D-Alanine
Peptidoglycan

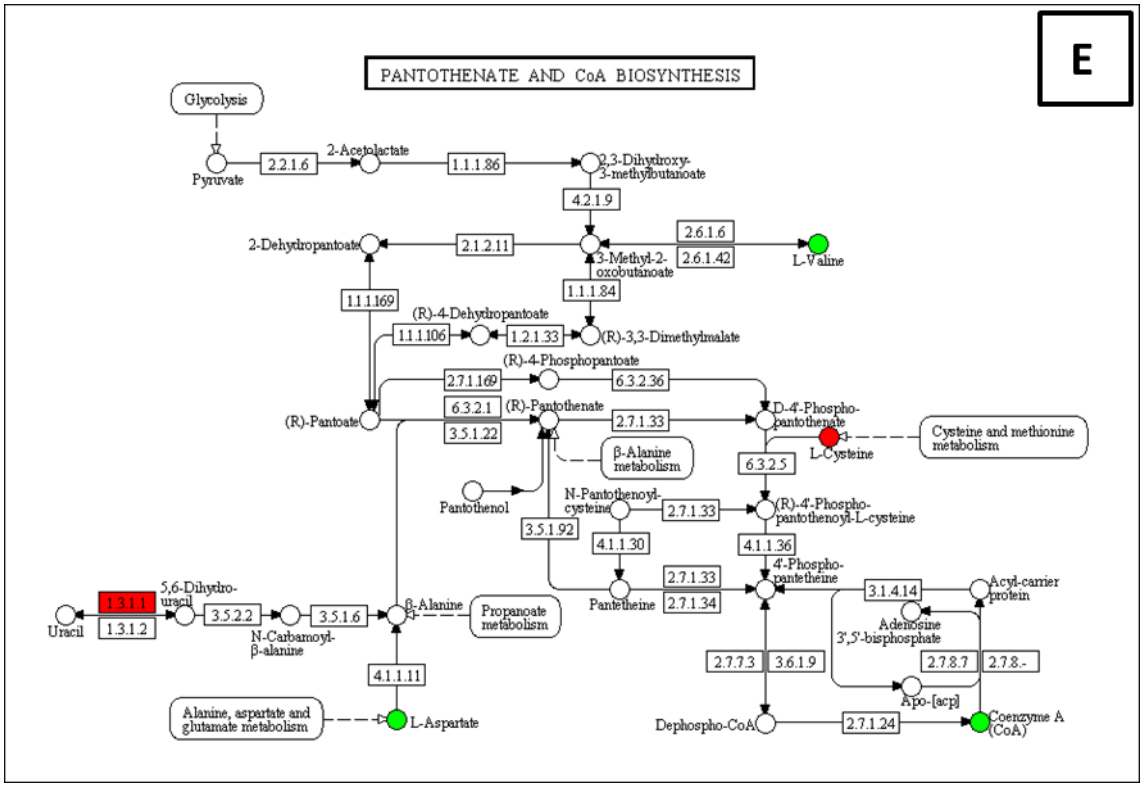

Figure 1. KEEG pathways highlighted by pathway-based integrative analysis: A. Purine metabolism. B. Nicotinate and nicotinamide metabolism. C. Sulfur metabolism. D. Peptidoglycan biosynthesis E. Pantothenate and CoA biosynthesis. Upregulated genes and metabolites with increased levels after reaching a new steady state in the presence 0.8 M NaCl are highlighted in green, whereas downregulated genes or metabolites with decreased levels are in red. As established in the Materials and Methods section, the minimum fold change was set to 2.

Chapter 5

Metabolic analysis in bioprocesses:

New insights into role of CobB in *Escherichia coli* using pathway-based analysis to integrate metabolomic and transcriptomic data in acetate-feeding chemostats

The contents of this chapter resulted in the following manuscript in preparation:

Bernal, C., Sevilla, A., Vidal, R., Gómez, M.T., Castaño-Cerezo, S., Suárez-Méndez, C., Iborra, J.L., Heijen, J., Wahl, A., Cánovas, M. New insights into role of CobB in Escherichia coli using pathway-based analysis to integrate metabolomic and transcriptomic datain acetate-feeding chemostats

ABSTRACT

Acetate assimilation is carried out in *E. coli* by two pathways, Acetyl CoA synthetase (ACS) and the pathway that involves two enzymes, acetate kinase (ACK) and phosphate acetyltransferase (PTA). ACS pathway is regulated by acetalylation, a post-translational modification (PTM), utilizing two enzymes YfiQ and CobB. The former is able to acetylate ACS repressing its activity, whereas the latter, CobB, belongs to the NAD+ dependent-Sir2 family and promotes ACS function by deacetylation. Furthemore, CobB has been found to be essential in additional processes such as flagella biosynthesis, motility and acid stress survival in glucose batch cultures and glucose-limited chemostats of ΔcobB. However, there is a lack of information of the effect of the ΔcobB when acetate was used as the sole carbon source.

Since CobB seems to be essential for the regulation of central carbon metabolism protein activities, the aim of this work was to study the effect of the deletion of the gene *cobB* in aerobic steady-state chemostats, using acetate as the sole carbon source. For this purpose, we used transcriptomics and metabolomics, integrating the data by using pathway-based analysis. The results obtained showed no statistical differences in the central carbon metabolism as previously reported in the case of limited-glucose chemostats. However, integration pathway analysis pointed to a strong metabolic effect, mainly in the nitrogen and also in the sulfur metabolisms, showing pathways such as the CoA biosynthesis (CoA resulted 2.4-fold higher in the cobB mutant), taurine, pyrimidines (higher content in pyrimidines, besides the downregulation of the operon *rut*ABCDEFG) and several amino acids (Cys, Gly and Glu were abruptly diminished in ΔcobB) metabolisms mainly affected. Taking into account the results obtained, it is suggested that the nitrogen metabolism is directly or indirectly regulated by protein acetylation. In the present work, Integration pathway-based analysis is seen to be useful for managing both, massive transcriptomic as well as metabolomic data in order to integrate them and to generate a better understanding of the CobB role.

INTRODUCTION

The acetate switch takes place when cells have depleted their acetate producing carbon sources, for example, glucose. When *Escherichia coli* grows using glucose as carbon source, it produces acetate that generates energy in the form of ATP. As shown in Figure 1, *E. coli* and other bacteria are able to express and activate the machinery responsible for acetate assimilation when the switch takes place (Wolfe, 2005). There are two pathways able to assimilate acetate in *E. coli*: the high-affinity pathway Acetyl CoA Synthetase (ACS) which works only in one direction, generating Acetyl CoA, and the low-affinity pathway that involves two enzymes, Acetate Kinase (ACK) and Phosphate acetyltransferase (PTA). These two enzymes are reversible, and can work in both directions. Acetate assimilation depends primarily on the ACS pathway while dissimilation depends on the PTA/ACK pathway. According to mutant phenotypes, the lack of PTA affects acetate production, while it is lower than that of the wild type strain. ACS and ACK/PTA are the only two pathways responsible for acetate assimilation since a double knockout is unable to grow when using acetate as the sole carbon source (Castaño-Cerezo et al., 2009)*****.

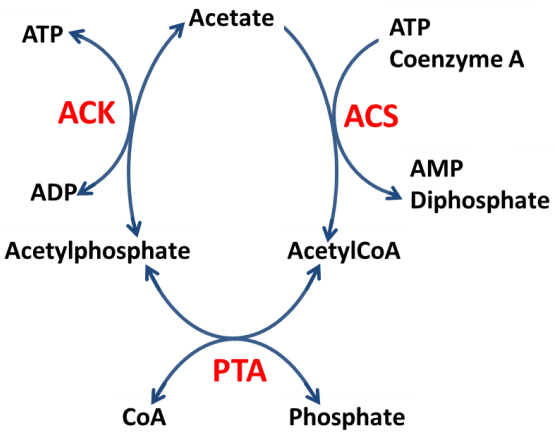

Figure 1. Acetate switch machinery. In this picture is depicted the high-affinity pathway (acetyl CoA synthase, ACS) and the low-affinity pathway that involves two enzimes (acetate kinase, ACK and phosphate acetyltransferase, PTA).

*****The citation Castaño-Cerezo is shown in the references as Castano-Cerezo.

A previous study (Castaño-Cerezo et al., 2011) described the regulation of the high-affinity pathway, ACS, by two enzymes: the protein acetyltransferase belonging to the Gcn5-related N-acetyltransferases (GNAT family) , YfiQ that represses ACS activity by acetylation, and the sirtuin-like deacetylase CobB, which promotes its function by deacetylation. The results obtained showed slight differences between the WT and the Δ*yfiQ* phenotypes when acetate was the sole carbon source. By contrast, the growth of the Δ*cobB* mutant was severely impaired in the same conditions. These results showed that CobB is

essential for the regulation of ACS activity. CobB belongs to the sirtuin family: NAD^+-dependent protein deacetylase enzymes that are broadly conserved from bacteria to human (Zhao et al., 2004). Sirtuins are involved in different roles such as gene regulation, metabolism and longevity (Satoh et al., 2011). In fact, several studies have reported that a great number of central metabolism enzymes are acetylated in lysine residues, (Choudhary et al., 2009; Herinksen et al., 2012; Kim et al., 2013; Lundby et al., 2012; Van Noort et al., 2012; Weinert et al., 2011, 2013, 2014). In bacteria, CobB stimulates ACS activity by deacetylating its active site, lysine 609 (Castaño-Cerezo et al., 2014; Zhao et al., 2004) and also Isocitrate lyase (ICL), the key enzyme of the glyoxylate shunt (Castaño-Cerezo et al., 2014).

The sirtuin role has been studied in other microorganisms, such as *Salmonella enterica* and *Saccharomyces cerevisiae*, where it was shown that the activation of acyl-coenzyme A synthetases requires sirtuin deacetylase protein functions (Starai et al., 2003). Although CobB has been also studied in *Bacillus subtilis* and *Rhodopseudomonas palustris*, the physiological role of *cobB* in bacteria still remain largely unknown (Li et al., 2010). In this latter, it is shown that CobB regulates *E. coli* chemotaxis by deacetylating CheY (chemotaxis response regulator), broadening our understandings of the physiological roles of the sirtuin protein family in bacteria and providing new insights into the regulation of bacterial chemotaxis.

A great contribution to our knowledge of the role of protein acetylation in *E.coli* physiology was provided in recent works (AbouElfetouh et al., 2014; Castaño-Cerezo et al., 2014; Kuhn et al., 2014; Weinert et al., 2013). In the study of

Kuhn and collaborators (2014) it was reported that the acetylation of thousands of lysine residues in hundreds of *E. coli* proteins are involved in essential cellular processes such as translation, transcription and the central metabolism. They concluded that *E. coli* possesses two mechanisms for lysine acetylation: the known AcCoA-dependent mechanism and the acetylphosphate (Acetyl-P)-dependent mechanism described in the study. In this latter, the effect of non-enzymatic acetylation of proteins by Acetyl-P appears to be quite extensive. Weinert and co-workers (2013), using an *E. coli* model, reported that most protein acetylation occurred at a low level and accumulated in growth-arrested cells depending on Acetyl-P formation through glycolysis, since mutants unable to convert Acetyl-P to acetate had high protein acetylation levels. Although it was found that this post-translational modification (PTM) occurs at a low level, these data do not preclude regulation of the metabolism by acetylation. In the work of AbouElfetouh and co-workers (2014), CobB showed no preference between enzymatic acetylated lysine sites and the non-enzymatic acetylated ones. Castaño-Cerezo and collaborators (2014) found that close to 17% of the quantified acetylated peptides were at least two-fold acetylated in Δ*cobB* mutant compared to wild-type strain. The number of peptides was higher in the case of acetate batch and glucose-limited chemostats where the Δ*cobB* mutant phenotype was clearly impaired. The acetylated proteins found in this study, especially those involved in amino acid and nucleotide biosynthesis and carbohydrate metabolism, were related to a metabolic function. Furthermore, in glucose-limited chemostats, flux through the glyoxylate shunt was decreased by 34% in the case of the Δ*cobB* strain and the ICL activity decreased almost 20 times. Besides these facts, transcriptomic and proteomic experiments demonstrated that protein deacetylation by CobB regulates the acetate metabolism, flagella biosynthesis, motility and acid stress survival in glucose batch cultures and glucose-limited chemostats.

In the recent work of AbouElfetouh and co-workers (2014) the preference of acetylated lysine sites of CobB was studied. The results obtained revealed that CobB presented special affinity for acetylated lysines adjacent to alanine, glycine, tyrosine and negative charge residues, independently if acetylation donor was AcCoA or Acetyl-P. However, an additional study of the structure is

needed since the secondary structure plays a key role in the ability of CobB to recognize these sites.

Apart from this, no other metabolic pathways regulated by the sirtuin-like CobB have been revealed. For this reason, the present work focused on the metabolic and transcriptomic characterization of the wild type and Δ*cobB* mutant in chemostat cultures with high concentrations of acetate as the sole carbon source, where the main acetate assimilation pathway is PTA-ACK. Further, since CobB seems to be essential for the regulation of the central carbon metabolism enzyme activities, the aim of this work was to broaden our knowledge about the metabolic and transcriptomic regulation by the sirtuin-like CobB in *E. coli* in aerobic chemostats using acetate-feeding. Furthermore, both sets of data were integrated using pathway analysis, highlighting pathways missed using transcriptomics data alone.

MATERIALS AND METHODS

Strain and cultivation conditions

The wild type strain of *E. coli* BW25113 and its derived *cobB* knockout (Baba et al., 2006) were used in the present study. Chemostat cultivations of these two strains, WT and Δ*cobB,* were carried out using sodium acetate as a carbon source. A 3L culture vessel with 2L working volume was used at 0.05 h^{-1} dilution rate. The temperature was set at 37^{o}C while the pH of 7.4 was controlled with HCl mainly. Minimal medium was the same as described in Taymaz-Nikerel, et al. (2010) but using 300 mM of acetate as a carbon source. In the case of the *cobB* knockout mutant, 30 µg/L of kanamycin was added to the medium since this strain presents kanamycin resistance. The aeration rate was set at 0.5 L/min and the pO2 was maintained above 40%, ensuring fully aerobic conditions. Experiments were performed in Biostat B (Braun Biotech International GMBH, Melsungen, Germany) reactors equipped with temperature, pH and oxygen probes, using pump controls for continuous operation. The stationary state was confirmed after 5 residential times when no modification in biomass concentration was observed, after which the samples

were harvested. In the steady state, a biomass dry weight of 2.5 g/L approx. was reached.

Chemicals

Standard metabolites were generally supplied by Sigma Aldrich (St Louis MO, USA), but glycine and histidine were from by Merck (Madrid, Spain). Phenylalanine, tryptophan, and the chemicals used as eluents (acetonitrile, acetic acid, ammonium acetate, ammonium hydroxide, and water) were obtained from Panreac (Barcelona, Spain). All chemicals were of HPLC grade quality.

Fermentation products excretion

Samples were withdrawn from the reactor and immediately centrifuged at 16,000 xg at 4^{o}C. Supernatants were used to determine external metabolites (acetate, ethanol, fumarate, pyruvate, and succinate) by an HPLC system from Shimadzu (Kyoto, Japan) with a cation exchange Aminex HPX-87H column supplied by BioRad Labs (Hercules, CA). The isocratic mobile phase was 5 mM H_2SO_4 at a flow rate of 0.5 mL min-1. The effluent was monitored using a refractive index detector (Shimadzu, Kioto, Japan).

Transcriptomic analysis

Sampling process

E. coli BW25113 (WT) and its derivative *cobB* knockout mutant (Δ*cobB*) were grown as described above. The samples were pelleted by centrifugation at 15000 x g and 4°C for 30 s. Total RNA was isolated using the Vantage RNA purification kit (Origene, MD, USA). Additionally, Dnase I digestion of the isolated RNA was performed using the Rnase-Free Dnase Set (QIAGEN Ibérica, Madrid, Spain) to avoid DNA interferences during the PCR steps. RNA quality and quantity were evaluated by microfluidic capillary electrophoresis on an Agilent 2100 Bioanalyzer (Agilent Technologies, Palo Alto, CA) using an Agilent RNA 6000 Pico kit. The GeneChip *E. coli* Genome 2.0 array of the Affymetrix system was used to compare gene expression. The processing of extracted RNA, cDNA labeling, hybridization, and slide-scanning procedures were performed according to the manufacturer's instructions (Affymetrix).

Statistical analysis

The statistical analysis was performed using the Bioconductor suite (Gentleman et al., 2005) in R (R Development Core Team, 2014). Affymetrix data files were processed with the affy package (Gautier et al., 2004). All of the microarrays were pre-processed simultaneously using Robust Multichip Average (RMA), as described by Irizarry et al. (2003) and scaled using log2. Afterwards, differentially expressed genes were identified from the limma package (Smyth 2005) with a P-value cut-off of 0.05, adjusted with Benjamini and Hochberg's method (Benjamini and Hochberg, 1995). Furthermore, the fold-change in gene expression of Δ*cobB* had to exceed a factor of 2 compared with the WT values for genes to be considered differentially expressed. Genes previously found differentially expressed were represented with a heatmap using package gplots (Warnes et al., 2012). Moreover, hierarchical clustering analysis was carried out using the complete agglomeration method from the stats package (R Development Core Team, 2014). Based on the different clusters found in the previous section, genes were analysed for gene term enriched analysis with the conditional hypergeometric test algorithm included in the GOstats Bioconductor package (Falcon and Gentleman, 2007). The p-value cut-off was set at 0.05. GO terms in the three categories, namely, BiologicalProcess (BP), Molecular Function (MF) and Cellular Component (CC), were included.

Endometabolome analysis.

Quenching

Quenching was performed by harvesting cells and introducing them into the quenching solution, 60% (vol/vol) methanol/water supplemented with 0.85% ammonium bicarbonate (AMBIC), kept at -40°C. AMBIC was added since it seemed to reduce osmotic shock and leakage in bacteria (Faijes et al., 2007) as well as in eukaryotic cells (Sellick et al., 2011); moreover, AMBIC is compatible with LC/MS analysis, despite controversial results (Kronthaler et al., 2012). Afterwards, the cells were pelleted by centrifugation at 3,000 x g for 5 min at -12ºC. The contact time with the methanol solution was kept as short as possible and the temperature was always kept below -12°C, since both factors have

been demonstrated to be critical (Schadel et al., 2011). The supernatant was removed by aspiration and kept for subsequent analysis to check and quantify leakage (Dietmair et al., 2010). Although, no leaking was detected, the results are expressed as fold-change and not as absolute concentrations since it is possible that no leakage was detected due to the sensitivity of the platform. Samples were kept at -86°C until extraction.

Extraction method validation.

The extraction method used based on Lazzarino et al., (2003) was previously validated (see chapter 2) by the use of several standard mixtures. Additionally, more metabolites (amino acids and other derivatives) were tested since a more complete metabolic analysis platform was available. Indeed, more than 70 metabolites were detected. The recovery was again more than 85% in all cases (results not shown). Besides, lyophilizing or freezing during and after the extraction procedure were avoided. For this reason, samples were prepared when the analysis platform was ready to avoid potential metabolic degradation, since lyophilization has been proven to alter the composition of metabolic mixtures (Oikawa et al., 2011) due to the presence of specific labile metabolites. Additionally, this method has been successfully tested in *E. coli* samples (Montero et al., 2014).

Extraction Method Description

Metabolite extraction was based on Lazzarino et al. (2003). First, samples from quenching step were re-suspended in 2 mL of extraction solution (acetonitrile + 10 mM KH_2PO_4 (3:1 v/v) at pH 7.4) and then incubated in a wheel for 30 minutes at 4^{o}C. This homogenate was then centrifuged at 15,000 xg for 20 min at 4^{o}C. The supernatant was separated and added to 4 mL of cold chloroform and centrifuged again at 15,000 x g for 5 min. This yielded a biphasic system, from which the aqueous phase was harvested. This process was carried out twice more. The extraction procedure was finished by filtering through a sterile 0.2 µm filter before being analyzed.

Analysis Method

The separation was carried out as previously described (Preinerstorfer et al., 2010) using an injection volume of 10 µl and a ZIC-HILIC as stationary phase: 150 mm x 4.6 mm internal diameter, and 5 µm particle size, provided with a guard column, 20 x 2.1 mm, 5 µm (Merck SeQuant, Marl, Germany) at a temperature of 25^{o}C. For metabolite elution, a gradient method was used with a flow rate of 0.5 ml/min. Mobile phases were 20 mM ammonium acetate (adjusted to pH 7.5 with NH_4OH) in H_2O (solvent A) and 20 mM ammonium acetate in AcN (solvent B). Gradient elution was performed, starting with 0% A and increasing to 80% A over 30 minutes, then return to starting conditions (80-0% A) for 1 minute followed by a re-equilibration period (0% A) of 14 minutes (total run time, 45 minutes). Data were acquired by a PC using the Agilent Chemstation software package provided by the HPLC manufacturer. Measurements for quantification were conducted using single ion monitoring (Bravo et al., 2011). The measured metabolites and the SIM ions used for quantification are summarized in Table 1. LC-MS experiments were performed on a 1200 series HPLC instrument (Agilent Technologies; California, USA) coupled to an Agilent 6120 single quadrupole mass spectrometer with orthogonal ESI source. The apparatus can be used in positive or negative ionization mode in either SCAN or SIM mode (Agilent Technologies). The mass spectrometer was operated in the positive ESI mode, using the SIM mode for the m/z of each compound. The ion spray voltage was set at 4000 V. Nitrogen with a flux of 12 L/min was used as the sheath gas (35 psi) and the auxiliary gas. The ion transfer capillary was heated to 300^{o}C. The fragmentation voltage was set at 100 V.

Metabolite Identification

Prior to the quantification process, the metabolites were identified using the retention time and relative intensities of the diagnostic ions of a pool of samples. For that, the mass spectra of single and pure standards were recorded and compared with the mass spectra of a pool of samples at the corresponding retention time. At least three diagnostic ions (preferably including the molecular ion) must be found, and their relative intensities should correspond to those of

the sample (see recent EU regulation for details) (Document No. SANCO/12495/2011). If the concentration of the metabolites in the sample was not sufficient to generate a clear spectrum, and a metabolite could not be unequivocally identified, pure calibration standards were spiked and the mass spectrum was recorded again. The diagnostic ions used as well as their relative intensities are summarized in Table 1. Due to the limitations of a single quadrupole for identifying isobaric compounds, their separation was confirmed by chromatography.

Quality control

The quality of the results was assessed by: (i) checking the extraction method with standard mixtures, (ii) internal standard (IS), and (iii) quality control samples (QC). The extraction method was validated by comparing the concentration of standard mixtures with and without the extraction process. Recoveries were higher than 85% in all of the analysed metabolites (results not shown). L-Phenyl-d5-alanine and Thymine-d4 (methyl-d3,6-d1) were added as internal standards (see Table 1), reaching a final concentration of 50 µM in each analysed sample, and the analysis was monitored by confirming that the internal standard area and retention time were always within an acceptable range. An acceptable coefficient of variation was set at 20% for the peak area and 2% for retention time. With respect to quality control samples, two types of QC were incorporated in the analysis: (i) a pool of samples and (ii) a pool of standards. QC analysis was performed in all of the analysed metabolites in the standard pool of samples and in all those in which concentrations were over the quantification limits of the sample pools. This was carried out by comparing the corrected areas. For the standard pool, the theoretical corrected area was calculated for the measured concentration. Regarding the pool of samples, the corrected areas were compared among all of the samples. An acceptable coefficient of variation was set at 20% for the peak area and 2% for retention time. QC samples were included in the analysis of the whole set of 20 biological samples. Additionally, random samples were analysed.

Quantitative analysis

The platform EasyLCMS (Fructuoso et al., 2012) was used for automated quantification. Standard and sample areas were normalized using the following formula, as previously established (Bunk et al., 2006):

$$A_N = \frac{A \cdot N}{A_{IS}}$$

In the formula above, A is the standard or sample area without normalization, A_N is the normalized area, N is the normalization value (10^6 by default), and A_{IS} is the internal standard area. Normalization with L-Phenyl-d5-alanine and Thymine-d4 (methyl-d3,6-d1) gave good results for several metabolic groups including nucleoside bases, nucleosides, nucleotides, amino acids, redox carriers, and vitamins, among others.

Table 1. LC-ESI-MS analytical parameters and method performance for compound standards of the quantified metabolites.

Metabolite	Abbreviation	Parent ion formula	Diagnostic ions (relative abundance)	RT (min)	SIM ion	LOD[a] (nmol/mL)	LOQ[b] (nmol/nM)	R^2	Intraday[c] RSD (%)	Interday[c] RSD (%)
Glycine	**Gly**	$C_2H_6NO_2^+$	76 (82), 98 (8), 150 (52)	15.0	76	4.71	15.71	0.9782	8.75	12.2
L-Alanine	**Ala**	$C_3H_8NO_2^+$	90 (100),112 (13), 134 (5)	14.3	90	4.81	16.03	0.9944	1.94	8.4
L-Serine	**Ser**	$C_3H_8NO_3^+$	88 (20), 106 (100),128 (10)	13.2	106	0.02	0.05	0.9826	1.50	9.3
L-Proline	**Pro**	$C_5H_{10}NO_2^+$	70 (2), 116 (100),138 (10)	25.8	116	0.90	3.0	0.9905	1.38	18.2
L-Valine	**Val**	$C_5H_{12}NO_2^+$	72 (5), 118 (80), 140 (15)	12.6	118	0.83	2.77	0.9935	1.14	11.5
L-Threonine	**Thr**	$C_4H_8NO_3^+$	74 (5), 120 (100),142 (10)	10.0	120[d]	0.91	3.03	0.9824	28.85	6.5
L-Homoserine	**HomoSer**	$C_4H_{10}NO^+$	74 (5), 120 (100),142 (8)	14.2	120[d]	0.28	0.94	0.9981	0.79	15.2
L-Cysteine	**Cys**	$C_3H_8NO_2S^+$	102 (10), 122 (42), 144 (44)	11.7	122	0.91	3.02	0.9992	1.36	7.9
Taurine	**Taurine**	$C_2H_6NO_3S^+$	126 (100), 146 (10), 148 (12), 251 (15)	12.1	126	3.11	10.36	0.9950	2.40	5.8
Thymine	**Thymine**	$C_5H_7N_2O_2^+$	127 (100),149 (10), 171 (10)	4.0	127	0.07	0.22	0.9991	0.45	13.7
L-Hydroxyproline	**HydroxyPro**	$C_5H_9NO_3^+$	86 (50), 132 (100),154 (10)	10.7	132[d]	1.73	5.77	0.9947	13.41	18.6
L-Isoleucine	**Ileu**	$C_6H_{14}NO_2^+$	86 (50), 132 (100),154 (10)	11.3	132[d]	0.45	1.5	0.9899	0.33	5.2
L-Leucine	**Leu**	$C_6H_{14}NO_2^+$	86 (10), 132 (100),154 (20)	14.1	132[d]	0.07	0.25	0.9926	1.22	16.7
L-Asparagine	**Asn**	$C_4H_9N_2O_3^+$	87 (10), 133 (100),155 (10)	14.5	133[d]	1.10	3.66	0.9834	1.31	0.9
L-Ornithine	**Orn**	$C_5H_{13}N_2O_2^+$	115 (25), 133 (100),155 (10)	26.5	133[d]	0.43	1.43	0.9902	0.44	2.5
L-Aspartic acid	**Asp**	$C_4H_6NO_4^+$	121 (20), 134 (100), 200 (75)	15.2	134	6.28	20.93	0.9837	2.78	4.9
L-HomoCysteine	**HomoCys**	$C_4H_{10}NO_2S^+$	90 (10), 136 (100),158 (10)	12.4	136	1.14	3.82	0.9859	0.37	6.7
Hypoxanthine	**Hypoxan**	$C_5H_5N_4O^+$	137 (70),159 (100), 175 (10)	11.0	137	0.23	0.77	0.9986	2.52	10.2
Acetylphosphate	**Acetyl-P**	$C_2H_4O_5P^+$	116 (100), 141 (23),163 (13)	15.3	141	0.76	2.53	0.9910	7.76	11.9
O-Phosphorylethanolamine	**OPE**	$C_2H_8NO_4P^+$	111 (5), 142 (100), 164 (10)	18.0	142	26.34	87.80	0.9705	4.0	8.4
L-Lysine	**Lys**	$C_6H_{15}N_2O_2^+$	84 (8), 130 (30), 147 (100),169 (8)	25.9	147[d]	0.10	0.35	0.9892	1.10	12.6
L-Glutamine	**Gln**	$C_5H_{11}N_2O_3^+$	130 (50), 147 (100),169 (67)	14.7	147[d]	0.73	2.45	0.9901	3.91	9.9
L-Glutamic acid	**Glu**	$C_5H_{10}NO_4^+$	102 (60), 148 (100), 170 (30),	14.9	148	0.37	1.23	0.9882	0.64	5.4
L-Methionine	**Met**	$C_5H_{12}NO_2S^+$	104 (8), 150 (100),172 (15)	11.6	150	0.01	0.04	0.99	1.50	3.4
L-Histidine	**His**	$C_6H_{10}N_3O_2^+$	137 (25), 156 (100), 178 (5)	15.0	156	0.24	0.79	0.9801	7.08	21.5

L-Carnitine	**Carnitine**	$C_7H_{16}NO_3^+$	149 (1), 162 (100),184 (5)	15.7	162	0.02	0.08	0.9899	4.04	7.9
L-Phenylalanine	**Phe**	$C_9H_{12}NO_2^+$	137 (35), 166 (100), 188 (20)	9.9	166	0.74	2.47	0.9987	2.08	12.5
L-Arginine	**Arg**	$C_6H_{13}N_4O_2^+$	140 (5), 175 (100),197 (2)	24.5	175	0.02	0.08	0.9950	1.47	16.4
L-Citrulline	**CIR**	$C_6H_{12}N_3O_3^+$	159 (19), 176 (100),198 (18)	15.3	176	0.38	1.26	0.9846	26.65	14.2
Glucosamine	**Glucosamine**	$C6H14NO_{5+}$	162 (35), 180 (100), 202 (10)	14.4	180	3.45	10.95	0.9940	14.3	7.9
L-Tyrosine	**Tyr**	$C_9H_{12}NO_3^+$	163 (15), 182 (100),204 (5)	12.1	182	0.76	2.55	0.9892	0.97	6.4
O-Phospho-L-Serine	**P-serine**	$C_3H_9NO_6P^+$	88 (18), 186 (100), 208 (5)	16.3	186	3.24	10.8	0.9923	1.19	0.5
2-Phosphogliceric acid	**2PG**	$C_3H_7O_7P^+$	187 (92),209 (33), 231 (19)	16.1	187 [d]	1.87	6.23	0.9924	0.70	3.1
3-Phosphogliceric acid	**3PG**	$C_3H_7O_7P^+$	187 (92),209 (33), 231 (19)	17.1	187 [d]	0.37	1.24	0.9932	0.82	4.0
N-Acetyl-L-Glutamine	**Ac-Gln**	$C_7H_{12}N_2O_4^+$	172 (15), 189 (80), 211 (60)	13.3	189	5.8	17.9	0.9812	2.6	0.6
L-Tryptophan	**Trp**	$C_{11}H_{13}N_2O_2^+$	177 (10), 205 (100),227 (30)	10.1	205	2.99	9.97	0.9897	5.13	2.4
L-Cystine	**Cystin**	$C_6H_{12}N_2O_4S_2^+$	156 (100), 241 (30), 263 (18)	17.0	241	12.07	40.24	0.9577	3.97	0.8
Thymidine	**Thymidine**	$C_{10}H_{13}N_2O_5^+$	243 (38), 265 (100), 281 (38)	4.2	243	0.17	0.57	0.9949	0.19	1.4
Biotin	**Biotin**	$C_{10}H_{17}N_2O_3S^+$	245 (43),267 (30), 527 (55)	10.8	245	1.52	5.07	0.9974	4.87	16.1
2'-Deoxyadenosine	**DA**	$C_{10}H_{14}N_5O_3^+$	139 (10), 252 (100), 274 (15)	5.2	252	0.04	0.13	0.9946	0.55	13.0
Glucosamine 6-phosphate	**GlucN6P**	$C_6H_{15}NO_8P^+$	242 (32), 260 (100),282 (8)	17.4	260	7.83	26.12	0.9993	2.06	5.1
L-Glutathione	**GSH**	$C_{10}H_{18}N_3O_6S^+$	308 (100),330 (10),618 (10)	14.6	308	5.64	18.82	0.9864	0.30	6.4
Thymidine monophosphate	**TMP**	$C_{10}H_{16}N_2O_8P^+$	207 (25), 323 (100),345 (50)	14.4	323	15.8	52.4	0.9799	4.1	0.8
Cytidine monophosphate	**CMP**	$C_9H_{15}N_3O_8P^+$	112 (20), 266 (10), 324 (100)	16.0	324	1.25	4.18	0.9881	5.07	0.9
Uridine monophosphate	**UMP**	$C_9H_{14}N_2O_9P^+$	172 (90), 325 (100), 342 (25)	15.0	325	26.55	88.51	0.9820	3.53	10.6
Thiamine monophosphate	**ThiaMP**	$C_{12}H_{18}N_4O_4PS^+$	122 (25), 345 (100), 367 (15)	20.5	345	2.3	7.6	0.9812	12.4	14.6
Adenosine monophosphate	**AMP**	$C_{10}H_{11}N_5O_6P^+$	268 (15), 348 (100), 370 (10)	14.7	348	0.64	2.15	0.9910	2.04	18.4
Inosine monophosphate	**IMP**	$C_{10}H_{14}N_4O_8P^+$	138 (50), 349 (100),371 (41)	15.4	349	93.71	312.39	0.9810	11.13	23.1
Guanosine monophosphate	**GMP**	$C_{10}H_{15}N_5O_8P^+$	344 (18), 364 (100), 386 (42)	16.3	364	4.48	14.92	0.9885	10.29	9.1
Xanthosine monophosphate	**XMP**	$C_{10}H_{14}N_4O_9P^+$	157 (50), 365 (100),387 (27)	15.7	365	17.85	59.49	0.9945	2.57	5.4
Cytidine diphosphate	**CDP**	$C_9H_{14}N_3O_{11}P_2^+$	381 (40),404 (100),426 (48)	16.0	404	2.32	7.74	0.9822	5.48	8.8
Uridine diphosphate	**UDP**	$C_9H_{13}N_2O_{12}P_2^+$	301 (95), 405 (100), 427 (60)	15.4	405	73.50	350.02	0.9949	2.42	0.9
Adenosine diphosphate	**ADP**	$C_{10}H_{14}N_5O_{10}P_2^+$	348 (40),428 (100), 450 (20)	15.7	428	1.95	5.50	0.9941	2.07	9.4
Guanosine diphosphate	**GDP**	$C_{10}H_{14}N_5O_{11}P_2^+$	150 (85), 444 (100),466 (38)	16.0	444	4.70	15.67	0.9940	5.33	5.4

Tetrahydrofolic acid	**THF**	$C_{19}H_{23}N_7O_6^+$	399 (100), 446 (20), 468 (17)	16.0	446	1.06	3.54	0.9930	1.55	16.4
Riboflavin-5'-monophosphate	**FMN**	$C_{17}H_{20}N_4O_9P^+$	399 (30), 457 (100),479 (30)	13.6	457	2.33	7.76	0.9942	2.17	11.5
Deoxycytidine triphosphate	**dCTP**	$C_9H_{15}N_3O_{13}P_3^+$	397 (50), 468 (100), 490 (75)	16.5	468	10.8	30.7	0.9991	18.6	22.1
Deoxythymidine triphosphate	**TTP**	$C_{10}H_{16}N_2O_{14}P_3^+$	419 (40), 483 (100), 505 (50)	15.2	483	34.72	115.75	0.9811	0.96	10.0
Cytidine triphosphate	**CTP**	$C_9H_{15}N_3O_{14}P_3^+$	177 (43) , 484 (100),506 (60)	16.7	484	0.62	2.08	0.9501	12.17	8.4
Uridine triphosphate	**UTP**	$C_9H_{14}N_2O_{15}P_3^+$	485 (100), 507 (50), 589 (20)	15.9	485	2.25	7.49	0.9961	5.56	13.7
CDP-choline	**CDP-choline**	$C_{14}H_{27}N_4O_{11}P_2^+$	112 (20), 489 (100), 511 (80)	17.0	489	9.41	31.38	0.9949	5.70	4.6
Deoxyadenosine triphosphate	**dATP**	$C_{10}H_{15}N_5O_{12}P_3^+$	252 (100), 492 (20),512 (5)	15.3	492	5.9	18.1	0.9926	9.7	5.7
adenosine triphosphate	**ATP**	$C_{10}H_{15}N_5O_{13}P_3^+$	410 (15),508 (100),530 (20)	15.6	508	7.68	25.62	0.9877	1.74	12.5
Inosine triphosphate	**ITP**	$C_{10}H_{14}N_4O_{14}P_3^+$	475 (50), 509 (100),531 (49), 553 (35)	16.4	509	11.71	30.06	0.9722	2.12	8.4
Guanosine triphosphate	**GTP**	$C_{10}H_{15}N_5O_{14}P_3^+$	213 (15), 524 (100),546 (30)	16.5	524	22.16	73.86	0.9883	9.11	20.4
L-Glutathione oxidised form	**GSSG**	$C_{20}H_{33}N_6O_{12}S_2^+$	307 (100),613 (100),635 (50)	16.5	613	4.09	13.63	0.9913	4.84	5.4
Nicotinamide adenine dinucleotide oxidised form	**NAD^+**	$C_{21}H_{26}N_7O_{14}P_2^+$	123 (20), 333 (30), 664 (100),686 (50)	15.2	664	3.44	11.46	0.9943	3.08	6.7
Nicotinamide adenine dinucleotide reduced form	**NADH**	$C_{21}H_{28}N_7O_{14}P_2^+$	334 (70), 666 (80),688 (50)	16.0	666	49.24	164.15	0.9834	4.51	7.8
Nicotinamide adenine dinucleotide phosphate oxidised form	**$NADP^+$**	$C_{21}H_{29}N_7O_{17}P_3^+$	123 (50), 744 (100),766 (37)	16.6	744	3.91	13.03	0.9947	2.12	0.8
Nicotinamide adenine dinucleotide phosphate reduced form	**NADPH**	$C_{21}H_{27}N_7O_{17}P_3^+$	315 (25), 746 (25), 768 (10)	16.0	746	0.33	1.12	0.9875	2.52	0.4
Coenzyme A	**CoA**	$C_{21}H_{37}N_7O_{16}P_3S^+$	385 (60),768 (100),790 (25)	14.8	768	18.65	62.18	0.9913	6.79	9.7
Acetyl-CoA	**AcCoA**	$C_{23}H_{39}N_7O_{17}P_3S^+$	406 (100),810 (95),832 (25)	14.1	810	16.38	54.60	0.9881	2.89	1.4

[a] LOD calculated from standard deviation of memory peak areas of blank runs: 3 x standard deviation of memory peak area (n=6)/slope of calibration function with neat standard solutions.

[b] LOD calculated from standard deviation of memory peak areas of blank runs: 10 x standard deviation of memory peak area (n=6)/slope of calibration function with neat standard solutions.

[c] The intra- and inter-day precision were determined by analyzing six replicates of the standards at the same concentration level and calculated as the relative standard deviation (RSD) defined as the ratio of the standard deviation to the mean response factor of each metabolite.

[d] Chromatographically separated.

Pathway-based integrative analysis

The transcriptomic and metabolomic results were integrated using pathway analysis based on KEGG pathways. Genes were annotated using the KEGG *Escherichia coli* K-12 MG1655 database. Similarly, traditional metabolite names were translated into KEGG compound database identifiers. KEGG XML data files were downloaded from the *Escherichia coli* K-12 MG1655 database, which are freely available for academic users from the KEGG website (Kanehisa et al., 2014). SubpathwayMiner (Li et al., 2009) was used for mapping previously identified genes and metabolites to pathways for overrepresentation analysis using the hypergeometric test. P-values were adjusted with Benjamini and Hochberg's method (Benjamini and Hochberg, 1995) and a cut-off value of 0.05 was set. This analysis led to a list of overrepresented pathways, which were visualized using Pathview R package (Luo and Brouwer, 2013).

RESULTS

Physiology

In Table 2 the physiological data of the process are shown. Biomass achieved (expressed as dry weight, DW, g/L) in the steady-state of the acetate-feeding chemostats did not show statistical differences between WT and *CobB* mutant. The same conclusion was found for other parameters such as respiratory coefficient (RQ), biomass yield (Yx/s, mmol/g/h) and the specific acetate consumption rate (qAcet, mmol/g/h).

Table 2. Biomass, RQ, biomass yield and specific acetate consumption rate during acetate-feeding chemostate cultures. All data are expressed in their averages ± s.e.m.

	DW(g/L)	RQ	Yx/s (mmol/g/h)	qAcet (mmol/g/h)
WT	2.56±0.20	0.84±0.02	0.14±0.01	-4.44±0.49
ΔcobB	2.43±0.16	0.86±0.01	0.13±0.01	-4.74±0.20

Fermentation products

No statistical differences were found between the WT and *CobB* mutant as regards excretion of the fermentation products (Table 3).

Table 3. Specific production rates of the fermentation product during acetate-feeding chemostate cultures.

(mmol/g/h) ±sem	qCitrate	qSuccinate	qLactate	qFormate	qEthanol	qPyruvate
WT	0.05±0.01	0.02±0.00	0.02±0.00	0.14±0.01	0.14±0.00	0.0026±0.000
ΔcobB	0.06±0.00	0.03±0.00	0.02±0.00	0.12±0.00	0.08±0.07	0.0026±0.000

Transcriptomics

Out of more than 10,000 genes represented in the microarrays, as few as 147 were significantly changed ($p \leq 0.05$ with at least 2-fold alteration). Clustering analysis revealed that 73 genes were significantly downregulated, whereas 75 genes were significantly upregulated in the steady-state of Δ*cobB* culture compared to WT (Figure 2, Clusters I and II, respectively).

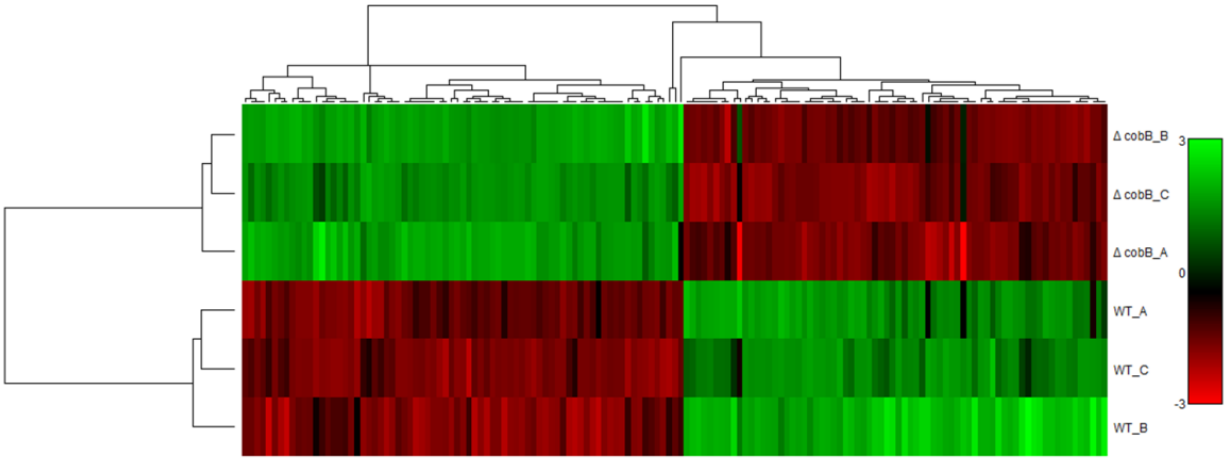

Figure 2. Clustering analysis of transcriptomic changes between WT and Δ*cobB* mutant in the stationary state of chemostats using acetate as the sole C-source.

A selection of GO terms is shown in Table 4. Interestingly, nitrogen utilization and transport was strongly hampered, including uracil degradation and the biosynthesis/ degradation/transport of several nitrogen rich amino acids such as lysine, arginine and glutamine.

Table 4: Selected Enriched Biological Process Gene Ontology clusters of transcriptomic analysis between WT and Δ*cobB* mutant in the stationary state of chemostats using acetate as sole C-source.

GO number	GO name	Count[1]	%[2]	P-value	Gene Ecocyc Ids[3]
		Cluster I. Downregulated Genes			
GO:0019740	nitrogen utilization	7	100.00	1.44E-14	*glnA*, ***rutE, rutF, rutC, rutD, rutB, rutA***
GO:0006212	uracil catabolic process	7	87.50	1.30E-13	***rutA, rutE, rutF, rutC, rutD, rutB,*** *rutG*
GO:0051454	intracellular pH elevation	3	75.00	5.47E-06	*gadB, gadC, gadA*
GO:0006536	glutamate metabolic process	3	18.75	6.26E-04	*gdhA, gadB, gadA*
GO:0009090	homoserine biosynthetic process	2	50.00	7.45E-04	*asd, lysC*
GO:0015847	putrescine transport	2	33.33	1.84E-03	*potF, potG*
GO:0009066	aspartate family amino acid metabolic process	5	5.95	2.44E-03	*asd, asnB, dapB, lysC, nadB*
GO:0009085	lysine biosynthetic process	3	12.00	2.65E-03	*asd, dapB, lysC*
GO:0006865	amino acid transport	5	4.81	6.11E-03	*yhdW, glnH, glnP, argT, gadC*
GO:0006476	protein deacetylation	1	100.00	1.13E-02	***cobB***
GO:0019544	arginine catabolic process to glutamate	1	100.00	1.13E-02	*astE*
GO:0019676	ammonia assimilation cycle	1	100.00	1.13E-02	*glnA*
GO:0072488	ammonium transmembrane transport	1	100.00	1.13E-02	*amtB*
GO:0009081	branched chain family amino acid metabolic process	3	6.67	1.40E-02	*leuD, ilvN, asd*
GO:0071468	cellular response to acidity	1	25.00	4.46E-02	*hdeA*

Cluster II. Upregulated Genes

GO:0040011	locomotion	35	63	9.30E-53	***flgF,*** *cheW****,*** *fliH****,*** ***flgE,*** *fliJ****,*** *fliO****,*** ***fliM****,* *flgK,* ***flgF****,* ***flgB****,* ***flgA****,* *flgJ,* ***fliF****, motA,* *fliE, cheY, flgI, fliN, tap, fliG, cheA,* *tap, motB,* ***flgG****, trg,* *fliC,* ***flgH****,* ***flgE****,* ***flgC****, mglB, flgL,* ***fliL****, tar, fliK, tsx*
GO:0071422	succinate transmembrane transport	1	1	1.37E-02	*dctA*
GO:0008643	carbohydrate transport	7	19.2	1.43E-02	*araF, mglC, rhaT, mglA, dctA, xylF, mglB*
GO:0009145	purine nucleoside triphosphate biosynthetic process	2	18	2.46E-02	*ndk, fliI*
GO:0015800	acidic amino acid transport	1	3	4.06E-02	*dctA*

[1]Number of genes found for each GO term.
[2]Coverage of the total number of genes for this GO term.
[3]Genes are underlined if they are up/down regulated with a fold-change of more than 5, and bold text indicates a fold change of more than 10.

Moreover, putrescine transport and ammonia transport and assimilation were transcriptionally downregulated. Besides, intracellular pH control seemed to be affected. In contrast, locomotion was strongly upregulated along with transport of carbon-rich metabolites such as succinate, acidic amino acids or carbohydrates. Additionally, *de novo* biosynthesis of purine nucleosides was upregulated.

Intracellular metabolomics

For a snapshot of the metabolism in the stationary state, 70 intracellular metabolites were measured in WT and Δ*cobB*, and for an overview of the results obtained, a PCA was carried out with all the data (Figure 3). A clearly different metabolic pattern was evident between the WT and Δ*cobB,* since the samples were clearly separate as regards their genetic background in the PC1, which encompassed more than 48% of the variance.

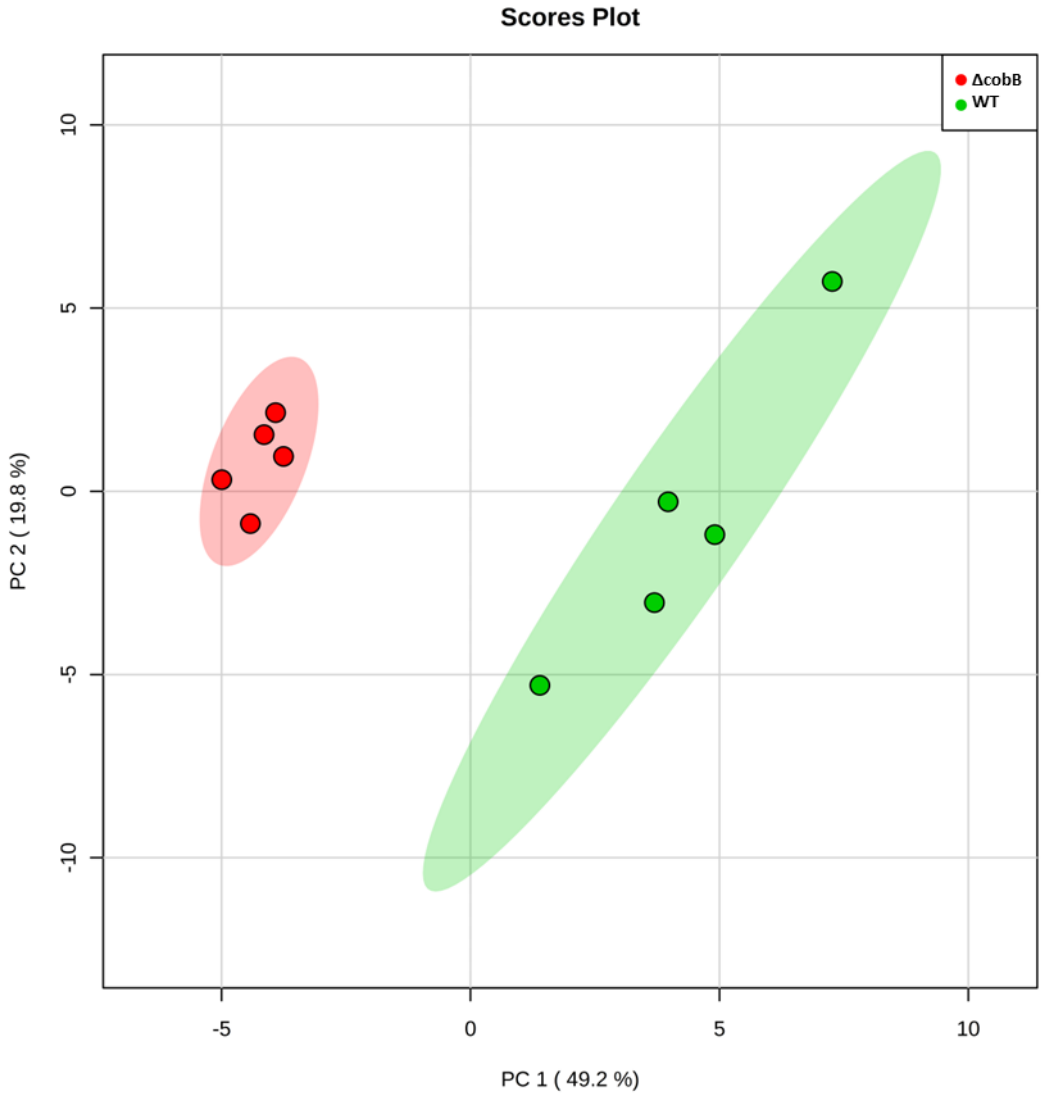

Figure 3. Scores plot from the PCA of the intracellular metabolites in the steady-state chemostats using acetate as a sole carbon source for wild type (WT,green) and Δ*cobB* mutant (cobB, red).

Figure 4 depicts the hierarchically clustered heat map of the metabolic levels of WT and mutant samples, as shows the main metabolic differences between *cobB* mutant and WT. Only the metabolic concentrations that presented a relevant statistical difference (t-test or welch test $p<0.05$) were included in the heatmap. In most cases, the intracellular metabolite levels in the mutant were lower than in the WT strain, with only a few exceptions, such as hypoxantine, thymine, thymidine, CoA and Arg which had higher levels in Δ*cobB*.

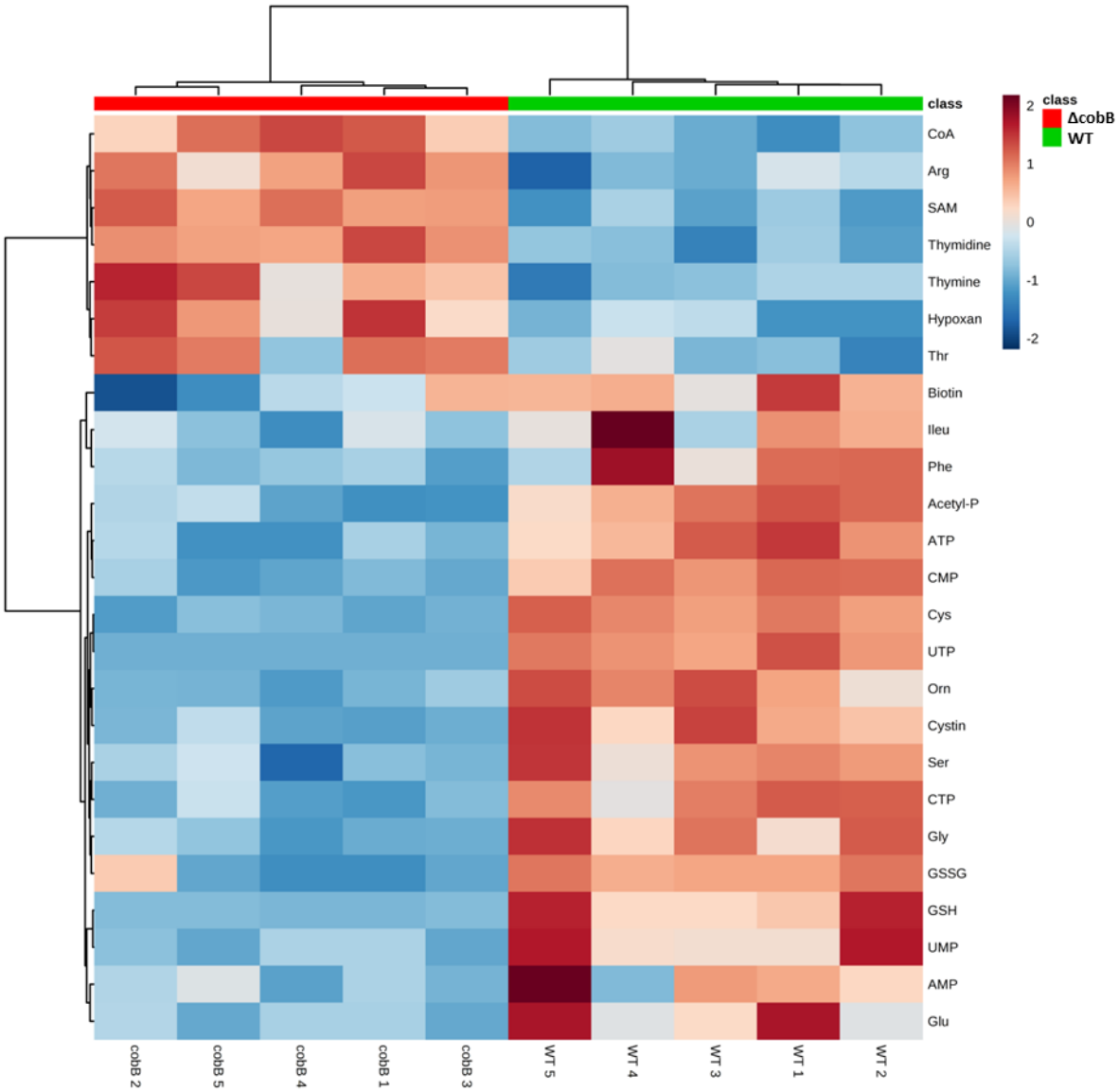

Figure 4. Heatmap of the intracellular metabolites of wild type strain (WT, green cluster) and Δ*cobB* mutant (cobB, red cluster) mutant in the stationary state of chemostats using acetate as the sole C-source.

The metabolites whose concentration changed to a statistically significant extent (t-test or welch test p<0.05) are listed in Table 5. Note the strong decrease in several amino acids such as glycine, L-serine, L-isoleucine and L-phenylalanine, whereas L-threonine and L-arginine were higher in Δ*cobB* mutant. The higher concentrations of the latter amino acids agrees with the fact that the genes related to their transport were strongly inhibited (Table 4).

Table 5. Metabolite fold-change and p-values between WT and Δ*cobB* mutant in stationary state chemostats using acetate as sole C-source. t-test was used to analyse differences between groups when variance was assumed to be homogeneous, or Welch correction was applied when data violated the assumption of homogeneity of variance. A p-value cut-off of 0.05 adjusted with Benjamini and Hochberg's method (FDR) was set. Shapiro-Wilk and Bartlett tests were used to check for normality and homoscedascity, respectively. Abbreviations are described in Table 1.

Metabolite	Compound	Δ*cobB* (FC)	FDR
Hypoxan	C00262	4.6	0.045*
Thymidine	C00214	2.9	<0.001***
Thr	C00188	2.8	0.017*
CoA	C00010	2.4	<0.001***
Arg	C00062	1.8	<0.001***
UTP	C00075	<-50#	<0.001***
Cys	C00097	-3.1	<0.001***
Gly	C00037	-2.9	<0.001***
ATP	C00002	-2.9	<0.001***
GSH	C00051	-2.7	<0.001***
Glu	C00025	-2.0	0.003**
Ser	C00065	-1.9	0.003**
CTP	C00063	-1.8	<0.001***
GSSG	C00127	-1.7	0.022*
UMP	C00105	-1.7	<0.001***
Cystin	C00491	-1.6	<0.001***
Orn	C00077	-1.6	<0.001***
3PG	C00197	-1.6	<0.001***
CMP	C00055	-1.5	<0.001***
AMP	C00020	-1.5	<0.001***
Acetyl-P	C00227	-1.4	<0.001***

Estimated value due to metabolite concentration was below quantification limit.

Moreover, sulfur containing metabolites such as GSH, Cystin and Cys decreased in the Δ*cobB* mutant, whereas CoA strongly increased, indicating a potential influence of the sirtuin-like deacetylase CobB in the sulfur metabolism. Additionally, the triphosphate nucleotides content dropped (see ATP, CTP and UTP, the last one being depleted) in the *cobB* mutant, whereas several bases

such as Thymidine, Thymine and Hypoxanthine strongly increased. Furthermore, the genetic regulation was in concordance with these results (GO:0009145 and GO:0006212 terms in Table 4).

The AcetylCoA/CoA ratio was also calculated in each case. In the steady state, this ratio was found to be two fold lower in the case of Δ*cobB* (Figure 5).

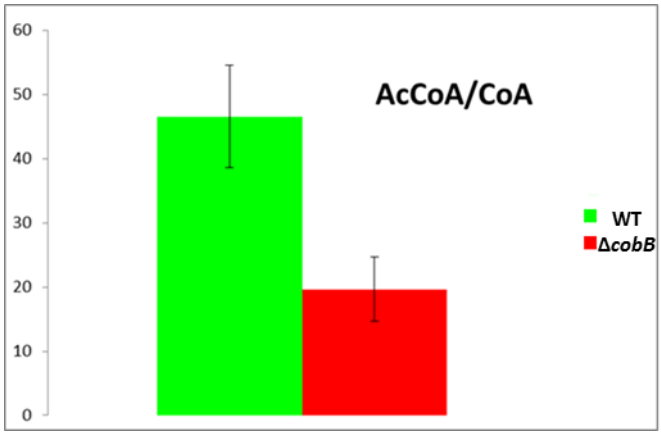

Figure 5. Intracellular AcCoA/CoA ratio at the chemostat steady-state for WT and Δ*cobB*.

Pathway-based integrative analysis.

In order to obtain information about the pathways affected, a pathway-based integrative analysis was made using the data obtained from the transcriptomic and metabolomic analyses. The results are listed in Table 6 and the most affected pathways are shown in Figure 6. Among pathways, some are related to sulfur containing metabolites, namely, (i) pantothenate and CoA biosynthesis (Figure 6A), (ii) GSH metabolism (Table 6) (iii) Cys and Met metabolism (Table 6) and (iv) taurine and hypotaurine metabolism (Figure 6D). It seems that all of them were highly inhibited, probably due to the drop in Cys (Table 5). However, CoA was strongly higher, even though the lower concentration of Cys, one of its precursors (Table 5), and the expression of critical enzymes of two additional precursors, β-Alanine (Figure 6B) and pantothenate (Figure 6A), were inhibited.

Table 6. KEGG pathway-based integrative analysis of metabolomic and transcriptomic data tested for overrepresentation using the hypergeometric distribution comparing WT and Δ*cobB* mutant in the stationary state of chemostats using acetate as sole C-source. The annMoleculeRatio is the number of molecules present in the pathway divided by the total number of provided molecules, annBgRatio is the number of molecules present in the pathway divided by the total number of molecules considering the whole set of pathways. The p-values for the hypergeometric test and FDR are the previous p values adjusted by the Benjamini–Hochberg false discovery rate (FDR).

Pathway KEGG Id	Pathway Name	annMoleculeRatio	annBgRatio	p value	FDR
eco02030	Bacterial chemotaxis	11/151	27/19425	0.00E+00	0.00E+00
eco02040	Flagellar assembly	33/151	36/19425	0.00E+00	0.00E+00
eco02010	ABC transporters	21/151	280/19425	5.00E-15	1.67E-13
eco00250	Alanine, aspartate and glutamate metabolism	10/151	55/19425	1.29E-11	2.93E-10
eco02020	Two-component system	15/151	184/19425	1.47E-11	2.93E-10
eco00240	Pyrimidine metabolism	13/151	127/19425	2.00E-11	3.33E-10
eco00330	Arginine and proline metabolism	10/151	132/19425	8.29E-08	1.18E-06
eco00430	Taurine and hypotaurine metabolism	5/151	28/19425	2.26E-06	2.82E-05
eco00480	Glutathione metabolism	6/151	56/19425	4.71E-06	4.80E-05
eco00270	Cysteine and methionine metabolism	7/151	86/19425	4.80E-06	4.80E-05
eco00650	Butanoate metabolism	6/151	74/19425	2.39E-05	2.18E-04
eco00260	Glycine, serine and threonine metabolism	6/151	84/19425	4.93E-05	4.11E-04
eco00290	Valine, leucine and isoleucine biosynthesis	4/151	39/19425	2.34E-04	1.80E-03
eco00460	Cyanoamino acid metabolism	4/151	41/19425	2.84E-04	2.03E-03
eco00230	Purine metabolism	6/151	180/19425	2.87E-03	1.91E-02
eco00660	C5-Branched dibasic acid metabolism	3/151	41/19425	3.95E-03	2.47E-02
eco00300	Lysine biosynthesis	3/151	42/19425	4.23E-03	2.49E-02
eco00410	beta-Alanine metabolism	3/151	46/19425	5.47E-03	3.04E-02
eco00770	Pantothenate and CoA biosynthesis	3/151	49/19425	6.53E-03	3.44E-02
eco00471	D-Glutamine and D-glutamate metabolism	2/151	17/19425	7.56E-03	3.78E-02

As regards the nitrogen metabolism, several pathways were found to be statistically relevant, namely, (i) Ala, Asp and Glu metabolism (Figure 6H), (ii) Arg and Pro metabolism (Figure 6F), (iii) Pyrimidine metabolism (Figure 6E), (iv) purine metabolism (Table 6), (v) Lys biosynthesis (Figure 6G) and (vi) Gln and Glu metabolism (Table 6), suggesting a strong cell metabolic alteration. Moreover, several transporters related to ammonia and amino acids were also inhibited (Table 4).

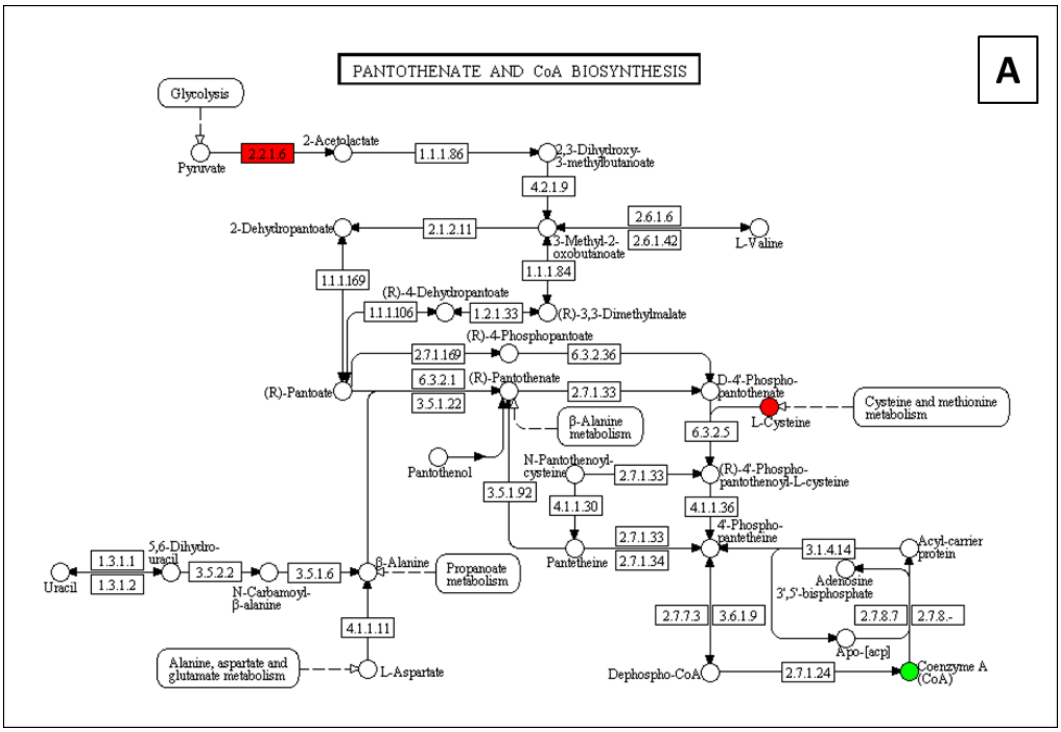
A
PANTOTHENATE AND CoA BIOSYNTHESIS
Glycolysis
Pyruvate
2.2.1.6
2-Acetolactate
1.1.1.86
2,3-Dihydroxy-3-methylbutanoate
4.2.1.9
2-Dehydropantoate
2.1.2.11
3-Methyl-2-oxobutanoate
2.6.1.6
2.6.1.42
L-Valine
1.1.1.169
1.1.1.84
(R)-4-Dehydropantoate
1.1.1.106
1.2.1.33
(R)-3,3-Dimethylmalate
(R)-4-Phosphopantoate
2.7.1.169
6.3.2.36
(R)-Pantoate
6.3.2.1
3.5.1.22
(R)-Pantothenate
2.7.1.33
D-4'-Phospho-pantothenate
L-Cysteine
Cysteine and methionine metabolism
β-Alanine metabolism
6.3.2.5
Pantothenol
N-Pantothenoyl-cysteine
2.7.1.33
(R)-4'-Phospho-pantothenoyl-L-cysteine
3.5.1.92
4.1.1.30
4.1.1.36
4'-Phospho-pantetheine
2.7.1.33
Pantetheine
2.7.1.34
3.1.4.14
Acyl-carrier protein
Adenosine 3',5'-bisphosphate
2.7.7.3
3.6.1.9
2.7.8.7
2.7.8.-
Apo-[acp]
Coenzyme A (CoA)
Dephospho-CoA
2.7.1.24
1.3.1.1
1.3.1.2
5,6-Dihydro-uracil
Uracil
3.5.2.2
N-Carbamoyl-β-alanine
3.5.1.6
β-Alanine
Propanoate metabolism
4.1.1.11
Alanine, aspartate and glutamate metabolism
L-Aspartate

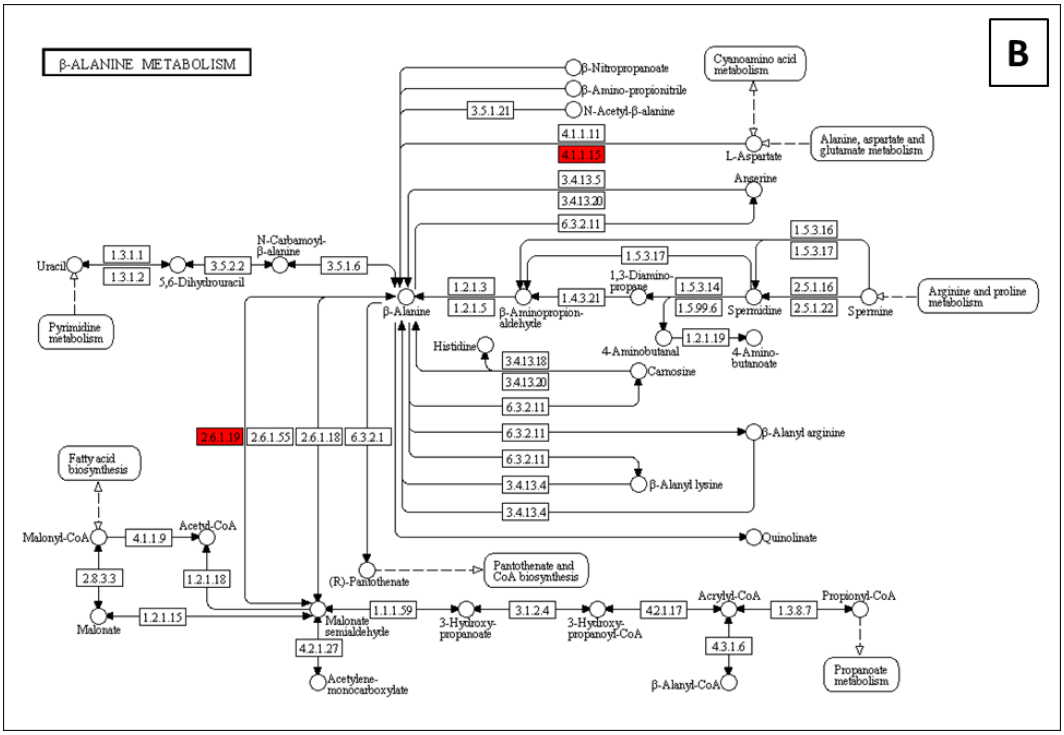
B
β-ALANINE METABOLISM
β-Nitropropanoate
β-Amino-propionitrile
N-Acetyl-β-alanine
3.5.1.21
Cyanoamino acid metabolism
4.1.1.11
4.1.1.15
L-Aspartate
Alanine, aspartate and glutamate metabolism
3.4.13.5
3.4.13.20
Anserine
6.3.2.11
1.5.3.16
1.5.3.17
1.5.3.17
N-Carbamoyl-β-alanine
Uracil
1.3.1.1
1.3.1.2
5,6-Dihydrouracil
3.5.2.2
3.5.1.6
1.2.1.3
1.2.1.5
β-Alanine
β-Aminopropion-aldehyde
1.4.3.21
1,3-Diamino-propane
1.5.3.14
1.5.99.6
Spermidine
2.5.1.16
2.5.1.22
Spermine
Arginine and proline metabolism
Pyrimidine metabolism
Histidine
3.4.13.18
3.4.13.20
6.3.2.11
4-Aminobutanal
1.2.1.19
4-Amino-butanoate
Carnosine
2.6.1.19
2.6.1.55
2.6.1.18
6.3.2.1
6.3.2.11
β-Alanyl arginine
6.3.2.11
3.4.13.4
β-Alanyl lysine
3.4.13.4
Fatty acid biosynthesis
Quinolinate
Malonyl-CoA
4.1.1.9
Acetyl-CoA
2.8.3.3
1.2.1.18
(R)-Pantothenate
Pantothenate and CoA biosynthesis
1.2.1.15
Malonate
Malonate semialdehyde
1.1.1.59
3-Hydroxy-propanoate
3.1.2.4
3-Hydroxy-propanoyl-CoA
4.2.1.17
Acrylyl-CoA
1.3.8.7
Propionyl-CoA
4.2.1.27
Acetylene-monocarboxylate
4.3.1.6
β-Alanyl-CoA
Propanoate metabolism

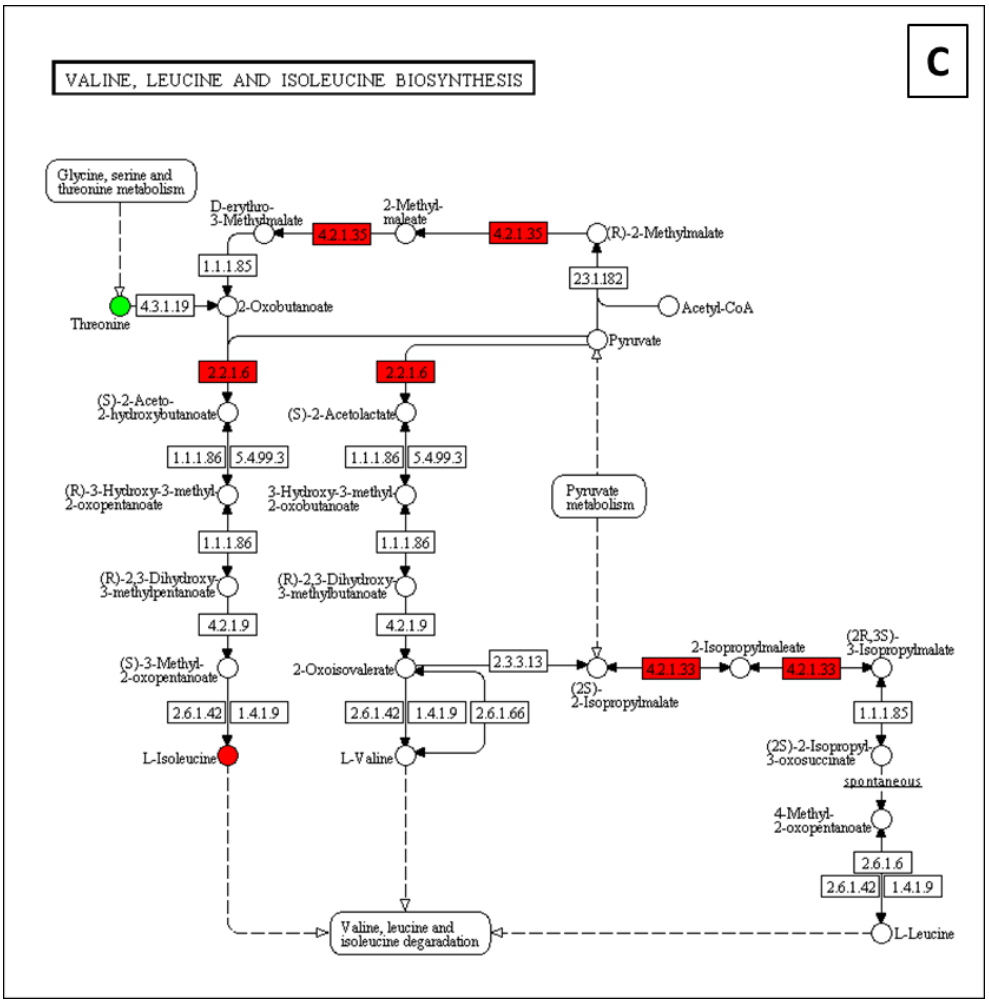
C
VALINE, LEUCINE AND ISOLEUCINE BIOSYNTHESIS
Glycine, serine and threonine metabolism
D-erythro-3-Methylmalate
2-Methyl-maleate
(R)-2-Methylmalate
4.2.1.35
4.2.1.35
1.1.1.85
2.3.1.182
Acetyl-CoA
Threonine
4.3.1.19
2-Oxobutanoate
Pyruvate
2.2.1.6
2.2.1.6
(S)-2-Aceto-2-hydroxybutanoate
(S)-2-Acetolactate
1.1.1.86
5.4.99.3
1.1.1.86
5.4.99.3
(R)-3-Hydroxy-3-methyl-2-oxopentanoate
3-Hydroxy-3-methyl-2-oxobutanoate
Pyruvate metabolism
1.1.1.86
1.1.1.86
(R)-2,3-Dihydroxy-3-methylpentanoate
(R)-2,3-Dihydroxy-3-methylbutanoate
4.2.1.9
4.2.1.9
(S)-3-Methyl-2-oxopentanoate
2-Oxoisovalerate
2.3.3.13
2-Isopropylmaleate
(2R,3S)-3-Isopropylmalate
4.2.1.33
4.2.1.33
(2S)-2-Isopropylmalate
2.6.1.42
1.4.1.9
2.6.1.42
1.4.1.9
2.6.1.66
1.1.1.85
L-Isoleucine
L-Valine
(2S)-2-Isopropyl-3-oxosuccinate
spontaneous
4-Methyl-2-oxopentanoate
2.6.1.6
2.6.1.42
1.4.1.9
Valine, leucine and isoleucine degradation
L-Leucine

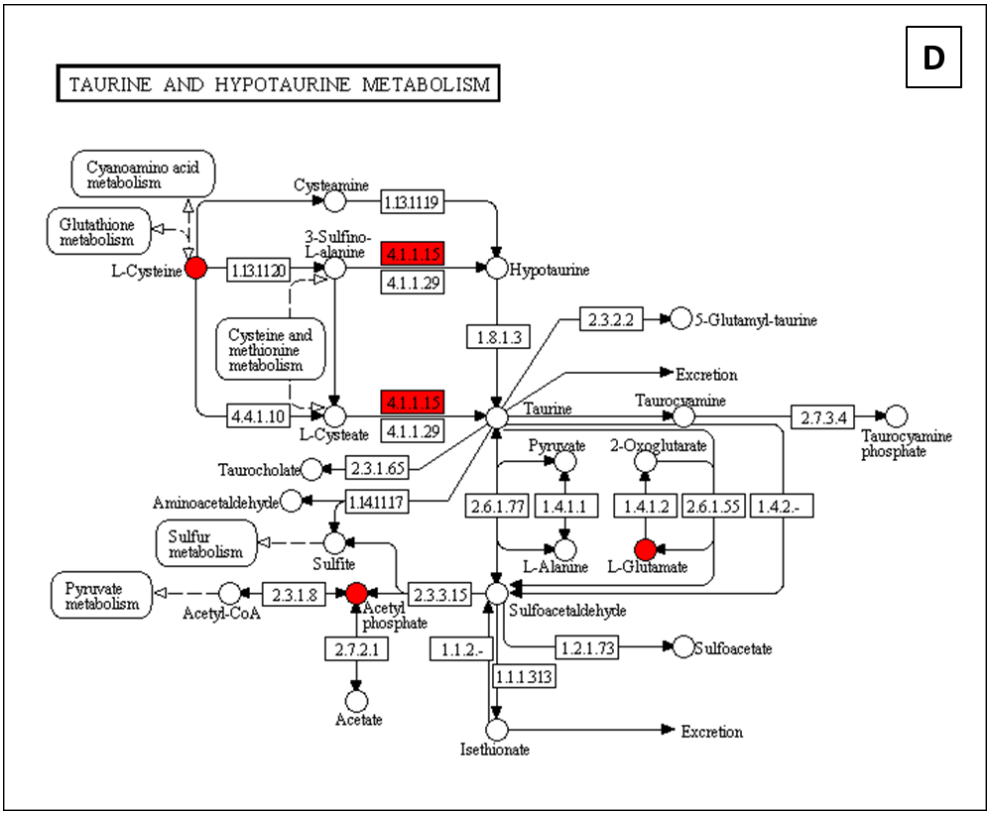
D
TAURINE AND HYPOTAURINE METABOLISM
Cyanoamino acid metabolism
Cysteamine
1.13.11.19
Glutathione metabolism
3-Sulfino-L-alanine
4.1.1.15
4.1.1.29
L-Cysteine
1.13.11.20
Hypotaurine
2.3.2.2
5-Glutamyl-taurine
1.8.1.3
Cysteine and methionine metabolism
Excretion
4.1.1.15
Taurine
Taurocyamine
2.7.3.4
Taurocyamine phosphate
4.4.1.10
4.1.1.29
L-Cysteate
Pyruvate
2-Oxoglutarate
Taurocholate
2.3.1.65
2.6.1.77
1.4.1.1
1.4.1.2
2.6.1.55
1.4.2.-
Aminoacetaldehyde
1.14.11.17
Sulfur metabolism
Sulfite
L-Alanine
L-Glutamate
Pyruvate metabolism
2.3.1.8
2.3.3.15
Sulfoacetaldehyde
Acetyl-CoA
Acetyl phosphate
1.2.1.73
Sulfoacetate
2.7.2.1
1.1.2.-
1.1.1.313
Acetate
Isethionate
Excretion

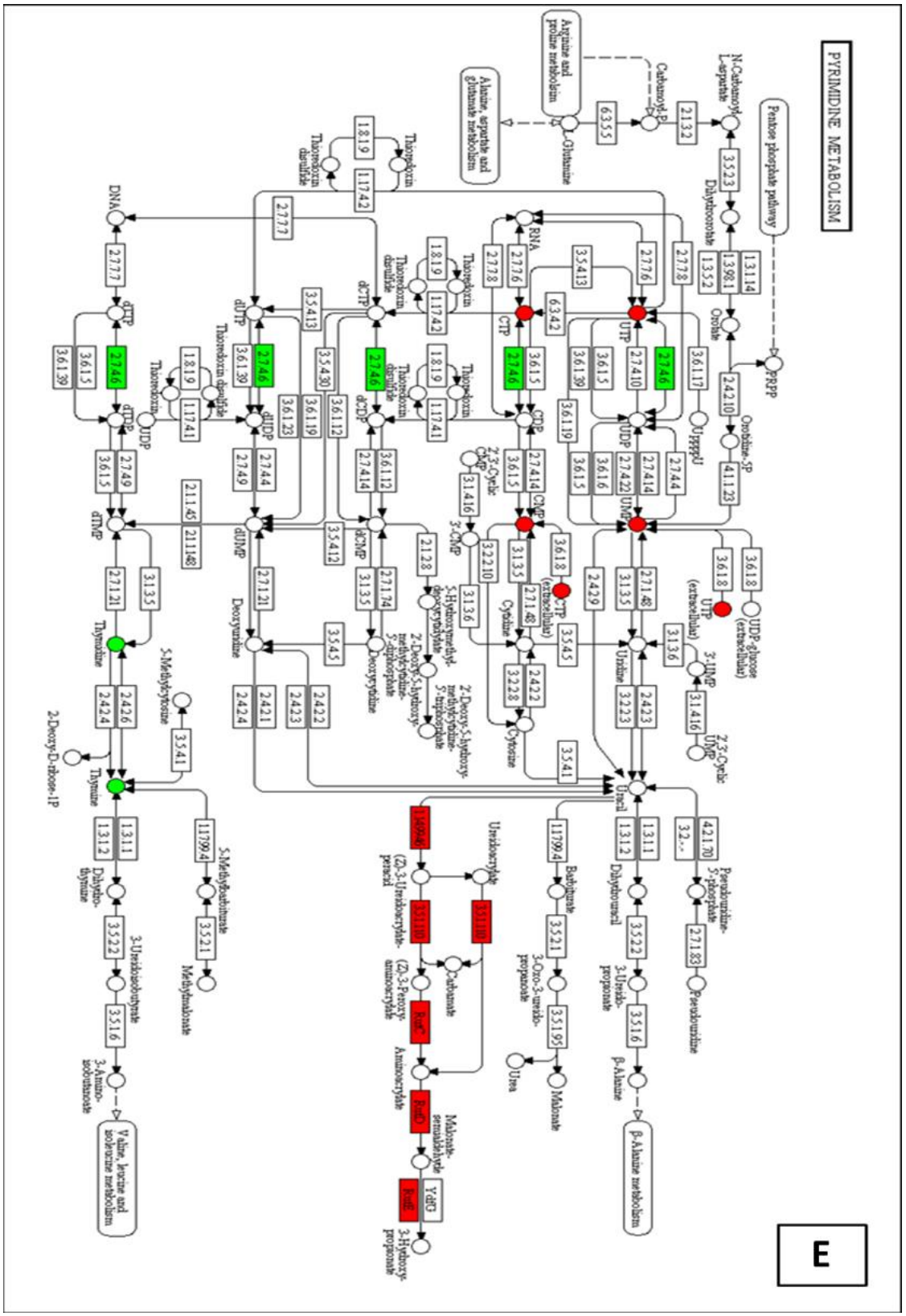
PYRIMIDINE METABOLISM
E

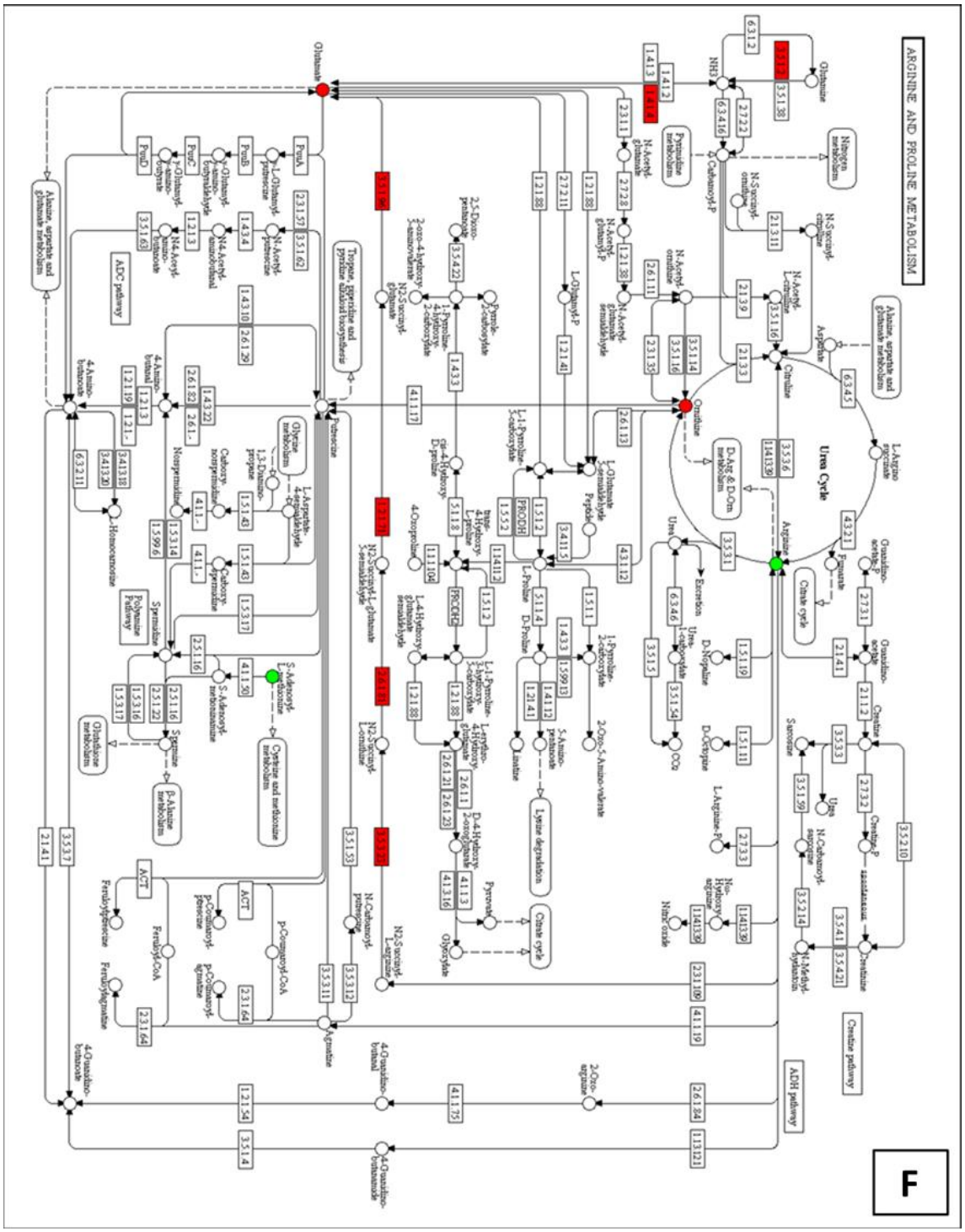
ARGINE AND PROLINE METABOLISM
Urea Cycle
F

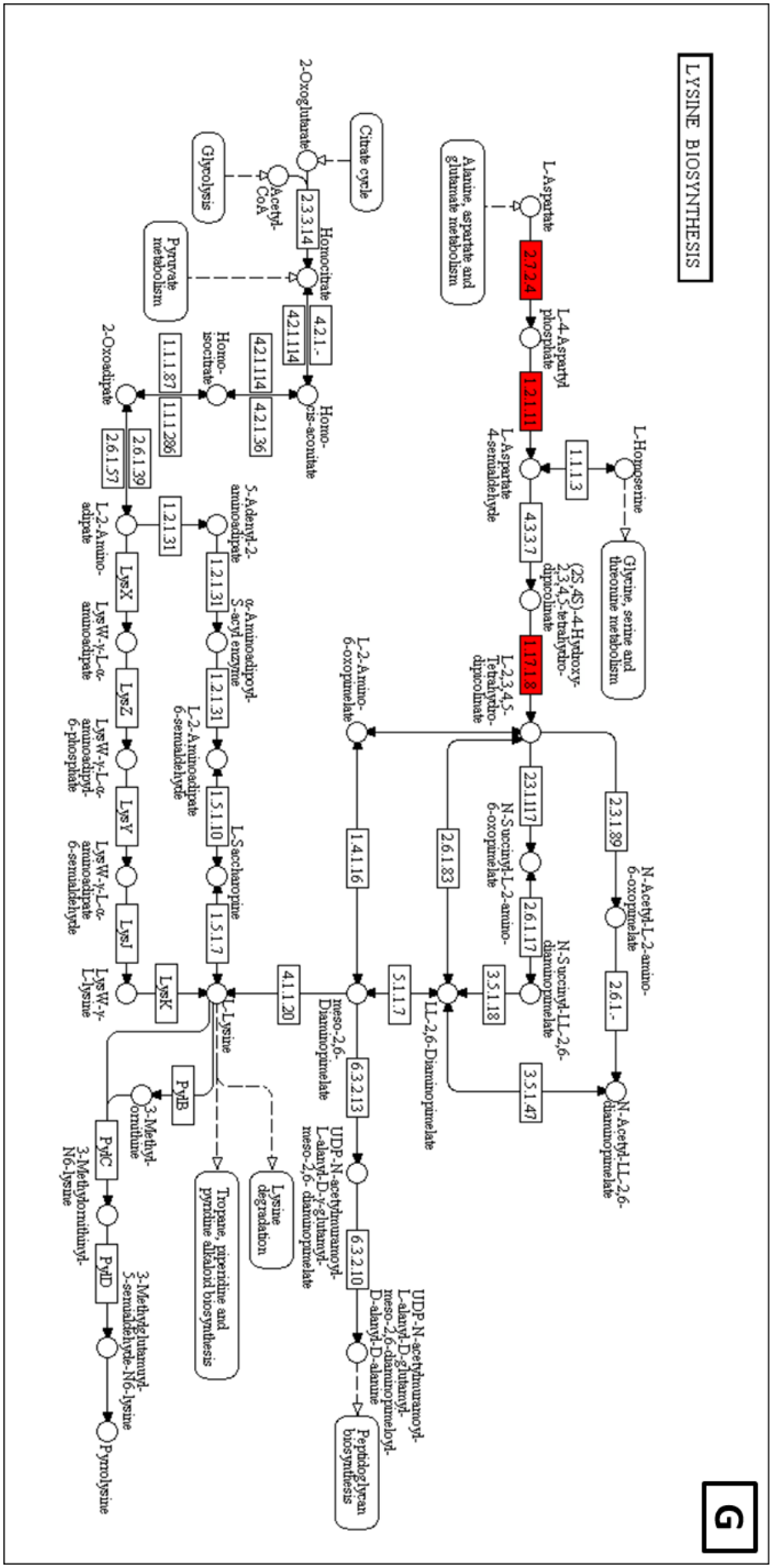
LYSINE BIOSYNTHESIS
G
L-Aspartate
2.7.2.4
L-4-Aspartyl phosphate
1.2.1.11
L-Aspartate 4-semialdehyde
1.1.1.3
L-Homoserine
4.3.3.7
(2S,4S)-4-Hydroxy-2,3,4,5-tetrahydro-dipicolinate
1.17.1.8
L-2,3,4,5-Tetrahydro-dipicolinate
Glycine, serine and threonine metabolism
Alanine, aspartate and glutamate metabolism
2.3.1.89
N-Acetyl-L-2-amino-6-oxopimelate
2.6.1.-
N-Acetyl-LL-2,6-diaminopimelate
2.3.1.117
N-Succinyl-L-2-amino-6-oxopimelate
2.6.1.17
N-Succinyl-LL-2,6-diaminopimelate
3.5.1.47
2.6.1.83
3.5.1.18
LL-2,6-Diaminopimelate
L-2-Amino-6-oxopimelate
1.4.1.16
5.1.1.7
meso-2,6-Diaminopimelate
6.3.2.13
UDP-N-acetylmuramoyl-L-alanyl-D-γ-glutamyl-meso-2,6- diaminopimelate
6.3.2.10
UDP-N-acetylmuramoyl-L-alanyl-D-glutamyl-meso-2,6-diaminopimeloyl-D-alanyl-D-alanine
Peptidoglycan biosynthesis
4.1.1.20
L-Lysine
Lysine degradation
Tropane, piperidine and pyridine alkaloid biosynthesis
PydB
3-Methyl-ornithine
PydC
3-Methylornithinyl-N6-lysine
PydD
3-Methylglutamyl-5-semialdehyde-N6-lysine
Pyrrolysine
LysK
LysW-γ-L-lysine
LysJ
LysW-γ-L-α-aminoadipyl-6-semialdehyde
1.5.1.7
L-Saccharopine
LysY
LysW-γ-L-α-aminoadipyl-6-phosphate
1.2.1.31
L-2-Aminoadipate 6-semialdehyde
LysZ
LysW-γ-L-α-aminoadipate
1.2.1.31
α-Aminoadipoyl-S-acyl enzyme
LysX
L-2-Amino-adipate
1.2.1.31
5-Adenyl-2-aminoadipate
2.6.1.39
2.6.1.57
2-Oxoadipate
1.1.1.86
1.1.1.87
Homo-isocitrate
4.2.1.114
4.2.1.36
Homo-cis-aconitate
4.2.1.-
4.2.1.114
Homocitrate
2.3.3.14
Acetyl-CoA
2-Oxoglutarate
Citrate cycle
Glycolysis
Pyruvate metabolism

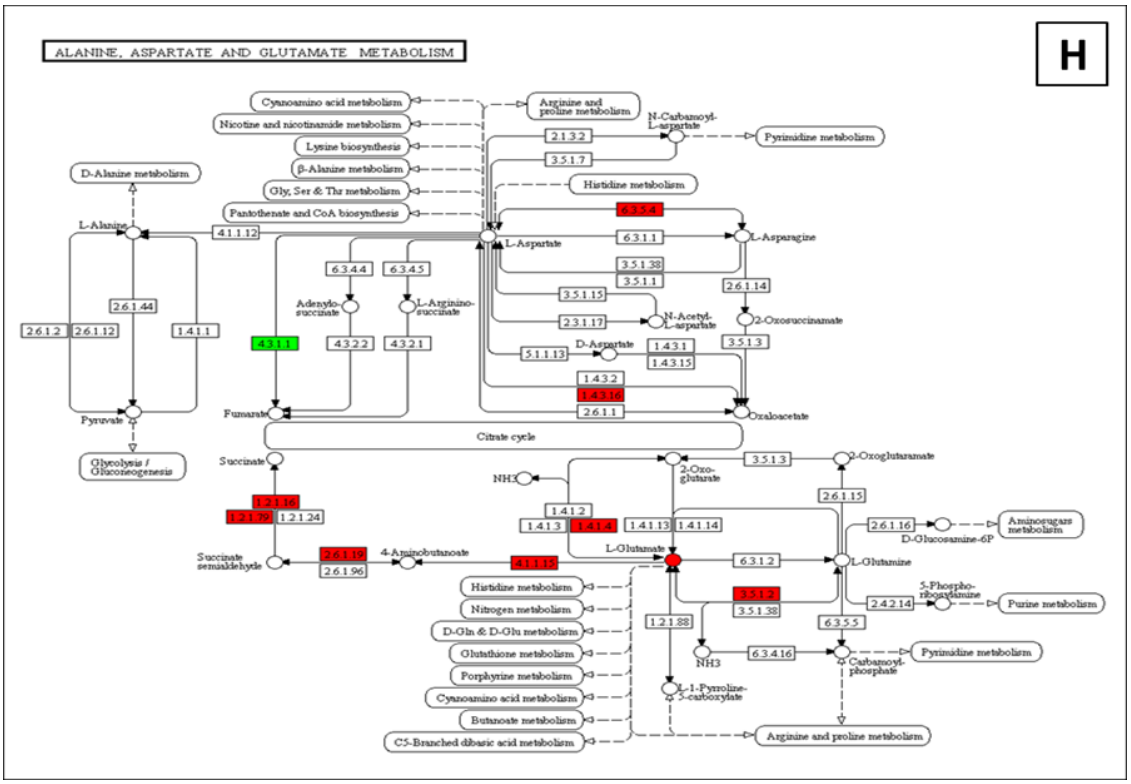

Figure 6. Results of the integrative pathway-based analysis in the case of ΔcobB acetate-feeding chemostat. A. Pantothenate and CoA biosynthesis. B. β-Alanine metabolism. C. Valine, leucine and isoleucine biosynthesis. D. Taurine and hypotaurine metabolism. E. Pyrimidine metabolism. F. Arginine and proline metabolism. G. Lysine biosynthesis. H. Alanine, aspartate and glutamate. Upregulated genes and metabolites with higher levels in ΔcobB compared with WT are highlighted in green, whereas downregulated genes or metabolites with lower levels are in red.

DISCUSSION

The role of the sirtuin-like deacetylase CobB, the only known deacetylase in *E. coli,* could be key player in metabolic network regulation since it has been reported that lysine acetylation of central metabolic enzymes is common in all living organisms (Barak et al., 2006 ; Choudhary et al., 2009; Kim et al., 2013; Kuo and Andrews, 2013; Lundby et al., 2012; Wang et al., 2010;. Weinert et al., 2011, 2013, 2014; Zhao et al., 2010). In the recent work of AbouElfetouh and co-workers (2014) evidence concerning CobB sustrate preferences is given. The authors reported that the most common adjacent residues to acetyllysines are glycine, alanine, tyrosine, glutamate and aspartate. However, the secondary structure is important since acetyllysines are more accesible to CobB when they are located in loops or α-helix. This work contributes to our knowledge of the role of CobB since the determination of CobB sustrates could unveil the enzyme

activity and the biological pathways regulated by CobB. In the present work, transcriptomic as well as metabolic analyses have been carried out in order to gain a new insight into the role of CobB in the regulation of metabolic networks in *E. coli*, when a high concentration of acetate is used as the sole carbon source. The global results of the present work showed that the nitrogen and sulfur metabolisms are strongly affected in Δ*cobB* mutant in high acetate feeding-chemostats of *E.coli,* which might indicate that protein lysine acetylation is directly or indirectly involved in the control of both metabolisms. Moreover, the results obtained with integrative pathway-based analysis showed that a lack of *cobB* gene in these conditions resulted in several metabolic pathways being affected such as those of several amino acids (Val, Leu, Ile, Ala, Asp, Glu, Arg and Pro), taurine and hypotaurine metabolism, pantothenate and CoA biosynthesis and pyrimidines metabolism.

Previous works (Castaño-Cerezo et al., 2011, Castaño-Cerezo et al., 2014) showed that Δ*cobB* mutant presented severe growth impairment compared to WT in acetate flask cultures and in limited-glucose chemostats. This phenotype is mainly caused by the inactivation of ACS in *cobB* mutant, but is also probably due to the inhibition/activation by lysine acetylation of other enzymes related with the central carbon metabolism. Despite its importance, this has not been explored. In the present work both WT and Δ*cobB* mutant were cultured in chemostats using a high concentration of acetate as the sole carbon source. The results pointed out no statistical differences in the biomass reached between them or in the fermentation products pattern. This could be the result of acetate assimilation through ACK/PTA, the low affinity pathway. Moreover, in this condition no significant differences regarding the central carbon metabolism were observed, unlike in the case of the limited-glucose chemostats where the flux through the glyoxylate shunt was 34% lower in the Δ*cobB* mutant (Castaño-Cerezo et al., 2014).

Regarding nitrogen metabolism and transport, several nitrogen molecule transporters, ammonia uptake and nitrogen fixation were transcriptionally downregulated, as seen from the GO term enrichment study (Table 4). Besides, important amino acid pathways were strongly hindered (Figure 6) with the

subsequent depletion/accumulation of some intermediates (Glu, Orn or Arg) (Table 5).

Additionally, both pyrimidine and purine metabolisms were found to be altered in Δ*cobB* (Figure 6E and Table 6) with higher concentrations of thymine, thymidine and hypoxanthine in the case of the mutant (Table 5). Thymine is the only pyrimidinic base without an amino group and it forms the nucleoside thymidine. The higher content in pyrimidines could be related to the fact that all the genes that constitute the operon *rutABCDEFG* were resulted downregulated in Δ*cobB* (Table 4). This operon encodes a pathway to degrade pyrimidines with the consequent release of two ring nitrogen atoms for assimilation (Parales and Ingraham 2010). In the case of purine derivatives, hypoxanthine is a product of adenine deamination with ammonium release. Taking all these results together, the deletion of *cobB* gene, and therefore post translational acetylation, could affect nitrogen fixation, which was highly inhibited in the mutant.

Regarding sulfur metabolism, important intermediates such as Cys, Cystin and GSH concentrations (with other components, Gly and Glu) were much lower in Δ*cobB* (Table 5) as well as it occurred with the taurine and hypotaurine metabolism (Figure 6D). Moreover, the fact that Cys and also Arg were altered could mean that these amino acids play an important role in the regulation of protein acetylation, as was reported in *Micromonospora aurantiaca* (Xu et al., 2014).

Regarding the AcCoA, there was no statistical difference between WT and Δ*cobB*. In the study of Barak et al. (2006) it was reported that AcCoA pools can be adjusted by the stability and activity of the central metabolic enzymes that can be acetylated. With regard to AcetylCoA/CoA ratio, it was lower in the case of the Δ*cobB* because the level of CoA was more than double than WT. This could be surprising since several of its precursors were strongly reduced and/or their biosynthesis was transcriptionally downregulated (Table 5, Figure 6AB).

Besides AcCoA, other acyl-CoAs and also Acetyl-P highly regulate the chemical acylation of proteins, which suggests a dependence on the metabolic state of the cell, as reported in the recent review of Bernal et al. (2014). Besides, in the

work of Weinert and co-workers (2013) it was concluded that Acetyl-P is a critical factor in protein acetylation in bacteria acting non-enzymatically. This study suggested that increased acetylation results from a combination of elevated Acetyl-P and prolonged exposure of proteins to the same. CobB suppressed acetylation in growing and growth-arrested cells and CobB-regulated sites were significantly more sensitive to Acetyl-P in vitro. In the present study, Acetyl-P in the *cobB* mutant was almost 40% lower than in WT. In the mutant, this could be explained by the double role played by Acetyl-P, which is thought to regulate the chemotaxis response regulator CheY through Acetyl-P-dependent phosphorylation and autocatalytic acetylation (Barak et al., 2006; Lukat et al., 1992).

Additionally, peptidoglycan synthesis was affected in the case of the *cob*B mutant since UTP, the energy source for the peptidoglycan synthesis, was below detection limits in the mutant (Table 5). Moreover, another critical intermediate, Glu, was found heavily diminished as occurred with pathways related to intermediates such as pyrimidine biosynthesis and Lys, which produce the meso-diaminopimelic acid (Figure 6G) essential in the *E. coli* peptidoglycan structure.

Finally, several genes related to cilliary, flagella and chemotaxis were found overexpressed in Δ*cobB*. These results agree with those obtained in the case of glucose flask and glucose-limited chemostats cultures (Castaño-Cerezo et al., 2014). In that work, Lys-154 of the transcription factor RcsB was seen to be acetylated, which supports the fact that CobB is proposed to deacetylate RcsB (Hu et al., 2013). The acetylation of this response regulator provokes the overexpression of the genes mentioned above (motility) and the diminished expression of the acid stress resistance genes. In the work of Li and collaborators (2010), it was proposed that CobB regulates *E. coli* chemotaxis by deacetylating the protein CheY, since this latter showed a higher level of acetylation and reduced the response to chemotactic stimuli in Δ*cobB* mutant. CheY is a chemotaxis regulator able to transmit the signal to flagellar motor components (Bren and Eisenbach 1998). In the present work, both GO set enrichment (Table 4) and pathway-based analysis highlighted that bacterial

chemotaxis and flagellar assembly is highly overexpressed (Table 6). Taking into account these findings, it can be hypothesized that the loss of response to chemotactic stimuli is not due to the lack of flagella. Besides, the genes that codify for the proteins FliN, FliG and FliM that constitute the Flagellar Motor Switch Complex (Lowder et al., 2005) were highly overexpressed in this mutant. CheY acetylation (mainly autoacetylation with AcetylCoA as a donor (Yan et al., 2008) reduces its binding to FliM. Therefore, these results suggest that the loss of response to chemotactic stimuli is due to the fact that acetylated CheY reduces its binding affinity to FliM (Li et al., 2010). In this way, the locomotor responses may not be sufficient to direct the cells favourably.

According to the transcriptomic analysis, genes related with the GO terms "intracellular pH elevation" and "cellular response to acidity" were found up-regulated in the case of Δ*cobB* (Table 4). The genes *hdeA* and *hdeB,* which code for acid resistance proteins, were more than four times inhibited in *cobB* mutant (Table 4). Moreover, these results agree with those previously reported in the work of Castaño-Cerezo et al. (2014). In fact, the protein HdeA has been proposed to be a chaperone that acts to prevent the aggregation of periplasmic denatured proteins under extremely acidic conditions. Besides, the genes, *gadA* and *gadB* that belong to the glutamate decarboxylase system were seen to be nearly five times inhibited in *cobB* mutant compared to WT as happened in the glucose-limited chemostats. That reflects the fact that GadA protein is more acetylated in *cob*B mutant (AbouElfetouh et al., 2014). These enzymes catalyse the conversion of glutamate to γ-aminobutyrate and help to maintain a neutral intracellular pH when the pH of the environment is very acidic (Masuda and Church 2003). These findings support the fact that RcsB is required for inducible acid resistance in *E. coli* and acts as gadE-dependent and -independent promoter (Johnson et al., 2011).

CONCLUDING REMARKS

No significant statistical differences were found between WT and *ΔcobB* as regards growth and fermentation products excretion since acetate is assimilated through the low-affinity pathway PTA-ACK due to the high concentration of

acetate present. Besides, no significantly different effects were found in the central metabolism as was reported in the case of glucose-chemostats. However the GO terms “intracellular pH elevation”, “cellular response to acidity” and “chemotaxis” in the present work indicated that CobB may play an important role in their regulation, as was reported in the previous work with glucose-chemostats. On the other hand, the Integration pathway-based analysis on KEGG pathways highlighted relevant interconnections with a strong metabolic effect related to sulfur and nitrogen metabolism, among other pathways, in these conditions. In the present work, relevant alterations were found in nitrogen metabolism, transport and fixation, and ammonia uptake was found transcriptionally downregulated as was highlighted in the GO term enrichment study. Besides, several amino acids and derivatives were observed to be altered. Moreover, pyrimidines concentration was higher in *ΔcobB,* which reflects the fact that the *rut*ABCDEFG operon was downregulated. In base of these results it can be hypothesized that nitrogen metabolism is directly or indirectly regulated by protein acetylation. Integration pathway-based analysis is seen to be a powerful tool to handle massive data from different –omics, helping to shed light on the role of CobB in the *E. coli* metabolism. Such analysis would also support works focused on the study of the CobB substrates.

REFERENCES

AbouElfetouh, A., Kuhn, M.L., Hu, L.I., Scholle, M.D., Sorensen, D.J., Sahu, A.K., Becher, D., Antelmann, H., Mrksich, M., Anderson, W.F, Gibson, B.W., Schilling, B., Wolfe, A.J. (2015). The *E. coli* sirtuin CobB shows no preference for enzymatic and nonenzymatic lysine acetylation substrate sites. *Microbiologyopen*, **4**, 66-83.

Baba, T., Ara, T., Hasegawa, M., Takai, Y., Okumura, Y., Baba, M., Datsenko, K.A., Tomita, M., Wanner, B.L., Mori, H. (2006). Construction of *Escherichia coli* K-12 in-frame, single-gene knockout mutants: the Keio collection. *Mol. Syst. Biol.,* **2,** doi: 10.1038/msb4100050.

Barak, R., Yan, J., Shainskaya, A., Eisenbach, M. (2006). The chemotaxis response regulator CheY can catalyze its own acetylation. *J. Mol. Biol.*, **359**, 251-265.

Benjamini, Y., Hochberg, Y., (1995). Controlling the false discovery rate - A practical and powerful approach to multiple testing. *J. R. Stat. Soc. Ser. B-Methodol.*, **57**, 289-300.

Bernal, V., Castano-Cerezo, S., Gallego-Jara, J., Ecija-Conesa, A., de Diego, T., Iborra, J. L. and Canovas, M. (2014). Regulation of bacterial physiology by lysine acetylation of proteins. *N. Biotechnol*., **31**, 586-95.

Bravo, E., Palleschi, S., Aspichueta, P., Buque, X., Rossi, B., Cano, A., Napolitano, M., Ochoa, B., Botham, K. M. (2011). High fat diet-induced non alcoholic fatty liver disease in rats is associated with hyperhomoCysteinemia caused by down regulation of the transsulphuration pathway. *Lipids Health Dis.*, **10**:60. doi:10.1186/1476-511x-10-60.

Bren, A., Eisenbach, M. (1998). The N terminus of the flagellar switch protein, FliM, is the binding domain for the chemotactic response regulator, CheY. *J. Mol. Biol.*, **278**, 507-514.

Bunk B., Kucklick M., Jonas R., Munch R., Schobert M., Jahn D., Hiller K. (2006). MetaQuant: a tool for the automatic quantification of GC/MS-based metabolome data. *Bioinformatics*, **22**(23), 2962-2965.

Castano-Cerezo, S., Bernal, V., Blanco-Catala, J., Iborra, J. L., Canovas, M. (2011). cAMP-CRP co-ordinates the expression of the protein acetylation pathway with central metabolism in *Escherichia coli*. *Mol. Microbiol.*, **82**, 1110-1128.

Castano-Cerezo, S., Pastor, J. M., Renilla, S., Bernal, V., Iborra, J. L., Canovas, M. (2009). An insight into the role of phosphotransacetylase (pta) and the acetate/acetyl-CoA node in *Escherichia coli*. *Microb. Cell Fact.*, **8,** 54. doi: 10.1186/1475-2859-8-54.

Castano-Cerezo, S., Bernal, V., Post, H., Fuhrer, T., Cappadona, S., Sanchez-Diaz, N. C., Sauer, U., Heck, A. J., Altelaar, A. F. and Canovas, M. (2014). Protein acetylation affects acetate metabolism, motility and acid stress response in *Escherichia coli*. Mol. Syst. Biol., **10**, 762. doi: 10.15252/msb.20145227

Choudhary, C., Kumar, C., Gnad, F., Nielsen, M.L., Rehman, M., Walther, T.C., Olsen, J. V., Mann, M. (2009). Lysine acetylation targets protein complexes and co-regulates major cellularfunctions. *Science*, **325**, 834–40.

Dietmair, S., Timmins, N. E., Gray, P. P., Nielsen, L. K., Kroemer, J. O. (2010). Towards quantitative metabolomics of mammalian cells: Development of a metabolite extraction protocol. *Anal. Biochem*., **404**, 155-164.

Document No. SANCO/12495/2011, 2011. Method Validation and Quality Control procedures for pesticide residues analysis in food and feed. http://ec.europa.eu/food/plant/protection/pesticides/docs/qualcontrol_en.pdf.

Falcon, S., Gentleman, R. (2007). Using GOstats to test gene lists for GO term association. *Bioinformatics*, **23**, 257-258.

Faijes, M., Mars, A. E., Smid, E. J. (2007). Comparison of quenching and extraction methodologies for metabolome analysis of *Lactobacillus plantarum*. *Microb. Cell. Fact*., **6**, 27. doi:10.1186/1475-2859-6-27.

Fructuoso, S., Sevilla, A., Bernal, C., Lozano, A. B., Iborra, J. L., Canovas, M. (2012). EasyLCMS: An asynchronous web application for the automated quantification of LC-MS data. *BMC Res. Notes*., **5**, 428. doi: 10.1186/1756-0500-5-428.

Gautier, L., Cope, L, Bolstad, B.M., Irizarry, R.A. (2004). affy—analysis of Affymetrix GeneChip data at the probe level. *Bioinformatics*, **20**, 307–315.

Gentleman, R. C., Carey, V. J., Bates, D. M., Bolstad, B., Dettling, M., Dudoit, S., Ellis, B., Gautier, L., Ge, Y., Gentry, J., Hornik, K., Hothorn, T., Huber, W., Iacus, S., Irizarry, R., Leisch, F., Li, C., Maechler, M., Rossini, A. J., Sawitzki, G., Smith, C., Smyth, G., Tierney, L., Yang, J. Y. and Zhang, J. (2004). Bioconductor: open software development for computational biology and bioinformatics. *Genome Biol*., **5**, R80.

Henriksen, P., Wagner, S.A., Weinert, B.T., Sharma, .S, Bacinskaja, G., Rehman, M., Juffer, A.H., Walther, T.C., Lisby, M., Choudhary, C. (2012) Proteome-wide analysis of lysine acetylation suggests its broad regulatory scope in *Saccharomyces cerevisiae*. *Mol. Cell Proteomics*, **11,** 1510 – 1522.

Hu, L.I., Chi, B.K., Kuhn, M.L., Filippova, E.V., Walker-Peddakotla, A.J., ., Becher, D., Anderson, W.F., Antelmann, H., Wolfe, A.J. (2013). Acetylation of the response regulator RcsB controls transcription from a small RNA promoter. *J. Bacteriol*., **195**, 4174-4186.

Irizarry, R. A., Hobbs, B., Collin, F., Beazer-Barclay, Y. D., Antonellis, K. J., Scherf, U., Speed, T. P. (2003). Exploration, normalization, and summaries of high density oligonucleotide array probe level data. *Biostatistics*. **4**, 249-264.

Johnson, M.D., Burton, N.A., Gutiérrez, B., Painter, K., Lund, P.A. (2011). RcsB is required for inducible acid resistance in *Escherichia coli* and acts at gadE-dependent and -independent promoters. *J. Bacteriol.,* **193,** 3653-3656.

Kanehisa, M., Goto, S., Sato, Y., Kawashima, M., Furumichi, M., Tanabe, M. (2014). Data, information, knowledge and principle: back to metabolism in KEGG. Nucleic Acids Res., **42**, D199-205.

Kim, D., Yu, B.J., Kim, J.A., Lee, Y.J, Choi, S.G, Kang, S., Pan, J.G. (2013) The acetylproteome of gram-positive model bacterium *Bacillus subtilis*. *Proteomics J.,* **13**, 1 – 28.

Kronthaler, J., Gstraunthaler, G. and Heel, C. (2012). Optimizing high-throughput metabolomic biomarker screening: a study of quenching solutions to freeze intracellular metabolism in CHO cells. *OMICS*, **16**, 90-7.

Kuhn, M.L., Zemaitaitis, B., Hu, L.I., Sahu, A., Sorensen, D., Minasov G., Lima B.P., Scholle, M., Mrksich, M., Anderson, W.F., Gibson, B.W., Schilling, B., Wolfe, A.J. (2014). Structural, kinetic and proteomic characterization of acetyl phosphate-dependent bacterial protein acetylation. *PLoS One*. **9**(4):e94816. doi: 10.1371/journal.pone.0094816.

Kuo Y-M, Andrews AJ. Quantitating the specificity and selectivity of Gcn5-mediated acetylation of histone H3. (2013). *PLoS One,* **8**(10):e54896. doi: 10.1371/journal.pone.0054896.

Lazzarino, G., Amorini, A. M., Fazzina, G., Vagnozzi, R., Signoretti, S., Donzelli, S., Di Stasio, E., Giardina, B., Tavazzi, B. (2003). Single-sample preparation for simultaneous cellular redox and energy state determination. *Anal. Biochem*., **322**, 51-59.

Li, C. Q., Li, X., Miao, Y. B., Wang, Q. H., Jiang, W., Xu, C., Li, J., Han, J. W., Zhang, F., Gong, B. S., Xu, L. D. (2009). SubpathwayMiner: a software package for flexible identification of pathways. *Nucleic Acids Res*., **37**(19): e131. doi: 10.1093/nar/gkp667.

Li, R., Gu, J., Chen, Y.-Y., Xiao, C.-L., Wang, L.-W., Zhang, Z.-P., Bi, L.-J., Wei, H.-P., Wang, X.-D., Deng, J.-Y., Zhang, X.-E. (2010). CobB regulates *Escherichia coli* chemotaxis by deacetylating the response regulator CheY. *Mol. Microbiol.*, **76**, 1162-1174.

Lowder, B. J., Duyvesteyn, M. D., Blair, D. F. (2005). FliG subunit arrangement in the flagellar rotor probed by targeted cross-linking. *J. Bacteriol.*, **187**, 5640-5647.

Lundby, A., Lage, K., Weinert, B.T., Bekker-Jensen, D.B., Secher, A., Skovgaard, T., Kelstrup, C.D, Dmytriyev, A., Choudhary, C., Lundby, C., Olsen, J.V. (2012). Proteomic analysis of lysine acetylation sites in rat tissues reveals organ specificity and subcellular patterns. *Cell Rep.*, **2**, 419–31.

Lukat, G. S., McCleary, W. R., Stock, A. M. and Stock, J. B. (1992). Phosphorylation of bacterial response regulator proteins by low molecular weight phospho-donors. Proc. Natl. Acad. Sci. U.S.A., **89**, 718-22.

Luo, W. J., Brouwer, C. (2013). Pathview: an R/Bioconductor package for pathway-based data integration and visualization. *Bioinformatics*. **29**, 1830-1831.

Masuda, N., Church, G. M. (2003). Regulatory network of acid resistance genes in *Escherichia coli*. *Mol. Microbiol.*, **48**, 699-712.

Montero, M., Rahimpour, M., Viale, A. M., Almagro, G., Eydallin, G., Sevilla, A., Canovas, M., Bernal, C., Lozano, A. B., Munoz, F. J., Baroja-Fernandez, E., Bahaji, A., Mori, H., Codoner, F. M. and Pozueta-Romero, J. (2014). Systematic production of inactivating and non-inactivating suppressor mutations at the *relA* locus that compensate the detrimental effects of complete *spoT* loss and affect glycogen content in E*scherichia coli*. *PLoS One* **9**(9): e106938. doi:10.1371/journal.pone.0106938.

Oikawa, A., Otsuka, T., Jikumaru, Y., Yamaguchi, S., Matsuda, F., Nakabayashi, R., Takashina, T., Isuzugawa, K., Saito, K., Shiratake, K. (2011). Effects of freeze-drying of samples on metabolite levels in metabolome analyses. *J. Sep. Sci*., **34**, 3561-3567.

Parales, R.E., Ingraham, J.L. (2010).The Surprising Rut Pathway: an Unexpected Way To Derive Nitrogen from Pyrimidines. *J. Bacteriol*., 192, 4086-4088.

Preinerstorfer, B., Schiesel, S., Lammerhofer, M. L., Lindner, W. (2010). Metabolic profiling of intracellular metabolites in fermentation broths from beta-lactam antibiotics production by liquid chromatography-tandem mass spectrometry methods. J. Chromatogr. A., **1217**, 312-328.

R Development Core Team. R: A Language and Environment for Statistical Computing (R Foundation for Statistical Computing, 2014).

Satoh, A., Stein, L., and Imai, S. (2011). The Role of Mammalian Sirtuins in the Regulation of Metabolism, Aging, and Longevity. *Handb. Exp. Pharmacol.*, **206**, 125–162.

Schadel, F., David, F., Franco-Lara, E. (2011). Evaluation of cell damage caused by cold sampling and quenching for metabolome analysis. *Appl. Microbiol. Biotechnol.,* **92**, 1261-1274.

Sellick, C. A., Hansen, R., Stephens, G. M., Goodacre, R., Dickson, A. J. (2011). Metabolite extraction from suspension-cultured mammalian cells for global metabolite profiling. *Nat. Protoc*., **6**, 1241-1249.

Smyth, G.K. (2005). Limma: linear models for microarray data, in Bioinformatics and Computational Biology Solutions Using R and Bioconductor, pp. 397–420, Springer, New York, NY, USA.

Starai, V. J., Takahashi, H., Boeke, J. D., Escalante-Semerena, J. C. (2003). Short-chain fatty acid activation by acyl-coenzyme A synthetases requires SIR2

protein function in *Salmonella enterica* and *Saccharomyces cerevisiae*. *Genetics*, **163**, 545-555.

Taymaz-Nikerel, H., Borujeni, A.E., Verheijen, P.J., Heijnen, J.J,, van Gulik, W.M. (2010). Genome-derived minimal metabolic models for *Escherichia coli* MG1655 with estimated in vivo respiratory ATP stoichiometry. *Biotechnol. Bioeng.*, **107**, 369-81.

Van Noort, V., Seebacher, J., Bader, S., Mohammed, S., Vonkova, I., Betts, M.J., Kühner,S., Kumar, R., Maier, T., O'Flaherty, M., Rybin, V., Schmeisky, A., Yus, E., Stülke, J.,Serrano, L., Russell, R.B., Heck, A.J.R, Bork, P., Gavin, A.C. (2012). Cross-talk between phosphorylation and lysine acetylation in a genome-reduced bacterium. *Mol. Syst. Biol.,* **8**, 571.

Wang, Q., Zhang, Y., Yang, C., Xiong, H., Lin, Y., Yao, J.,Li, H., Xie, L., Zhao, W., Yao, Y., Zhi-Bin Ning, Z. B., Zeng, R., Xiong, Y., Kun-Liang Guan, K.L., Zhao, S., Zhao, G.P. (2010). Acetylation of metabolic enzymes coordinates carbon source utilization and metabolic flux. *Science*, **327**, 1004–7.

Warnes, G.R., Bolker, B., Bonebakker, L., Gentleman, R., Liaw, W.H.A., Lumley, T., Maechler, M., Magnusson, A., Moeller, S., Schwartz, M., Venables, B. (2012). gplots: various R programming tools for plotting data. http://CRAN.R-project.org/package=gplots.

Weinert, B.T., Wagner, S.A., Horn, H., Henriksen, P., Liu, W.R., Olsen, J.V., Jensen, L.J., Choudhary, C. (2011). Proteomewide mapping of the *Drosophila* acetylome demonstrates a high degree of conservation of lysine acetylation. *Sci. Signal*, **4**, ra48.

Weinert, B.T., Lesmantavicius, V., Wagner, S.A.A., Schölz, C., Gummesson, B., Beli, P., Nyström, T., Choudhary, C. (2013). Acetyl-phosphate is a critical determinant of lysine acetylation in *E. coli*. *Mol. Cell*, **51**, 265–72.

Weinert, B.T., Lesmantavicius, V., Moustafa, T., Schölz, C., Wagner, S.A., Magnes, C., Zechner, R., Choudhary, C. (2014). Acetylation dynamics and stoichiometry in *Saccharomyces cerevisiae*. *Mol. Syst. Biol.*, **10**:716.

Wolfe, A. J. (2005). The acetate switch. *Microbiol. Mol. Biol. Revi.*, **69**, 12-50.

Xu, J.Y., You, D., Leng, P.Q., Ye, B.C. (2014). Allosteric regulation of a protein acetyltransferase in *Micromonospora aurantiaca* by the amino acids cysteine and arginine. *J. biol. Chem.,* **289**, 27034-45.

Zhao, K. H., Chai, X. M., Marmorstein, R. (2004). Structure and substrate binding properties of cobB, a Sir2 homolog protein deacetylase from *Escherichia coli*. *J. Mol. Biol.*, **337**, 731-741.

Chapter 6

Discussion

The aim of this Thesis was to design a metabolic profile platform able to identify and quantify unequivocally metabolites from different chemical familiessimultaneously, to be applied in a wide range of biological systems such as eukaryotic cells (Chapter 2), tissues (Chapter 3) and prokaryotic cells (Chapter 4 a 5).

The validation of a neutral extraction protocol based on ACN/$CHCl_3$ was essential in the development of the metabolic platform profile. This protocol efficiently recovers labile metabolites in standard mixture such as CoA, AcCoA, GSH, NADH or NADPH (Chapter 2). This extraction protocol was combined with an analysis method based on HPLC/UV able to quantify more than 20 metabolites simultaneously (nucleotides, coenzymes and redox metabolites) and it was applied to study the intracellular concentrations of murine leukaemia cell lines under DNM exposure (Chapter 2).

In the following Chapters (3-5) an analysis method based on HPLC-MS was used, which was able to identify and quantify more than 80 metabolites, including amino acids and derivatives. In Chapter 3, the validated extraction protocol was used to obtain the metabolic pattern of healthy and non-alcoholic fatty liver disease (NALFD) rat livers. In Chapter 4, the metabolic profile platform was used to determine the metabolic alterations when an osmotic up-shift took place in *E.coli* anaerobic chemostats with glycerol as a C-source. Additionally, metabolic flux analysis was carried out. In Chapter 5, the metabolic state of *E.coli ΔcobB* in acetate-feeding chemostats was studied. Besides, transcriptomics analysis was carried out in this chapter. In both Chapters 4 and 5, integrative pathways analysis was used to combine both transcriptomic and metabolomics data sets.

In all the chapters, relevant metabolic information has been obtained showing that metabolic analysis is a powerful tool able to give extensive information regarding the metabolic state in different biological systems (Chapter 2 to 5) and also a complement for classical biomarkers (Chapter 3) and other –omics such as fluxomics (Chapter 4) and transcriptomics (Chapter 4 and 5).

The studies carried out in this Thesis have been summarized above but for a better understanding, a final discussion of the results obtained is presented in the following.

Some metabolites have been difficult to quantify due to their instability under several conditions (Gao et al., 2007; Oikawa et al., 2011; Wu et al., 1986). In base of that, a mixture of standards of 21 metabolites (nucleotides, coenzymes and redox metabolites) were subjected to 3 extraction protocols. These 3 protocols, namely acn+chloro (based on lazzarino et al., 2003), meoh (based on Sellick et al., 2010) and acn (base on Dietmair et al., 2010), were selected from literature since they were able to quantify a wide range of metabolites from different chemical families. Moreover, since lyophilization has been widely used in literature but controversial results have been found (Oikawa et al., 2011), this process (namely lyo) was also tested in the 21 metabolite mixture named above.

The recovery (%) of each metabolite after the different protocols was obtained. Out of 21 metabolites, 4 showed significant differences with an ANOVA p-value <0.001 (NADH, NADPH, AcCoA and GSSG), whereas the remaining recoveries were close to 100% (Chapter 2, Figure 5). Regarding lyophilization (lyo), the recoveries of GSSG, CoA and AcCoA were significantly lower (60%, 65% and 50%, respectively) and also in the protocols (meoh and acn) where lyophilization was carried out. These results agree with Oikawa et al. (2011) and highlight that lyophilization should be avoided for measuring GSH and AcCoA/CoA ratios. With respect to MeOH extraction protocol (meoh), the recovery of NADH and NADPH were 66% and 17%, respectively showing that it could not be the most suitable protocol for these metabolites. The metabolites CoA, AcCoA and GSSG were only efficiently recovered when neutral extraction with ACN/$CHCl_3$ (acn+chloro) was applied (87%, 100% and 100% recoveries respectivelly), whereas recoveries were 50-60% for CoA, around 82% for AcCoA and around 60% for GSSG with the other protocols (meoh, and acn). Besides, the recoveries obtained with the acn+chloro extraction method were higher than 85% for all the analysed metabolites. In based of that, neutral extraction based on lazzarino et al., (2003) was used in the present work for all the studies.

As regards quenching 60% methanol supplemented with 0.85% AMBIC (ammonium bicarbonate) at -40ºC has been used in the present work. Although Dietmair et al. (2010) stated that this solution could lead to metabolite leakage, it has been shown to be most suitable solution for mammalian cells (Sellick et al. (2010, 2011). Besides, although metabolite interconversions might not be completely prevented even at -50ºC (Wellerdiek et al., 2009), Sellick et al. (2011) did not find any substantial leakage in the case of small metabolites (TCA intermediates). Besides eukaryotic cells, AMBIC was added since it seemed to reduce osmotic shock and leakage in bacteria (Faijes et al., 2007). In the present work, the results obtained did not show any relevant leakage, probably due to the fact that most of the measured metabolites presented a high molecular weight (Canelas et al., 2009). Besides, although no leaking was detected in Chapter 4 and 5, in which target were bacterial samples, results were expressed as fold-change and not as absolute concentrations since it is possible that no leakage was detected due to the sensitivity of the platform.

In Chapter 2, the selected extraction protocol was used to study the metabolic state of leukaemia cells: L1210 cell line (sensitive to DNM), L1210R (multidrug-resistant phenotype, MDR-cells) and CBMC-6 (L1210 that expresses glycoprotein P, p-gP). Before daunomycin treatment, the metabolic state of the cells mentioned above was studied. Regarding GSH, its concentration was five-fold higher in L1210R ($p<0.001$) and two-fold higher in CBMC-6 than in the parental cell line, L1210 (Chapter 2, Figure 7). The difference in GSH concentration between chemotherapy-resistant and sensitive cell lines have been described in previous works (Bohacova et al., 2000, Suzukake et al., (1982); Ramu et al., 1984). This could be related to its role as a major antioxidant by maintaining the homeostasis of the redox status (Marí et al., 2009). In addition, NADH/NAD+ ratio was higher in MDR cells than in both L1210 and CBMC-6 cell lines (Chapter 2, Figure 7, $p<0.05$ for both), which could help to protect cells from ROS-induced cell death (Kuznetsov et al., 2011). With regard to AcetylCoA/CoA ratio, it was higher in L1210R and CBMC-6 cell lines ($p<0.05$) than in L1210 parental cell line (Chapter 2, Figure 7) which could be related to P-gp is also involved in the movement of lipids (Aye et al., 2009, Foucaud-Vignault et al., 2011). Regaring nucleotides, the adenylate

energy charge value (AEC), uracilate energy charge value (UEC) as well as guanylate energy charge value (GEC) were calculated as in Atkinson and Walton (1967). It was more appropriate to look at the nucleotide balance including the corresponding triphosphates (XTP), diphosphates (XDP) and monophosphates (XMP), since several enzymatic reactions are devoted to their interconversion. Our results showed a higher level of AEC, GEC and UEC (Chapter 2, Figure 8) in MDR-cells compared to the sensitive one and an intermediate value for CBMC-6 cells. AEC has been shown higher in several leukaemic cell lines compared with lymphocytes from healthy human subjects (Baranowska-Bosiacka et al., 2005). P-gP could contribute to the slightly higher AEC in CBMC-6 cells since this subline presents 20% P-gp expression of MDR cells and P-gp ATPase activity inhibition has showed a drastic sensitization of MDR tumors (Oberlies et al., 1997). Similar results were obtained for GEC and UEC.

Besides, the metabolic analysis was applied to study the metabolic state of these cells under 1h of 0.15µM DNM exposure. Based on the results obtained, it could be hypothesized that cell survival during DNM exposure is highly influenced by cellular GSH content since this metabolite was completely depleted in sensitive-cells after one hour of DNM-exposure (12% cell survival), whereas it was constant in MDR cells during DNM exposure (90% cell survival). Regarding NADH/NAD+ ratio, only L1210R cells presented an initial sharp increase after daunomycin addition. In this regard, MDR cells could have developed mechanisms to increase NADH levels in order to be protected from ROS-induced cell death, as also shown by Kuznetsov et al., (2011). Regarding AEC, it could be concluded that MDR cells have developed different metabolic strategies in order to keep high values of AEC under DNM treatment. Finally, AcetylCoA/CoA ratio strongly decreased in the MDR and CBMC-6 cells after daunomycin treatment (Chapter 2, Figure 8). This could be related to the metabolic changes that take place in cancer cells and also chemotherapy resistance affecting to ATP source pathways, fatty acid oxidation and glycolysis (Carvalho et al., 2010, Harper et al., 2002). Further experiments are necessary to corroborate this hypothesis and establish the contribution of P-gp, for example, down-regulating P-gp expression in L1210R and CBMC-6 cells.

In Chapter 3, the metabolic profile platform gave a specific metabolic pattern for each type of sample, healthy and NAFLD livers. In this regard, an unknown sample would be easily classified as healthy or NALFD if the metabolic analysis described in this work is carried out. Besides, the intracellular metabolite concentrations agreed with the classical biomarkers (AST, ALT, LDL, HDL and isoprostanes) (Chapter 3, Appendix 1). ATP concentration was 5-fold higher in NAFLD liver rats, which was in concordance to the high-fat intake. Lipid metabolism could be affected since CoA was completely depleted and carnitine was two-fold lower compared to rats fed with normal diet, which agreed with previous results (Kim et al., 2011, Noland et al., 2009; Vinaixa et al., 2010). Regarding amino acid concentrations, Lys and Tyr were two-fold lower, as shown in previous studies (Xie et al., 2010; Garcia-Canaveras et al., 2011; Kim et al., 2011).On the contrary, Arg was 8 times higher in NALFD rats, which could be related to the fact that this amino acid regulates lipid metabolism, modulating the expression and function of the enzymes involved in lipolysis and lipogenesis (Jobgen et al., 2009). Cys, Glu and Gly were found also diminished in NAFLD which is concordance with the the abrupt GSH decrease (almost 60 fold) since these amino acids form the tripeptide GSH. Besides, homocys and GSSG were also lower. These facts could suggest that both glutathione synthesis and the trans-sulphuration pathway were impaired (Abdelmalek et al., 2009; Bravo et al. 2011). The redox state was also affected in high fatty acid diet since NADH was very high in the case of high-fat diet fed rats. This alteration could be due to the fact that NAD^+ acts as electron acceptor in the β-oxidation. Summarizing, 51 targeted metabolites were unambiguously quantified and 26 metabolites presented a statistically significant difference ($p<0.05$ in Welch t-test) in rats in the initial phase of the NAFLD improving the knowledge from previous studies (Barr et al., 2010; Xie et al., 2010; Garcia-Canaveras et al., 2011; Kim et al., 2011; Vinaixa et al., 2010).

In chapter 4 and 5, this Thesis is focused in the metabolic state of *Escherichia coli* under specific situations since this microorganism is frequently used as a model in microbiology studies. In chapter 4, metabolic analysis was performed to study the metabolic response of anaerobic osmoadaptation and in Chapter 5, the role of the only known deacetylase (CobB) in acetate-feeding chemostats.

In Chapter 4, the most relevant metabolic events during the response to the long-term anaerobic NaCl exposure in *E.coli* with glycerol as C-source and using conditions closed to its natural environment (anaerobiosis, complex media and high osmolarity) was studied. To study the metabolic response of the *E. coli* anaerobic osmoadaptation, two NaCl concentrations (0.5 and 0.8 M) were selected according to the previous work carried out in our group (Arense et al., 2010). The results obtained suggested that *E. coli* was able to develop different strategies in order to keep cellular homeostasis.

Extracellular amino acids were depleted after 0.5M and 0.8M NaCl up-shift (Chapter 4, Figure 1). Apparently, this was carried out to save energy and redirect cofactor redox and coenzymes to other pathways, as it might avoid their de novo synthesis (Jozefczuk et al., 2010). These results agreed with transcriptomic analysis since four genes (*pheP, proW, proV and proX*) with the GO term "amino acid transport" resulted significantly upregulated in the NaCl exposure conditions (Chapter 4, Appendix) with a concentration-dependent pattern. Metabolic fluxes distribution was changed depending on NaCl concentration, as was showed using a large-scale stationary *E. coli* model (Sevilla et al., 2005). The metabolic fluxes redistribution seemed to be focused to maintain cellular homeostasis (Chapter 4, Figure 3) by increasing ATP production (higher glycerol consumption) and minimize NADH production (flux through PDH was decreased, whereas higher ethanol production at 0.5 M NaCl and higher lactate production at 0.8 M were measured). PCA analysis showed clear different intracellular metabolic patterns for these three situations (Chapter 4, Figure 2). Intracellular amino acids accumulation was measured (except Cys and His), being more accused at 0.8M NaCl. Val and Gln should be highlighted since they showed a >2000 and 100-fold increase respectively in the case of 0.8M NaCl. Regarding Val, it is highly accumulated in plants in case of salt stress (Parida and Das 2005). And Gln was also one of the amino acids highest accumulated during osmotic stress in wheat (Kovács et al., 2012). Additionally, carnitine, glycerol assimilation intermediates and CoA derivatives were accumulated at 0.8M of NaCl. Strong alterations in the redox coenzymes ratios were measured, with higher values of the NADPH and NADP forms, whereas NADH was almost depleted (Chapter 4, Table 2). Finally, the integration

pathway analysis showed also the main affected pathways: GSH metabolism, glycolysis/glyconeogenesis, amino acid biosynthesis/degradation, purine metabolism, phosphorylative oxidation, pyruvate metabolism, TCA cycle and glyoxylate shunt. However, further studies should be carried out to establish the relevance of the switch of redox cofactors observed and the effect of the oxidation state in these conditions.

In Chapter 5, acetate-feeding chemostats of *E.coli* WT and *ΔcobB* knockout were carried out in order to study the role of CobB deacetylase from a metabolic point of view. Besides, transcriptomic analysis was performed and both data sets were combined by integrative pathway analysis. Previous works (Castaño-Cerezo et al., 2012, Castaño-Cerezo et al., 2014) showed that Δ*cobB* mutant presented severe growth impairment compared to WT in acetate flask cultures and in limited-glucose chemostats. This phenotype is mainly caused by the inactivation of ACS. On the contrary, in this case of acetate-feeding chemostats no significant statistical differences were found between WT and *ΔcobB* regarding growth and fermentation patterns. In this case, acetate was mainly assimilated through the low-affinity pathway PTA-ACK due to its high concentration. Besides, no significantly different effects were found in the central metabolism as was reported in the case of glucose-chemostats (Castaño-Cerezo., 2014). However the GO terms “intracellular pH elevation”, “cellular response to acidity” and “chemotaxis” in the present work indicated that CobB may play an important role in their regulation, as was reported in the previous work with glucose-chemostats.

Integration pathway-based analysis on KEGG pathways highlighted relevant interconnections with a strong effect on sulfur and nitrogen metabolism in the acetate-feeding chemostats. Results showed relevant alterations in nitrogen metabolism, transport and fixation, ammonia uptake, amino acids and pyrimidines concentrations. In base of these results, it can be hypothesized that nitrogen metabolism is directly or indirectly regulated by protein acetylation. Regarding sulfur metabolism, Cys, Cystin and GSH concentration were much lower in *ΔcobB* (Chapter 4, Table 3) as well as taurine and hypotaurine metabolism (Chapter4, Figure 8D). Besides Cys, Arg was also altered which could be related to the fact that these amino acids are key in protein acetylation

regulation, as was reported in *Micromonospora aurantiaca* (Xu et al., 2014). In the present study, Acetyl-P in the Δ*cobB* mutant was almost 40% lower than in WT (Chapter 4, table 4), which could be as a consequence of the double role played by Acetyl-P, which is thought to regulate through Acetyl-P-dependent phosphorylation and autocatalytic acetylation (Barak et al., 2006; Lukat et al., 1992). Additionally, the peptidoglycan synthesis was affected since intermediates and pathways involved were altered, such as (i)UTP (main energy source for the peptidoglycan synthesis), which was below detection limits in the mutant (Chapter 4, Table 4); (ii) Glu, (iii) Lys, which produce the meso-diaminopimelic acid and (iv) pathways related to intermediates such as pyrimidine biosynthesis (Chapter 4, Figure 9D).

To sum up, a metabolic profile platform has been developed in this work and it has been applied to study the metabolic state different biological systems such as mammal cells, tissues and microorganisms. The validation of a neutral extraction protocol based on HCN/$CHCl_3$, which avoids lyophylization, has been essential in order to apply a general protocol to different biological systems and to obtain extensive information regarding different metabolites (nucleotides, amino acids and derivatives, coenzymes and redox metabolites). This protocol was used to study the metabolic alterations in leukaemia cell lines (sensitive and chemotherapy-resistant) under daunomycin treatment. Besides, the previous protocol was applied to obtain the metabolic pattern of NAFLD rat livers. Furthermore, metabolome analysis was used to study the metabolic effect of high NaCl concentrations in *E.coli* anaerobic chemostats using glycerol as C-source. Finally, the same protocol was also used to study the metabolic pattern in *E.coli* ΔcobB mutant using acetate as the sole carbon source. In these latter studies, integrative pathway analysis was carried out to combine metabolic and transcriptomic data to highlight the most affected pathways.

It can be conclude that some of the key metabolites have been GSH, ATP, AcCoA, CoA and some amino acids since at least one of them has resulted altered in any of the situations described along Chapters 2 to 5. GSH plays an important protective role, as it has been shown in Chapter 2 in which its concentration was five-fold higher in chemotherapy resistant-cells than in sensitive cells. In Chapter 3 and 4 GSH was almost depleted, in livers with a

high fatty acid and hypercolesterolemic diet pointing out the effect of this diet and during 0.8M NaCl up-shift in *E.coli* chemostats. In Chapter 5, GSH was also lower (almost 3 times) in the case of Δ*cobB* knockout. Taking all together, it is seen that GSH is lower or even depleted because it is used to cell protection when a perturbation is taking place (hypercolesteloremic diet, high osmolarity or gene deletion). However, in the case of MDR cells GSH remained constant during DNM incubation since these cells could have been adapted to this perturbation and they have probably developed different strategies to keep high concentrations of GSH and ATP. This latter metabolite is commonly called the molecular unit of energy transfer since it plays an important role in the majority of the metabolic pathways in any biological systems from bacteria to human. As it has been shown, ATP was found altered in all the studied systems. For example, the AEC was kept high in MDR cells even during daunomycine exposure (Chapter 2); ATP was also higher NAFLD livers (Chapter 3); *E. coli* metabolic fluxes reorganized towards ATP production increasing glycerol consumption when high osmotic up-shift took place (Chapter 4) and ATP was 3 times lower in the case of Δ*CobB* mutant (Chapter 5). Regarding AcCoA/CoA, this ratio and its metabolites (CoA and AcCoA concentrations) are key to understand the metabolic state of the system. This ratio was found higher in the case of chemotherapy resistant cells compared to sensitive ones (Chapter 2). In the case of NAFLD livers, CoA, which was completely depleted, is essential in the fatty acid metabolism (Chapter 3). AcCoA and CoA were seven times higher in the case of 0.8M NaCl up-shift in *E.coli* chemostats and CoA was more than double in Δ*cobB* mutant in the case of acetate-feeding chemostats. In any metabolic perturbation studied, even in different biological systems, CoA, AcCoA or the ratio AcCoA/CoA has resulted altered. Finally, with regard to amino acids, it has been shown that they could present important alterations during different perturbations. In the case of NAFLD livers most of the intracellular amino acid concentrations were lower than in healthy livers with the exception of Arg which it is involved in lipid metabolism regulation (Jobgen et al., 2009) (Chapter 3). In Chapter 4, total depletion of extracellular amino acids at the osmotic up-shift was shown in *E. coli* anaerobic chemostats. Finally, in Chapter 5 the integrative-based pathway analysis revealed that metabolic

pathways of several amino acids (Val, Leu, Ile, Ala, Asp, Glu, Arg and Pro) were affected in in Δ*cobB* mutant in acetate-feeding chemostats.

In base of that, we can conclude that the quantification of redox cofactors, nucleotides, coenzymes and amino acids is highly important for the understanding of the whole metabolic state in biological systems. Surprisingly, some of the key molecules described, such as GSH, AcCoA, CoA and also NAD(P)H are labile and their concentrations could be easily altered during the extraction process (Chapter 2). Because of that, the use of an appropriate unbiased extraction protocol for the determination of these metabolites has been proved to be essential.

REFERENCES

Abdelmalek, M. F., Sanderson, S. O., Angulo, P., Soldevila-Pico, C., Liu, C., Peter, J., Keach, J., Cave, M., Chen, T., McClain, C. J., Lindor, K. D. (2009). Betaine for Nonalcoholic Fatty Liver Disease: Results of a Randomized Placebo-Controlled Trial. *Hepatology*, **50**, 1818-1826.

Arense, P., Bernal, V., Iborra, J. L., Cánovas, M. (2010). Metabolic adaptation of Escherichia coli to long-term exposure to salt stress. *Process Biochem*., **45**, 1459-1467.

Atkinson, D. E. and Walton, G. M. (1967). Adenosine triphosphate conservation in metabolic regulation - rat liver citrate cleavage enzyme. *J. Biol. Chem*., **242**, 3239-3241.

Aye, I., Singh, A. T. and Keelan, J. A. (2009). Transport of lipids by ABC proteins: Interactions and implications for cellular toxicity, viability and function. *Chem. Biol. Interact*., **180**, 327-339.

Barak, R., Yan, J., Shainskaya, A., Eisenbach, M. (2006). The chemotaxis response regulator CheY can catalyze its own acetylation. J. Mol. Biol., 359, 251-265.

Baranowska-Bosiacka, I., Machalinski, B. and Tarasiuk, J. (2005). The purine nucleotide content in human leukemia cell lines. *Cell. Mol. Biol. Lett*., **10**, 217-226.

Barr, J., Vazquez-Chantada, M., Alonso, C., Perez-Cormenzana, M., Mayo, R., Galan, A., Caballeria, J., Martin-Duce, A., Tran, A., Wagner, C., Luka, Z., Lu, S. C., Castro, A., Le Marchand-Brustel, Y., Martinez-Chantar, M. L., Veyrie, N., Clement, K., Tordjman, J., Gual, P., Mato, J. M. (2010). Liquid

Chromatography-Mass Spectrometry-Based Parallel Metabolic Profiling of Human and Mouse Model Serum Reveals Putative Biomarkers Associated with the Progression of Nonalcoholic Fatty Liver Disease. *J. Proteome Res.*, **9**, 4501-4512.

Bohacova, V., Kvackajova, J., Barancik, M., Drobna, Z. and Breier, A. (2000). Glutathione S-transferase does not play a role in multidrug resistance of L1210/VCR cell line. *Physiol. Res*., **49**, 447-453.

Bravo, E., Palleschi, S., Aspichueta, P., Buque, X., Rossi, B., Cano, A., Napolitano, M., Ochoa, B., Botham, K. M. (2011). High fat diet-induced non alcoholic fatty liver disease in rats is associated with hyperhomocysteinemia caused by down regulation of the transsulphuration pathway. *Lipids Health Dis.*, **10;** doi:10.1186/1476-511x-10-60.

Canelas, A. B., ten Pierick, A., Ras, C., Seifar, R. M., van Dam, J. C., van Gulik, W. M. and Heijnen, J. J. (2009). Quantitative Evaluation of Intracellular Metabolite Extraction Techniques for Yeast Metabolomics. *Anal. Chem*., **81,** 7379-7389.

Carvalho, R. A., Sousa, R. P. B., Cadete, V. J. J., Lopaschuk, G. D., Palmeira, C. M. M., Bjork, J. A. and Wallace, K. B. (2010). Metabolic remodeling associated with subchronic doxorubicin cardiomyopathy. *Toxicol.,* **270**, 92-98.

Castano-Cerezo, S., Bernal, V., Post, H., Fuhrer, T., Cappadona, S., Sanchez-Diaz, N. C., Sauer, U., Heck, A. J., Altelaar, A. F. and Canovas, M. (2014). Protein acetylation affects acetate metabolism, motility and acid stress response in *Escherichia coli*. Mol. Syst. Biol., **10**, 762. doi: 10.15252/msb.20145227

Castano-Cerezo, S., Bernal, V., Blanco-Catala, J., Iborra, J. L., Canovas, M. (2011). cAMP-CRP co-ordinates the expression of the protein acetylation pathway with central metabolism in *Escherichia coli*. *Mol. Microbiol.*, **82**, 1110-1128.

Dietmair, S., Timmins, N. E., Gray, P. P., Nielsen, L. K. and Kroemer, J. O. (2010). Towards quantitative metabolomics of mammalian cells: Development of a metabolite extraction protocol. *Anal. Biochem*., **404**, 155-164.

Foucaud-Vignault, M., Soayfane, Z., Menez, C., Bertrand-Michel, J., Guy, P., Martin, P., Guillou, H., Collet, X. and Lespine, A. (2011). P-glycoprotein Dysfunction Contributes to Hepatic Steatosis and Obesity in Mice. *PLoS One,* **6**: e23614. doi: 10.1371/journal.pone.0023614.

Faijes, M., Mars, A. E., Smid, E. J. (2007). Comparison of quenching and extraction methodologies for metabolome analysis of *Lactobacillus plantarum*. *Microb. Cell. Fact.*, **6**.

Gao, L., Chiou, W., Tang, H., Cheng, X., Camp, H. S. and Burns, D. J. (2007). Simultaneous quantification of malonyl-CoA and several other short-chain acyl-CoAs in animal tissues by ion-pairing reversed-phase HPLC/MS. *J. Chromatogr. B Analyt. Technol. Biomed. Life. Sci.*, **853**, 303-313.

Garcia-Canaveras, J. C., Donato, M. T., Castell, J. V., Lahoz, A. (2011). A Comprehensive Untargeted Metabonomic Analysis of Human Steatotic Liver Tissue by RP and HILIC Chromatography Coupled to Mass Spectrometry Reveals Important Metabolic Alterations. *J. Proteome Res.*, **10**, 4825-4834.

Harper, M. E., Antoniou, A., Villalobos-Menuey, E., Russo, A., Trauger, R., Vendemelio, M., George, A., Bartholomew, R., Carlo, D., Shaikh, A., Kupperman, J., Newell, E. W., Bespalov, I. A., Wallace, S. S., Liu, Y., Rogers, J. R., Gibbs, G. L., Leahy, J. L., Camley, R. E., Melamede, R. and Newell, M. K. (2002). Characterization of a novel metabolic strategy used by drug-resistant tumor cells. *FASEB J.*, **16**, 1550-1557.

Jobgen, W., Fu, W. J., Gao, H., Li, P., Meininger, C. J., Smith, S. B., Spencer, T. E., Wu, G. (2009). High fat feeding and dietary L-arginine supplementation differentially regulate gene expression in rat white adipose tissue. *Amino Acids*, **37**, 187-198.

Jozefczuk, S., Klie, S., Catchpole, G., Szymanski, J., Cuadros-Inostroza, A., Steinhauser, D., Selbig, J., Willmitzer, L. (2010). Metabolomic and transcriptomic stress response of *Escherichia coli*. *Mol. Syst. Biol.*, **6**:364. doi: 10.1038/msb.2010.18.

Kim, H. J., Kim, J. H., Noh, S., Hur, H. J., Sung, M. J., Hwang, J. T., Park, J. H., Yang, H. J., Kim, M. S., Kwon, D. Y., Yoon, S. H. (2011). Metabolomic Analysis of Livers and Serum from High-Fat Diet Induced Obese Mice. *J. Proteome Res.*, **10**, 722-731.

Kovács, Z., Simon-Sarkadi, L., Vashegyi, I. and Kocsy, G. (2012). Different accumulation of free amino acids during short- and long-term osmotic stress in wheat. ScientificWorldJournal, **2012**, 216521.

Kuznetsov, A. V., Margreiter, R., Amberger, A., Saks, V. and Grimm, M. (2011). Changes in mitochondrial redox state, membrane potential and calcium precede mitochondrial dysfunction in doxorubicin-induced cell death. *Biochim. Biophys. Acta*, **1813**, 1144-52.

Lazzarino, G., Amorini, A. M., Fazzina, G., Vagnozzi, R., Signoretti, S., Donzelli, S., Di Stasio, E., Giardina, B. and Tavazzi, B. (2003). Single-sample preparation for simultaneous cellular redox and energy state determination. *Anal. Biochem.*, **322**, 51-59.

Lukat, G. S., McCleary, W. R., Stock, A. M. and Stock, J. B. (1992). Phosphorylation of bacterial response regulator proteins by low molecular weight phospho-donors. Proc. Natl. Acad. Sci. U.S.A., **89**, 718-22.

Marí, M., Morales, A., Colell, A., García-Ruiz, C., & Fernández-Checa, J. C. (2009). Mitochondrial Glutathione, a Key Survival Antioxidant. *Antioxid. Redox Signaling*, **11**(11), 2685–2700.

Noland, R. C., Koves, T. R., Seiler, S. E., Lum, H., Lust, R. M., Ilkayeva, O., Stevens, R. D., Hegardt, F. G., Muoio, D. M. (2009). Carnitine Insufficiency Caused by Aging and Overnutrition Compromises Mitochondrial Performance and Metabolic Control. *J. Biol. Chem.*, **284**, 22840-22852.

Oberlies, N. H., Croy, V. L., Harrison, M. L. and McLaughlin, J. L. (1997). The Annonaceous acetogenin bullatacin is cytotoxic against multidrug-resistant human mammary adenocarcinoma cells. *Cancer Lett.*, **115**, 73-79.

Oikawa, A., Otsuka, T., Jikumaru, Y., Yamaguchi, S., Matsuda, F., Nakabayashi, R., Takashina, T., Isuzugawa, K., Saito, K. and Shiratake, K. (2011). Effects of freeze-drying of samples on metabolite levels in metabolome analyses. *J. Sep. Sci*., **34**, 3561-3567.

Parida, A.K., Das, A.B. (2005). Salt tolerance and salinity effects on plants: a review. *Ecotoxicol. Environ. Saf.*, **60,** 324-49**.**

Ramu, A., Cohen, L. and Glaubiger, D. (1984). Oxygen radical detoxification enzymes in doxorubicin-sensitive and doxorubicin-resistant P388 murine leukemia-cells. *Cancer Res.,* **44**, 1976-1980.

Sellick, C. A., Hansen, R., Stephens, G. M., Goodacre, R. and Dickson, A. J. (2011). Metabolite extraction from suspension-cultured mammalian cells for global metabolite profiling. *Nat. Protoc*., **6,** 1241-1249.

Sellick, C. A., Knight, D., Croxford, A. S., Maqsood, A. R., Stephens, G. M., Goodacre, R. and Dickson, A. J. (2010). Evaluation of extraction processes for intracellular metabolite profiling of mammalian cells: matching extraction approaches to cell type and metabolite targets. *Metabolomics*, **6**, 427-438.

Sevilla, A., Schmid, J. W., Mauch, K., Iborra, J. L., Reuss, M., Cánovas, M. (2005). Model of central and trimethylammonium metabolism for optimizing L-carnitine production by *E. coli*. *Metab. Eng.*, **7**, 401-425.

Suzukake, K., Petro, B. J. and Vistica, D. T. (1982). Reduction in glutathione content of L-pam resistant L1210 cells confers drug sensitivity. *Biochem. Pharmacol*., **31**, 121-124.

Vinaixa, M., Rodriguez, M. A., Rull, A., Beltran, R., Blade, C., Brezmes, J., Canellas, N., Joven, J., Correig, X. (2010). Metabolomic Assessment of the Effect of Dietary Cholesterol in the Progressive Development of Fatty Liver Disease. *J. Proteome Res.*, **9**, 2527-2538.

Wu, J. T., Wu, L. H. and Knight, J. A. (1986). Stability of NADPH - effect of various factors on the kinetics of degradation. *Clin. Chem*., **32**, 314-319.

Xie, Z. Q., Li, H. K., Wang, K., Lin, J. C., Wang, Q., Zhao, G. P., Jia, W., Zhang, Q. H. (2010). Analysis of transcriptome and metabolome profiles alterations in fatty liver induced by high-fat diet in rat. *Metab.-Clin. Exp.*, **59**, 554-560.

Xu, J.Y., You, D., Leng, P.Q., Ye, B.C. (2014). Allosteric regulation of a protein acetyltransferase in *Micromonospora aurantiaca* by the amino acids cysteine and arginine. *J. biol. Chem.,* **289**, 27034-45.

Chapter 7

Conclusions

and

future perspectives

CONCLUSIONS

- Metabolome analysis is shown to be a powerful tool that provides extensive information regarding the metabolic state in a wide range of biological systems.
- The metabolite extraction method has been carefully validated with pure standards, neutral extraction based on ACN/$CHCl_3$ and avoiding lyophilization being especially important for the quantification of of redox intermediates (NADH,NADPH and GSSG) and CoA derivatives (AcCoA and CoA).
- The analysis method based on HPLC-UV was used to study the metabolic differences among the murine leukaemia cell line (L1210) and two derived sublines L1210R (MDR phenotype) and CBMC-6 (P-gp expressed L1210) before and after daunomycin exposure. The results provided a better understanding of the defense mechanisms developed by MDR cells such as a 5-fold higher GSH concentration and higher AEC, UEC and GEC ratios compared to the L1210 line. However, further experiments should be carried out for a better understanding of the P-gp contribution to the MDR phenotype since CBMC-6 subline showed an intermediate behavior between sensitive and MDR cells.
- The metabolic platform based on HPLC-MS was able to quantify the metabolic differences between healthy and NALFD rat livers. In the latter, the ATP concentration was found to be 5-fold higher and the lipid metabolism was deeply altered since carnitine was 2-fold lower and CoA was completely depleted. Moreover, the amino acid content and redox state were altered in this disease.
- The same analytical platform as mentioned above was applied to the study of the metabolic events that took place in *E. coli* in response to anaerobic long-term high (0.5M) and very high (0.8M) NaCl concentrations using glycerol as C-source in complex medium. The metabolic effects were more pronounced in the case of very high salt concentration. Main mechanisms involved in this situation were (i) the total depletion of extracellular amino acids; (ii) the accumulation of

intracellular aminoacids (except Cys and His), carnitine, CoA derivarives and glycerol assimilation intermediates and (iii) alterations in the redox state and in the fermentation fluxes.

- Regarding the deletion of *cobB* gene *in E. coli* chemostats using acetate as a sole carbon source, metabolomics and transcriptomics data sets were combined by the use of pathway-based integration analysis. This approach highlighted strong impairment of the sulfur and nitrogen metabolisms in this situation. Besides, flagella biosynthesis, motility and acid stress survival were altered as observed in glucose-limited chemostats.

FUTURE PERSPECTIVES

According to the studies carried out in the present work, some future perpectives could be proposed:

- In the case of the metabolic response of leukamia cells under DNM treatment, the metabolic study of the equivalent human leukaemia cell lines would be of interest in order to establish a comparison between murine and human models. Besides, another study could be the metabolic analysis of these cells under low temperatures treatment, since totally opposite behavior was observed compared with the DNM treatment.
- In the case of NAFLD, it would be useful to carry out the analysis of NAFLD human livers in order to establish a comparison between murine and human studies and increase the knowledge concerning this common medical problem.
- Due to the interesting results obtained in the study of *E. coli* during the anaerobic long-term NaCl adaptation, these results of this study could be applied in the L-carnitine production process.
- With regard to *cobB* mutant, the present study will be complemented with further studies carried out in the TUDELFT based on ^{13}C labeling experiments.